NONLINEAR ALGORITHMS FOR FAST AND ROBUST CONTROL OF ELECTRICAL DRIVES

by

Dusan Borojevic

Dissertation submitted to the Faculty of the
Virginia Polytechnic Institute and State University
in partial fulfillment of the requirements for the degree of
DOCTOR OF PHILOSOPHY
in
Electrical Engineering

APPROVED:

F. C. Lee, Chairman

L. Garces

D. K. Lindner

H. Naitoh

C. E. Nunnally

January, 1986
Blacksburg, Virginia

NONLINEAR ALGORITHMS FOR FAST AND ROBUST CONTROL OF ELECTRICAL DRIVES

by

Dusan Borojevic

Committee Chairman: Fred C. Lee
Electrical Engineering

(ABSTRACT)

Several new nonlinear algorithms for speed control of electrical drives are developed. They are compared with the algorithms for integral-proportional (I-P) control, sliding mode control (SLM) and adaptive control which uses the torque and parameter observer. To achieve fast and robust response, all algorithms use very large gains.

In a new, variable limit PI (VLPI) control algorithm, integrator windup is completely prevented by using a high gain, "variable dead zone" nonlinearity as a local feedback over the integrator.

Recently proposed soft variable structure (SVS) control, derived by using the Liapunov direct method, is modified so that the algorithm can be implemented with only the output measurements. Proper operation is achieved for any value of the output variable. The new control is very robust, but exhibits a steady state error.

Two versions of the adaptive PI (API) control algorithm are developed that have fast and robust transient response with zero steady state error. The SVS API version operates similarly as the modified SVS control, but does not have its drawbacks. The SLM API version operates like the SLM control during large transients, and like VLPI control when close to the steady state. The local stability of the control is proved using the "small gain theorem". Its global behavior is analyzed by describing functions.

Very good operation of the SVS API speed control within the proportional position loop is demonstrated. Faster transient response is achieved by implementing the SLM adaptive proportional control in the position loop. The operation is the same as the operation of the SLM API control in the speed loop.

Similarity between modified SVS control, API control, and classical adaptive algorithms is shown. All the algorithms are simulated and compared for twofold and tenfold changes in plant parameters. The experimental verification of the results for I-P control, SLM control, and modified SVS control, are presented.

Theory of the new algorithms is general, such that the results are applicable to any SISO plant that can be stabilized.

ACKNOWLEDGEMENTS

I am grateful to my advisers, Dr. Fred C. Lee and Dr. Luis Garces, for the guidance, encouragement and caring support. Their impressive knowledge and technical skills have been an invaluable help and challenge, throughout this research.

A special thanks to Dr. D. K. Lindner, who served on my advisory committee and taught the large part of my course work. My appreciation of automatic control theory is due mainly to his provocative teaching.

I wish to thank my committee members, Dr C. E. Nunnally and Dr H. Naitoh, and past committee members Dr F. C. Brockhurst and Dr S. J. Skar, for their help and support.

I am indebted to for his efforts in organizing and supporting my stay at VPI & SU, and for his constant moral support.

It is a pleasure to acknowledge the faculty and graduate students in the Power Electronics Research Group at VPI & SU, for providing a constructive and enjoyable educational atmosphere. I particularly appreciate the enlightening discussions with my fellow students, and

Also thanks to for her assistance in typing the manuscript.

With much love, I thank my parents, and for their constant support.

Most importantly, I wish to pay tribute to my wife, , for her many contributions to this and other projects throughout the years. Without her constant assistance and moral support, these projects could never have been accomplished.

This work has been supported by the General Electric Co., IEDL, Charlottesville, Va., under a research fellowship grant J80-G1772.

To my wife

and my children

and

TABLE OF CONTENTS

NOMENCLATURE

Some of the symbols and abbreviations used in the text are defined below.

$\tilde{\bullet}$	Approximate value; estimate.
$\bullet_e$	Equilibrium value.
$\|\bullet\|$	Eucledean norm on R^n ; absolute value.
$\underline{\bullet}$	Laplace or z- transform.
$\bullet'$	Transpose of a vector or a matrix.
$\hat{\bullet}$	Offset by a constant.
R	Field of real numbers.
R^n	n-dimensional linear vector space with elements in R.
PI	Proportional plus Integral (control)
SVS	Soft Variable Structure (control)
SLM	Sliding Mode (control)
API	Adaptive PI (control)
SAPI	Sliding API (control)
SVSPI	Soft variable structure API (control)
SISO	Single Input Single Output
VLPI	Variable limit PI (control)

Chapter 1

INTRODUCTION

Electrical motors are literally the driving force of the modern industry. In most applications they need to be controlled in a closed loop system. Until the 1950's the control was implemented using Ward-Leonard sets, amplidynes, magnetic amplifiers and similar electromechanical and electromagnetic devices. High cost and large dimensions of these systems limited their widespread use, which to a great extent hampered the development of industry automation.

The invention of power semiconductor devices and development of power electronic circuits marked the emergence of the new generation high performance and reliable, compact and economical, solid-state motor drives. Due to the availability of cheaper drives the industry automation increased very fast, which then increased demand for high-quality, controlled electrical drives. This has resulted in vast improvements in electrical machine performances, power electronic circuit techniques, power semiconductor device

characteristics, and in nonlinear control theory. The effect of this development was that in the 1970's, old systems were completely replaced by electronically controlled motor drives, which also found many new application areas.

The advances in analog and digital signal processing electronic components, especially the advent of microprocessors, made the implementation of more complicated control algorithms possible. That enabled the development of sophisticated motion control systems, like numerically controlled machine tools, precision manipulators, high density disc drives, etc. [10].

Today, the electronic control of electrical drives is a maturing technology. Further developments will be mainly directed towards technological refinements on one side, and towards meeting ever increasing performance standards on the other. The latter requires very fast, highly accurate and robust designs.

1.1. ELECTRICAL MOTOR CONTROL SYSTEM

The general block diagram of a motor control system is shown in Fig. 1.1. The objective of the control is to efficiently convert the supplied electrical energy into useful

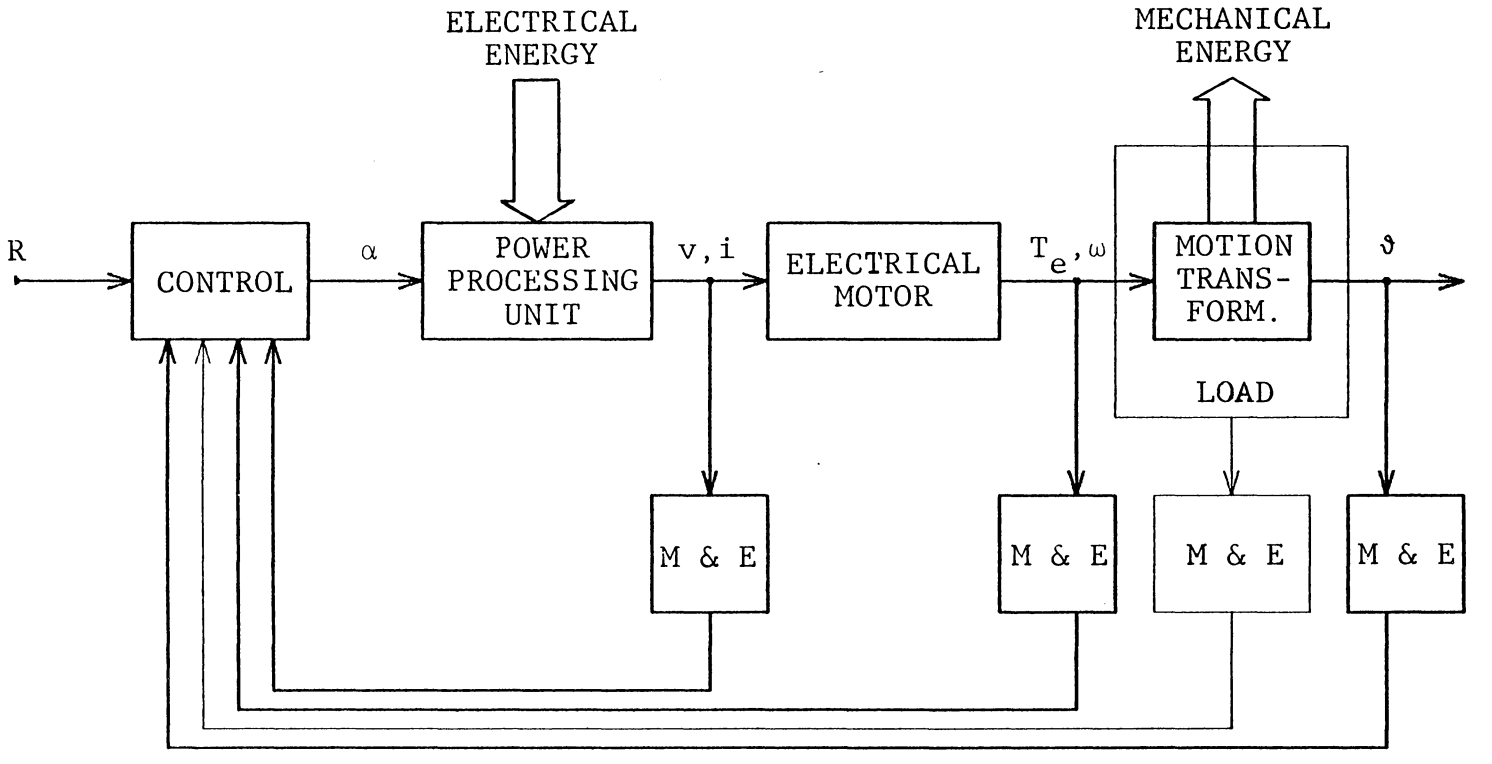

Fig. 1.1: General block diagram of an electrical drive control system.

mechanical energy, in such a way that the output variable ϑ is some predetermined function of the reference input R.

The central part of the system is the electrical motor which actually performs the electromechanical conversion. Its inputs are voltages (v) and currents (i), and outputs are the developed torque T_e and the speed ω at its shaft.

The power processing unit is an electronic converter, which transforms electrical energy from the easily available form, to the form suitable for the motor. The energy flow is continuously directed by the control unit, in such a way that the objective of the control is achieved. For the proper operation of the converter, a feedback loop from the motor electrical variables v and i, to the converter control input α is usually necessary.

For a long time, and still today, dc motors are used for high performance, motion control applications. However, with the new developments in motor construction, in power electronic devices and circuits, and in the nonlinear control algorithms, this situation is rapidly changing. Electronically commutated dc motors (also called brushless dc motors), synchronous motors, and induction motors, are used more frequently instead of the classical dc motors. They provide the same performance characteristics, with the added benefit of lower maintenance, cost, volume, and weight [8, 66, 31]. By using the field oriented control, any of these

motors together with the power processing unit and the associated control, can be treated as an equivalent, current driven dc motor, as shown in Fig. 1.2.

The mechanical torque and speed, developed by the motor, always undergo some kind of "motion transformation", before the final output variable ϑ is obtained. This part of the system, together with the delivered mechanical energy, is usually referred to as load.

The amount of energy demanded by the load is, in practically all applications, a stochastic variable. Therefore, it is standard to consider this quantity as disturbance. In a control system, it is convenient to represent the effect of this disturbance, as an additional input to the plant which, when referred to the motor shaft, becomes the load torque, T_ℓ.

In many cases, load can be represented as a single inertia and damping. In such case, load parameters can be lumped together with the parameters of the motor mechanical part. If the output variable ϑ, is proportional to the position of the motor shaft θ, the simplest block diagram of the motor control system can be represented as shown in Fig. 1.2.

Because the load parameters are never exactly known, the feedback control must be used in order to achieve the objective of the control. Therefore, measurement and estimation

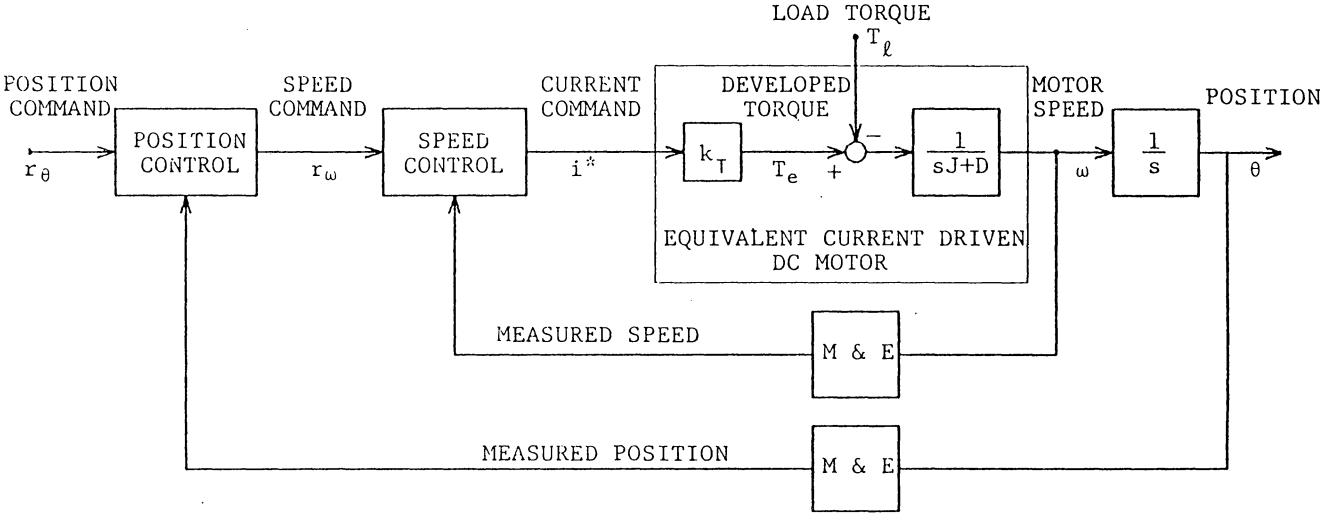

J - moment of inertia, D - mechanical damping, M & E - measurement & estimation

Fig. 1.2: Functional block diagram of an electrical motor controller, commonly used in motion control systems.

of the system variables is necessary. Beside the inner current and/or voltage loop, the speed control loop is always present and in most applications it is placed within an outer, output control loop. The control algorithms that are used in these feedback loops depend on the application and on performance requirements.

1.2. PROBLEM FORMULATION

The major performance characteristics of any motor control system are:

- transient response,
- accuracy,
- robustness,
- cost.

In motion control, the requirements are usually severe. Very fast and non-oscillatory transient response is required together with high accuracy (usually better than 0.01%). Such performance has to be maintained for a very wide range of system parameters variation, up to the ratios of 1 to 100 in some robotics applications. Such requirements cannot be met with classical linear control algorithms. Therefore nonlin-

ear algorithms, like the sliding mode control or adaptive control, have been used recently in motion control systems.

Another motive for the application of robust algorithms in the motion control systems is a need for the electrical drive systems which do not have to be adjusted for each application. The elimination of the infield tuning and setup time, reduces the cost of the motion control systems, which is very important for the further enhancement of the industry automation.

The objective of this research was to investigate the possibilities of using nonlinear control algorithms in the speed loop of electrical drives, for achieving very fast transient response, very high accuracy, and high degree of robustness to parameter variations and external disturbances. The investigation consisted of analyses of several known control algorithms and their modifications, of proposing new control algorithms, and of comparing their merits and demerits.

The speed control loop was selected because the system parameters which are varying are contained within this loop. Also, the speed of response and accuracy of the outer loop is directly related to the transient response and accuracy of the speed loop.

A dc motor was selected as the sample electrical drive, because it is the simplest to model and experiment with.

This in no way limits the results of this work because, as mentioned earlier, the other commonly used electrical drives can be treated as equivalent dc motors, if the field oriented control is used within the inner control loop.

Although the cost is a very important performance requirement because it includes such important factors as efficiency, complexity, reliability, manufacturing costs, installation costs, maintenance costs, etc. - which are all influenced by the selection of the control algorithm - it is only marginally considered in this research.

1.3. DISSERTATION OUTLINE

The presentation of the material follows two patterns. First, the chapters are mainly ordered by ascending complexity and novelty of the material presented. Second, most of the derivations and formal proofs, as well as the practical details, are presented in appendices. The exception is Appendix A, which contains models of the dc motor which are referred to, throughout the text.

In the following chapter, the major problems that are encountered in the application of the high gain proportional-plus-integral (PI) control are presented. Two

ways of alleviating the problem of integrator wind-up, are also demonstrated.

The third chapter introduces the concept of the sliding mode (SLM) control and gives an example of its implementation for the speed control of the voltage driven dc motor.

In Chapter 4, a recent concept of the soft variable structure (SVS) control is explained. The major problems in the original version of that concept are analyzed, and the new, modified SVS control algorithm is proposed.

The results that were developed in the first four chapters led to the development of a new, adaptive PI (API) control algorithm. Its principles are presented in Chapter 5. Two versions of the algorithm, the soft variable structure PI (SVSPI) control, and the sliding API (SAPI) control are analyzed in detail.

Chapter 6 presents the performance comparison between the algorithms developed in previous chapters, particularly from the aspect of robustness.

For the purpose of completing the assessment of the new algorithms, already known adaptive control results, are discussed and compared with the SVS and API control in Chapter 7.

Chapter 8 briefly investigates the properties of the position control with SVSPI control implemented in the speed

loop. A possibility of using the SAPI control concept in the position loop itself, is also presented.

In the last chapter, the summary, conclusions and closing remarks are given.

Chapter 2

NONLINEAR ELEMENTS IN PI CONTROL

The linear proportional plus integral (PI) regulator is the most widely used one in control of motor drives, as well as in many other applications. Its wide acceptance can be chiefly attributed to its accuracy in steady state; namely to the property that in the equilibrium, the output is always exactly equal to the reference input, regardless of the parameter values or constant external disturbances. Other advantages of the PI control are its uncomplicated design and relatively good transient response in many applications. However, it has the serious disadvantage in that the control dynamics is quite sensitive to parameter variations and nonlinearities of the plant.

In his classical text on synthesis of feedback systems, Horowitz [40], presented many methods of designing robust control systems - or as he stated "...achieving objectives despite ignorance" - by using classical, linear control theory. As repeatedly pointed out in [40], most of these

results fail in the presence of "severe nonlinearities". One often encountered nonlinearity is saturation, and its effect on the PI control is the subject of this chapter.

2.1. PI CONTROL AND INPUT SATURATION

The basic structure of a system with PI control is shown in Fig. 2.1. Here, $G(s)$ is the plant transfer function, d is the unmeasurable disturbance, and g_p and g_i are proportional and integral gains, respectively. The transfer function of the controller from Fig. 2.1 is

$$G_c(s) \triangleq \frac{u}{e} = g_p + \frac{g_i}{s} \triangleq g_p \frac{s + z_c}{s} \quad . \qquad (2.1)$$

The PI control is usually quite sensitive to plant parameter variations, especially for higher order plants. One way to reduce the sensitivity in any feedback control system, is to increase the loop gain. However, if the plant $G(s)$ in Fig. 2.1 has two more poles than zeros, the closed loop system is very oscillatory for the large loop gains. With larger number of poles the system may become unstable. Even if instability does not occur, or if it is avoided by the use of additional compensators, the problem of reaching saturation effects becomes prominent, whenever the large controller gains are used.

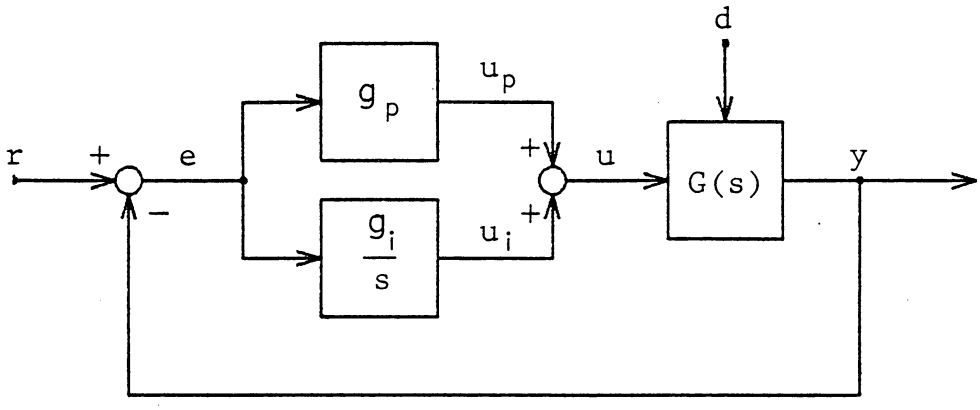

Fig. 2.1: Basic proportional plus integral (PI) control with the plant input saturation.

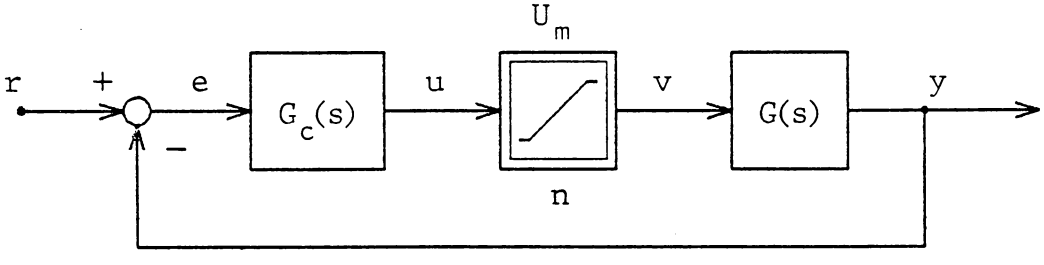

Fig. 2.2: Linear feedback system with saturation.

To investigate the effect of saturation, consider the system on Fig. 2.2. If $u(t)$ is larger than U_m, the feedback loop is practically open, although the state variable within $G_c(s)$ is changing according to $e(t)$. This will definitely deteriorate the system response, and can be the cause for instability. It is of interest to find the stability conditions in this case.

The sufficient conditions for the system in Fig. 2.2 to be globally asymptotically stable is that $G_c(s)\cdot G(s)$ has no poles with positive real part, and that the Nyquist diagram of $G_c(j\omega)\cdot G(j\omega)$ lies completely to the right of the vertical line passing through the point (-1,0). Proof of this statement is based on the circle criterion and is given in Appendix B.1. These conditions are quite conservative, i.e., there exist many systems which do not satisfy them but are still stable. A useful technique for investigating the stability of such systems is the describing function analysis. An example of its use, for the system that does not satisfy the above conditions, is given in Appendix B.2.

In motor control, saturation is always present. For voltage controlled drives, both the input voltage and the armature current (a state) are limited. In the case of current drives, the voltage limit is seldomly reached under normal operating conditions, so that the plant can be represented with the single saturation at the input, as in Appendix A.3. Using the transfer function, of the current

controlled motor with output filter, as G(s), from (A.22) we have

$$G(s) = \frac{36 \cdot 10^3}{s\,(s + 2 \cdot 10^3)} \quad . \tag{2.2}$$

If the proportional and integral gains are chosen as

$$g_p = 32 \quad , \qquad g_i = 5 \cdot 10^3 \quad , \tag{2.3}$$

the controller transfer function $G_c(s)$ is

$$G_c(s) = 32 \cdot \frac{s + 160}{s} \quad , \tag{2.4}$$

and the closed loop poles within the linear region are

$$s_1 = -250 \; , \qquad s_2 = -640 \; , \qquad s_3 = -1100 \quad . \tag{2.5}$$

If the disturbance input d (which for the motor is the load torque T_ℓ), is taken into account, the plant output is, from (A.26), given by

$$y = \frac{36 \cdot 10^3}{s \cdot (s + 2 \cdot 10^3)} \cdot (u - 50 \cdot T_\ell) \tag{2.6}$$

Due to the saturation, this system will have different transient response for different input amplitudes. In order to illustrate that effect, the system was simulated with the very small step change in the speed command r , which is

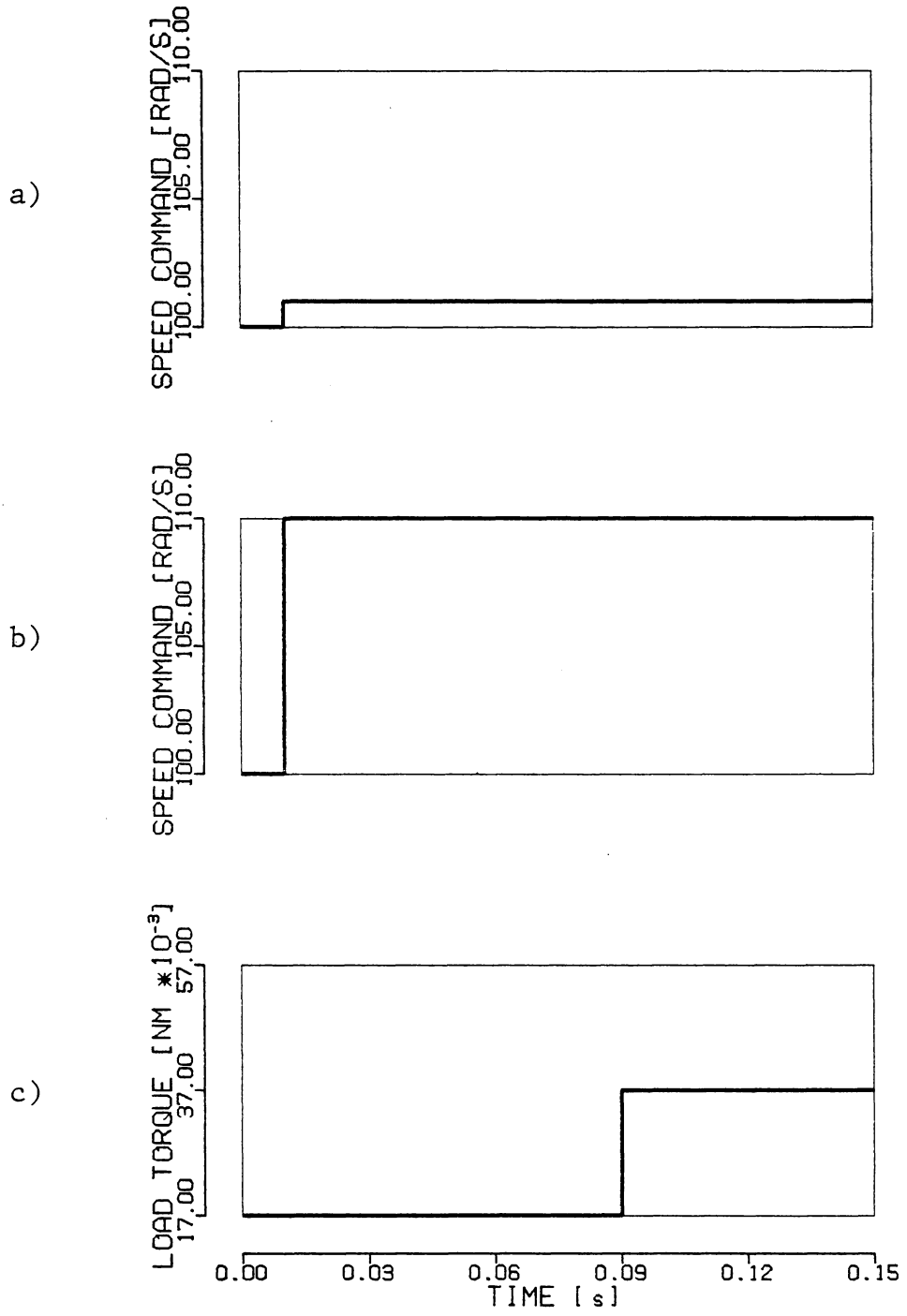

Fig. 2.3: Test inputs used in simulations and experiments.

shown in Fig. 2.3a, and with the larger step change shown in Fig. 2.3b. In both cases, the disturbance rejection of the system was tested by applying the step in the load torque shown in Fig. 2.3c.

The waveforms of speed, armature current, integral and proportional components of the control (which correspond to y, u, u_i and u_p in Fig. 2.1, respectively) for the small command step, are shown in Fig. 2.4. If the saturation were not present the same waveshapes would be obtained for any step amplitude. However, if the saturation is present, with

$$U_m = I_m = 3.6 \text{ A} \quad , \tag{2.7}$$

the response of the system to the larger command step from Fig. 2.3b, is shown in Fig. 2.5. It can be observed that the large overshoot of the output is primarily caused by the uncontrolled increase of the integral component while the system was in saturation. This phenomenon is usually called the integrator windup.

From this discussion, it follows that high gain PI control should be avoided whenever saturation is present, unless some modifications are made. The problem of the integrator windup has been studied in the literature for a long time, and many solutions have been suggested [77, 61, 50, 11, 32, 67]. Two examples of modifying the PI regulator in order to reduce the negative effects of the integrator windup, will be presented in the following sections. These results were

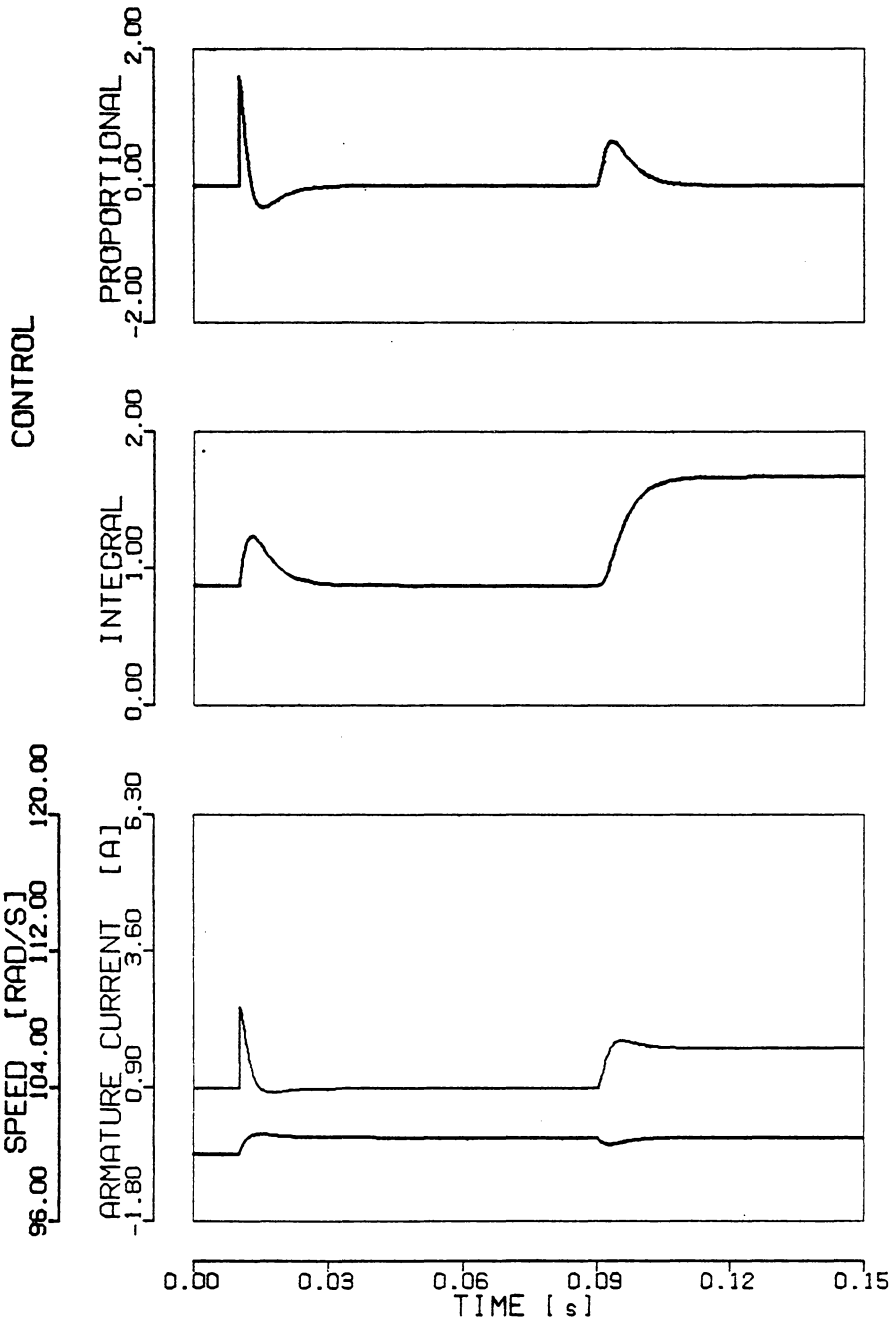

Fig. 2.4: Transient response of the motor control system with linear PI regulator, for the command from Fig. 2.3a, and the load torque change from Fig. 2.3c.

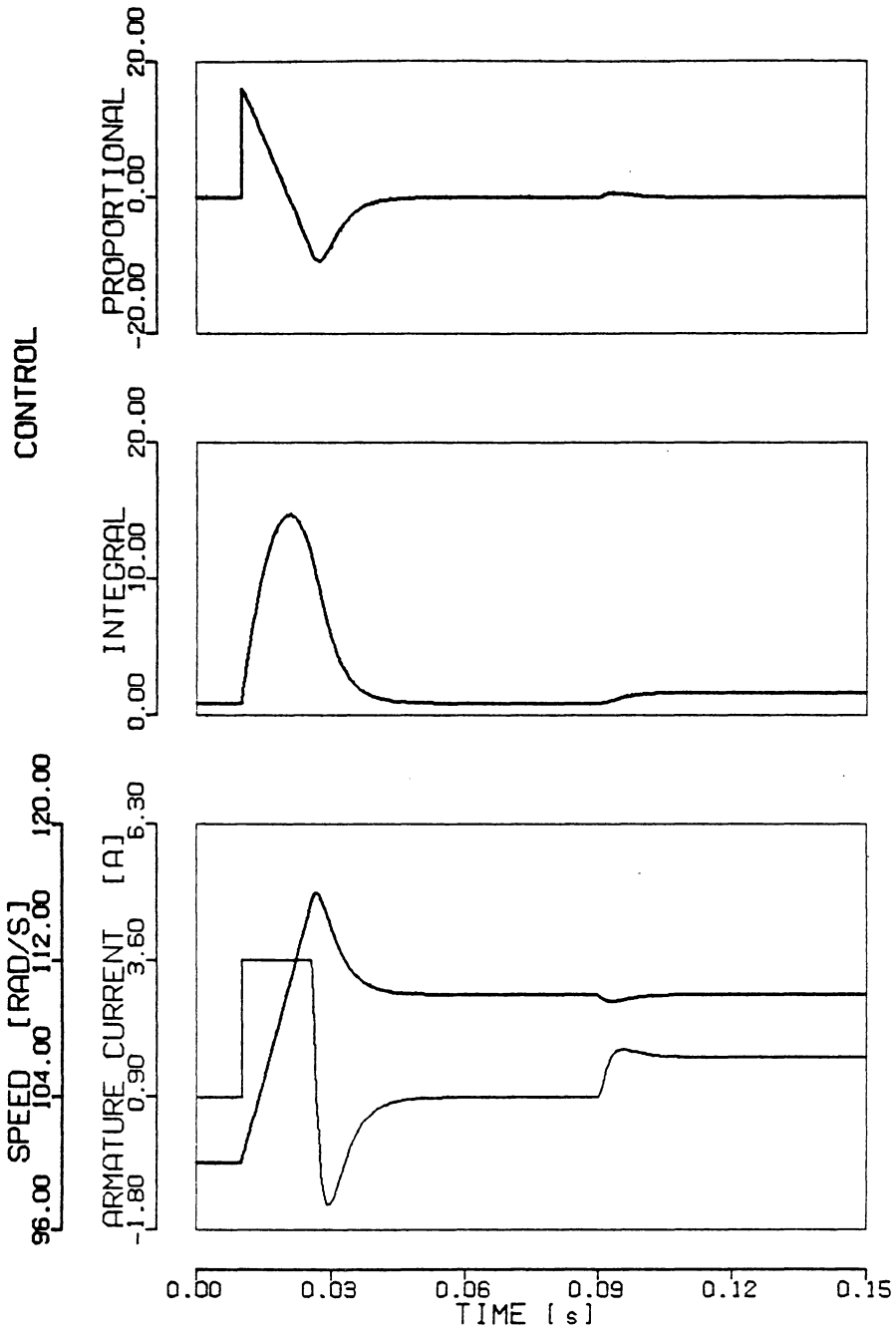

Fig. 2.5: Transient response of the motor control system with linear PI regulator, for the speed command from Fig. 2.3b, and the load torque from Fig. 2.3c.

motivated by the solutions given in the above references, but they are new in some details.

2.2. I-P CONTROL WITH FIXED INTEGRATOR LIMITS

High gain is used in the PI control, in order to increase the speed of response and robustness of the closed loop system. If only the proportional control is used, the problem of the integrator windup is avoided, but the system has steady state error.

In the "pseudo-derivative feedback", developed in [61], or in the "integral-proportional" (I-P) control, suggested by Harashima [34], the high gain proportional feedback loop is closed first, in order to achieve the desired transient response and reduction in sensitivity. This closed loop system is then considered as a new plant for which an integral regulator is designed in order to eliminate the steady state error.

The idea is illustrated in Fig. 2.6. Here, F is the output feedback gain, and the gain 1+F is used in the direct path to restore the steady state gain of the plant. The concept works if the output feedback alone can produce satisfactory transient response and robustness. The added PI (or just I) control will slow down the system somewhat, but it will assure zero steady-state error. The above condition

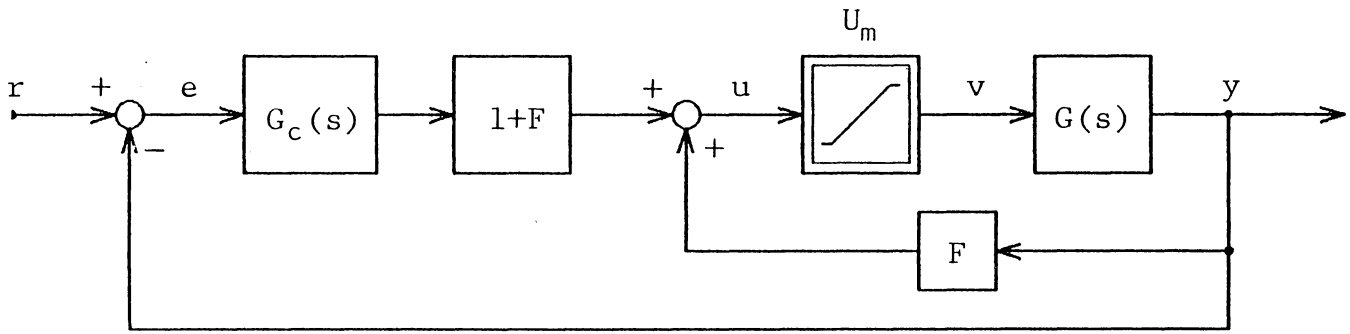

Fig. 2.6: I-P control system.

is generally not valid if the plant is not dominantly single-pole, or dominantly double-pole, with both poles real. However, the desired transient response may still require an integral gain large enough for saturation to be reached.

Since large overshoots are caused by an uncontrolled increase of the integrator output during saturation, the idea of limiting that output may be considered, [77]. One way of implementing such limits, motivated by [77] and [2], is shown in Fig. 2.7.

The nonlinear feedback over the integrator was originally suggested by West and Somerville [77]. Its purpose is to limit the output of the integrator in such a way that the plant would not be driven into saturation if u_p were zero. To explain this, consider the differential equation governing the integrator:

$$\dot{u}_i = g_i \cdot e_v - g_i \cdot \mu(u_i, U_m) \quad , \tag{2.8}$$

where $\mu(\bullet,\bullet)$ is given by

$$\mu(x,X) = \begin{cases} 0 & , \quad |x| < X \\ \mu_0 \cdot [x - X \cdot \mathrm{sign}(x)] & , \quad |x| \geq X \end{cases} \quad , \tag{2.9}$$

and is shown on Fig. 2.8. If $|u_i| < U_m$, integrator output is within the limits, and normal integral action takes place. When the limit is exceeded, (2.8) becomes

$$\dot{u}_i = g_i \cdot e_v - g_i \cdot \mu_0 \cdot [u_i - U_m \cdot \mathrm{sign}(u_i)] \quad . \tag{2.10}$$

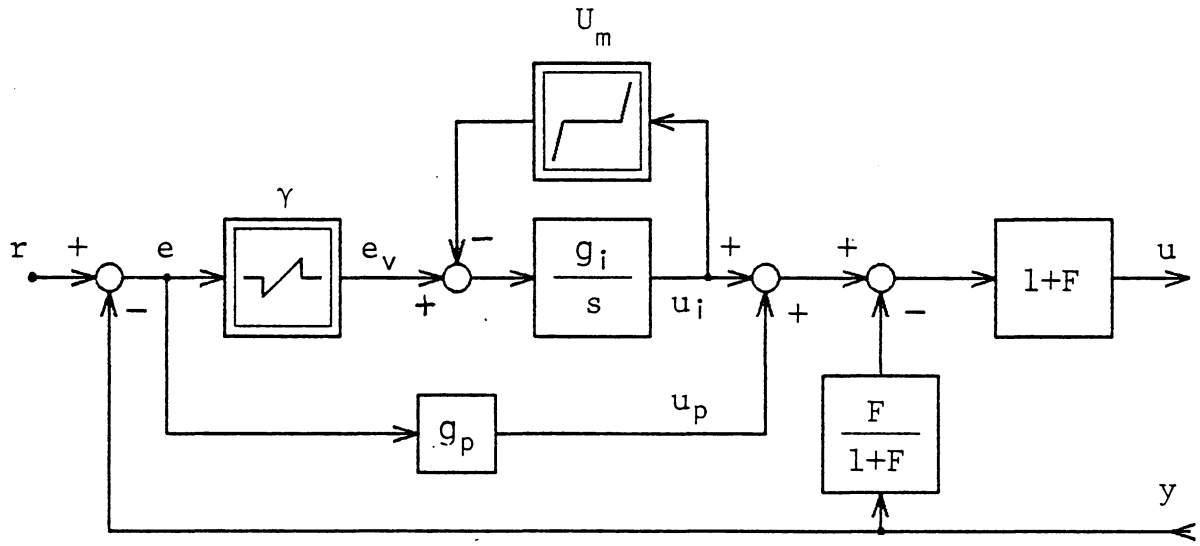

Fig. 2.7: I-P control with fixed integrator limits.

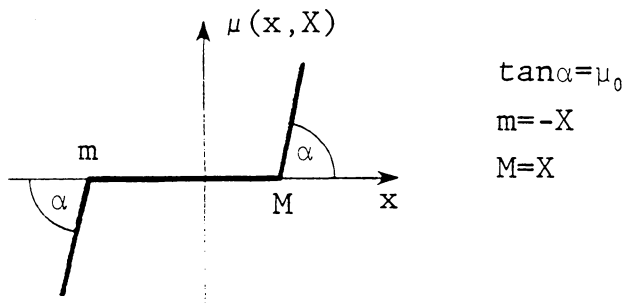

Fig. 2.8: Limiting function for the integral component of PI control.

If μ_0 is very large (ideally $\mu_0 \to \infty$), the equation (2.10) is singularly perturbed, and after a very short transient the equilibrium point that is reached, is

$$u_i = U_m \cdot \text{sign}(u_i) \quad . \tag{2.11}$$

Even with this control, during the initial part of a transient, the plant input may be driven into saturation by the proportional component alone. Thus, the change in u_i is still uncontrollable, in the sense that its effect does not influence the plant. Actually, limiting with (2.9), gives only an upper bound on the possible overshoots under varying operating conditions, [67].

A further improvement can be expected if an additional, "limited field of view", nonlinearity is placed in front of the integrator, as shown in Fig. 2.7. Its effect is to zero the input to the integral part of the controller at the beginning of the transient, when the error e is large. In that way the integral action will be present only for small errors, when the proportional part $g_p \cdot e$ is small so that the saturation is not reached. The cut-in value of the error, γ, must be sufficiently large, to allow the proportional feedback to bring the error within the "field of view", for the worst case of plant parameter variations and external disturbances. However, if these variations are to large, the effect of the limited field of view, will be considerably diminished.

The control in Fig. 2.7 was implemented for the speed control of a voltage driven dc motor. The motor model is described in Appendix A.2. In the linear region, the motor with the input amplifier and output filter can be represented by the transfer function (A.12):

$$G(s) = \frac{K_v}{(s \cdot T_m + 1) \cdot (s \cdot T_e + 1) \cdot (s \cdot T_f + 1)} \quad . \qquad (2.12)$$

The parameter values are given by (A.4), (A.11) and (A.13). If the desired closed loop dominant time constant is T_c = 30 ms, then the output feedback should move the motor dominant pole beyond $-1/T_c$. With the choice of the output feedback constant as

$$F = 20 \quad , \qquad (2.13)$$

the closed loop poles are

$$s_1 = -140 \ , \qquad s_2 = -1800 \ , \qquad s_3 = -3\ 10^4 \quad . \qquad (2.14)$$

The PI control can then be designed, around the above loop, and with

$$G_c(s) = 6 \cdot \frac{s + 33}{s} \qquad (2.15)$$

the final closed loop poles are

$$s_1 = -\ 30 \ , \qquad s_{2,3} = -\ 1000 \pm j\ 870 \quad . \qquad (2.16)$$

Assuming that in the worst case an input of $u = U_m$ will be able to overcome the influence of all disturbances, the "field of view" is determined as

$$\gamma = \frac{U_m}{g_p} = \frac{V_m}{g_p} = 2 \quad , \tag{2.17}$$

where $V_m = 12$ from (A.6).

This system was simulated, and its step response is shown in Fig. 2.9. The result shows a small overshoot and a very fast transient response.

The system was experimentally tested with the same structure and parameter values. An analog controller, using operational amplifiers, was built. For the implementation of the "limited field of view" nonlinear characteristic a waveform shaping network, consisting of operational amplifiers and diodes was used. The circuit schematic of the controller is shown in Appendix F.4. The experimentally measured waveforms are given in Fig. 2.10, and although the result is generally satisfactory, it is somewhat oscillatory.

The problem with this kind of control is the exceptional severity of the "limited field of view" nonlinearity. Atherton [2, pp. 190-193] has shown that this nonlinearity can cause oscillatory behavior and even "jump phenomena". This behavior was not observed in the simulations, but it did appear in experiments as can be clearly seen in Fig. 2.10. The oscillatory behavior was even more pronounced when the

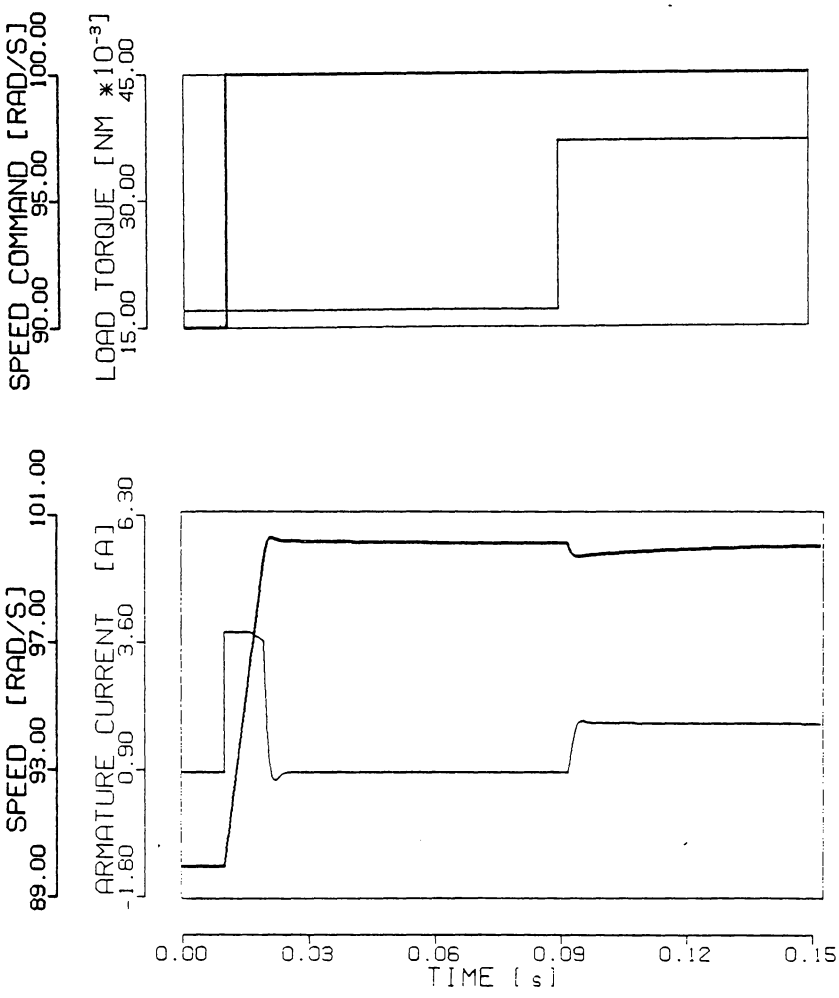

Fig. 2.9: Simulated transient response of the I-P control system with fixed integrator limits.

a) Test inputs.

b) Speed and current response.

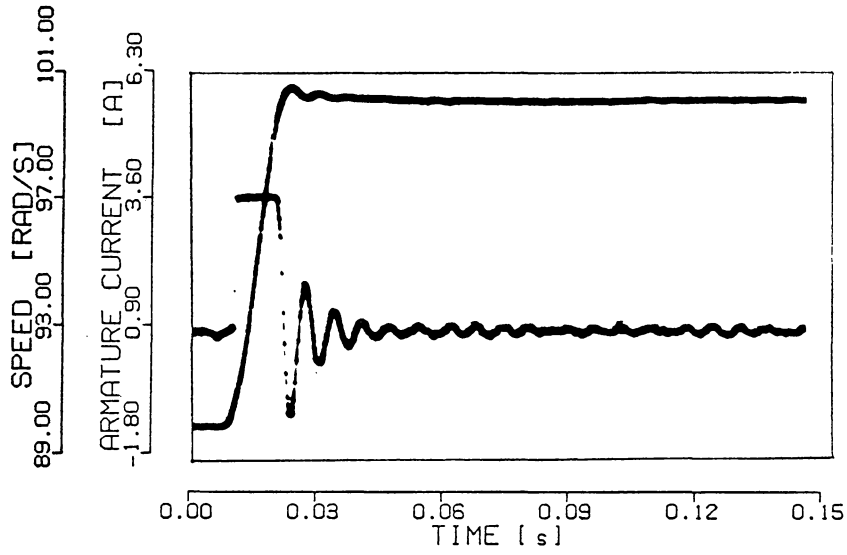

Fig. 2.10: Experimental transient response of the I-P control system with fixed integrator limits for the speed command from Fig. 2.9a, and $T_\ell = 0.017$ N m .

gain K_v was increased, as is shown in Chapter 6, together with the other robustness related experimental and simulation results.

2.3. VARIABLE LIMIT PI (VLPI) CONTROL

From the discussions in the preceding sections, a more general idea is emerging: If some nonlinear elements are present in the plant, for optimum performance these nonlinearities have to be accounted for, by appropriate nonlinear effects in the controller. The question of which nonlinear effect is appropriate, has to be answered for each class of plants, as is usually the case with nonlinear control. In the PI control of a plant with an input saturation, the clue is to limit the controller variables in such a way, that the input limit is never exceeded. Then all changes of the controller output have effect on the plant, and therefore a closed-loop feedback exists at all times. One way of achieving this is presented in this section.

Consider the system in Fig. 2.11. In the proportional branch of the controller, a fixed, saturation type, nonlinearity is added, so that u_p never exceeds $\pm U_m$. The integral component has a variable feedback limiter, the output of which is given by

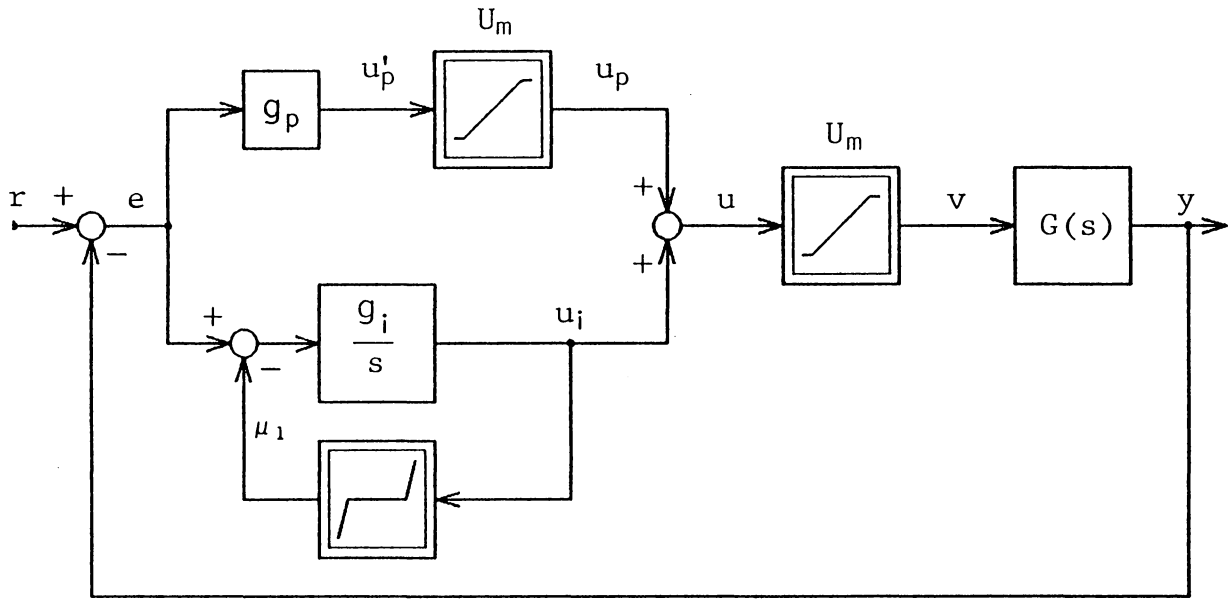

Fig. 2.11: Variable limit PI (VLPI) control.

$$\mu_1(u_i,u_p,U_m) = \begin{cases} 0 \quad , \text{ for } \quad -U_m - u_p < u_i < U_m - u_p \\ \\ \mu_0 \cdot \{u_i - [U_m \text{sign}(u_i) - u_p]\} \quad , \text{ elsewhere.} \end{cases} \qquad (2.18)$$

$$|u_p| \leq U_m$$

This nonlinearity has the same form as the one shown in Fig. 2.8 with $x = u_i$, and variable limits

$$\begin{aligned} m &= -U_m - u_p \\ M &= U_m - u_p \quad . \end{aligned} \qquad (2.19)$$

Operation of this limiter is also similar to the one described in the previous section. During the interval when $|u_i+u_p| < U_m$, the system operates as linear PI. When the limit is even slightly exceeded, u_i is governed by

$$\dot{u}_i = g_i\{e - \mu_0 \cdot [u_i - U_m \cdot \text{sign}(u_i) + u_p]\} \qquad (2.20)$$

Since μ_0 is large, after a very short time we have

$$u = u_i + u_p \simeq U_m \cdot \text{sign}(u_i) \quad . \qquad (2.21)$$

Therefore, the input limit is never exceeded considerably, and the sign of u_i is preserved. Obviously, for $u_p = U_m$, the integral component is u_i is equal to zero.

This control algorithm was implemented for the speed control of a current driven dc motor. Except for the added nonlinearities, the system is exactly the same as the one simulated in Section 2.1. For the very small step-input from

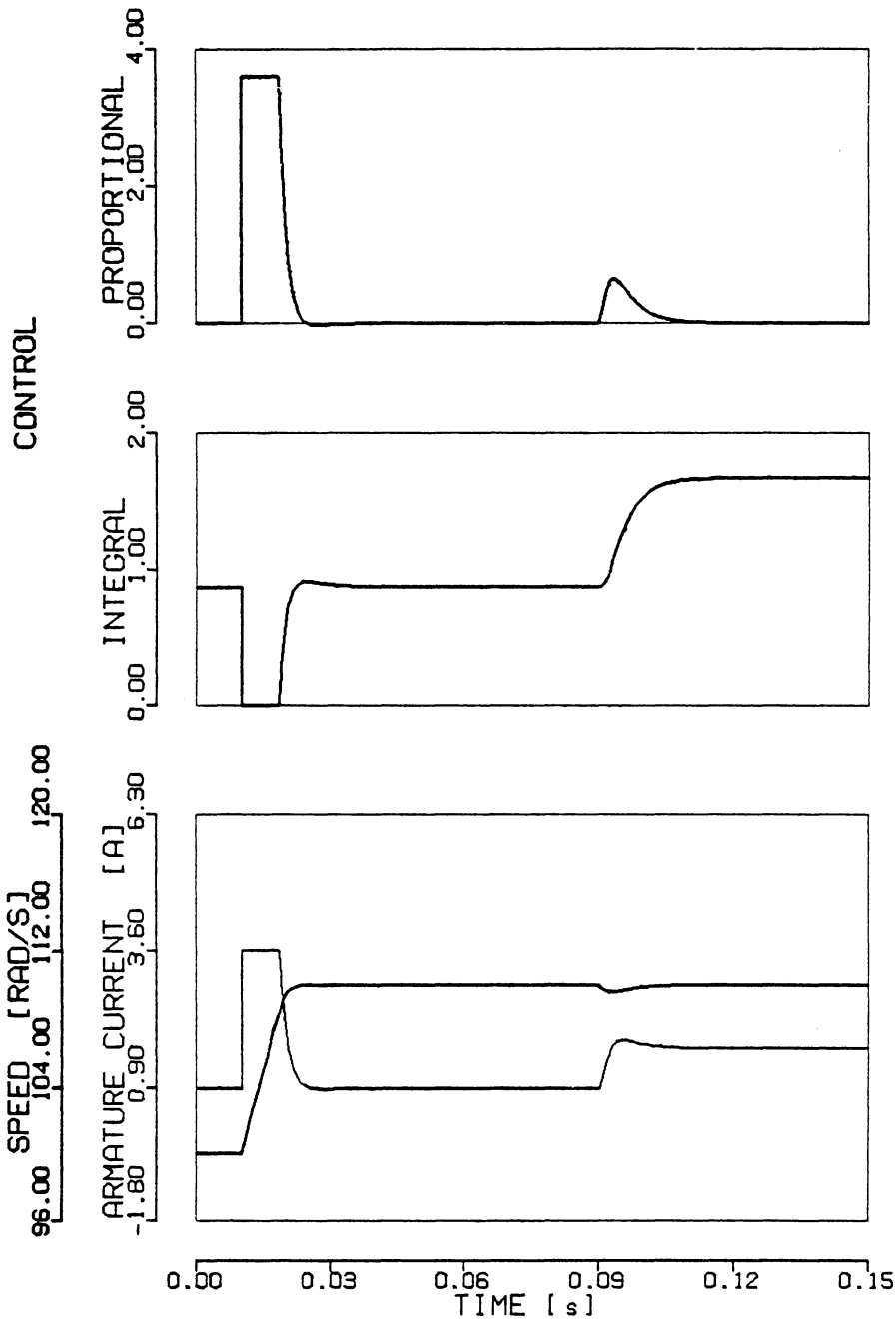

Fig. 2.12: Transient response of the VLPI control system for the inputs from Figures 2.3b and 2.3c.

Fig. 2.3a, the response is exactly the same as in Fig. 2.4. For the larger step-input from the Fig. 2.3b, the response is shown in Fig. 2.12. An improvement of the transient response is clearly seen when compared with Fig. 2.5. It is important to note that the overshoot in Fig. 2.5 varies with the input-step amplitude, whereas the response in Fig. 2.12 is the same for all amplitudes for which saturation is reached.

The improvement achieved in this particular case is apparent. However, we were unable to generalize this approach, although intuitively at least some level of generalization should be possible. A short discussion of the stability concerns is given in Appendix B.3.

The VLPI control is quite similar to the methods of avoiding the integrator windup by using the fixed feedback limiting of the integrator, [77, 50]. However, because the integrator limiting function μ_1 is varying, the plant input saturation is never exceeded in the VLPI control, which is not the case with the fixed limiting. In this way, the overshoot is completely avoided if the linear controller has real poles. The idea presented here was derived from the work of Franke [28], where the same kind of limiter was used, however, in a particular nonlinear controller, which is described in Chapter 4.

* * *

The influence of the plant-input saturation on the performance of the systems with PI control has been discussed and illustrated in this chapter. Several ways of dealing with the problem are also presented. Although none of these methods infer an increased robustness explicitly, they nonetheless imply it, by allowing the use of higher gains without detrimental effect on transient performance and stability.

A completely different and totally nonlinear approach to the problem of system robustness is presented in the next chapter.

Chapter 3

SLIDING MODE CONTROL

Sliding mode control is a control algorithm which intentionally introduces discontinuous (i.e., switching) action in the feedback, in order to increase the robustness of the closed loop system. In the ideal case the system response is insensitive to plant parameter variations and external disturbances. In fact this is the only control algorithm which can guarantee (at least theoretically) total system invariance for a wide class of plants and disturbances [17]. Due to this unique property it has attracted a great deal of interest in recent years.

There are already many papers presenting applications of the sliding mode (SLM) control to dc drives [14, 15, 73, 46, 35, 47, 24] and in several cases to ac drives [63, 64, 4, 58, 9]. However, there are hardly any commercial drive systems that use SLM control. This discrepancy can be partially attributed to the novelty of the method, but it also

indicates the presence of practical difficulties in implementing the SLM control.

This chapter presents some of the problems in using SLM control for speed control of dc motors, and ways to solve them. The same problems were treated in detail by Balestrino et al. in [3], where they used SLM in the model reference adaptive control. The major reason for including the treatment of SLM control in this work, is to provide a common reference against which the robustness of other control algorithms can be evaluated.

3.1. STRUCTURE AND OPERATION OF THE CONTROLLER

There exists already a vast amount of references on analyses and design of systems with sliding modes, most of it is in the Soviet literature. However, much is available in English, either as translations, or original works [69, 42, 70, 18, 79, 71, 78]. Only a special case of designing SLM control for a linear, second order, single input single output (SISO) plant, will be described here.

Consider a plant in phase canonical form:

$$\begin{bmatrix} \dot{x}_1 \\ \dot{x}_2 \end{bmatrix} = \begin{bmatrix} 0 & 1 \\ -a_1 & -a_2 \end{bmatrix} \cdot \begin{bmatrix} x_1 \\ x_2 \end{bmatrix} + \begin{bmatrix} 0 \\ b \end{bmatrix} \cdot v + \begin{bmatrix} 0 \\ -h \end{bmatrix} \cdot d \qquad (3.1)$$

$$v = \begin{cases} U_u , & u > U_u \\ u , & U_\ell \le u \le U_u \\ U_\ell , & u < U_\ell \end{cases} \qquad (3.2)$$

where d is a constant but unknown disturbance. Suppose that it is desirable to drive the state x_1 to the origin from some initial condition x_{10} , with a transient that is characterized by a single time constant T_c, i.e.,

$$x_1 = x_{10} \cdot \exp(-\frac{t}{T_c}) \quad . \qquad (3.3)$$

Since $\dot{x}_1 = x_2$ the above condition is satisfied whenever

$$\sigma = \sigma(x_1, x_2) = 0 \quad , \qquad (3.4)$$

where

$$\sigma = \frac{1}{T_c} \cdot x_1 + x_2 \quad . \qquad (3.5)$$

If the plant parameters and the disturbance d were precisely known, the design objective (3.3) could be achieved with a simple state feedback. However, in a practical situation, a different kind of control is necessary.

In SLM control, the idea is to keep the equation (3.4), at least approximately satisfied, by using a special switching-type control. The control that achieves this for the plant (3.1), (3.2) is given by, [42, 46],

$$u = - \psi_1 \cdot x_1 - \psi_2 \cdot x_2 - \delta \cdot \mathrm{sign}(\sigma) \tag{3.6}$$

$$\psi_1 = \begin{cases} \alpha_1 , & x_1 \cdot \sigma > 0 \\ \beta_1 , & x_1 \cdot \sigma < 0 \end{cases} \tag{3.7}$$

$$\psi_2 = \begin{cases} \alpha_2 , & x_2 \cdot \sigma > 0 \\ \beta_2 , & x_2 \cdot \sigma < 0 \end{cases} \tag{3.8}$$

The operation of the controller is illustrated in Fig. 3.1, where a trajectory of the system is shown in the phase plane. Equation (3.4), representing a straight line in that plane is called sliding line. If the system was originally at point A, the control (3.6) will be

$$u = - \alpha_1 \cdot x_1 - \beta_2 \cdot x_2 + \delta \quad , \tag{3.9}$$

because $x_1 < 0$, $x_2 > 0$ and $\sigma < 0$. The coefficients in (3.9) have to be such as to move the system towards the sliding line, preferably as fast as possible. This corresponds to the segment A-C in the figure, where the part B-C shows the system in saturation. After crossing the sliding line at point C, σ changes sign while x_1 and x_2 do not, so that the control is

$$u = - \beta_1 \cdot x_1 - \alpha_2 \cdot x_2 - \delta \quad . \tag{3.10}$$

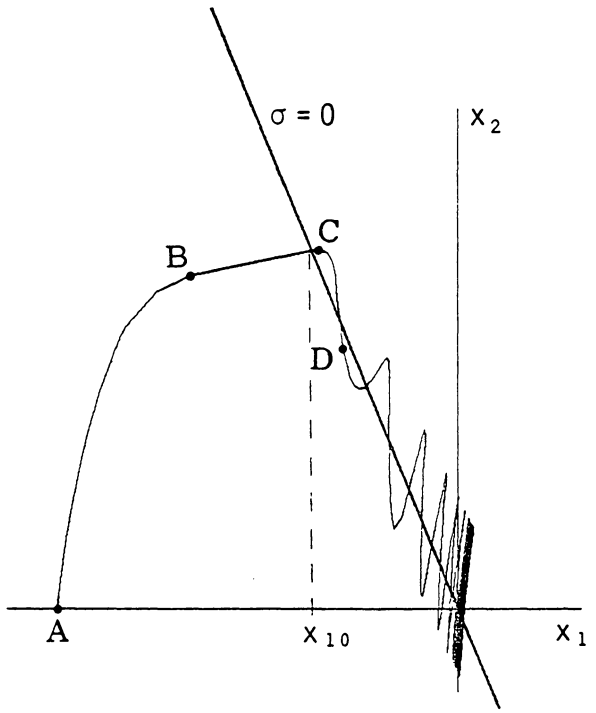

Fig. 3.1: Sliding mode trajectory.

The coefficients in (3.10) now have to be such that the system is forced back across the sliding line. This corresponds to the segment C-D. At D, another change of the sign of σ is detected, so the control given in (3.9) is applied again. The above described process repeats, which results in a chattering motion along the sliding line to the origin. If it is possible to detect the sign-changes, and switch the control as soon as they are occur, the chattering will be negligible, and the motion of the system (3.1), after leaving the saturation, will be described by (3.3).

The values of coefficients in (3.6), that will guarantee this behavior, can be found from the sufficient condition for existence and reachability of the sliding mode [71], which is

$$\sigma \cdot \dot{\sigma} < 0 \quad , \quad \forall x \quad \text{except when} \quad \sigma = 0 \quad . \tag{3.11}$$

For our system, this conditions are satisfied if the following relations hold.

$$a_1 > 0 \quad , \quad a_2 > 0 \tag{3.12}$$

$$U_u \cdot U_\ell < 0 \tag{3.13}$$

$$\alpha_1 \geq -\frac{a_1}{b} \geq \beta_1 \tag{3.14}$$

$$\alpha_2 \geq \frac{1 - a_2 \cdot T_c}{b \cdot T_c} \geq \beta_2 \qquad (3.15)$$

$$\delta > \frac{h}{b} \cdot \max(|d|) \qquad (3.16)$$

The conditions (3.12) and (3.13) are necessary due to the presence of the saturation at the input of the plant. The first one requires that the open loop plant is stable, so that starting with any initial conditions the system will come within the input limits. The second one ensures that the origin (equilibrium state) is within the limits.

The conditions (3.14)-(3.16) assure the reachability and existence of sliding mode, within the limits. They are easily obtained from (3.11) by performing the differentiation and then substituting (3.1) and (3.6) into it. The following expression is obtained

$$\begin{aligned} \sigma \cdot \dot{\sigma} = & -(a_1 + b \cdot \psi_1) \cdot x_1 \cdot \sigma - \\ & - (a_2 - \frac{1}{T_c} + b \cdot \psi_2) \cdot x_2 \cdot \sigma - \\ & - b \cdot \delta \cdot \sigma \cdot \mathrm{sign}(\sigma) - \sigma \cdot h \cdot d \quad , \end{aligned} \qquad (3.17)$$

and then by using (3.7) and (3.8), the conditions follow directly. Stability of the system, when operating in the sliding mode, is automatically assured by T_c being positive.

The remarkable result is that the relations (3.14)-(3.16) are single sided, i.e., given any plant parameters and disturbances, an appropriate set of control parameters can be found, such that these relations hold. Even more, if the parameters and the disturbances are varying but bounded, choosing the controller parameters in such a way that (3.14)-(3.16) are always satisfied, will guarantee complete invariance, i.e., the system response will still be governed by (3.3), as desired. Also, from (3.14)-(3.16) there is no theoretical limit on T_c. However, for $T_c \to 0$, from (3.15) it follows that $\alpha_2 \to \infty$, so some practical limit must be imposed.

In many cases, much simpler control can be used to obtain the sliding mode. If the plant is open-loop stable, as required by (3.12), then a bounded input produces bounded output. So, there are bounds on x_1 and x_2 that correspond to the bounds on the input v. From (3.17) it is then obvious that there exists some δ, such that (3.11) is satisfied even for $\psi_1=\psi_2=0$. In that case, the resulting control

$$u = - \delta \cdot \mathrm{sign}(\sigma) \ , \qquad \delta = \max(|U_u|, |U_\ell|) \ , \qquad (3.18)$$

is extremely simple. However, in practical implementations, such control very often results in excessive chattering.

In practice, a successful implementation depends on the ability to switch the input fast at the right instants. Fast

switching is usually not a problem with the modern power electronic devices. But, accurate observation of the system states is by no means trivial. Some states may not be measurable, so some kind of state estimation must be used. Also, noise is always present and filtering has to be employed, which causes delays. In digital implementation there is also computational delay. Combined effect of all or some of these factors makes the estimation of the right instants of switching very difficult in most cases. This results in the chattering along the sliding line, instead of ideal "sliding". These oscillations may cause excessive power dissipation, strain on system components, and they can excite higher order resonances that may be present in the system. Some of these problems are illustrated in the next section.

3.2. IMPLEMENTATION OF SLM CONTROL FOR SPEED REGULATION

A sliding mode control algorithm described in the previous section was implemented for dc motor speed regulation. A voltage controlled motor was used. Its model and block diagram are given in Appendix A.2. The appropriate phase cannonical form, with speed and speed derivative as state variables, is given in Appendix A.4. Speed measurement y, is obtained through the output filter with the time constant T_f, Fig. 3.2. The desired time constant of the closed loop

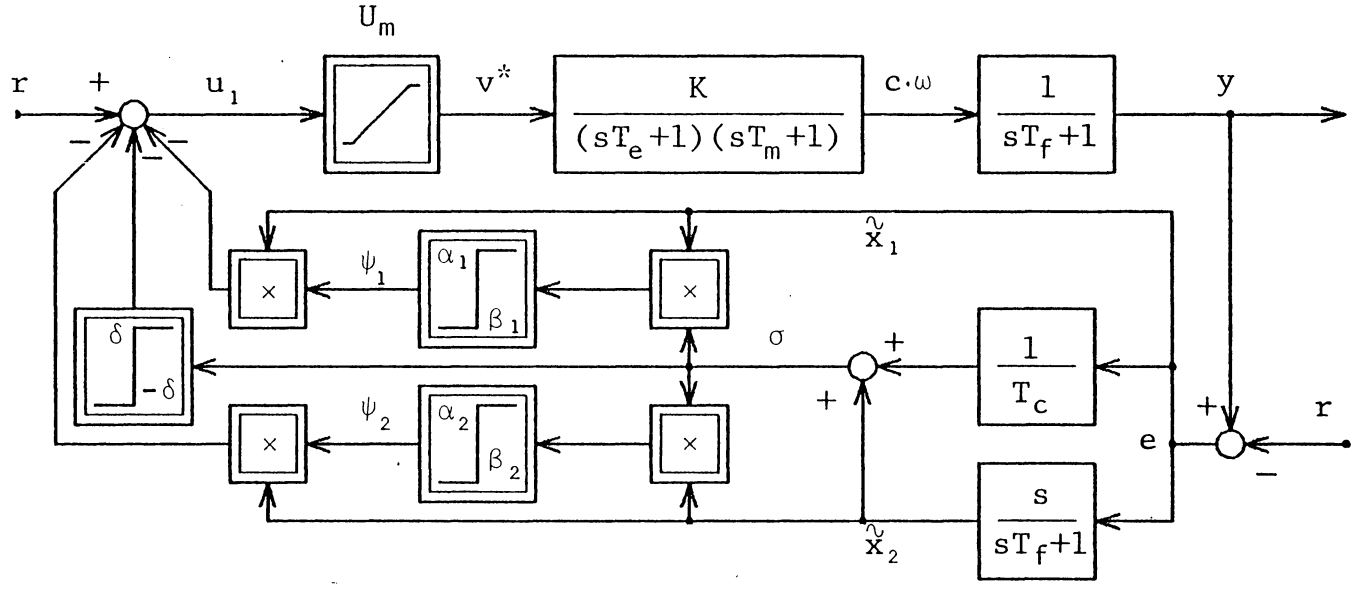

Fig. 3.2: Sliding mode (SLM) control of the voltage driven motor.

system was chosen to be 100 times smaller than the motor mechanical time constant T_m,

$$T_c = 3 \text{ ms} \quad . \tag{3.19}$$

Using the parameter values from (A.13), (A.35) and (3.19), the conditions (3.14)-(3.16) were evaluated and the system was simulated. The motor response to step changes in command and torque is shown in Fig. 3.3a. Very fast transient response and excellent disturbance rejection are exemplified.

These results are just theoretical. For the control that will ensure the existence of the sliding mode along the sliding line, the knowledge of both states x_1 and x_2 is necessary. However, only the speed measurement y is known. Since the system is observable, an observer can be used. If the classical Luenberger observer [55] is used, the robustness of the SLM control is lost, since the observer does not provide an accurate estimate if the plant parameters, and all inputs (including T_ℓ) are not known. A common way out is to neglect the output filter dynamics and assume that

$$x_1 \approx \tilde{x}_1 \triangleq y - r \triangleq e \quad . \tag{3.20}$$

Although (3.20) can be satisfied with small error, the estimation of x_2 based on (3.20) can be very erroneous. This is

a)

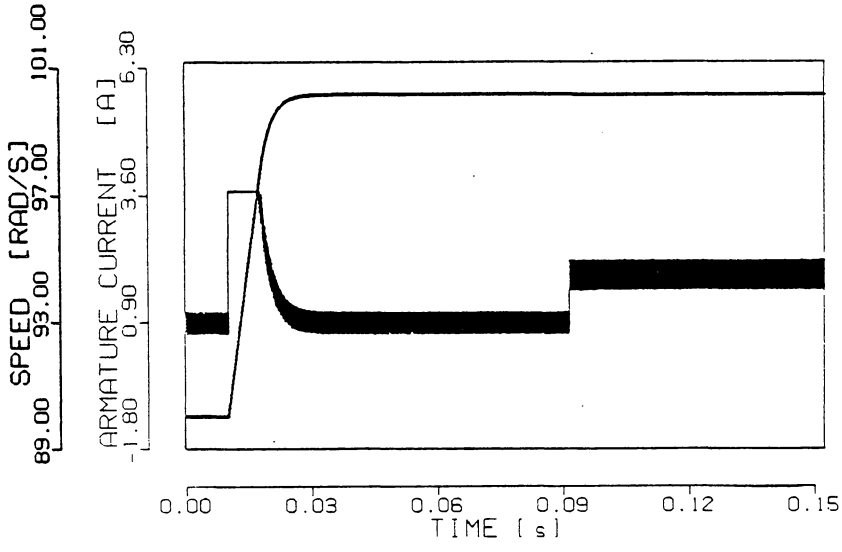

b)

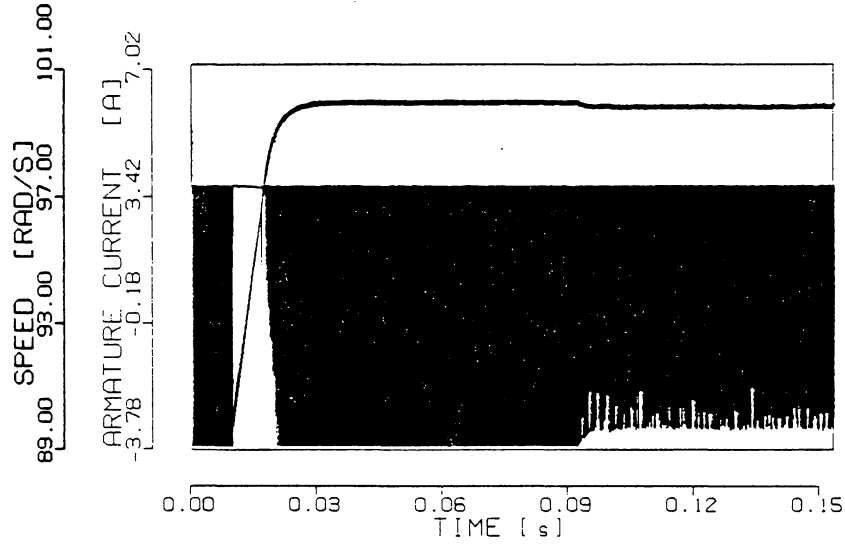

Fig. 3.3: Transient response of the SLM control system for the inputs from Fig. 2.9a.

a) Motor speed and its derivative are known exactly.

b) Motor speed and its derivative are estimated from the filter output.

due to the fact that the dynamics of the armature current and therefore of the $x_2 = \dot{x}_1$, is much faster than the output filter dynamics ($T_e << T_f$). To illustrate this effect the SLM control system was simulated with the same parameters as for Fig. 3.3a, but instead of the original states, $\tilde{x}_1$ from (3.20) and $\tilde{x}_2 = \dot{\tilde{x}}_1$ was used. The result is shown in Fig. 3.3b. The armature current oscillations are now limited only by the current limit. Although the speed response may still be acceptable, the increased power dissipation is intolerable.

In order to reduce the current oscillations, a choke may be added in the armature circuit if a voltage control is used. For the current controlled drive, an integrator may be added in front of the current controller, as was done in [15]. In both cases the armature current dynamics is slowed down enough, so that the estimation of x_2 based on the approximation (3.20) is possible. In the current controlled case, it was also possible to build an unbiased, robust observer. However, such an approach can be used only if a slow transient response of the closed loop system is desired. In our case, the objective is to achieve a transient response, and instead of an observer, the nonideal differentiator is used:

$$\tilde{x}_2 = \frac{s}{T_f \cdot s + 1} \tilde{x}_1 \quad . \tag{3.21}$$

This implies that for the approximation $\tilde{x}_2 \simeq x_2$ to hold, at least the following has to be satisfied:

$$T_c > T_e > T_f \quad . \tag{3.22}$$

Since we are using the voltage control, a choke was added, so that the armature circuit inductance is increased to

$$L = 5 \text{ mH} \quad , \tag{3.23}$$

which resulted in

$$T_e \simeq 2.17 \text{ ms} \tag{3.24}$$

so that, with $T_c = 3$ ms and $T_f = 0.5$ ms, (3.23) is barely satisfied. With these values, the new set of the system parameters is given by (A.38). Then the conditions (3.14)-(3.16) are evaluated again and the following values are chosen:

$$\begin{aligned} \alpha_1 &= 0 \quad , \quad \beta_1 = -1.5 \\ \alpha_2 &= 0.1 \quad , \quad \beta_2 = -0.2 \\ \delta &= 5 \quad . \end{aligned} \tag{3.25}$$

With the new parameter values from (3.24) and (3.25) the system was simulated again, and the result is shown in Fig. 3.4a. The resulted chattering is considerably reduced.

An experimental sliding mode controller was designed, based on the diagram in Fig. 3.2. A nonideal differentiator (3.21) and the control components $\beta_1 e$, $\alpha_2 e$, and $\beta_2 e$ were implemented by using analog amplifiers. Detection of sign changes necessary for synthesizing the control (3.6)-(3.8) was done using the fast comparators and logic circuitry. The circuit diagram is shown in Appendix F.5. The controller and motor parameters are the same as those used in the simulation, equation (3.25). Experimentally measured waveforms are shown in Fig. 3.4b, and good agreement with the simulation can be observed.

Further simulation and experimental results are presented in Chapter 6, where they are compared with other types of control, for different plant parameters.

* * *

The basic principles used in designing a sliding mode control for dc motor speed regulation were presented in this chapter. A major obstacle in implementing SLM control is the problem of accurate estimation of instantaneous values of state variables. One way to resolve the difficulty in the specific case, was presented and the validity of the approach

a)

b)

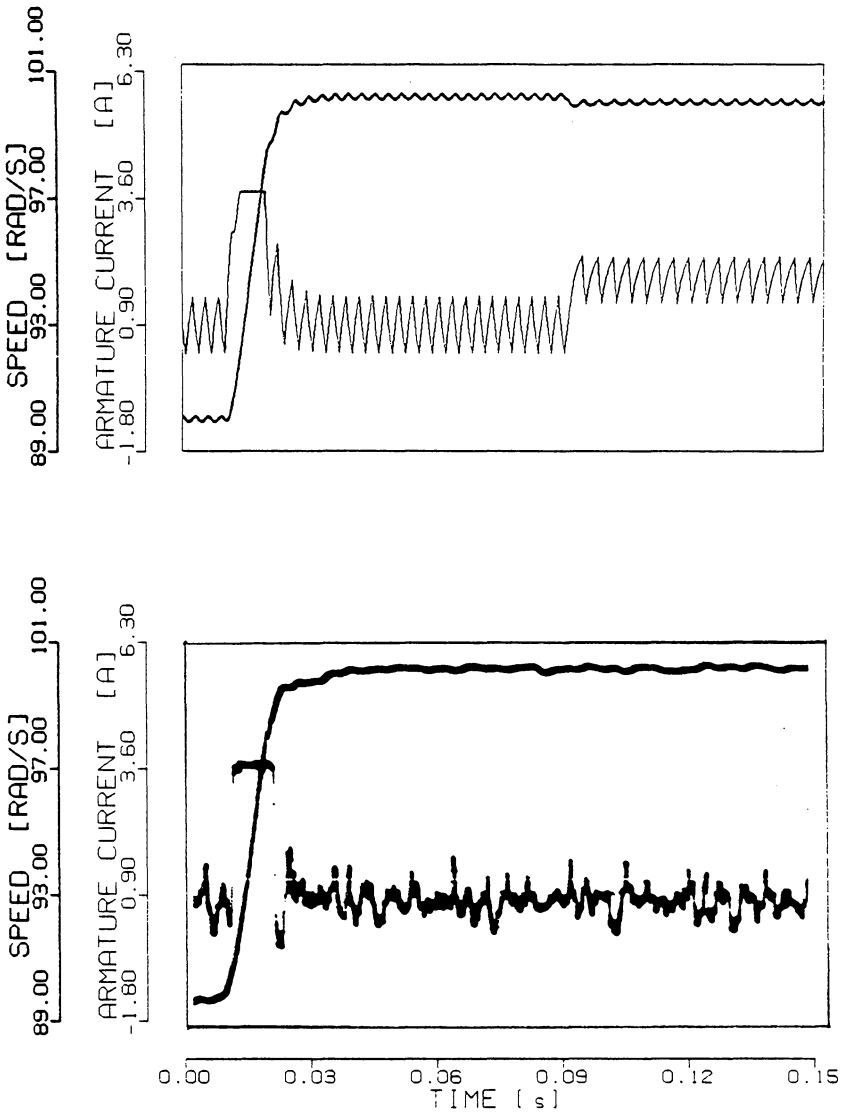

Fig. 3.4: Transient response of the SLM control system when the choke is added in the armature circuit.

a) Simulation with the inputs from Fig. 2.9a.

b) Experiment with the step speed command from Fig. 2.9a, and T_ℓ = 0.017 N·m .

was testified by simulation and experimental results. However, the problem of chattering remains as the major drawback. Methods of retaining the robustness of SLM control and eliminating the undesired chattering, are still the object of current research, [65, 24, 58]. In the next two chapters some new results in the same direction are presented.

Chapter 4

SOFT VARIABLE STRUCTURE CONTROL

In the control of electrical drives a simple output feedback usually provides satisfactory transient response. The PI control assures that the equilibrium error is always zero, but it is sensitive to plant parameter variations. On the other hand, the SLM control described in the previous chapter, provides excellent robustness. A method of directly combining last two algorithms in such a way that their good properties are retained, and that their drawbacks are eliminated, does not exist. Therefore, some kind of compromise has to be searched for.

Recently, two significant theoretical results have been reported, which combine some kind of integral control with very high gain feedback control, in such a way that sliding motion is avoided. One method is due to the German researcher Franke [28, 27, 29], and the method is named the soft variable structure (SVS) control. Another one was in-

dependently developed by Soviet scientists Emelyanov[1] and Korovin [20, 19, 22, 23, 21], and it is called the integral coordinate-parametric feedback. The two concepts are characteristically similar, although SVS just permits the use of an infinite gain, whereas the integral coordinate-parametric feedback uses the infinite gain explicitly through the "sign" function. Also, Franke's formulation is much less structured.

The present research was concentrated on the SVS control and its application to the electrical drives. In this chapter the concept of SVS is introduced first; then the structure of the modified controller suitable for speed control of electrical drives, is formulated. Finally, implementation results are presented.

4.1. CONCEPT OF SVS CONTROL

Soft variable structure control evolved from the study of bilinear systems [26], and the control algorithm is derived by Liapunov's direct method [45]. The results were originally obtained for multivariable, as well as distributed

---

[1] It is interesting to note that Emelyanov headed the research group which developed in 1960s the first systematic theory of sliding modes.

parameter, linear systems [28, 27]. However, for our purposes, only a single-input, single-output (SISO) case is of interest, and it will be presented here in a somewhat simplified form.

Consider a SISO plant described by the following equations:

$$\begin{aligned} \dot{x} &= A \cdot x + b \cdot v \quad , \qquad x \in R^n \\ y &= c'x \qquad\quad , \qquad u,v,y \in R \end{aligned} \tag{4.1}$$

$$v = \begin{cases} u & , \quad |u| \leq U_m \\ U_m \cdot \text{sign } u & , \quad |u| > U_m \end{cases} \tag{4.2}$$

It is assumed that the plant is stable and that it has unity steady state gain, i.e.

$$c' \cdot A^{-1} \cdot b = -1 \quad . \tag{4.3}$$

Assumption (4.3) is for notational reasons, and does not influence the generality. Under these assumptions a soft variable structure controller is given by:

$$u = r + p \cdot y \tag{4.4}$$

$$\dot{p} = - q \cdot [(x - x_s)' \cdot Q_1 \cdot b \cdot y + \mu_2(p,y,r,U_m)] \tag{4.5}$$

$$x_s = - A^{-1} \cdot b \cdot r \quad , \tag{4.6}$$

where r is a reference input, x_s is desired equilibrium point of x, and μ_2 is given by:

$$\mu_2(p,y,r,U_m) \underset{|r|<U_m}{=} \begin{cases} 0 \quad , & - U_m - r \leq py \leq U_m - r \\ \mu_0 \cdot \left[p - \dfrac{U_m \cdot \mathrm{sign}(p \cdot y) - r}{y} \right] , & \text{elsewhere.} \end{cases} \tag{4.7}$$

Function μ_2 has the same form as μ depicted in Fig. 2.8 with x corresponding to p, and the variable limits

$$\begin{aligned} m &= \frac{- U_m - r}{y} \\ M &= \frac{U_m - r}{y} \quad . \end{aligned} \tag{4.8}$$

In [28, 27] Franke proved that this system is globally asymptotically stable if $q > 0$, and Q_1 is a solution of

$$A' Q_1 + Q_1 A = - R_1 \quad , \tag{4.9}$$

where R_1 is any $n \times n$ positive definite matrix. We have found a flaw in Franke's proof, so that it does not hold if reference input r is equal to zero.

The fact that the system is not asymptotically stable when $r = 0$ can be directly observed from equations (4.1)-(4.6). If $r = 0$, it follows from (4.6) that $x_s = 0$, and then from (4.5) and (4.1) the equilibrium values of the plant output and states are also equal to zero. However, from (4.4), the controller state p, can have any value in equilibrium. Therefore, the system is not asymptotically stable by definition. The problem is further elaborated in Appendix C.1.

However, if $r \neq 0$ the system is stable, and therefore throughout this section we will assume that $r \neq 0$. Much of the research effort that will be presented in the rest of this chapter and in the next chapter, is directed towards removing this deficiency.

Control (4.4) can be viewed as an output feedback with adaptive gain p. The mechanism of adaptation is then given by (4.5). In order to increase the speed of adaptation process, the gain q in (4.5) is usually very large.

The transient response of the SVS control can be divided into three modes of operation. In which mode the system operates, depends mainly on the size of the state error $|x - x_s|$.

Input limit mode: $|x - x_s| >> 1$

If $y \neq 0$, due to very large q, $|\dot{p}|$ is very large, and p will reach the limit, set by the function μ_2, after very short transient. Thereafter p is given by

$$p = \frac{U_m \cdot \text{sign}(p \cdot y) - r}{y} \quad , \tag{4.10}$$

as obtained from (4.5), after substituting (4.7) and letting $\mu_0 \to \infty$. Hence, the plant input is $u = U_m \cdot \text{sign}(p \cdot y)$, i.e., the "feedback gain" p is continuously adjusted to the value just large enough to keep the plant in the limit.

Integral action mode: $|x - x_s| \approx 0$

Due to (4.3) it follows from (4.4) that in equilibrium $p_e = 0$, and therefore p is not in the limit, in this mode. Also, $y \approx y_e$, so from (4.4) and (4.5) it follows that the input to the plant is

$$u \approx r - q \cdot y_e^2 \cdot \int_0^t (x - x_s)' \cdot Q_1 \cdot b \cdot dt \quad . \tag{4.11}$$

This shows that an integral-type feedback is present when the system is very close to steady state.

Transition mode: $|x - x_s| << 1$

The system operates in this mode during the transient between the two previous modes. The action of the limiting function

μ_2 during the input limit mode has a profound effect on the operation of the system in this transient. If μ_2 were identically equal to zero, the variable gain p would have increased considerably beyond the limits during the input limit mode. In that case, there will be some delay from the moment when $(x-x_s)'Q_1by$ changes sign, until the plant input u comes within the limits. For sufficiently large q, such effect would produce a limit cycle with u(t) varying as:

$$\begin{aligned} u &\simeq U_m \cdot \text{sign}(p \cdot y) \\ &\simeq U_m \cdot \text{sign}[(x - x_s)' \cdot Q_1 \cdot b \cdot y^2] \\ &= U_m \cdot \text{sign}[(x - x_s)' \cdot Q_1 \cdot b] \quad , \quad y \neq 0 \quad . \end{aligned} \tag{4.12}$$

The control of this type was considered in Section 3.2, and from equation (3.18) it follows that a sliding mode control will result along the sliding line:

$$\sigma = (x - x_s)' \cdot Q_1 \cdot b \quad . \tag{4.13}$$

However, with μ_2 given by (4.7), the system will leave the input limit mode immediately after $(x-x_s)'Q_1by$, (i.e. p) changes sign. Then, because the system is globally asymptotically stable, the state error will reduce enough for the system to enter the integral action mode.

This discussion shows that the SVS control possesses the features of the high gain output feedback, and of the integral control. Also, a close proximity of the SVS control and SLM control (also called variable structure systems) can be observed. This implies a possible robustness of the SVS control. In [29] Franke has actually derived the conditions under which the soft variable structure control is invariant to parameter variations and external disturbances. Although these conditions are not satisfied in most cases, it has been shown that the control nonetheless has excellent robustness, due to the large gain q .

There are two major problems with the SVS control. One is, as already mentioned, lack of asymptotic stability for $r = 0$. The condition that $y \neq 0$, which was needed in qualitative description of the regions of operation is directly related to this problem. Even if y is close to zero, it is seen from (4.5) and (4.11) that the influence of the large gain q is diminished. Hence, the system will be more sensitive in this region.

Another problem is that an output feedback was attempted, but the full state feedback resulted. In particular cases, b and Q_1 may contain many zeros, so that just a partial state vector may be necessary for the controller synthesis. The SVS control can be pure output feedback only if

$$c' \cdot b \neq 0 \quad . \tag{4.14}$$

The proof of this statement is in Appendix C.2. The condition (4.14) is very restrictive, because it requires that the number of plant poles is exactly by one smaller than the number of zeros, [78]. This is not satisfied for many plants, and specifically not for dc motor.

The severity of the second problem is even more pronounced in systems with unmeasurable disturbances. For, even if all the necessary states are accessible, their equilibrium values are no longer given by (4.6) since they also depend on disturbances.

4.2. MODIFIED SVS CONTROLLER

Due to the problems outlined in the previous section, it was not possible to implement the SVS control in its original version. In a dc motor there are two states: rotor speed and armature current. The equilibrium value of the armature current is almost solely determined by the applied torque, i.e. unmeasurable disturbance, and therefore the current cannot be used in the SVS controller. In order to solve the problem, the system (4.1) is augmented with the new, "dummy" state variable z, such that

$$\dot{z} = - \lambda \cdot z + \lambda \cdot v \quad , \tag{4.15}$$

where v is the input to the plant. Then the equation that governs the adaptation of the feedback gain p is given by

$$\dot{p} = - q \cdot [k_1 \cdot (y - r) + k_3 \cdot p \cdot y + k_4 \cdot (z - r)] \cdot y +$$

$$+ q \cdot \mu_2(p, y, r, U_m) - \varepsilon \cdot p \quad , \tag{4.16}$$

instead of (4.5). In Appendix C.3 it is proved, that for any positive q, ε, k_1, k_3 there exist some positive λ^* and k_4^* such that the system (4.1) with the control (4.4), (4.7), (4.15) and (4.16) is globally asymptotically stable for all $\lambda > \lambda^*$ and $k_4 > k_4^*$, provided that (4.1) has all poles with negative real part.

The major improvements over the original Franke's control are:

i) High-gain, output-only, feedback is possible, regardless of the plant structure, (4.1).

ii) The system is asymptotically stable for all $|r| < U_m$ (including $r = 0$).

The price paid for these improvements is the addition of a new state z to the controller, and the presence of the factor $\varepsilon \cdot p$.

The dummy state variable z, may appear as an observer which substitutes for the ignored state variables of the plant. However, it is not, because only one variable is needed regardless of the order and structure of the plant, and it has only lower boundary on the value of its pole λ. Consequently, λ may be chosen as infinite. In that case, from (4.15)

$$z \simeq u = r + p \cdot y \quad , \tag{4.17}$$

which gives

$$k_3 \cdot p \cdot y + k_4 \cdot (z - r) \triangleq k_2 \cdot p \cdot y \quad . \tag{4.18}$$

In this way, equation (4.15) can be completely eliminated from the controller.

Factor $\varepsilon \cdot p$ provides additional dynamics to the adaptation mechanism (4.16) and assures the stability for $r = 0$. The system is stable with any $\varepsilon > 0$, but if ε is very large (say $\varepsilon \simeq q$), the feedback becomes quite weak. This is obvious from (4.16), because the plant output then has much smaller influence. The problem is especially pronounced for $r = 0$, i.e. when $y \simeq 0$. Therefore, the system still does not have satisfactory performance when the output is close to zero, although the theoretical problem of stability at $r = 0$ has been solved. To alleviate the problem, all the variables in the plant model (4.1) can be offset by

their maximum negative equilibrium values. Since it was assumed that the plant gain is unity, (4.3), the offsetting is done as

$$\hat{v} = v + U_m, \qquad \hat{y} = y + U_m \quad . \tag{4.19}$$

The plant model is then

$$\dot{\hat{x}} = A\,\hat{x} + b\,\hat{v} \tag{4.20}$$

$$\hat{v} = \begin{cases} 2\,U_m & , \quad \hat{u} > 2\,U_m \\ \hat{u} & , \quad 0 \le \hat{u} \le 2\,U_m \\ 0 & , \quad \hat{u} < 0 \end{cases} \tag{4.21}$$

$$\hat{x} = x - A^{-1}\cdot b\cdot U_m \quad , \qquad \hat{u} = u + U_m \quad . \tag{4.22}$$

With offsetting, the case $\hat{r} = \hat{y} = 0$ is placed outside the range of interest, so that the global stability is not required. The offset system is still asymptotically stable in the domain $0 < \hat{r} < 2U_m$, even with $\varepsilon \equiv 0$.

With the modifications (4.18) and (4.19), the modified SVS control of the plant (4.20)-(4.22), is given by

$$\hat{u} = \hat{r} + p\cdot\hat{y} \tag{4.23}$$

$$\dot{p} = -\,q\cdot\{[k_1\cdot(\hat{y} - \hat{r}) + k_2\cdot p\cdot\hat{y}]\cdot\hat{y} + \mu_3(p,\hat{y},\hat{r},U_m)\} \quad ,$$

where (4.3) still holds, and

$$\mu_3(p,\hat{y},\hat{r},U_m)_{0<\hat{r}<2U_m} = \begin{cases} \mu_0 \cdot (p + \dfrac{\hat{r}}{\hat{y}}) & , \quad p\cdot\hat{y} < -\hat{r} \\ 0 & , \quad -\hat{r} \le p\cdot\hat{y} \le 2\cdot U_m - \hat{r} \\ \mu_0 \cdot \left[p - \dfrac{2\cdot U_m - \hat{r}}{\hat{y}}\right] & , \quad p\cdot\hat{y} > 2\cdot U_m - \hat{r} \end{cases} \tag{4.24}$$

$$\hat{r} = r + U_m \quad . \tag{4.25}$$

Variable μ_3 serves the same function as μ_2, except it is also offset by U_m. It still has the form depicted in Fig. 2.8, with x corresponding to p, and the limits

$$m = -\frac{\hat{r}}{\hat{y}}$$

$$M = \frac{2\cdot U_m - \hat{r}}{\hat{y}} \quad . \tag{4.26}$$

4.3. IMPLEMENTATION RESULTS

The modified SVS controller described by equations (4.19)-(4.26) of the previous section was implemented for the

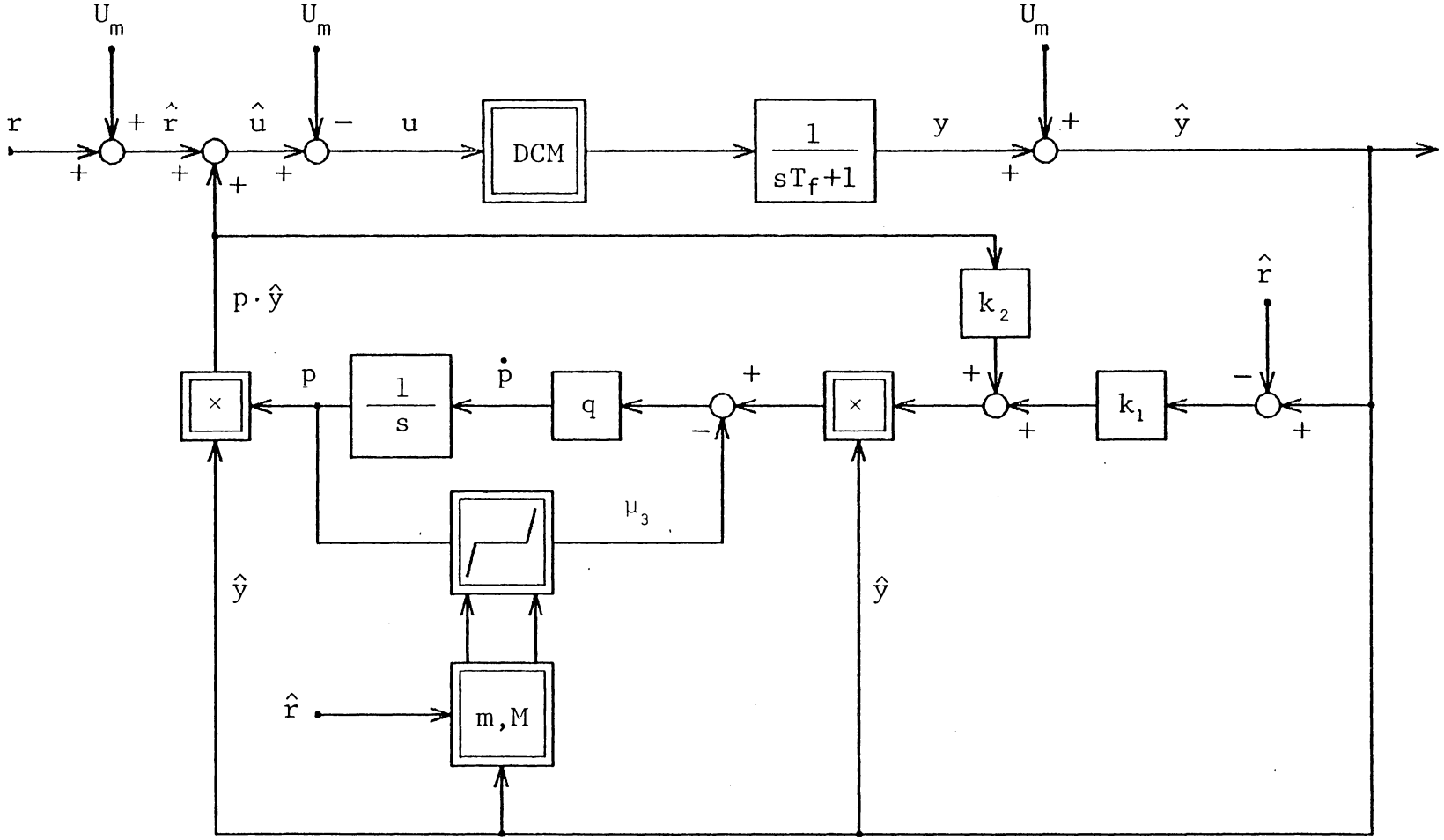

Fig. 4.1: Modified soft variable structure (SVS) control.

dc motor speed control. The block diagram of the system is shown in Fig. 4.1. The plant is the voltage driven dc motor, whose model and parameter values are given in Appendix A.2. An output filter is used for noise reduction, and the plant steady state gain is unity, as explained in Appendix A.2. Upper and lower limits of p, (m and M) are calculated according to equation (4.26) with two dividers needed to perform that calculation. In addition, two multipliers are necessary to perform the noted multiplications. The rest of the algorithm is simple, and is easily realized using scaled summers.

The whole system was simulated and built experimentally. Analog components were used in the experiment, and the circuit diagram is shown in Appendix F.6.

The modified SVS controller has five parameters: U_m, μ_0 , q, k_1 and k_2. U_m is given by the plant saturation level, and in our case it is the voltage limit V_m from (A.6). The constant μ_0 should be as large as possible, limited only by the available gain. In our case, $\mu_0 \approx 10^5$. The remaining three parameters can be reduced to two, $q \cdot k_1$, and k_2/k_1 , by factoring k_1 in front of the brackets in equation (4.23).

The effect of different values of q is shown in Fig. 4.2. Both simulation and experiment show considerable improvement in the transient response when q is increased. So, the gain q should be chosen as large as possible, limited only by the noise level in the measurement signals.

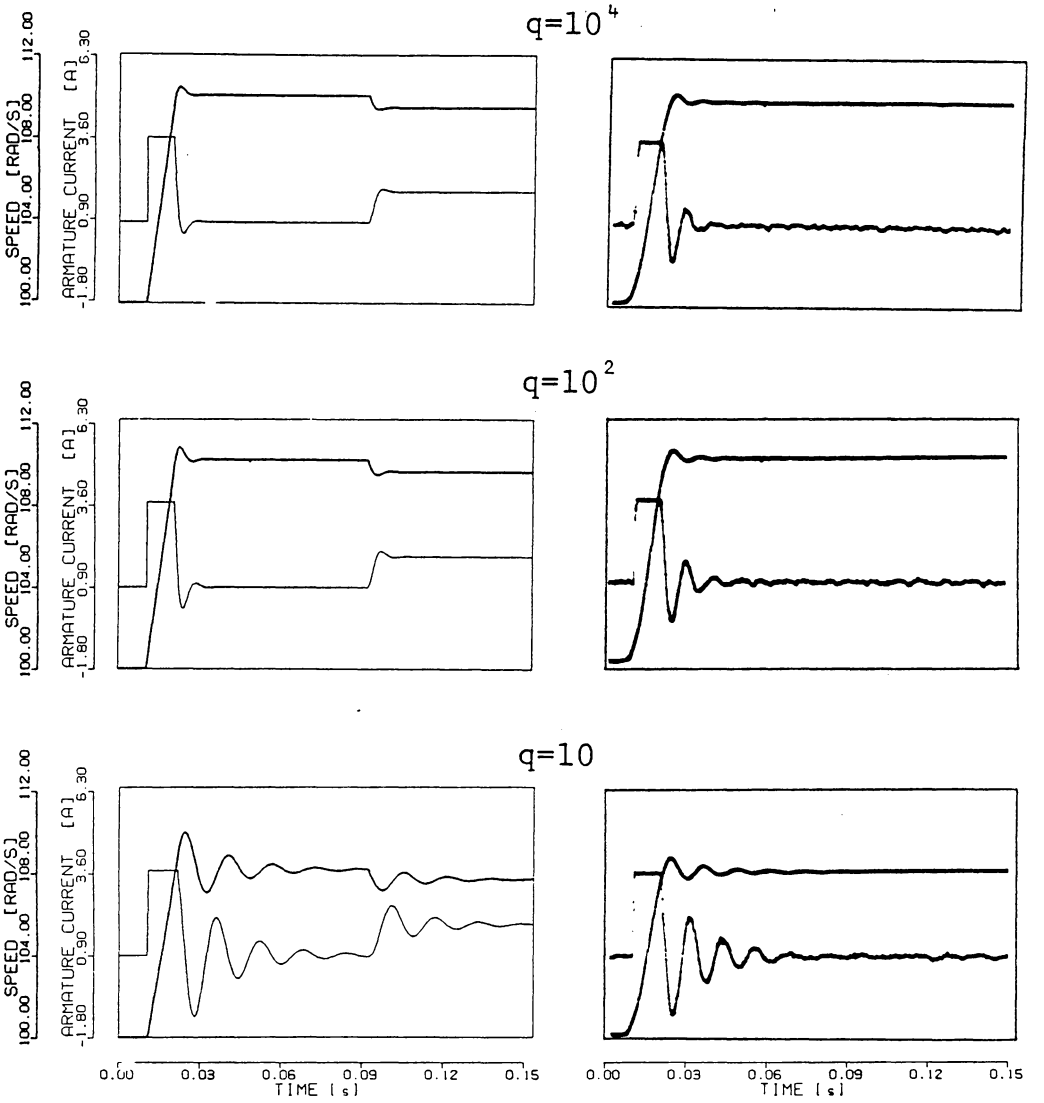

Fig. 4.2: Transient response of the modified SVS control system for different values of q, and $k_1 = 30$, $k_2 = 0.3$.

a) Simulation with the inputs from Figures 2.3b and 2.3c.

b) Experiment with the step speed command from Fig. 2.3b, and $T_\ell = 0.017$ N·m.

The magnitude of q does not influence the steady state error, as can be observed in Fig. 4.2a. From (4.23) the equilibrium value of $p \cdot y$ is

$$(p \cdot \hat{y})_e = \frac{k_1}{k_2} (\hat{r}_e - \hat{y}_e) \quad ,$$

and then

$$\hat{v}_e = \hat{r}_e + \frac{k_1}{k_2} \cdot (\hat{r}_e - \hat{y}_e) \quad . \tag{4.27}$$

Using (4.27) and the motor model in Appendix A.2, it is easily obtained that

$$\hat{y}_e = \hat{r}_e - \frac{k_2/k_1}{1 + k_2/k_1} \cdot \frac{R \cdot c}{k_m^2 + R \cdot D} \cdot T_\ell \quad , \tag{4.28}$$

where R, c, D and k_m are motor parameters, and T_ℓ is load torque. It is now obvious that the equilibrium error $\hat{y}_e - \hat{r}_e$, does not depend on q, but on the ratio k_2/k_1. From (4.28) it follows that the error would be zero if $k_2 = 0$. However, from the stability analysis in the previous section and in Appendix C.3 it follows that $k_2 > k_2^* > 0$. The effect of the various values of k_2/k_1 is shown in Fig. 4.3. Both, simulation and experiment are in the excellent agreement with the theory: large k_2/k_1 causes large equilibrium error, and too small k_2/k_1 causes instability.

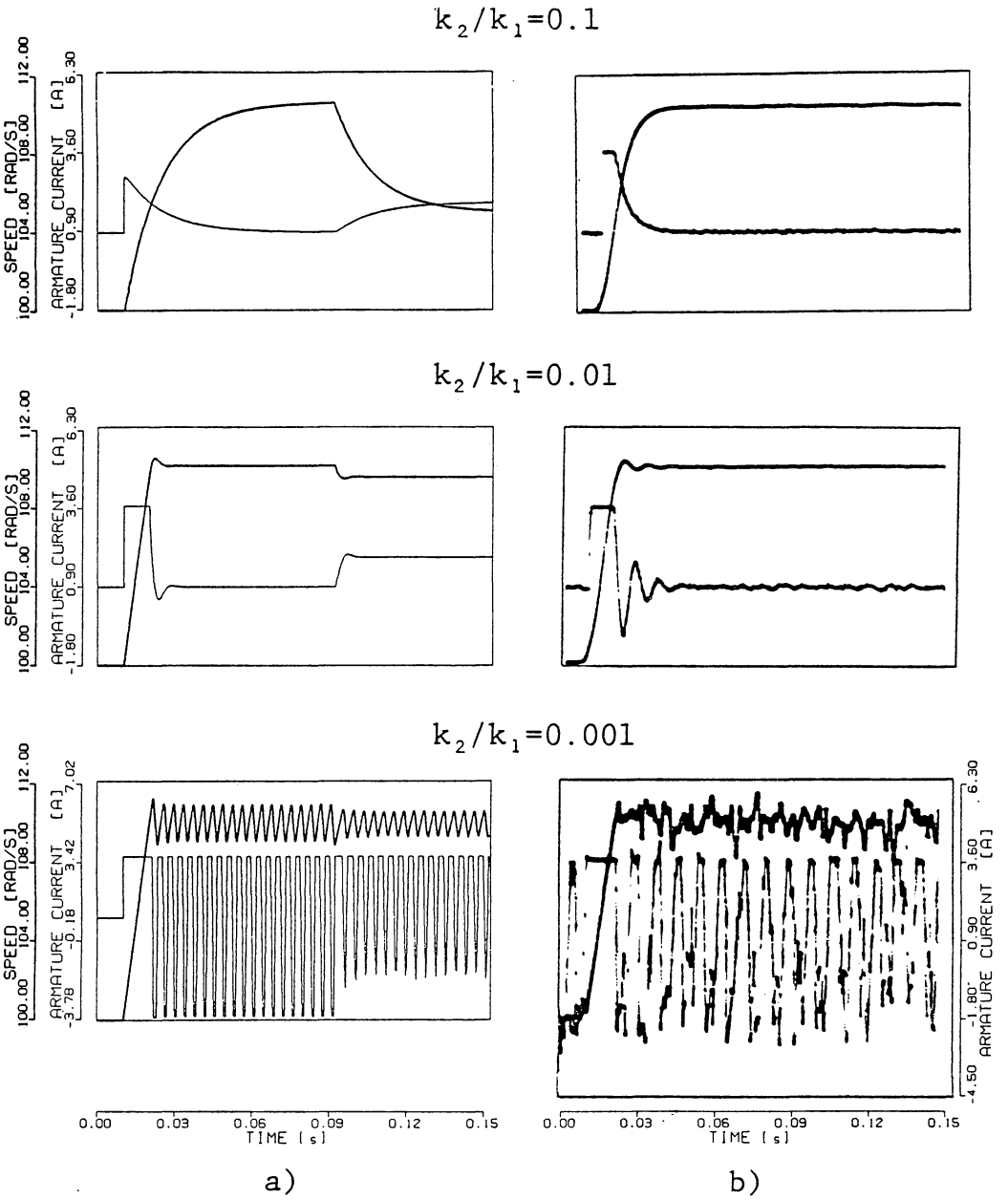

Fig. 4.3: Transient response of the modified SVS control system for different values of k_2/k_1 , and $q = 10^3$, $k_1 = 30$.

a) Simulation with the inputs from Figures 2.3b and 2.3c.

b) Experiment with the step speed command from Fig. 2.3b, and $T_\ell = 0.017$ N·m .

From these results it follows that the only critical parameter of the controller is k_2/k_1. From Appendix C.3 and equation (4.18), a lower bound on k_2 can be found as a function of k_1 and the Liapunov function of the plant. Since a Liapunov function is never unique, it is very difficult to estimate the smallest k_2^*. In our case, direct simulation showed to be quite simple, and the minimum k_2^* was obtained by trial and error.

Finally the controller parameters that we have decided upon, are

$$\begin{aligned} q &= 500 \\ k_1 &= 30 \\ k_2 &= 0.3 \quad . \end{aligned} \tag{4.29}$$

Simulation and experimental results for the motor start-up, when these parameters are used, are shown in Fig. 4.4.

In order to investigate the effect of the asymmetry of controller operation induced by offsetting, (4.19), the steady state error and the small signal bandwidth were evaluated over the operating region. Variation of the steady state error for a nominal torque, as obtained by simulations, is shown in Fig. 4.5. Measured small signal bandwidth variation is shown in Fig. 4.6. Both results show that the var-

a)

b)

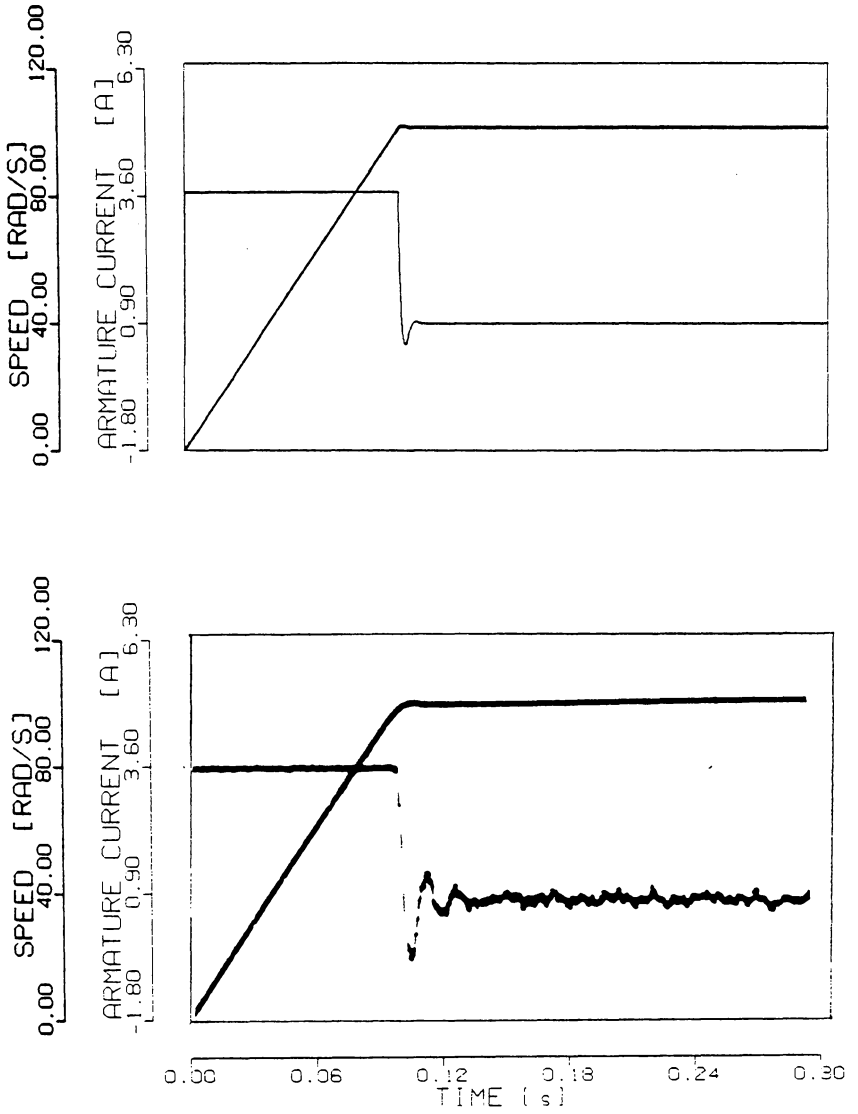

Fig. 4.4: Start-up of the motor with the modified SVS control, for the controller parameter values of $q = 500$, $k_1 = 30$, $k_2 = 0.3$.

a) Simulation.

b) Experiment.

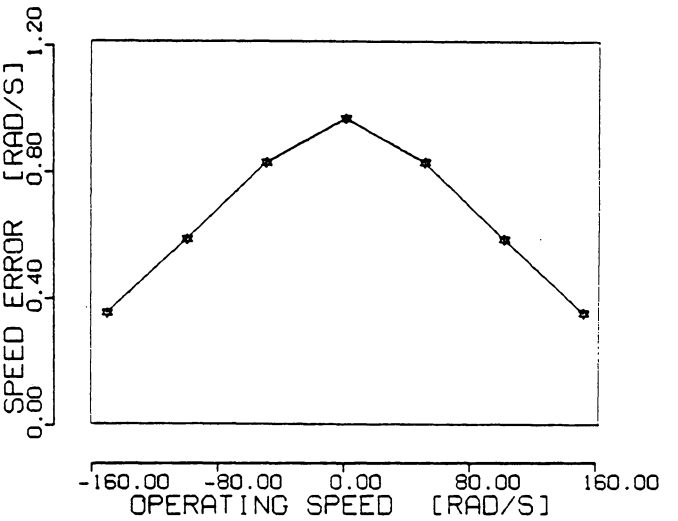

Fig. 4.5: Variation of the steady state error, as a function of operating speed.

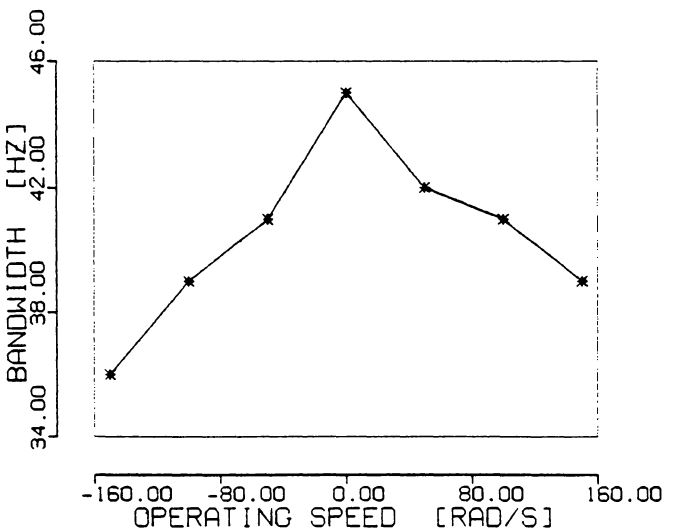

Fig. 4.6: Variation of the measured bandwidth, as a function of operating speed.

iation of the system performance over the operating region is quite small, and that asymmetry is negligible.

The controller was further tested, and the results relating to robustness are presented in Chapter 6.

4.4. DIGITAL IMPLEMENTATION

The controller shown in Fig. 4.1, with the parameter values from (4.29) was also implemented on a microprocessor system with INTEL 8751 as the main processor. This implementation, and its analysis was reported by Lee in his master's thesis, [53]. Detailed description of the hardware and software used, as well as simulation and experimental results are presented there.

It has been demonstrated that digital implementation of the SVS algorithm is considerably simpler than the analog one. The hardware configuration was minimal, i.e. the same as is necessary for implementation of even the simplest speed control algorithm. The whole software was successfully executed within a cycle time of 1 ms, which is sufficiently fast for most applications.

However, the nonlinearities present in the SVS controller, in conjunction with the offsetting of variables (equations (4.19), (4.23)) caused problems which were not present in the analog implementation. To explain these

problems consider equation (4.23) near steady state, where $\hat{y} \approx \hat{y}_e$ and $\mu_3 = 0$. In s-domain we then have

$$s \cdot \underline{p} \approx - q \cdot k_1 \cdot \hat{y}_e \cdot (\underline{\hat{y}} - \underline{\hat{r}}) - q \cdot k_2 \cdot \hat{y}_e^2 \cdot \underline{p}$$

or

$$\underline{p} \approx - \frac{q \cdot k_1 \cdot \hat{y}_e}{s + q \cdot k_2 \cdot \hat{y}_e^2} \cdot (\underline{\hat{y}} - \underline{\hat{r}}) \quad . \tag{4.30}$$

This linearized form of the SVS algorithm shows that, around steady state, the feedback gain p is changing as a filtered error. The filter is of the first order, with a variable gain and a variable pole. However, throughout the operating range ($0 < \hat{y}_e < 2U_m$) the pole is always negative and real. This assures the "well-behavedness" of the system in analog implementation.

The same is not true for the digital implementation. The discrete time version of equation (4.23), which was used by Lee [53, pp. 53-55] is (in our notation):

$$\begin{aligned} p(n) \cdot \hat{y}(n) = {} & p(n-1) \cdot \hat{y}(n-1) + \\ & - T_s \cdot q \cdot k_1 \cdot [\hat{y}(n) - \hat{r}(n)][\hat{y}(n)]^2 + \\ & - T_s \cdot q \cdot k_2 \cdot p(n-1) \cdot \hat{y}(n-1) \cdot [\hat{y}(n)]^2 \quad , \end{aligned} \tag{4.31}$$

where T_s the is sampling period. Close to steady state we have

$$\hat{y}_e \approx \hat{y}(n) \approx \hat{y}(n-1) \quad , \tag{4.32}$$

and the z-domain equivalent of (4.30) is then from (4.31) and (4.32), given by

$$\underline{p} \approx - \frac{T_s \cdot q \cdot k_1 \cdot \hat{y}_e \cdot z}{z - (1 - T_s \cdot q \cdot k_2 \cdot \hat{y}_e^2)} [\underline{\hat{y}} - \underline{\hat{r}}] \quad . \qquad (4.33)$$

This again represents a first order filtering of the error, with the filter pole given by

$$z_1 = 1 - T_s \cdot q \cdot k_2 \cdot \hat{y}_e^2 \quad . \qquad (4.34)$$

With the digital, scaled range of $\hat{y}_e$ ($0 < \hat{y}_e < 16$), and the values of the constants ($T_s = 0.7$ ms, $q = 500$, $k_2 = 1/64$) used in [53], z_1 lies in the interval

$$-0.4 < z_1 < 1 \quad . \qquad (4.35)$$

Although (4.35) assures stability, it is also known [51], that negative real poles in the z-domain produce an alternating sequence in the time domain. Hence, a considerably increased fluctuation of the control input, and therefore of the armature current, was noticed for positive speeds ($8 < \hat{y}_e < 16$) than for negative speeds ($0 < \hat{y}_e < 8$), Fig. 4.7. This effect was also aggravated by the increase of gain in (4.33), at positive speeds.

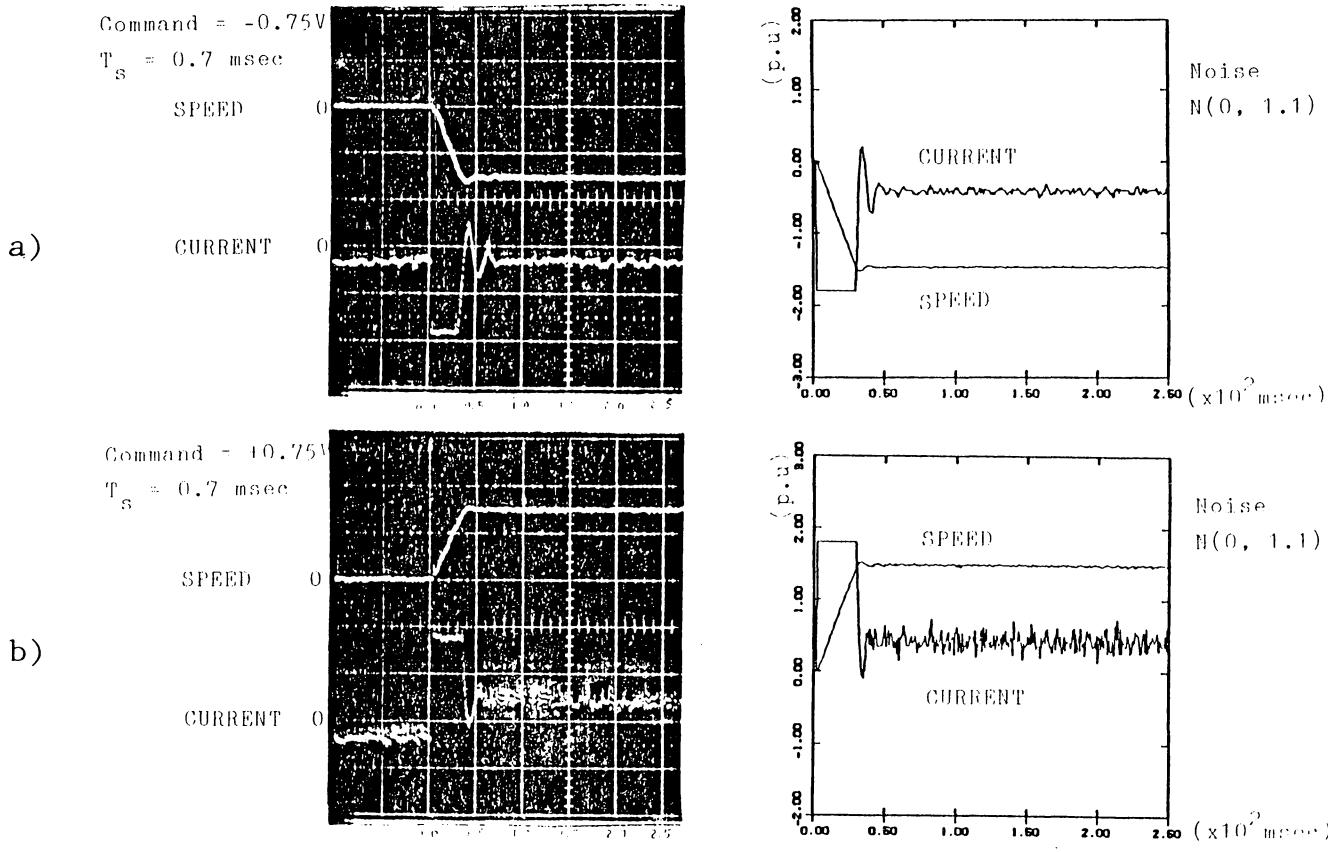

Fig. 4.7: Effect of offsetting in the digital implementation. Experimental and simulation results.

a) Negative speed.

b) Positive speed.

(Reproduced from [53] with permission.)

The problem outlined above, can be solved by decreasing the sampling time and/or decreasing gain q. However, using a faster microprocessor will unduly increase the cost of the system, and using smaller q causes deterioration of the performance of the SVS control algorithm (see Fig. 4.2).

* * *

In this chapter, a novel, modified SVS control algorithm, for use in dc motor speed control, was presented. The control system is robust and has very fast response without significant overshoot. It is easy to design, although somewhat complex to implement. The steady state error is present. Due to large gains and offsetting, there are are serious problems in the digital implementation.

The difficulties experienced in the digital implementation directed further research towards finding the control algorithms which can operate satisfactorily at the plant output close to zero, and therefore avoid the offsetting. These results are presented in the next chapter.

Chapter 5

ADAPTIVE PI CONTROL

One way of implementing a control algorithm which combines the properties of the output feedback integral control and the very high gain feedback, but avoids sliding mode, has been presented in the previous chapter. The resulting modified SVS control achieved very fast and smooth transient response and excellent robustness. However, a steady state error was still present, and offsetting of the system variables produced undesired chattering in the digital implementation.

In this chapter, a method of directly combining a PI control with an SVS control, is presented. The method, named adaptive PI (API) control, has operation and performance characteristics between SLM and PI control, and does not exhibit the problems present in the modified SVS control.

5.1. CONCEPT OF API CONTROL

In order to eliminate the steady state error present in the SVS control, the SVS controller can be used in parallel with a constant gain integrator. In that case, the input to this composite controller has to be the error between the reference signal and the plant output, instead of the plant output itself, as was in the SVS control.

The functional block diagram of the proposed API control system is shown in Fig. 5.1a, whereas the details of the controller are shown in Fig. 5.1b. The API control is essentially a PI control with an adaptive proportional gain p, because the input to the plant $G_s(s)$ is given by

$$u = u_p + u_i = p \cdot e_f + g_i \cdot \int_0^t e_f \cdot dt \quad . \tag{5.1}$$

The block $G_f(s)$ in the figure, is an output filter. Gain adaptation mechanism is given by

$$\dot{p} = q \cdot H(e_f, p) \cdot e_f - \mu_4 - \varepsilon \cdot (p - g_p) \quad , \tag{5.2}$$

where q, ε, and g_p are positive constants. Function μ_4 is

$$\mu_4 \triangleq \mu_2(p, e_f, 0, U_m) \quad , \tag{5.3}$$

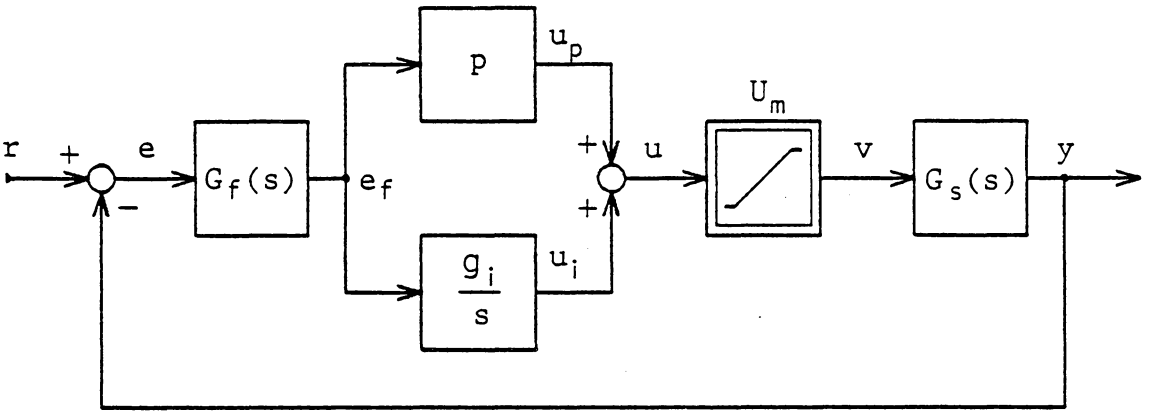

a) Functional block diagram.

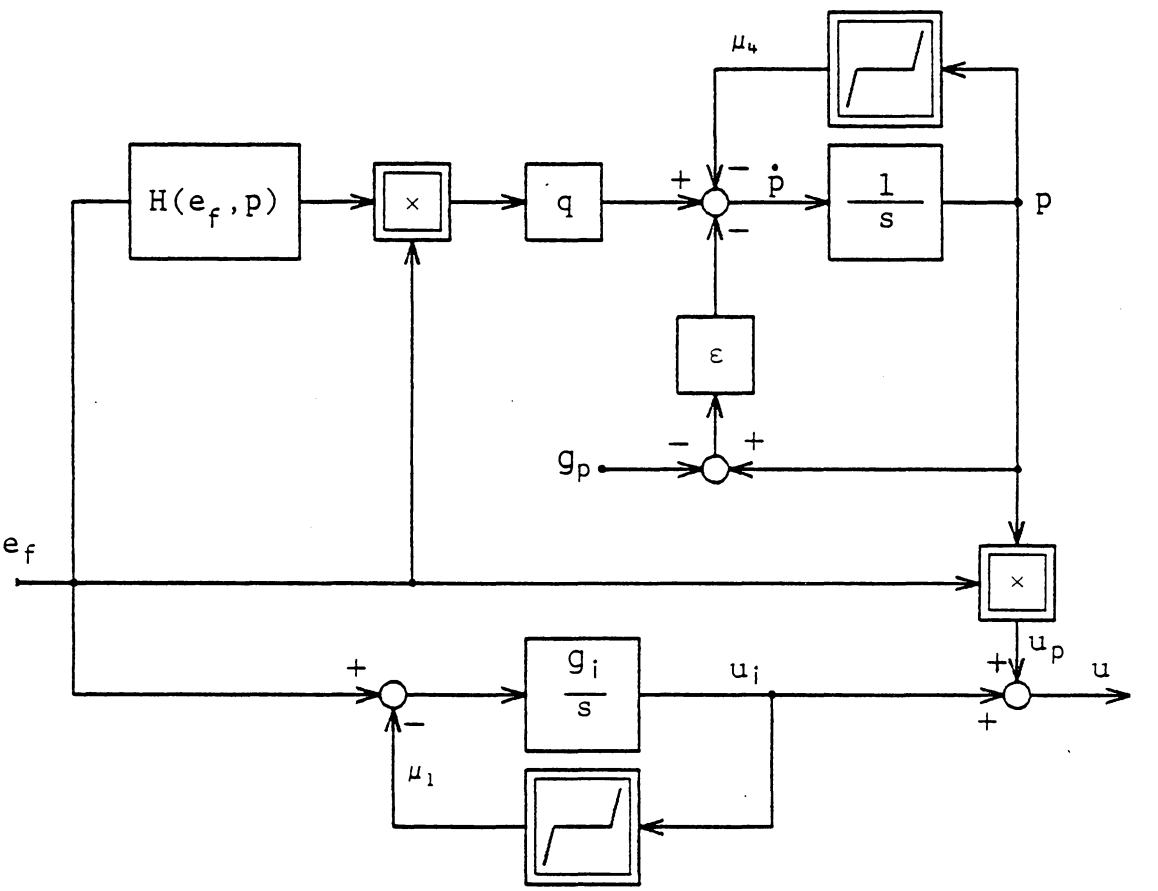

b) Structure of the controller.

Fig. 5.1: Adaptive PI (API) control.

where μ_2 is defined in (4.7). H is a linear operator on e_f and it may depend, linearly or nonlinearly on the adaptive gain p, i.e.,

$$H(\alpha e_{f1}+\beta e_{f2},p) = \alpha H(e_{f1},p) + \beta H(e_{f2},p) \ , \quad \forall\, p,e_f \ . \tag{5.4}$$

The integral component of the control is given by

$$\dot{u}_i = g_i \cdot e_f + g_i \cdot \mu_1(u_i,u_p,U_m) \ , \tag{5.5}$$

where μ_1 is given by (2.16), and g_i is a positive constant.

Operation of the controller can be explained in the following way. The limiting function μ_4 restrains the values of the adaptive gain p, in such a way that the proportional component of the control $u_p = p \cdot e_f$ never exceeds $\pm U_m$. Then the limiting function μ_1 assures that the total control $u = u_p + u_i$ does not exceed the plant saturation limit, in the same way as was explained in Section 2.3.

The adaptation gain q is always chosen much larger than ε and g_i, and therefore p is in the limit whenever the error e_f is large. In this case u_p is equal to either U_m or $-U_m$ so that the integral control u_i is reset to zero by the limiting function μ_1. This corresponds directly to the operation in the input limit mode of the SVS control (Section 4.1), where the "feedback gain" p is continuously

adjusted to the value just large enough to keep the plant input in the saturation.

When $e_f \approx 0$, and both limits μ_1 and μ_4 are equal to zero, it follows from (5.2) that

$$\dot{p} \approx - \varepsilon \cdot (p - g_p) \quad , \tag{5.6}$$

so that in equilibrium

$$p = g_p \quad . \tag{5.7}$$

Therefore, from (5.1), (5.5) and (5.7) it follows that in equilibrium or very close to it,

$$u \approx g_p \cdot e_f + g_i \cdot \int_0^t e_f \, dt \quad , \tag{5.8}$$

i.e. the control reduces to the constant gain PI control. This corresponds to the integral action mode of the SVS algorithm described in Section 4.1. The transition between these two modes of operation depends on the nature of H, as well as on the parameter values.

The main advantage of the API control over the standard PI control is in the possibility of using much larger gains. Namely, a constant gain PI control of the form (5.8), used with large g_i and small g_p, will produce slow and/or oscillatory transient response. If g_p is also large, in-

stability may occur. However, in the API control, the adaptive proportional gain p, is adjusted in such a way that it is large during the initial part of the transient, and small when most of the transient is over. Depending on the choice of H, this can result in fast and robust behavior.

In order to investigate the structure of the API controller further, let us introduce the following change of variables:

$$p_1 = p - g_p \quad . \tag{5.9}$$

Then, equations (5.1), (5.2) and (5.3) become

$$u = (g_p \cdot e_f + u_i) + p_1 \cdot e_f \tag{5.10}$$

$$\dot{p}_1 = q \cdot H(e_f, p_1 + g_p) \cdot e_f - \mu_4 - \varepsilon \cdot p_1 \tag{5.11}$$

$$\mu_4 = \mu_2(p_1 + g_p, e_f, 0, U_m) \quad , \tag{5.12}$$

respectively. From (5.10) it follows that the control u can be separated in two components, given as:

$$\begin{aligned} u &= u_c + u_a \\ u_c &= g_p \cdot e_f + u_i \quad , \qquad u_a = p_1 \cdot e_f \quad . \end{aligned} \tag{5.13}$$

The component u_c, with u_i given by (5.5), represents a control which would be generated by the VLPI controller, described in Section 2.3. The other component u_a is then, an additional, adaptive, SVS control.

Block diagram of the transformed system is shown in Fig. 5.2a. When close to equilibrium, the limiting function, μ_1 is zero, so that the variable limit PI control becomes a linear one, with the controller transfer function $G_c(s)$ same as in (2.1):

$$G_c(s) = g_p + \frac{g_i}{s} \tag{5.14}$$

In this region, API control from Fig. 5.2a, can be represented as shown in Fig. 5.2b, where the SVS control part, given by (5.11), is applied to the linear "plant" $G_1(s)$. The difference from the modified SVS control described in Section 4.2, is that now both the input and the output of the "plant" are equal to zero in equilibrium, regardless of the reference value r or any constant disturbance. This results in uniform operation of the API controller for any given value of the reference input r and output y.

Obviously, the performance and stability of the system depend on the choice of H. Two alternatives will be presented in the following sections.

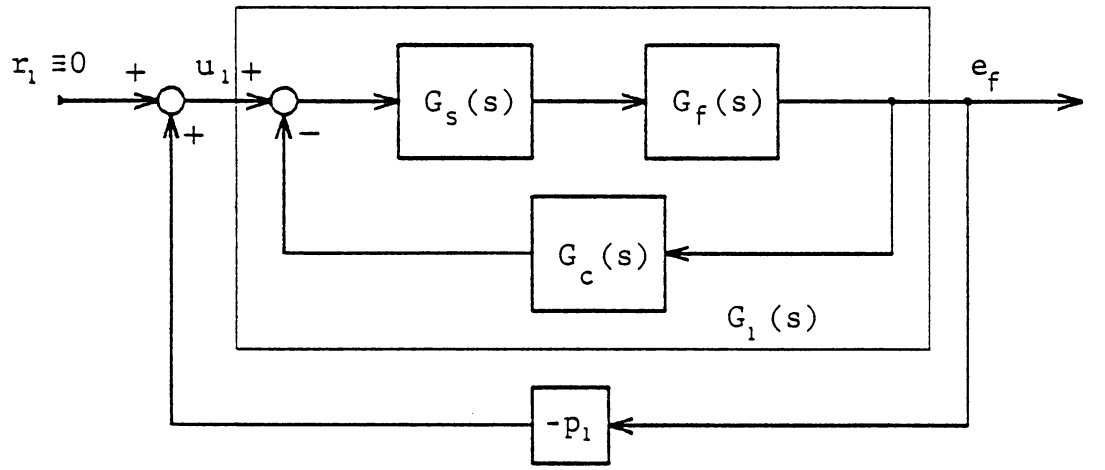

a) Complete system.

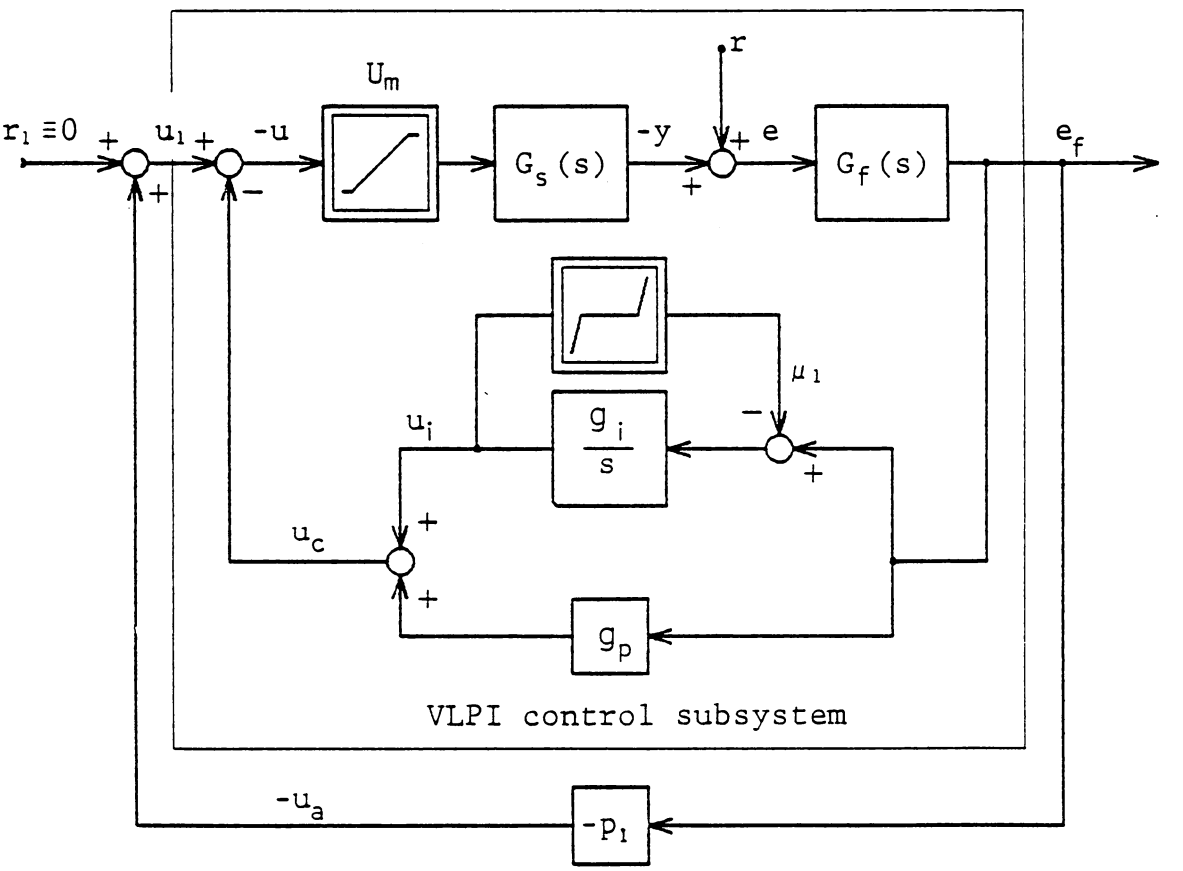

b) Equivalent system when close to equilibrium

Fig. 5.2: Representation of the API control as a combination of the VLPI control and the modified SVS control.

5.2. SOFT VARIABLE STRUCTURE PI (SVSPI) CONTROL

The modified SVS control described in Chapter 4, is fast and robust, but not accurate enough. If it is implemented together with the VLPI control, as shown in Fig. 5.2, all three design objectives are achieved. This, soft variable structure PI (SVSPI) control is developed in this section.

5.2.1. CONTROLLER STRUCTURE: Suppose that the VLPI control subsystem in Fig. 5.2 is asymptotically stable, i.e.

$$u_1 = 0 \quad \Rightarrow \quad e_{fe} = 0 \quad , \quad \forall\, r \in (-U_m, U_m) \quad . \tag{5.15}$$

From equations (4.16)-(4.18), the modified SVS control algorithm is given by

$$\begin{aligned} u &= r + p \cdot y \\ \dot{p} &= - q \cdot \{[k_1 \cdot (y - r) + k_2 \cdot p \cdot y] \cdot y + \mu_2\} - \varepsilon \cdot p \quad . \end{aligned} \tag{5.16}$$

If the VLPI subsystem is now considered as a plant which is controlled by the SVS algorithm (5.16), then with the following change of notation

$$\begin{aligned} r &= r_1 \quad , \quad & y &= + e_f \quad , \\ u &= + u_1 \quad , \quad & p &= - p_1 \quad , \end{aligned} \tag{5.17}$$

control law (5.16) becomes

$$u_1 = - p_1 \cdot e_f \tag{5.18}$$

$$\dot{p}_1 = q \cdot (k_1 \cdot e_f - k_2 \cdot p_1 \cdot e_f) \cdot e_f - \mu_4 - \varepsilon \cdot p_1 \quad . \tag{5.19}$$

for $r_1 \equiv 0$. With these substitutions, the limiting function μ_4 would be defined as $\mu_4 = -q \cdot \mu_2(-p_1, e_f, 0, U_m)$. By using (4.7), this is the same as $\mu_4 = \mu_2(p_1, e_f, 0, U_m)$ if the constant $q \cdot \mu_0$ is denoted as a new constant μ_0 . However, because the plant saturation nonlinearity in Fig. 5.2 is at the input u , and not u_1 , the limiting function μ_4 has to be defined as in (5.12).

The control (5.18)-(5.19) is the same as the one in Fig. 5.2 with (5.10)-(5.12), and with

$$H(e_f, p_1 + g_p) = (k_1 - k_2 \cdot p_1) \cdot e_f \quad . \tag{5.20}$$

Therefore, according to the results in Appendix C.3, the system in Fig. 5.2 with H given by (5.20), is globally asymptotically stable, provided that the VLPI subsystem is stable, q, ε, and k_1 are positive, and k_2 is greater than some positive constant k_2^*.

In order to obtain a form of the control system suitable for implementation, let us first backsubstitute p_1 from (5.9) into (5.18) - (5.20). Then

$$u = u_i + p \cdot e_f$$

$$\dot{p} = q \cdot (k_1 + k_2 g_p) \cdot \left(1 - \frac{k_2}{k_1 + k_2 g_p}\, p\right) \cdot e_f^2 - \mu_4 - \varepsilon (p - g_p) \quad . \tag{5.21}$$

The adaptation gain q is usually impractically large for implementation. However, it can be evenly distributed by the following substitutions

$$p = q_1 \cdot p_2 \quad , \quad e_1 = q_1 \cdot e_f \quad . \tag{5.22}$$

Substituting (5.22) into (5.21), and denoting

$$k = \frac{k_2}{k_1 + k_2 \cdot g_p} \quad , \quad g_p' = \frac{g_p}{q_1} \quad , \tag{5.23}$$

it follows that

$$u = u_i + p_2 \cdot e_1 \tag{5.24}$$

$$\dot{p}_2 = (1 - k \cdot p_2) \cdot e_1^2 - \mu_5 - \varepsilon (p_2 - g_p') \quad , \tag{5.25}$$

where the gain q is now

$$q = q_1^3 \cdot (k_1 + k_2 \cdot g_p) \quad . \tag{5.26}$$

The limiting function μ_5 is equal to μ_4 defined in (5.3) with the substitutions (5.22), and with $q_1 \cdot \mu_0$ considered

as a new μ_0 . Then, by using (4.7), μ_5 can be expressed as

$$\mu_5(p_2, e_1, U_m) = \begin{cases} 0 \ , & |p_2 e_1| \le U_m \\ \mu_0 \cdot \left[p_2 - \dfrac{U_m \cdot \mathrm{sign}(p_2)}{|e_1|} \right] \ , & \text{elsewhere.} \end{cases} \tag{5.27}$$

The block diagram of this controller is shown in Fig. 5.3. The filter $G_f(s)$ is a simple first order filter given by

$$G_f(s) = \frac{1}{s \cdot T_f + 1} \ . \tag{5.28}$$

5.2.2. CONTROLLER OPERATION: The SVSPI algorithm can be directly applied to the motor speed control. For the stability of the system it is required that the plant together with the VLPI controller (i.e. the VLPI subsystem in Fig. 5.2) is stable. Therefore, it is irrelevant whether the plant is a current or a voltage driven dc motor, because a stable, constant gain PI control system can be designed for either one.

The system shown in Fig. 5.3 was implemented and simulated for the current controlled motor described in Appendix A.3. The stable, VLPI control for that drive was already designed in Chapter 2. The combined plant and filter transfer function, $G_s(s) \cdot G_f(s)$, is given by (2.2), and the PI

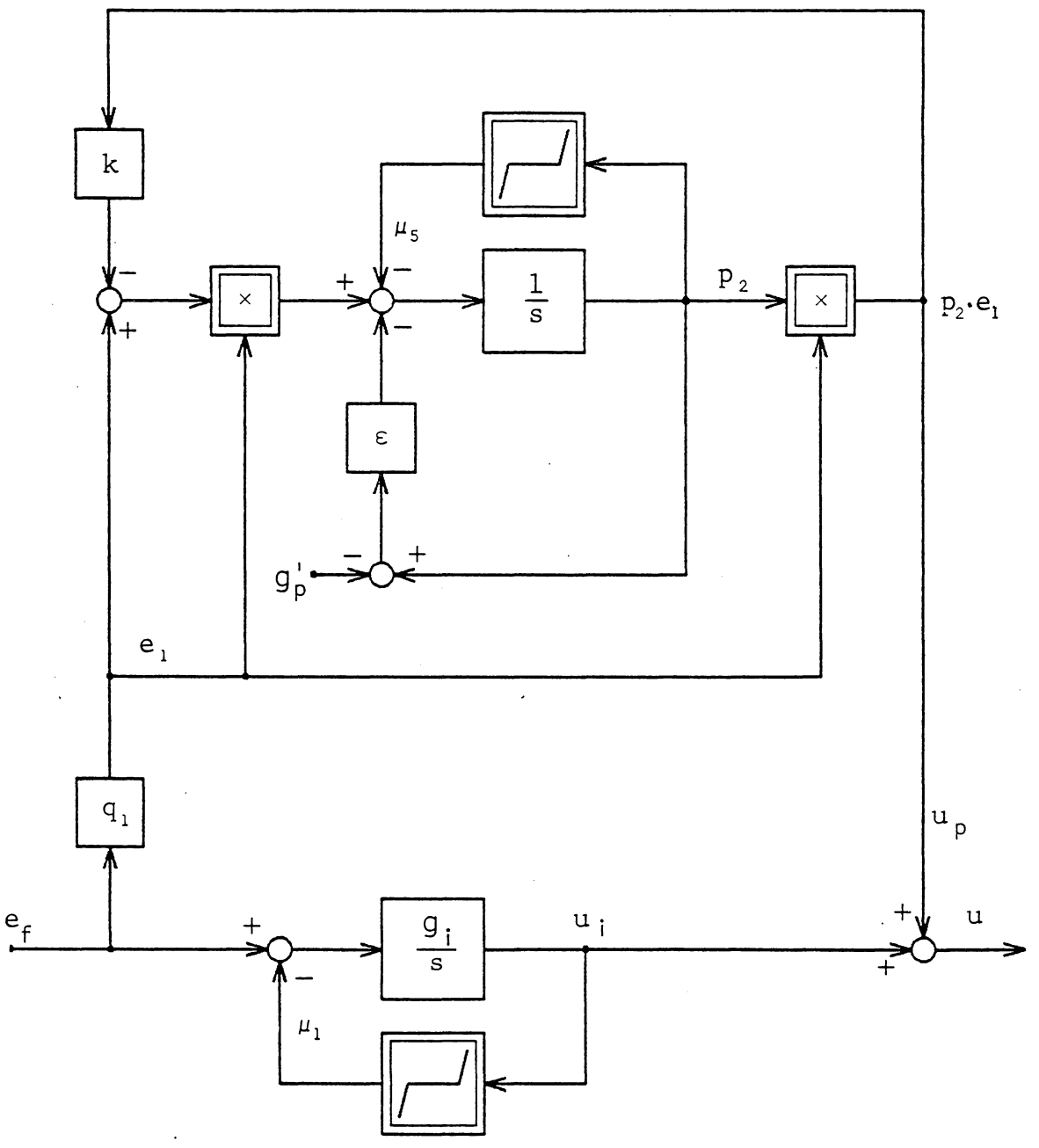

Fig. 5.3: Soft variable structure PI (SVSPI) controller.

controller transfer function by (2.4). The closed loop poles are given by (2.5), and they are all real.

The system was simulated with the following values for the adaptive controller parameters

$$q_1 = 500, \quad \varepsilon = 200, \quad k = 0.1 \tag{5.29}$$

The waveforms of the motor speed, armature current, adaptive gain $p = p_2 q_1$ and the integral control u_i, are shown in Fig. 5.4 for the small step input from Fig. 2.3b. and the step disturbance from Fig. 2.3c. In steady state p is equal to 32 so that the proportional gain is as in (2.3). The integral component, u_i has the value necessary to support the constant load torque that is present.

After the step command is applied at $t = 0.01$ s in Fig. 5.4, three distinct modes of operation can be observed in the resulting transient. In the input limit mode, the integrator output u_i is reset to zero, and p is decreased by the limiting functions μ_1 and μ_5, so that the plant input is exactly enough to keep the current in saturation. Due to the very large q_1, the adaptive gain p is increased hyperbolically as the error e_f is decreasing, assuring that the current stays in saturation almost until e_f becomes zero. The small overshoot in speed, at the end of this mode, is due to the phase lag, introduced by the filter $G_f(s)$.

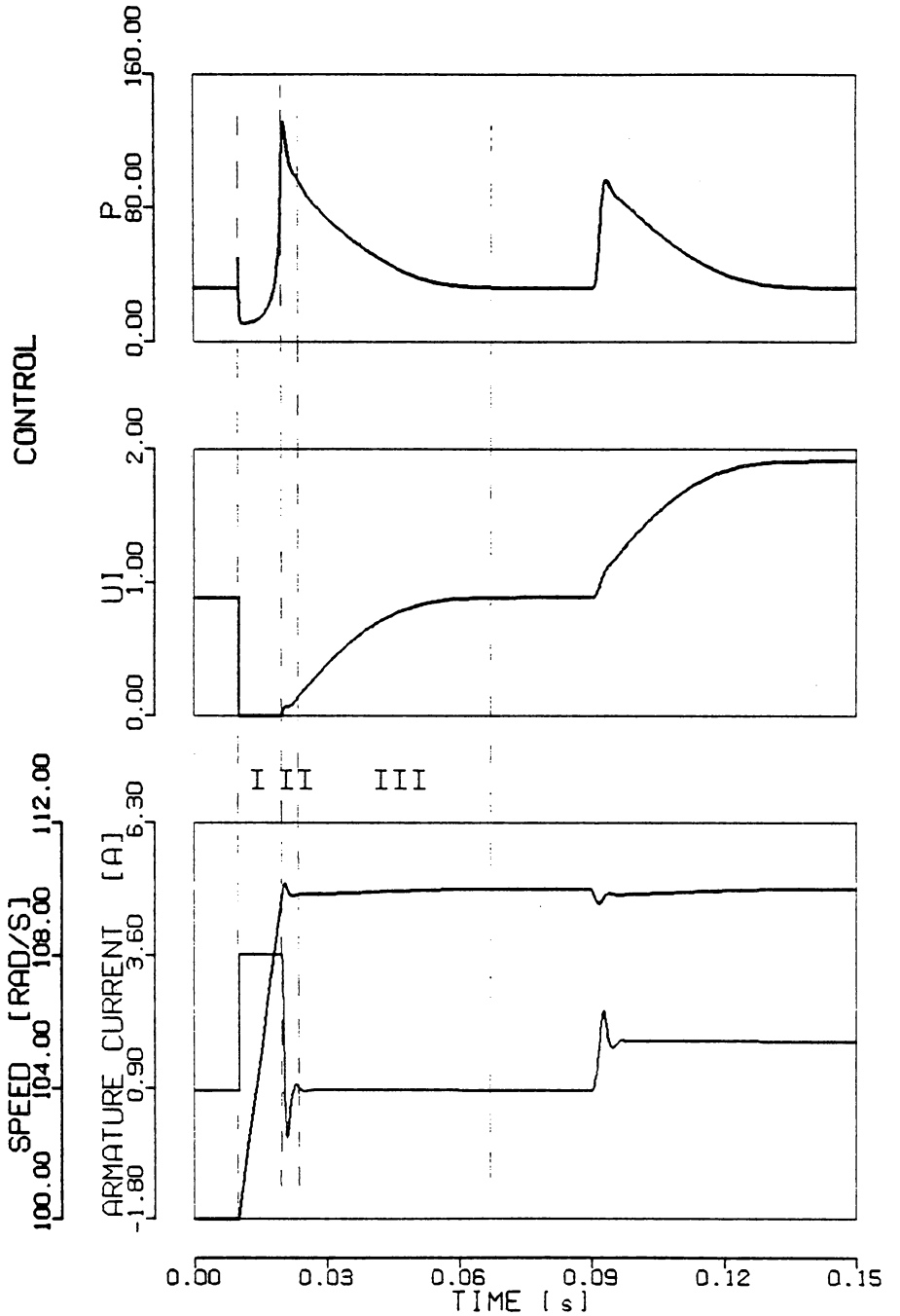

Fig. 5.4: Transient response of the SVSPI control system for the inputs from Figures 2.3b and 2.3c. Marked modes of operation are:

I - Input limit mode.
II - Transition mode.
III - Integral action mode.

The moment when e_f becomes zero, marks the beginning of the transition mode. Because the effective proportional gain p is large at this moment, the overshoot is very small, and the speed returns below the reference value, in very short time. The error e_f is very small and the factor $\varepsilon(p_2-g'_p)$ becomes dominant in the adaptation law (5.25). As a consequence, the adaptive gain p is reduced very fast, so that the onset of oscillations is prevented. At the same time the integrator output u_i starts to increase faster. This is the end of the transition mode, and the system enters the integral action mode.

This last stage of the transient is characterized by resetting of the adaptive gain p to its steady state value g_p, by increasing of the integral control component u_i, and by decreasing of the output error e to zero. The rate of change of these variables is determined by the values of the gains ε and g_i, and to some extent, by the plant parameters. However, the exact dependence is quite complicated because the system is still truly nonlinear.

When the step in the load torque is applied, similar behavior of p and u_i results, providing for the negligible influence of the disturbance. Unless the load step is larger than rated, the input limit mode is absent in this transient.

The same system was simulated with a moment of inertia increased 10 times. The waveforms for the same inputs, are shown in Fig. 5.5. As can be observed, p increased con-

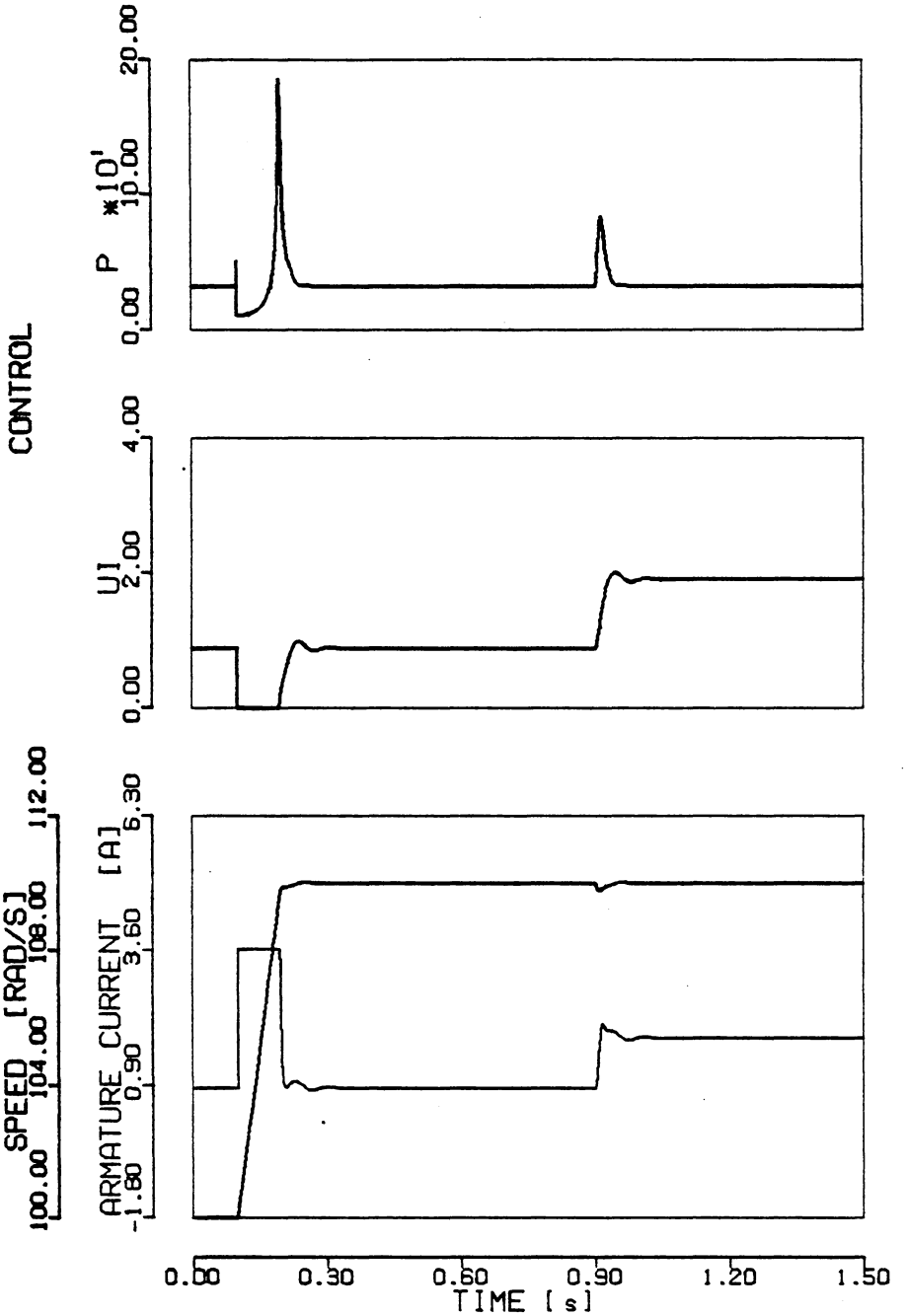

Fig. 5.5: Transient response of the SVSPI control system with the moment of inertia increased 10 times.

siderably more during the transient, than in the case of small inertia. This prevented the oscillatory behavior which would be otherwise rather pronounced because the integral component u_i would increase much beyond the necessary equilibrium value, due to the slowness of the plant. The residual effect of such an oscillation can still be observed in Fig. 5.5 at the beginning of the integral action mode.

5.2.3 PARAMETER SELECTION: From the discussion of the controller operation, several conclusions can be made, regarding the parameter selection. First, if the parameter k is small, from (5.25) and Figures 5.4 and 5.5, it follows that the adaptive gain p is always increased during transients. The increase of p is larger for a slower plant, i.e. for a plant with lower gain. This is the major source of robustness of the algorithm. With a smaller increase of the controller gain for a plant with a larger gain, and a larger increase of the controller gain for a plants with a smaller gain, the effective "loop gain" is approximately constant during transients. Therefore, the VLPI subsystem should be designed for the fastest plant that will be encountered in the application. The value of the adaptation gain q_1 should be chosen as the largest one, that will not cause excessive overshoot and ringing for the fastest plant. The actual value will have to be determined by simulations. The re-

sponses of the same system, with the same inputs as for Fig. 5.3, but with different values of q_1 are shown in Fig. 5.6.

Second, from (5.25) it follows that the parameter ε determines the rate at which the adaptive gain p is resetting to its steady state value g_p, at the end of a transient. Since it is desirable to have the overall transient settled as fast as possible, ε should be relatively large. However, if it is too large, the effect of the increasing gain p is diminished, and an oscillatory behavior may result for slower plants. The optimum value, again, has to be found through simulations, and in the cases that were considered, it was always between the values of g_p and g_i. The system responses for different values of ε are shown in Fig. 5.7.

Third, the influence of the parameter k is not quite clear. From the stability proof in Appendix C.3 and from (5.23), there is a lower bound on k. On the other hand, for the operation described previously it is necessary that the factor $(1 - k \cdot p_2)$ in equation (5.25) is always positive. This sets the upper bound on k. If $k > 1/g_p'$, the gain p will be decreased, instead of increased, during transient. Although, possibly, this may be desirable in some applications, for our case such value of k should be avoided. Again, the final choice has to be made by simulations. The system responses for different values of k are shown in Fig. 5.8. An interesting result is that a satisfactory step re-

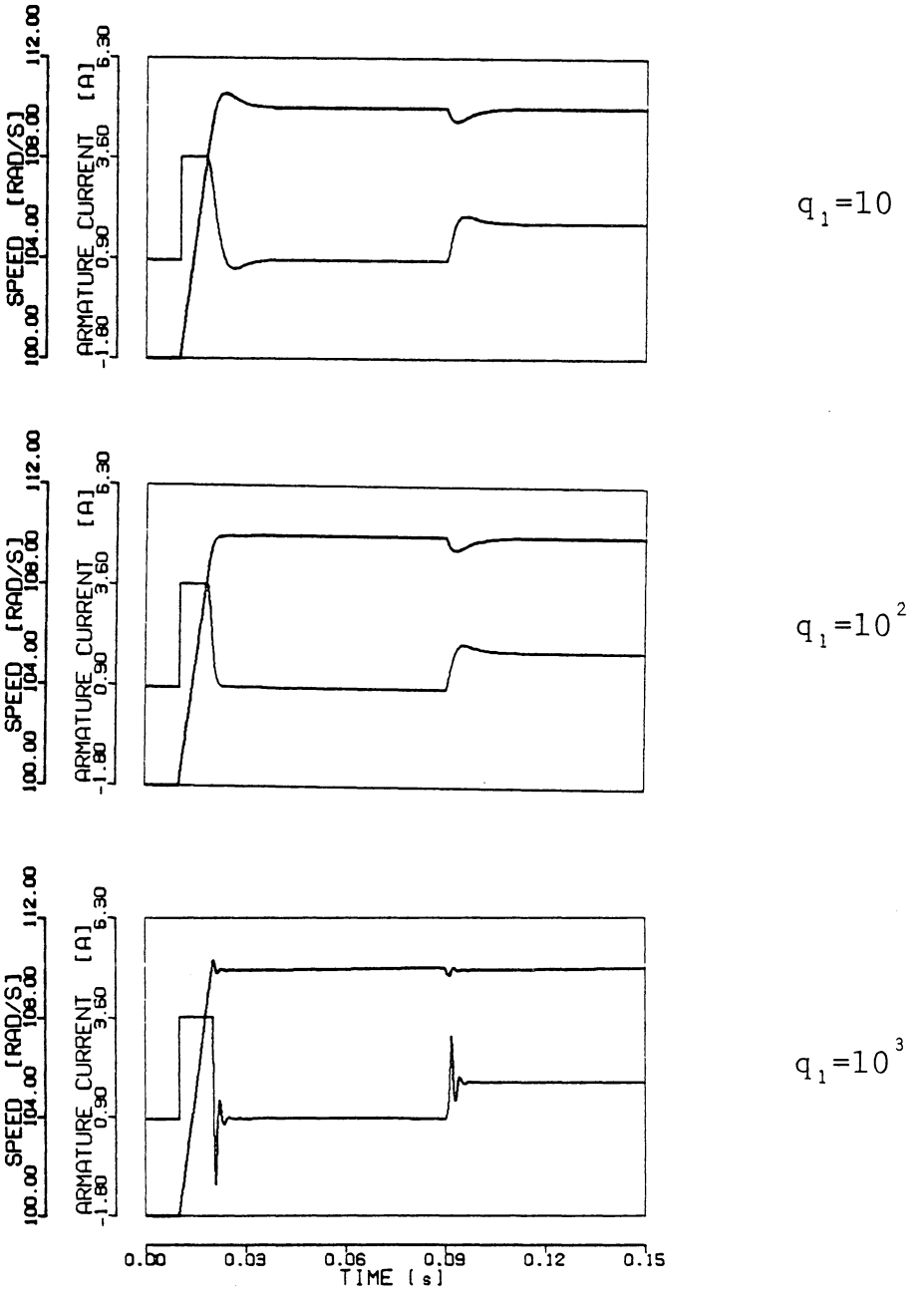

Fig. 5.6: Transient response of the SVSPI control system, for different values of q_1 , and $\varepsilon = 200$, $k = 0.1$. The inputs are from Figures 2.3b and 2.3c.

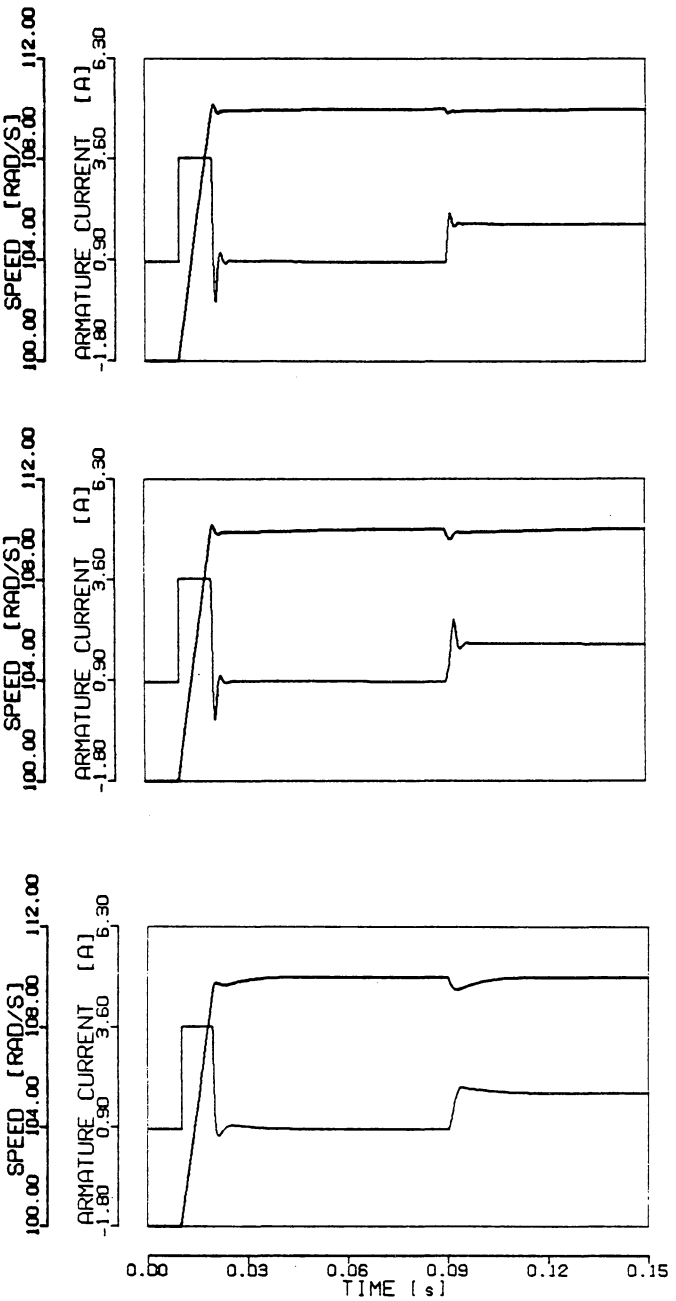

$\varepsilon=1$

$\varepsilon=10^2$

$\varepsilon=10^4$

Fig. 5.7: Transient response of the SVSPI control system, for different values of ε, and $q_1 = 500$, $k = 0.1$. The inputs are from Figures 2.3b and 2.3c.

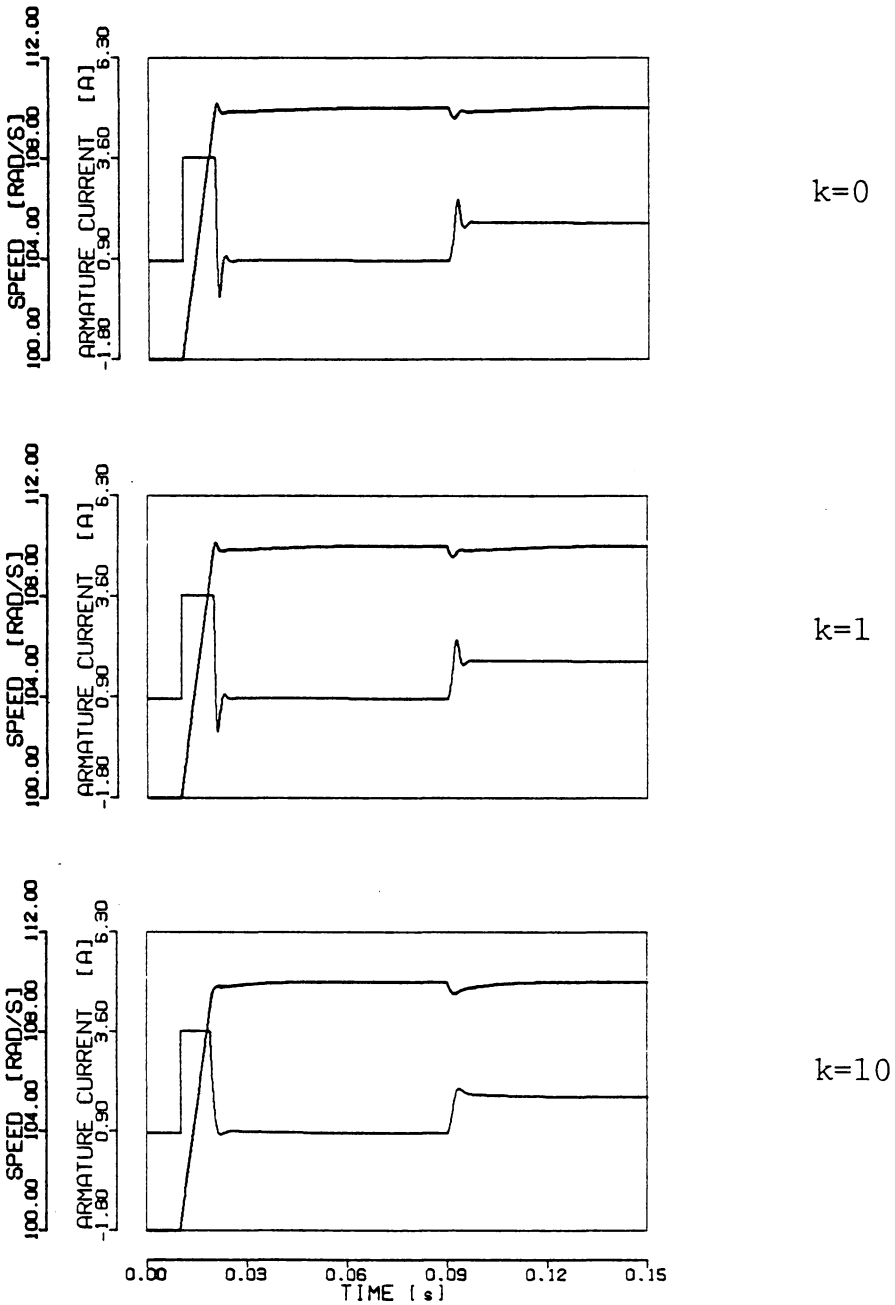

Fig. 5.8: Transient response of the SVSPI control system, for different values of k, and $q_1 = 500$, $\varepsilon = 200$. The inputs are from Figures 2.3b and 2.3c.

sponse is obtained for $k = 0$. We have also obtained practically the same response even for $k < 0$. This is in conflict with the stability proof, and shows that either the conditions used in the proof are overly conservative, or that with $k \leq 0$ only local stability is achieved. The influence of k on stability and performance, clearly needs further investigation. At this stage, the "rule-of-thumb" is that

$$0 < k < 1/g'_p \quad . \tag{5.30}$$

Due to the nonlinear nature of the SVSPI control, and relatively large number of parameters, it was not possible to derive an exact design procedure. However, the previous examples demonstrated that large variations in the controller and plant parameters do not adversely effect the performance of the system. Therefore, high performance and robust SVSPI control system can be designed simply by using the presented guidelines, while the precise tuning is not necessary.

5.3. SLIDING API (SAPI) CONTROL

The sliding mode control described in Chapter 3 is almost completely invariant to plant parameter variations and external disturbances. It would be desirable to obtain the same properties, but without the characteristic chattering.

Suppose that the conditions for the existence of the sliding mode, (3.11)-(3.16), can be satisfied with $\psi_2=\delta=0$. Then the control (3.6) will be in the form

$$\begin{aligned} u &= -\alpha \cdot x_1 \cdot \mathrm{sign}(\sigma \cdot x_1) \\ \sigma &= x_1 + T_c \dot{x}_1 \quad , \end{aligned} \tag{5.31}$$

where in (3.7) it was taken that $\alpha_1=-\beta_1=\alpha$. Variable x_1 is the output error and can be denoted by $-e$. Also, the sign function can be realized by using an integrator with infinite gain and limits. Then the function realized by (5.31) can be implemented as

$$u = e \cdot p \tag{5.32}$$

$$\dot{p} = q \cdot [(e + T_c \cdot \dot{e}) \cdot e] - \mu(p,\alpha) \tag{5.33}$$

where μ is given by (2.9). Indeed, if $q \to \infty$, from (5.33) p will be equal either to $-\alpha$ or α, depending on the sign of $(e+T_c\dot{e})\cdot e$, which is the same as (5.31).

The control given by (5.32)-(5.33) has almost the same form as the API control in (5.1)-(5.2), with $H = e + T_c \cdot \dot{e}$. It is of interest to investigate whether this control, with the finite q, can be realized as a stable API control.

5.3.1. CONTROLLER STRUCTURE: The output error e in (5.32) - (5.33) cannot be obtained exactly due to noise, so that the filtered error e_f has to be used instead. Also, if $\dot{e}$ is not measurable directly, it can be estimated by using a non-ideal differentiator as was done for SLM in (3.21), i.e.

$$\underline{\dot{e}} \simeq \underline{\tilde{\dot{e}}}_f \simeq G_d(s)\cdot\underline{e}_f$$

$$G_d(s) = \frac{s}{s\cdot T_f + 1} \quad . \tag{5.34}$$

Now, by setting

$$H(s) = 1 + T_c\cdot G_d(s) \quad , \tag{5.35}$$

the API control from (5.1)-(5.2) becomes

$$u = u_p + u_i \quad , \qquad u_p = p\cdot e_f$$

$$\dot{p} = q\cdot(e_f + T_c\cdot\tilde{\dot{e}}_f)\cdot e_f - \mu_4 - \varepsilon\cdot(p - g_p) \quad . \tag{5.36}$$

where u_i is given by (5.5). From (5.36), the proportional part of the API control has the same form as the sliding mode controller described by (5.33), except for the resetting factor $\varepsilon(p-g_p)$. If the adaptation gain q is not infinitely large, this controller has the same modes of operation as the general API algorithm. In the transition mode it may be

expected that the system behaves similarly to the SLM control. Hence the name sliding-adaptive PI (SAPI) control.

In order to make the resulting controller easier to implement, the gain q can be distributed in the same way as was done for SVSPI control with substitutions (5.22). Then the controller is given by

$$u = (p_2 \cdot q_1) \cdot e_f + u_i \tag{5.37}$$

$$\dot{p}_2 = q_2 \cdot (e_1 + T_c \cdot e_2) \cdot e_1 - \varepsilon \cdot (p_2 - g_p') - \mu_5 \tag{5.38}$$

where

$$\begin{gathered} \underline{e}_2 \triangleq G_d(s)\, \underline{e}_1 \\ e_1 \triangleq q_1 \cdot e_f \,, \qquad q = q_1^3 \cdot q_2 \,, \qquad g_p' = \frac{g_p}{q_1} \,, \end{gathered} \tag{5.39}$$

and μ_5 is given by (5.27). The block diagram of this controller is shown in Fig. 5.9.

Even though the system (5.37)-(5.39) is very similar to the previously described SVS controllers, it was not possible to use the same Liapunov methods to prove stability. This is due to the absence of the stabilizing factor $p \cdot y$, in equation (5.38), which was introduced in the modified SVS algorithm in order to substitute for the unobserved states. For that reason, the theory of input-output (I/O) stability for nonlinear systems was used instead. Even then, a truly

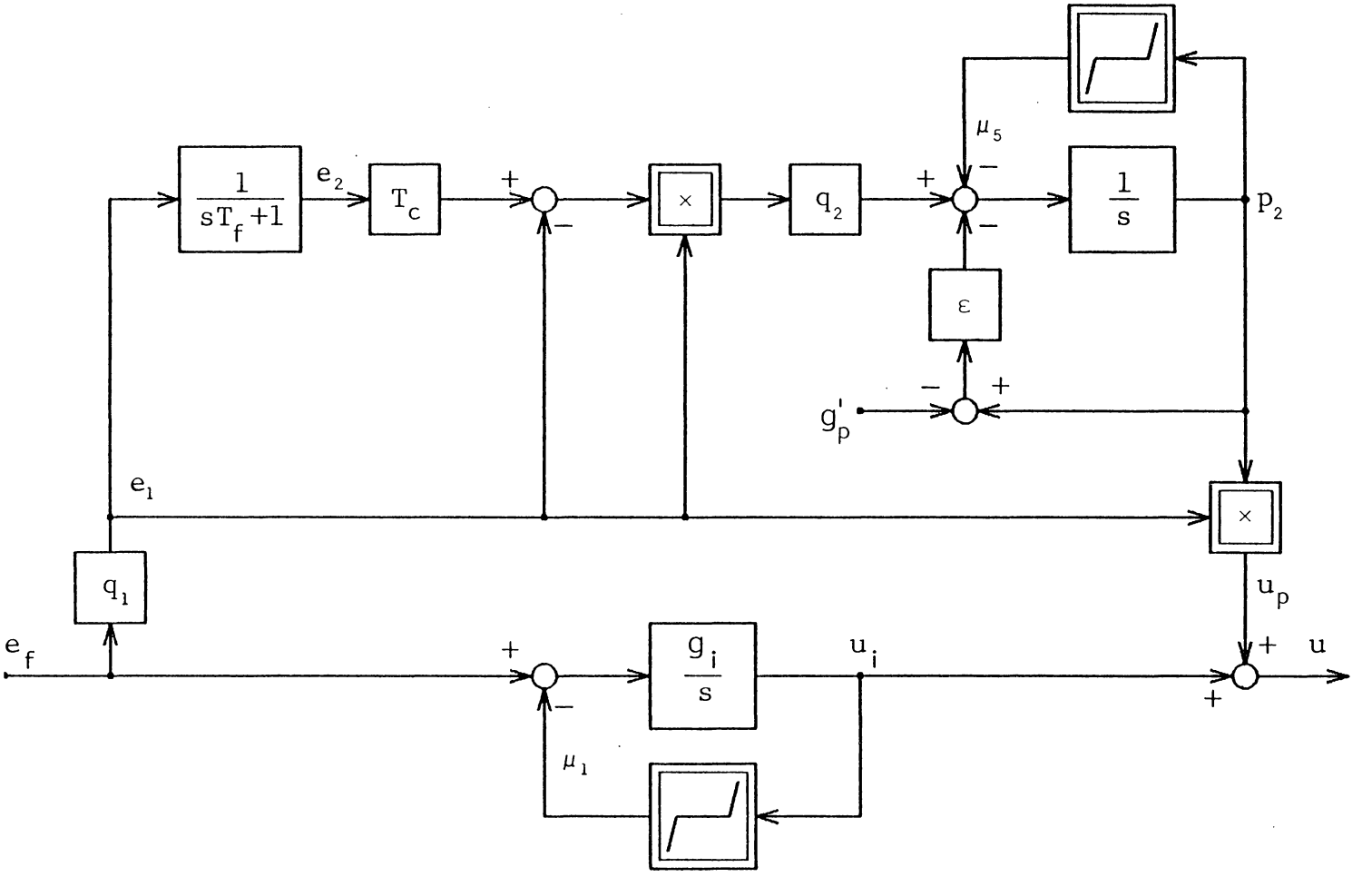

Fig. 5.9: Sliding API (SAPI) controller.

global result could not be obtained. Two assumptions, which reflect the conditions present in the practical systems had to be made.

First, due to the physical limitations, variables e_1 and e_2 in Fig. 5.9 do not take infinite values, but always belong to some restricted domain. This is explicitly accounted for, by placing the saturation-type limits in the controller, as shown in Fig. 5.10.

The second assumption deals with the influence of the plant input saturation, and limiting functions μ_1 and μ_5, on the stability. The system in Fig. 5.10, in which these nonlinearities are not present, is identical to the system in Fig. 5.9 for very small perturbations around steady state. Therefore, if the system in Fig. 5.10 is globally asymptotically stable, the system in Fig. 5.9 is at least locally asymptotically stable.

Using the small gain theorem from the theory of I/O stability [13, 39], it is proved in Appendix D.1 that the system in Fig. 5.1a, with the controller shown in Fig. 5.10, and with $G_c(s)$, $G_f(s)$ and $G_d(s)$ given by (5.14), (5.29) and (5.34) respectively, is globally asymptotically stable provided that

i) $q_1 > 0$, $q_2 > 0$, $\varepsilon > 0$;

ii) the constant gain subsystem, defined as

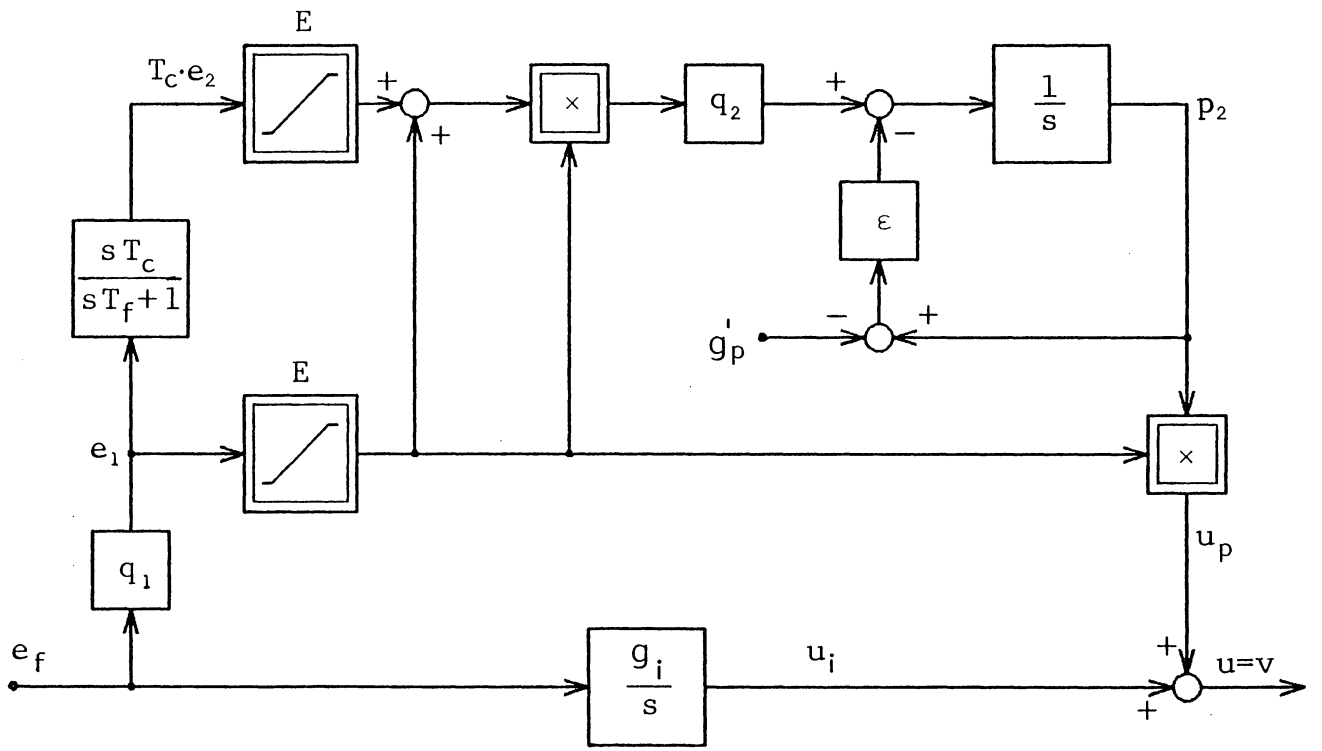

Fig. 5.10. Simplified structure of the SAPI controller used in the I/O proof of stability.

$$G_1(s) \triangleq \frac{\underline{e}_f}{\underline{u}} = \frac{G_s(s)\cdot G_f(s)}{1 + G_s(s)\cdot G_c(s)\cdot G_f(s)} \qquad (5.40)$$

has all poles with negative real part;

iii)

$$q_1 < 1/(\sqrt{2}\cdot E\cdot F_m) \qquad (5.41)$$

$$q_2 < \varepsilon/(\sqrt{2}\cdot E) \qquad (5.42)$$

where F_m is the maximum absolute value of the function

$$F(j\omega) = G_1(j\omega)\cdot[1 + T_c^2\cdot|G_d(j\omega)|^2]^{\frac{1}{2}} \quad . \qquad (5.43)$$

Several remarks can be made about this result. First, as already mentioned, the statement assures only the local stability of the original SAPI control system with the controller in Fig. 5.9. Second, when the conditions (i)-(iii) are evaluated numerically, impractically conservative bounds on the gains q_1 and q_2 are obtained.

Nonetheless, the result is very important theoretically for several reasons. It indicates that the stability of the constant gain PI control subsystem is an important requirement for the overall stability. From (5.41) and (5.43), it follows that the product of the adaptation gain and the maximum gain of the linear subsystem, has an upper bound, which

can be useful in design. Most important, the result shows that there exists a region of stable operation, which justifies the use of approximate methods (like describing functions) for the estimation of maximum allowable gains, and the region of stability.

5.3.2. DESCRIBING FUNCTION ANALYSIS: The nonlinear parts of the controller in Fig. 5.9, which were omitted in the I/O proof of stability, are the plant input saturation, and the limiting functions μ_1 and μ_5. With such nonlinearities, instability is usually manifested through the existence of a limit cycle. An appropriate method of investigating this possibility is the method of harmonic balance, or describing functions. In order to derive the describing function for the system in Fig. 5.9, some simplifications have to be made.

Let us consider the original SAPI controller, given by (5.36). It was explained in the Section 5.1 that in the input limit mode of operation, the proportional component of control, u_p, is equal to either U_m or $-U_m$, while the integral component u_i is equal to zero. After leaving the input limit mode, the plant input is not in saturation, and $\mu_1=\mu_5=0$. In this region the system is stable according to the proof of I/O stability, unless it again enters the input limit mode. Therefore, the only way for the limit cycle to exist, is that the proportional component u_p oscillates between U_m and $-U_m$. The existence of a limit cycle is even

more probable if the limiting function μ_5 is replaced by the saturation function at the output of the proportional part of the controller, as shown in Fig. 5.11. Therefore, if the conditions for existence of the limit cycle for the controller in Fig. 5.11 are not satisfied, it is even less probable that the limit cycle will exist in the original SAPI control system.

In Appendix D.2, describing function relating u_p and e_f in Fig. 5.11, for the frequences of

$$\omega > 10 \cdot \varepsilon \tag{5.44}$$

is shown to be given by the following set of equations:

$$N(a,\omega) = g_p + P(a,\omega) \tag{5.45}$$

$$P(a,\omega) = f_1(\rho) \cdot (g_p + p_0) - g_p + f_1(\rho) \cdot \frac{a_p}{2} \cdot \exp(j\phi_p) \ , \tag{5.46}$$

where

$$p_0 = \frac{q \cdot a^2 \cdot g_z(\omega)}{2 \cdot \varepsilon} \cos[\phi_z(\omega)]$$

$$a_p = \frac{q \cdot a^2 \cdot g_z(\omega)}{2 \cdot (4 \cdot \omega^2 + \varepsilon^2)^{\frac{1}{2}}}$$

$$\phi_p = \phi_z(\omega) - \tan^{-1}(2\omega/\varepsilon) \tag{5.47}$$

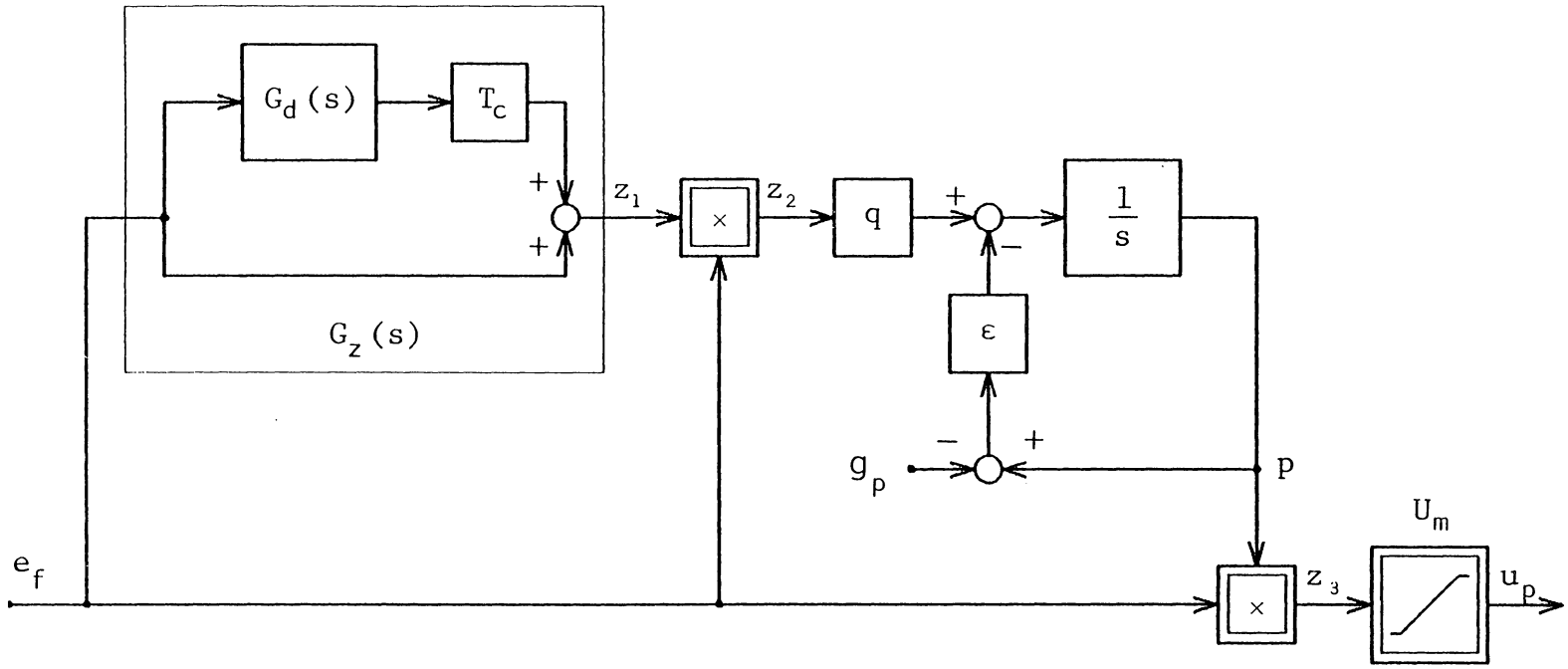

Fig. 5.11. Modified structure of the SAPI controller used in the derivation of the describing function.

$$G_z(j\omega) \triangleq 1 + T_c \cdot G_d(j\omega) \triangleq g_z(\omega) \cdot \exp[j\phi_z(\omega)]$$

$$\rho = \frac{U_m}{a \cdot a_3}$$

$$a_3 = [(p_0 + g_p)^2 + a_p \cdot (p_0 + g_p) \cdot \cos(\phi_p) + (a_p/2)^2]^{\frac{1}{2}} \quad ,$$

and $f_1(\rho)$ is the describing function of the unit saturation function given in (B.7).

The block diagram of the original SAPI control system, with the nonlinear part represented by the describing function is shown in Fig. 5.12a. From $N(a,\omega)$ in (5.45) it is obvious that g_p and g_i/s can be again combined to form the constant gain PI controller $G_c(s)$. The resulting system is shown in Fig. 5.12b.

Finally, using the harmonic balance method (Atherton [2, pp. 114-116]), a limit cycle of amplitude a, and frequency ω may exist if the following equation is satisfied

$$G_1(j\omega) = - \frac{1}{P(a,\omega)} \quad , \qquad (5.48)$$

where $G_1(j\omega)$ is the transfer function of the linear part in Fig. 5.12b, and it is same as the one given by (5.40). It is convenient to test the condition (5.48) graphically, in the complex plane. The linear transfer function $G_1(j\omega)$ is relatively easy to calculate, and/or measure, as a func-

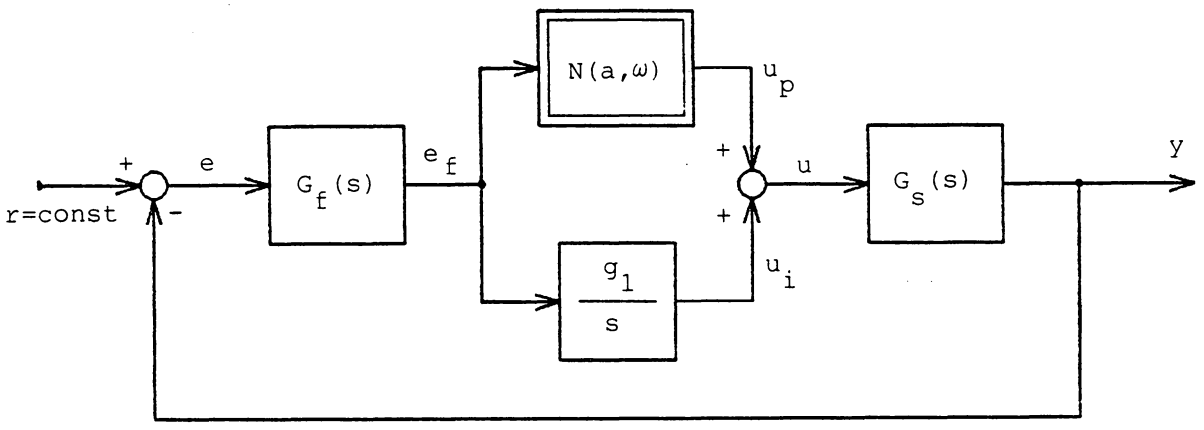

a)

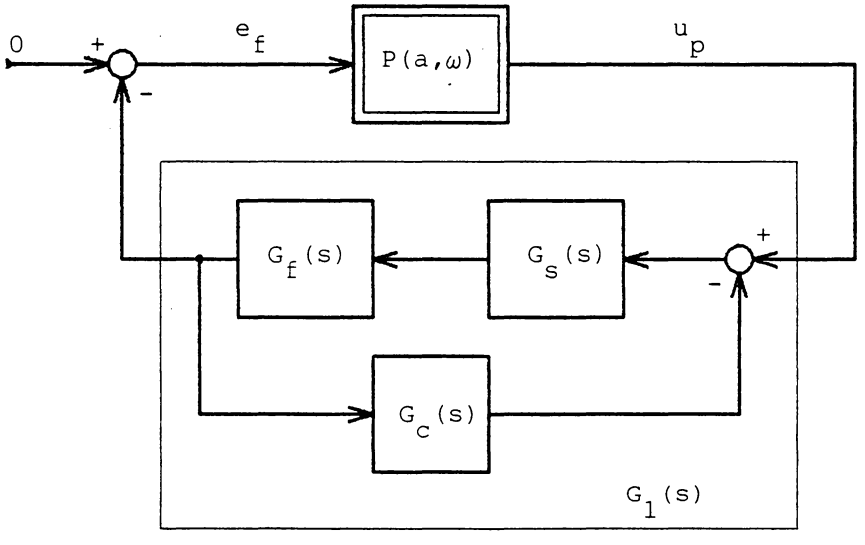

b)

Fig. 5.12. SAPI control system with the nonlinear part represented by a describing function.

a) Using $N(a,\omega)$ from (5.45)

b) Using $P(a,\omega)$ from (5.46)

tion of frequency. Then its Nyquist plot can be drawn in the complex plane.

Function $-1/P(a,\omega)$, given by (5.46) and (5.47) is quite cumbersome. However, being in the closed form it is an easy task to program it on a digital computer. Since $P(a,\omega)$ is a complex function of two variables, $-1/P(a,\omega)$ is represented in the complex plane as a family of curves for varying a, with ω as the running parameter, or vice versa. It is of interest to find the region in the complex plane where this family of curves is located, if such bounded region exists. Then if the Nyquist plot of $G_1(j\omega)$ lies completely outside that region, the condition (5.48) cannot be fulfilled, and a limit cycle most probably will not exist.

The calculation of the function $-1/P(a,\omega)$ from equations (5.46) and (5.47) has been programmed on a computer. It has been found that for any given ω, the function $-1/P(a,\omega)$ is contained within the third quadrant of the complex plane. As the amplitude a increases from zero to infinity, the function $-1/P(a,\omega)$ changes from $-(\infty+j\infty)$ to some finite value, close to the origin, and then decreases again. Therefore, the region of the complex plane which contains all the points of $-1/P(a,\omega)$ lies below the negative real axis and to the left of the boundary function $C(\omega)$. With the parameter values which are given in (5.51)-(5.58) below, the boundary function $C(\omega)$ for $\omega/(2\pi) > 2$ kHz is shown in Fig. 5.13, and the the region of

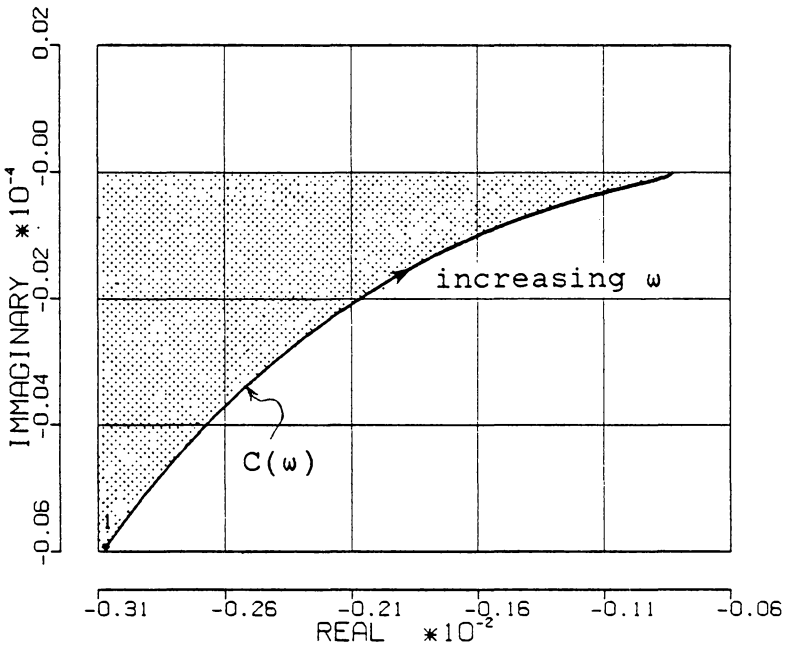

Fig. 5.13: Region of the complex plane which contains all the points of $-1/P(a,\omega)$ for $a > 0$ and $\omega/(2\pi) > 2$ kHz . The region extends to infinity, below the negative real axis, and to the left of $C(\omega)$.

the complex plane which contains $-1/P(a,\omega)$ for $a > 0$ is indicated by shading.

5.3.3. CONTROLLER OPERATION: The operation of the SAPI controller, and the ways for selecting the adaptation gain q, will be illustrated on a somewhat abstract example. The example is chosen so that the salient features of the operation can be easily observed.

Let us apply the controller from Fig. 5.9 to the current driven dc motor given in Appendix A.2, in a closed loop arrangement shown in Fig. 5.1a. Since the controller was derived from the SLM control, the similar problems may be expected in implementing it. These problems, as pointed out in Chapter 3, are the estimation of the speed derivative e_2/q_1 , and the resulting current chattering. In order to prevent the onset of these problems, in this example the armature current control parameters are changed to

$$L = 1 \text{ mH} \quad , \quad g_a = 20 \quad , \tag{5.49}$$

and the filter time constant is decreased to

$$T_f = 10 \ \mu s \quad . \tag{5.50}$$

This value is unrealistic in most applications, but it allows us to theoretically investigate the case when the speed derivative can be estimated with very small error.

The current limit is set to a round value of

$$I_m = 4\ A = U_m \quad . \tag{5.51}$$

With the rest of the motor drive parameters being the same as in Appendix A.2, from (A.6), (5.28) and (5.34) we have

$$G_s(s) = \frac{360 \cdot 10^3}{(s + 0.36)(s + 22 \cdot 10^3)} \tag{5.52}$$

$$G_f(s) = \frac{10^5}{s + 10^5} \tag{5.53}$$

$$G_d(s) = \frac{10^5 \cdot s}{s + 10^5} \quad . \tag{5.54}$$

If the PI controller parameters are chosen, close to ones given in (2.3), as g_p=20 and g_i=5000, we have from (5.14)

$$G_c(s) = 20 \cdot \frac{s + 250}{s} \quad . \tag{5.55}$$

The dominant time constant of the closed loop system in the transition mode, is chosen as

$$T_c = 2\ ms \quad . \tag{5.56}$$

The parameter ε has the same effect as in the SVSPI control, i.e. it determines the rate at which the system settles to the steady state in the integral action mode. Since this final part of the transient should not be much slower than the response in the transition mode, the reasonable choice of ε, considering $1/T_c = 500$ rad/s , may be

$$\varepsilon = 100 \text{ rad/s} \quad . \tag{5.57}$$

The initial estimate of the values of adaptation gains q_1 and q_2 can be obtained by using the relations (5.41) and (5.42) from the conditions for I/O stability. However, the results are very conservative. With the smallest physically justifiable value for the error limit E in Fig. 5.10, the values that are obtained are $q_1 \approx 10$ and $q_2 \approx 50$. From (5.39) this gives the value of the total adaptation gain of $q \approx 5 \cdot 10^4$. For this reason, the gain values were selected such that the total adaptation gain is close to the one used in SVSPI control, (5.29). Therefore,

$$q_1 = 100 \quad , \qquad q_2 = 500 \quad ,$$

which gives

$$q = q_1^3 \cdot q_2 = 5 \cdot 10^8 \quad . \tag{5.58}$$

With these values, the system was analyzed and simulated. Function $G_1(j\omega)$ is calculated by substituting (5.52), (5.53) and (5.55) into (5.40). The Nyquist diagram of $G_1(j\omega)$ is plotted in Fig. 5.14a together with the describing function boundary $C(\omega)$. The details around the origin from Fig. 5.14a are shown in Fig. 5.14b, together with the sample plot of the describing function $-1/P(a,\omega_2)$, for $\omega_2/(2\pi) = 7475$ Hz. It is easily observed that, although huge q was used, the condition for the existence of a limit cycle is not satisfied.

The whole control system has also been simulated in the time domain. The system response to small step change in speed command from Fig. 2.3b, and the step change in load from Fig. 2.3c, is shown in Fig. 5.15a. The state plane trajectory of the response to the step command, is shown in Fig. 5.15b. As can be observed, the system is in saturation (i.e., moving as fast as possible) until the line with the slope $-1/T_c$ is reached. From that point, the system behaves as a first order system with a time constant T_c.

Now, suppose that the control system remains unchanged, but that the motor inertia is decreased 2.5 times. (This is physically impossible for the experimental motor we are using, but may represent a model of a motor with 2.5 times larger torque-to-inertia ratio). The plant transfer function is then

b)

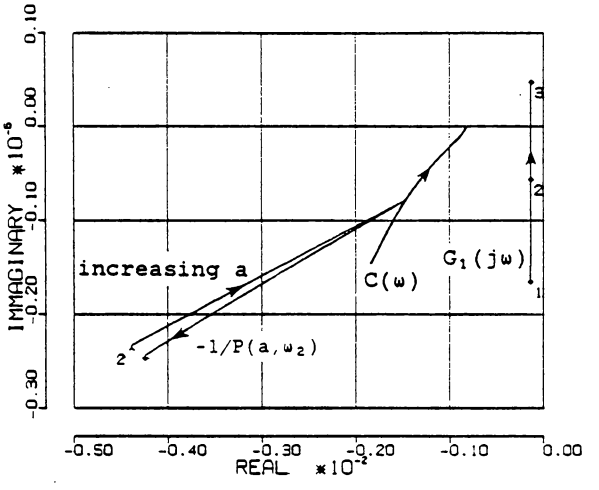

$\omega_1 = 2\pi$ 7400 rad/s

$\omega_2 = 2\pi$ 7475 rad/s

$\omega_3 = 2\pi$ 7550 rad/s

a)

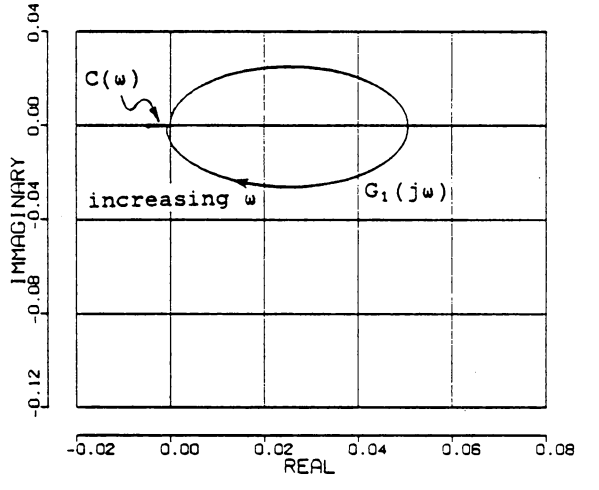

Fig. 5.14: Complex plane diagrams for the describing function analysis of SAPI control system.

a) Nyquist plot of $G_1(j\omega)$ for $\omega > 0$, and plot of the describing function boundary $C(\omega)$ for $\omega/(2\pi) > 2$ kHz .

b) Detail around origin from Fig. a): plots of

- $G_1(j\omega)$ for $\omega_1 < \omega < \omega_3$
- $C(\omega)$ for $\omega/(2\pi) > 5$ kHz
- $-1/P(a,\omega)$ for $\omega = \omega_2$

a)

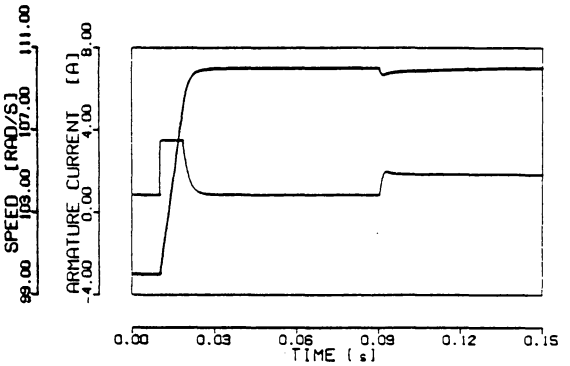

b)

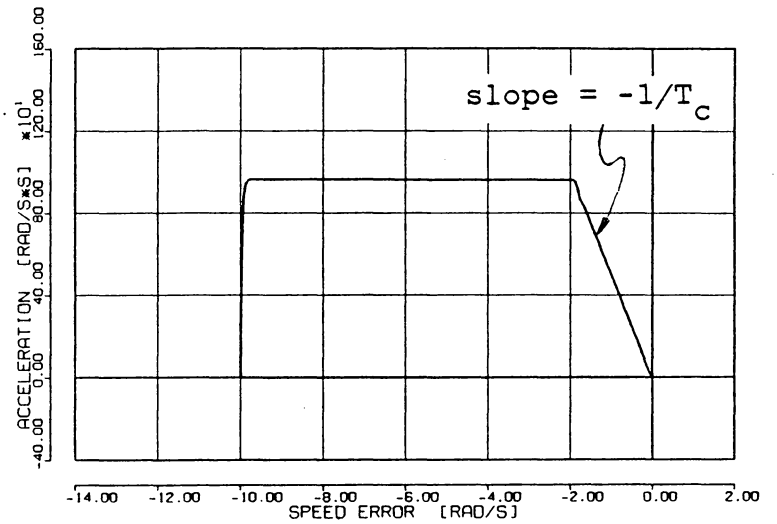

Fig. 5.15: Transient response of the SAPI control system with the nominal plant parameters.

a) Time domain response for the inputs from Figures 2.3b and 2.3c.

b) State plane trajectory for the input from Fig. 2.3b.

$$G_s(s) = \frac{2.5 \cdot 360 \cdot 10^3}{(s + .91)(s + 22 \cdot 10^3)} \qquad (5.59)$$

while the describing function remains unchanged. The Nyquist diagram, transient response, and the state plane trajectory of the new system are shown in Fig. 5.16. The conditions for the existence of a limit cycle are again not satisfied, but a short oscillatory period - or equivalently nonideal sliding mode - is present during the transition mode of operation. The transient response is still dominantly single-time-constant, and unlike in the SLM control, the chattering disappears in steady state.

If the moment of inertia is further decreased, so that it is 10 times lower than the original one, the plant transfer function is

$$G_s(s) = \frac{10 \cdot 360 \cdot 10^3}{(s + 3.6)(s + 22 \cdot 10^3)} \quad . \qquad (5.60)$$

Diagrams characterizing this system are shown in Fig. 5.17. It is obvious from the Nyquist diagram, that the existence of a limit cycle is now very likely. Indeed, the time response and the state plane trajectory show that the nonideal sliding mode is now present. If this is undesirable it can be avoided by decreasing the gain q. However, if the sliding mode behavior is acceptable, the armature current fluctuation can be reduced by further increasing the armature inductance.

a)

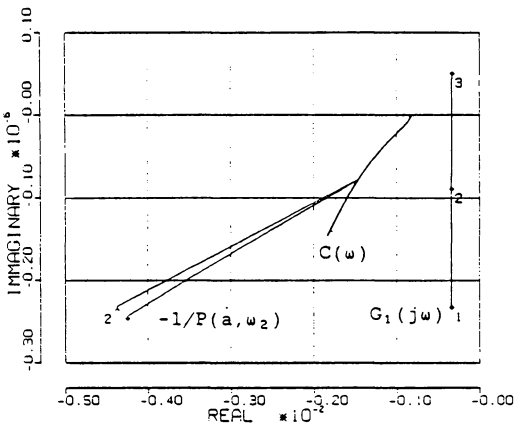

$\omega_1 = 2\pi$ 7450 rad/s

$\omega_2 = 2\pi$ 7490 rad/s

$\omega_3 = 2\pi$ 7530 rad/s

b)

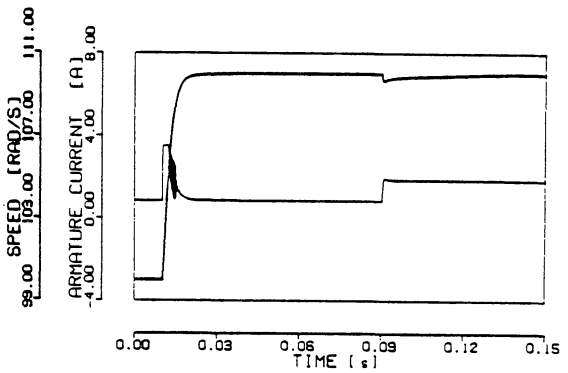

c)

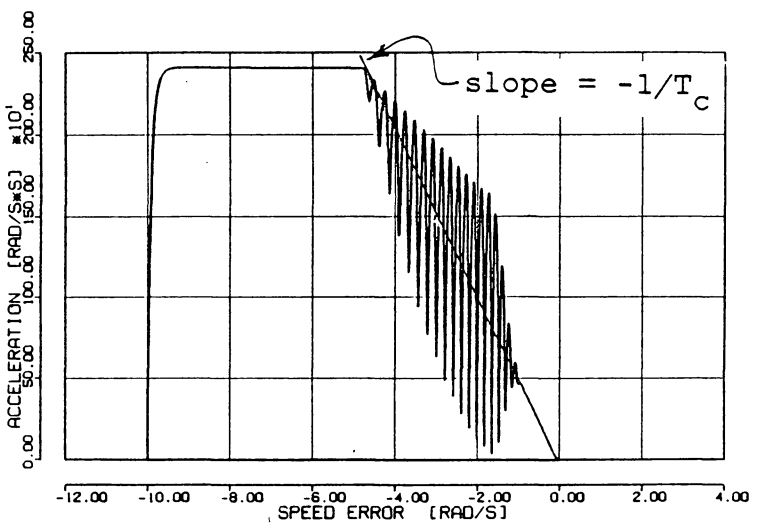

Fig. 5.16: Characteristics of the SAPI control system with the moment of inertia decreased 2.5 times.

a) Complex plane diagrams.
b) Time domain transient response.
c) State plane trajectory

a)

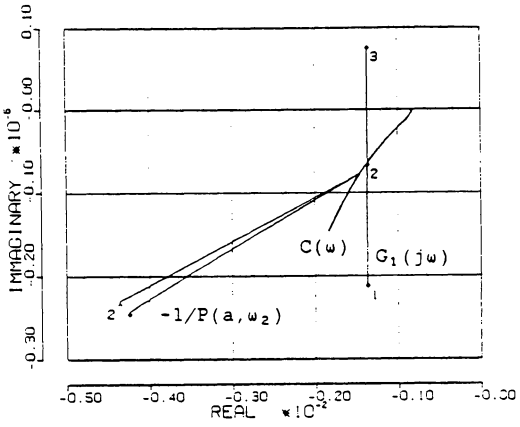

$\omega_1 = 2\pi$ 7500 rad/s

$\omega_2 = 2\pi$ 7510 rad/s

$\omega_3 = 2\pi$ 7520 rad/s

b)

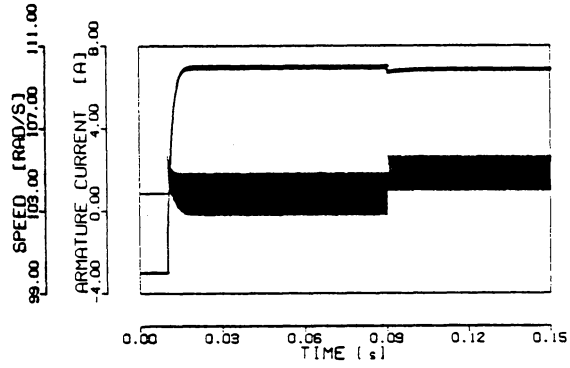

c)

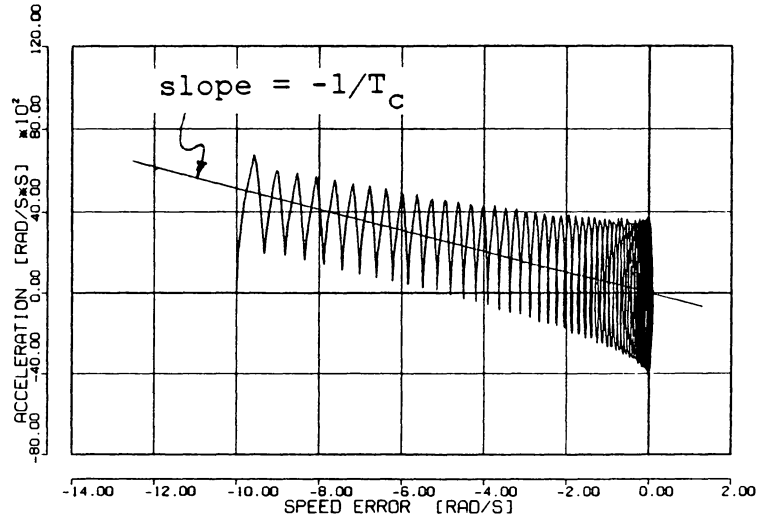

Fig. 5.17: Characteristics of the SAPI control system with the moment of inertia decreased 10 times.

a) Complex plane diagrams.
b) Time domain transient response.
c) State plane trajectory.

The SAPI control has also been implemented and simulated for the speed control of the same current driven dc motor, as was the SVSPI controller. Therefore, the same constant gain subsystem, given by (2.2)-(2.4), is used. From (2.2), the filter time constant is $T_f = 0.5$ ms , so that the nonideal differentiator $G_d(s)$ in (5.39) is then specified. The adaptive controller parameters were chosen through simulations, and the following values were finally used:

$$T_c = 2 \text{ ms}, \quad \varepsilon = 200 \text{ rad/s}, \quad q_1 = 100, \quad q_2 = 100. \qquad (5.61)$$

The system transient response is shown in Fig. 5.18. High amplitude oscillations of the armature current can be observed in the transition mode. They correspond to the nonideal sliding mode in the previous examples. The larger amplitude and lower frequency, are caused by the larger phase lag which is now present in the output filter and differentiator. This control system is further compared with other algorithms, in the next chapter.

* * *

This chapter has illustrated that it is feasible to achieve a high-gain adaptive controller which has fast transient response, zero steady-state error, and excellent disturbance rejection. The resulting adaptive PI control

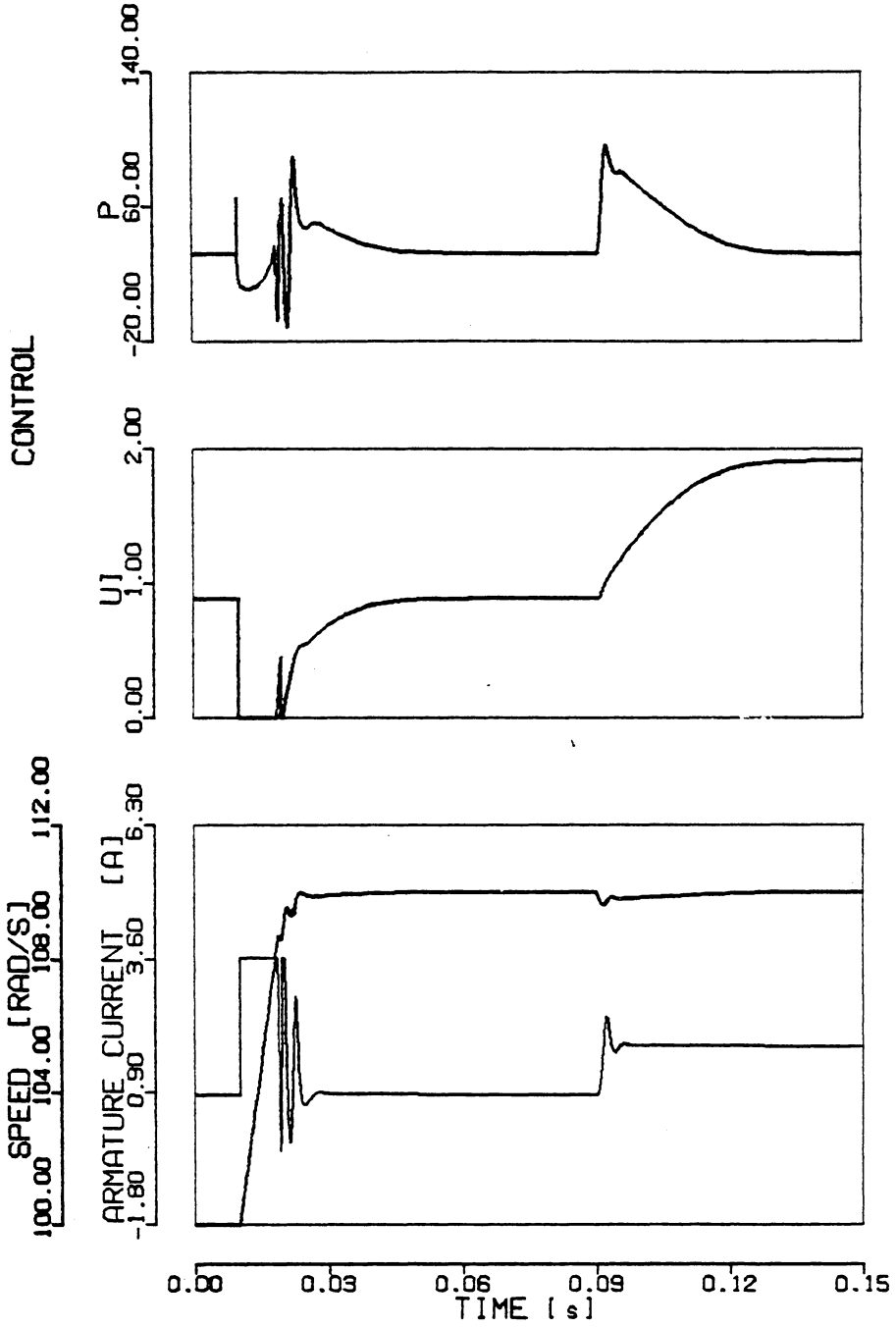

Fig. 5.18: Transient response of the SAPI control system, for the same plant parameters as used in the examples of VLPI and SVSPI control systems. The controller parameters are given in (2.3) and (5.61).

algorithm has nonoscillatory transient response in the SVS design, and may have somewhat oscillatory response in the sliding-adaptive case. The controller has the structure, operation and properties between those of the VLPI control and the SLM control. However, the two are not merged by simply switching between the algorithms (as was done, e.g., in [58]), but through the original use of the soft variable structure concept, thus guaranteeing stability and well behaved operation.

Chapter 6

PERFORMANCE COMPARISON

In previous chapters several different control algorithms were described. All of them were implemented for the speed control of either a current or voltage driven dc motor. Some were implemented also experimentally. The common objectives in all designs were accuracy, fast transient response, and robustness to parameter variations. Accuracy and fast transient response were demonstrated for each algorithm in corresponding chapters. However, robustness was only implied by the stability proofs and the fact that in all algorithms, exceptionally large gains had been used. The purpose of this chapter is to comparatively demonstrate the robustness of the algorithms for large changes of plant parameters.

All the algorithms studied are nonlinear. Furthermore, due to large gains, the plant is also forced to operate in the nonlinear region. Finally, we are interested in the robustness to large parameter variations. Therefore, none of the sensitivity results for linear systems that are

available [40, 60, 80] can be applied. This situation has forced us to assess the robustness of the algorithms by examining their transient response and disturbance rejection obtained through simulations and/or experiment, for varying plant parameters.

Algorithms implemented for the voltage controlled drive are presented in the first, whereas the algorithms used with the current controlled drive are examined in the second section.

In order to facilitate the comparison all variables are normalized with respect to the following base quantities

$$\omega_B = 100 \text{ rad/s} \quad , \qquad i_B = I_m/2 = 1.8 \text{ A}$$

$$t_B = \frac{R \cdot J}{k_m^2} \quad , \qquad T_\ell = 0.036 \text{ N}\cdot\text{m} \quad . \tag{6.1}$$

where R, k_m and nominal value of J are given in (A.2). Base quantity for time t_B, was changed accordingly, when the total moment of inertia was changed.

6.1. VOLTAGE CONTROLLED DRIVE

The control algorithms that were applied to the voltage driven dc motor are:

- I-P control with fixed integrator limits (Section 2.2),
- sliding mode control (Chapter 3),
- modified soft variable structure control (Chapter 4).

The motor model used for the first and third algorithm is given in Appendix A.2, and the model used for SLM control is given in Appendix A.4. Even though different models were used, plant structure is the same and is shown in Fig. A.2. Nominal plant parameter values are those given in (A.2), with the exception of the SLM control, where the choke of 5 mH was added in the armature circuit. The controller parameters for the I-P control are given in (2.13), (2.15) and (2.17), for the SLM control in (3.25), and for the modified SVS control in (4.29).

In the linear region, the transfer function of the plant (i.e., motor and the output filter) is given by (A.12). From the transfer function it follows that the influence of all plant parameters can be examined by varying just three of them. Since the electrical time constant T_e is not dominant in I-P and SVS control, only the changes in K_v, T_f and T_m need to be examined. In the SLM control, the electrical time constant becomes important due to addition of the choke in the armature circuit. However, from the discussion in Section 3.2, it is obvious that actually only the ratio T_f/T_e

is important, the influence of which may be studied again through the change in T_f.

As was described in the respective sections, all three controllers were designed, simulated and experimentally tested. Simulation test inputs are shown in Fig. 6.1a, and the experimental test signal is shown in Fig. 6.1b. Due to the unavailability of the apparatus for abrupt torque loading of the motor, only the response to the step in reference command was tested experimentally.

The responses of the three control systems, with the plant having nominal values, are shown in Fig. 6.2. It may be observed that very fast transient response has been achieved for all three control laws.

The systems' responses, when the output filter time constant was increased two times, are shown in Fig. 6.3. The most significant change can be observed in the response of the SLM control system, where a considerable increase in the amplitude of chattering appeared.

The influence of a twofold increase in the power amplifier gain g_a (and therefore in K_v), is illustrated in Fig. 6.4. From simulation result it could be concluded that the I-P control responded also reasonably well to this large change. However, the system was very oscillatory in the experiment. Combined influence of several factors may be the cause for this discrepancy. First, the "limited field of view" nonlinear characteristic (Fig. 2.7) is extremely se-

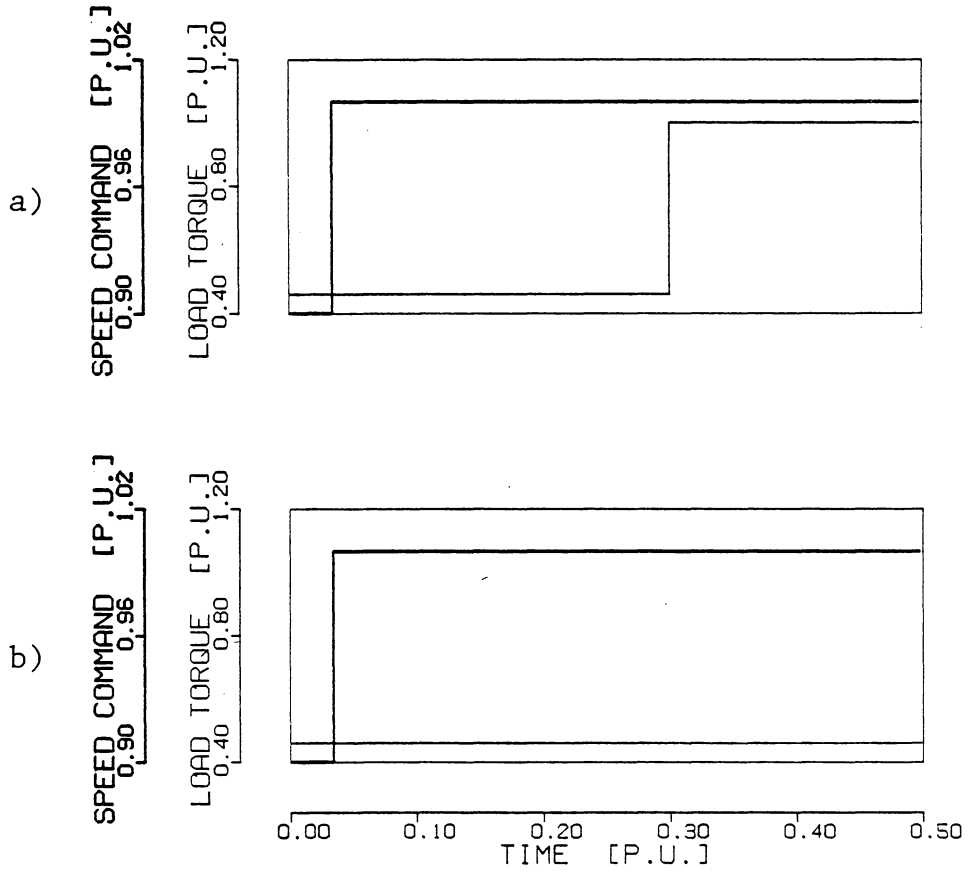

Fig. 6.1: Test inputs,

a) used in simulation;

b) used in experiment.

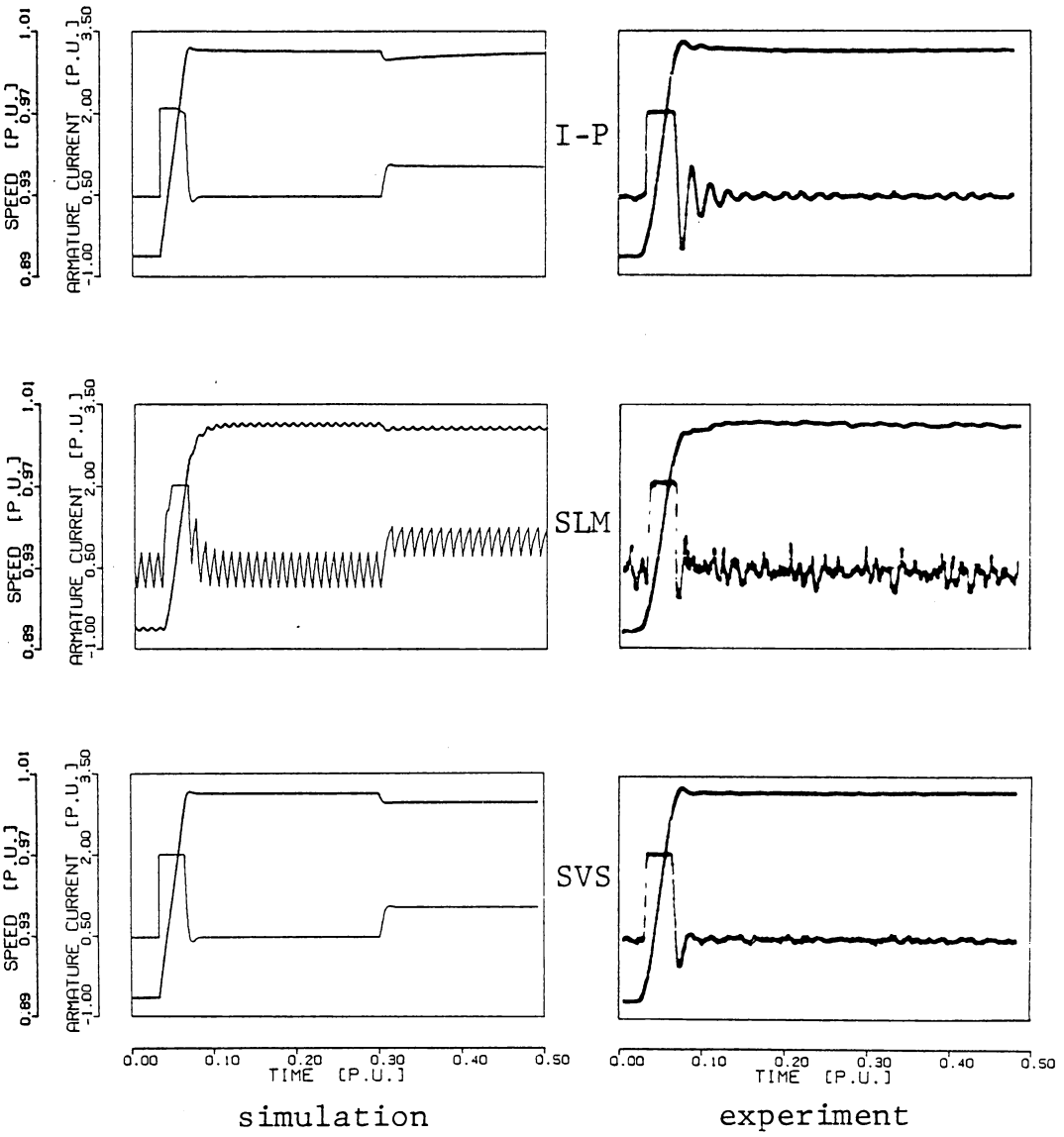

Fig. 6.2: Transient responses of the motor control systems, with the nominal plant parameters.

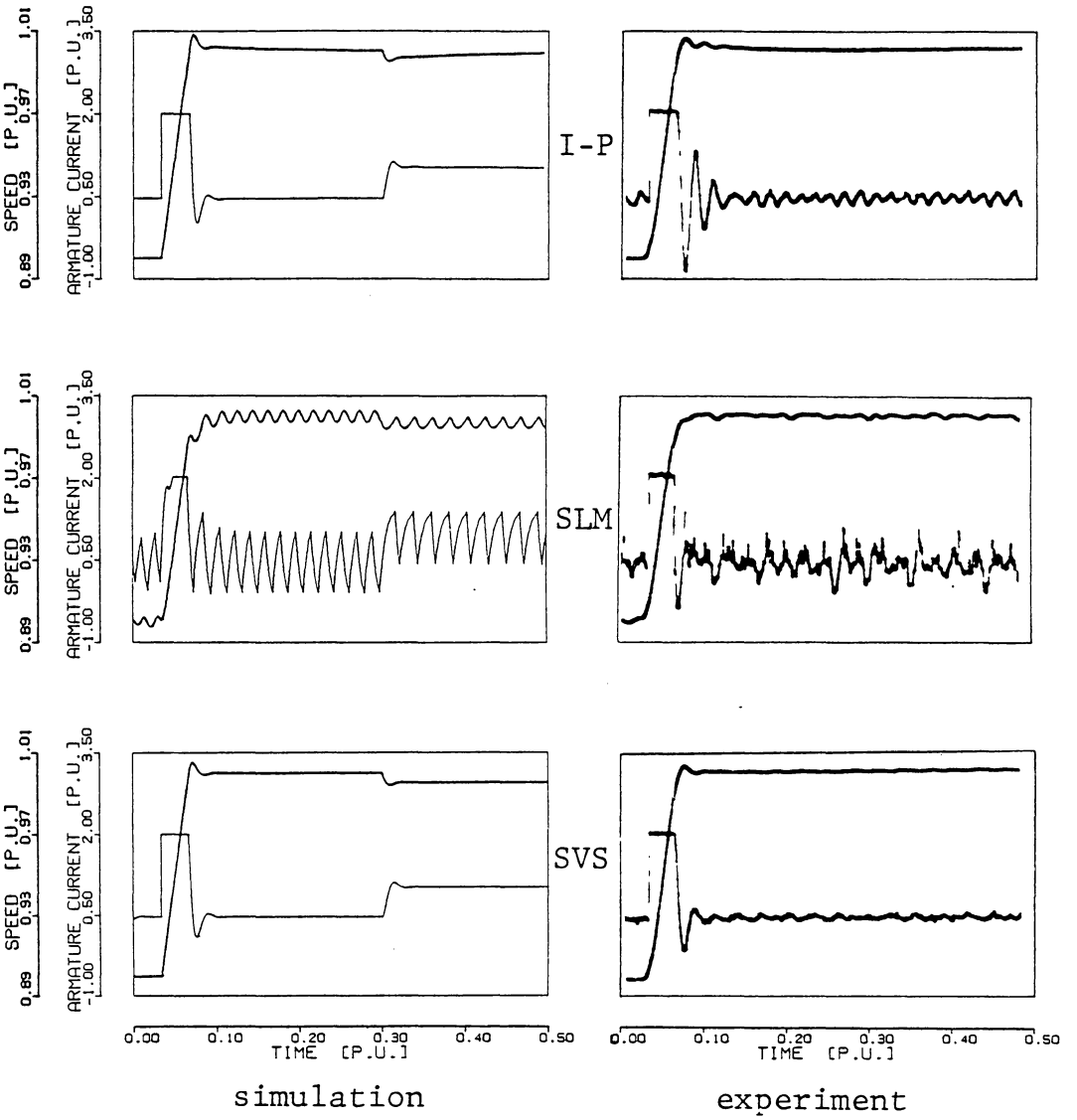

Fig. 6.3: Transient responses of the motor control systems, with the filter time constant T_f increased 2 times.

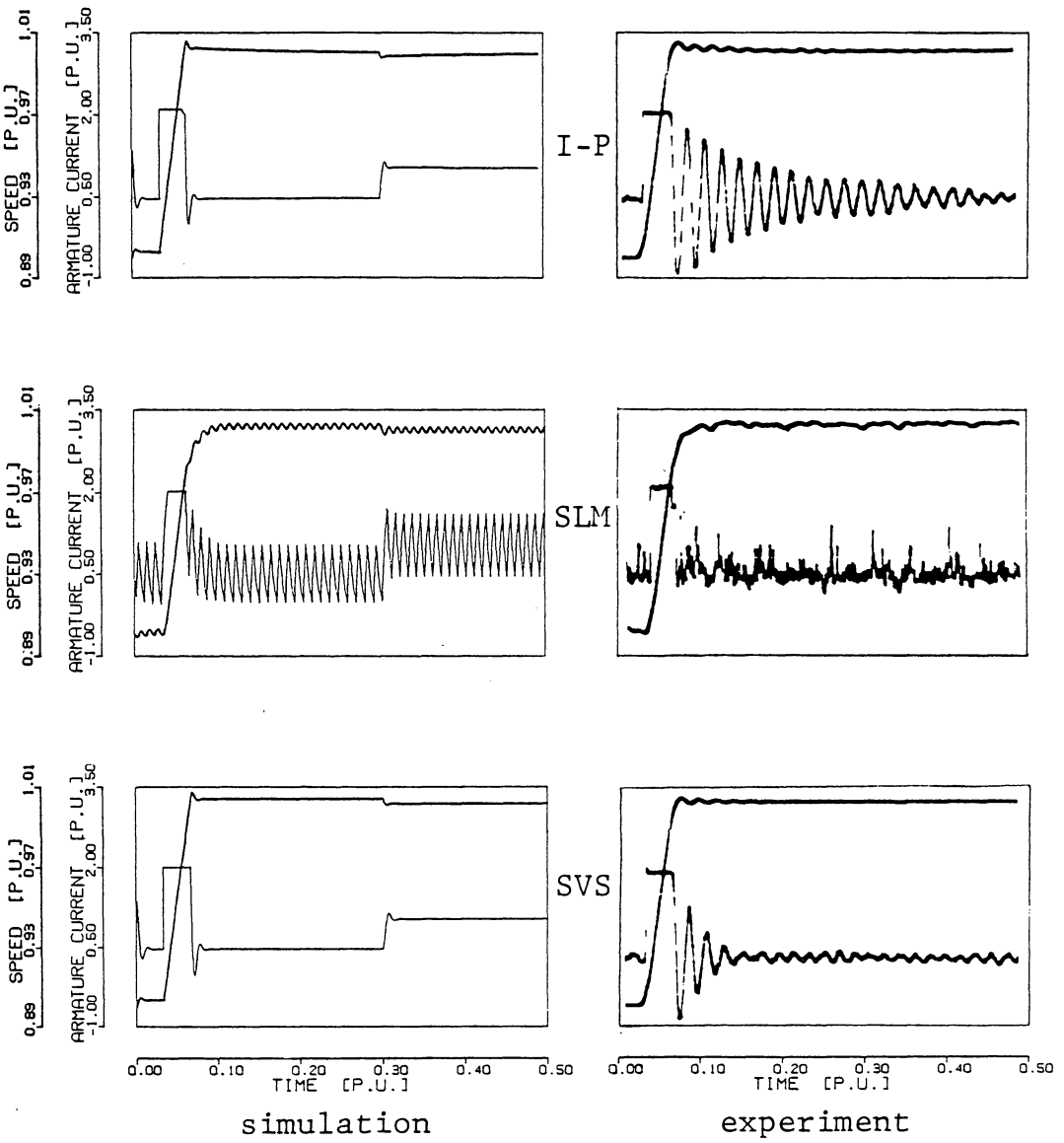

Fig. 6.4: Transient responses of the motor control systems, with the gain K_v increased 2 times.

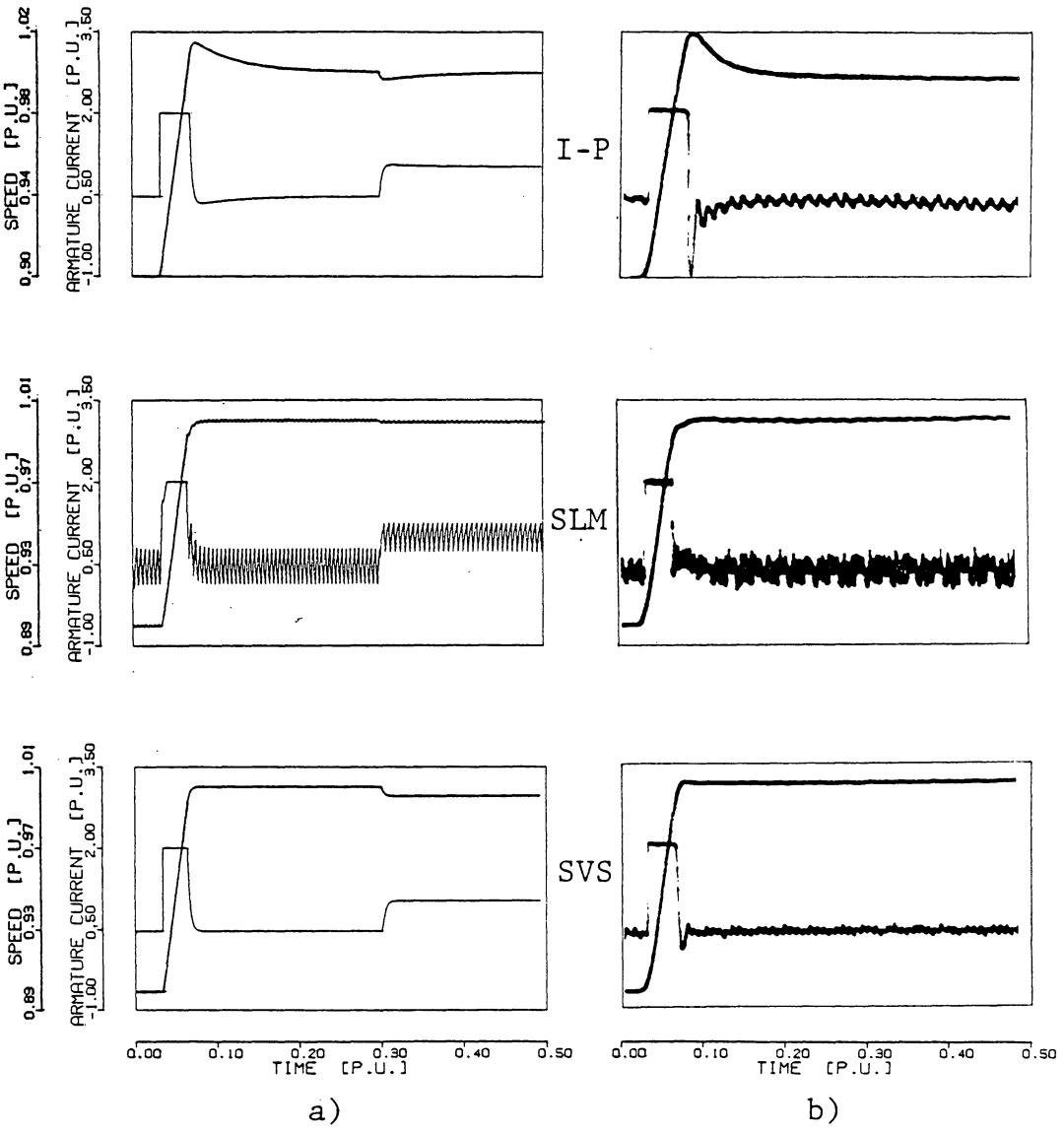

Fig. 6.5: Transient responses of the motor control systems.

a) Simulation with the moment of inertia increased 2 times.

b) Experiment with the moment of inertia increased 3 times.

vere, and its experimental implementation has many parasitic elements (finite negative gain, diode capacitances, etc.). Also, the plant itself, has higher order effects which were neglected in simulation (finite amplifier bandwidth, mechanical and amplifier nonlinearities, etc.). These oscillations show that, although this algorithm may be theoretically viable, it has serious practical limitations.

In Fig. 6.5 the response of the control systems, with the increased moment of inertia (and therefore T_m), is shown. It may be observed that I-P control, although still stable, departed strongly from the required performance. The SVS control became somewhat slower, while there is almost no difference in the SLM control response.

In order to quantify, at least to some extent, the results presented, six performance characteristics are defined. They are:

e_s - steady state error

t_{sr} - settling time to command change

ov_r - overshoot to command change

t_{st} - settling time to load torque change

ov_t - overshoot to load torque change

p_{ds} - relative increase in the steady state power dissipation.

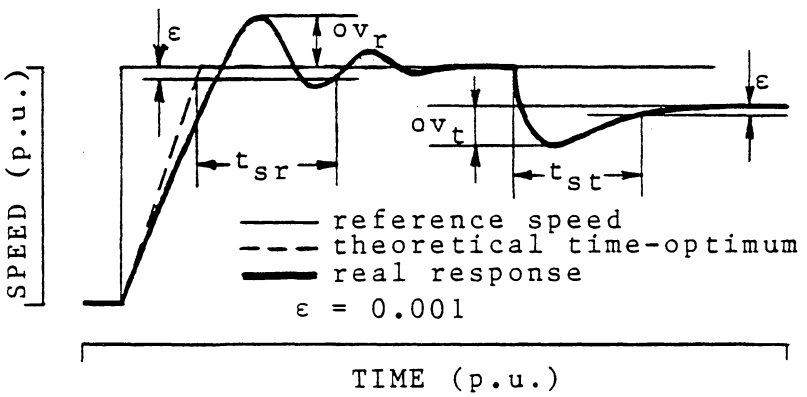

Fig. 6.6: Definitions of the transient performance characteristics.

Definitions of the settling times and overshoots are clear from Fig. 6.6.

Steady state error is defined as the maximum absolute value of the difference between the reference speed and the actual speed, for any steady state operating speed and load torque in the range between zero and two times the base values from (6.1).

Steady state power dissipation is increased only for the SLM control, due to the chattering. Therefore, p_{ds} is defined as the increase in power dissipation relative to the minimum possible power dissipation, at rated speed and half of the rated torque.

Since all quantities are normalized, the performance characteristics are relative to the base values (6.1), and are expressed as percentages.

These performance characteristics were evaluated from simulations, first for the nominal plant parameters for each control algorithm, and then reevaluated for all three variations of the parameters that were simulated. The results are given in Table 6.1.

From the obtained results, the following general remarks can be made about the quality of performance.

TRANSIENT RESPONSE: SVS control has the fastest transient response, with the overshoot within its steady state error. SLM control, contrary to the previous assertions [34] can be

Table 6.1: Performance characteristics of the three control laws for different parameter values. All entries are in %.

Parameters	Control	e_s	t_{sr}	t_{st}	ov_r	ov_t	p_{ds}
Nominal	I-P	0.0	5	16.4	0.26	0.40	0
	SLM	0.24	5	5.1	none	0.05	20
	SVS	0.46	0.05	1.8	0.01	0.02	0
2 T_f	I-P	0.0	11.8	14.3	0.83	0.46	0
	SLM	0.56	4.9	4.9	none	0.05	60
	SVS	0.46	1.1	4.3	0.53	0.12	0
2 K_v	I-P	0.0	11.2[1]	16.3	0.56	0.22	0
	SLM	0.35	4.1	0.5	none	0.03	50
	SVS	0.40	0.6	0.3	0.32	0.22	0
2 T_m	I-P	0.0	15.3[2]	7.8[2]	1.46	0.34	0
	SLM	0.12	1.4[2]	0.5[2]	none	0.0	10
	SVS	0.46	0.3[2]	-	none	none	0

[1] Experimentally this was much longer.
[2] Base time is two times longer.

designed to be very fast, and there is no possibility for overshoot. Although a fast I-P control can be also obtained, the design is very critical.

STEADY STATE PERFORMANCE: I-P control has by far the best steady state accuracy, under any operating conditions. SVS control has a steady state error. Although that error can be changed by adjusting the parameters, the practical minimum possible error, under the full torque, was found to be around 0.1%. In SLM control, the steady state error is basically determined by the amplitude of the speed chattering. The excess power dissipation, present in the SLM control, can be adjusted to a relatively small value, but depends heavily on operating conditions and plant parameter variations.

ROBUSTNESS: SLM control is almost completely insensitive to torque disturbances and changes of the moment of inertia. However, inasmuch it is insensitive to variations of the mechanical part of the system, it is sensitive to changes in the electrical part. SVS control, aside of the steady state error, is very robust. As expected, the I-P control was the most sensitive to parameter variations.

6.2. CURRENT CONTROLLED DRIVE

The control algorithms that were applied to the current driven motor are:

- PI control with variable integrator limits (Section 2.3),
- soft variable structure PI control (Section 5.2),
- sliding API control (Section 5.3).

All the algorithms were implemented for the same motor model given in Appendix A.3. Nominal plant parameter values are given in (A.2), (A.6), (A.8) and (A.14). The constant gain part of each of the controllers is also the same, and is given in (2.2)-(2.4). Other controller parameters for the SVSPI control are given in (5.29), and for the SAPI control in (5.61).

In the linear region the approximate transfer function of the plant is given by (A.24). It can be observed that for the current driven motor, the influence of all plant parameters can be examined by changing just two of them: the gain ck_m/J , and the filter time constant T_f.

As was described in the respective sections, all three controllers were implemented and simulated on a digital computer. However, these controllers were not experimentally tested at this stage, but it is expected that the exper-

imental results would have the same degree of agreement with the simulations, as was shown for the voltage driven motor. It also should be noted, that these three algorithms are in no way restricted to the current controlled drives. They could be equally well applied for the voltage controlled drives.

Simulation test inputs used, are shown in Fig. 6.1a. The transient response of the three control systems is shown in Fig. 6.7, for the nominal plant parameters. All three algorithms show fast transient response and excellent disturbance rejection.

The systems' responses for the moment of inertia increased two times (thus decreasing the gain ck_m/J), are shown in Fig. 6.8. All three algorithms responded exceptionally well to this large parameter change. If the moment of inertia is increased even further, to ten times the nominal one, the responses are as shown in Fig. 6.9. In this case the advantage of adaptive change of the proportional gain in the API control becomes more pronounced, preventing overshoot and oscillations that appeared in the PI control.

The influence of a twofold increase in the filter time constant T_f is shown in Fig. 6.10. Overshoot is slightly larger in the case of VLPI control and SVSPI control. However, there is a significant increase of the armature current oscillations in the SAPI control. This was to be expected due to the critical dependence of the sliding API algorithm

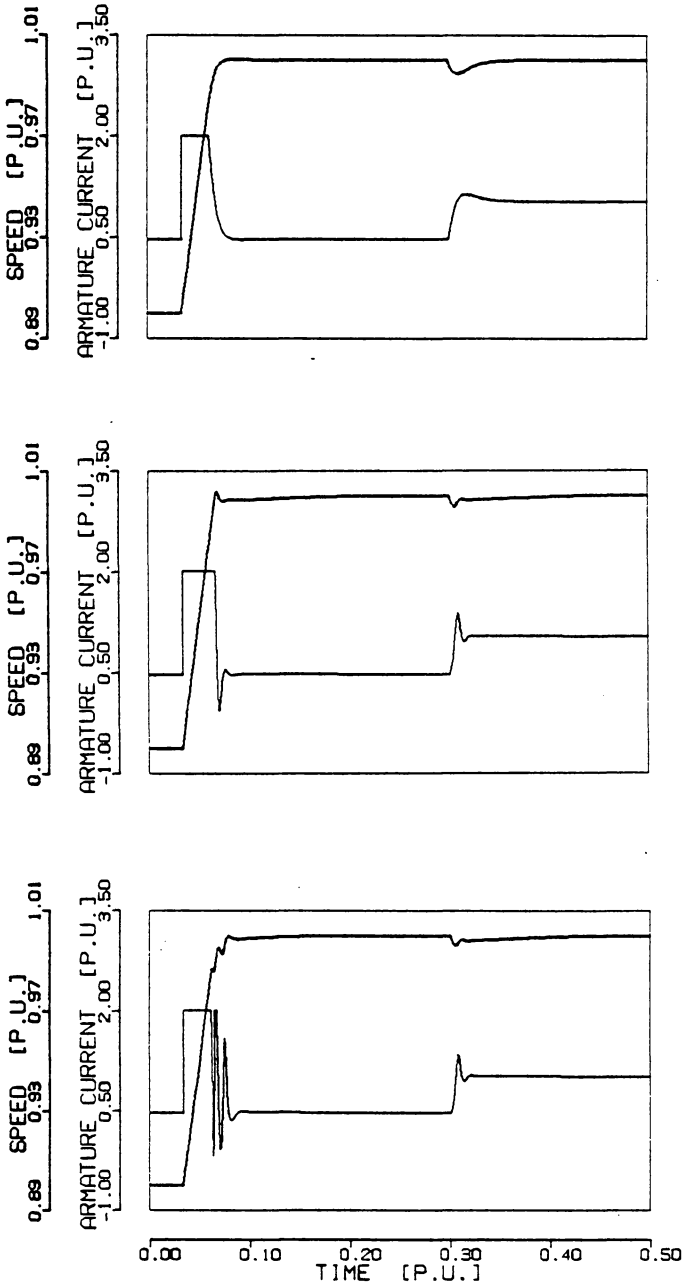

Fig. 6.7: Transient responses of the motor control systems, with the nominal plant parameters.

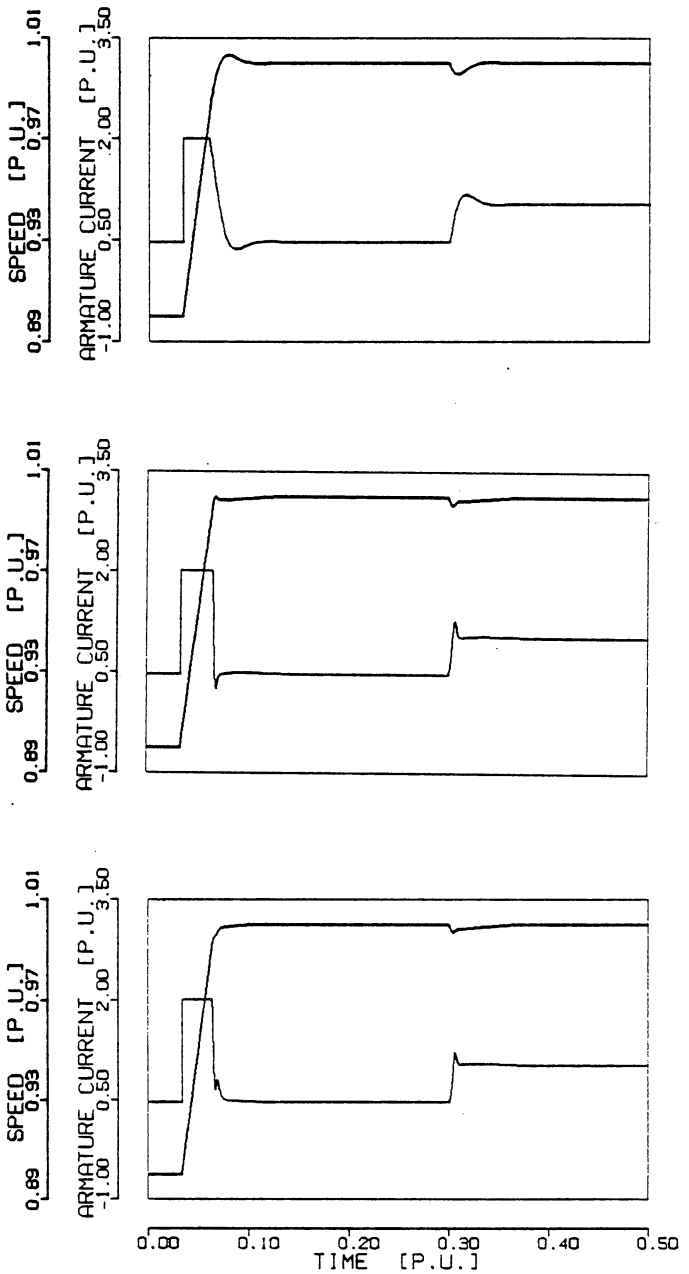

Fig. 6.8: Transient responses of the motor control systems, with the moment of inertia increased 2 times.

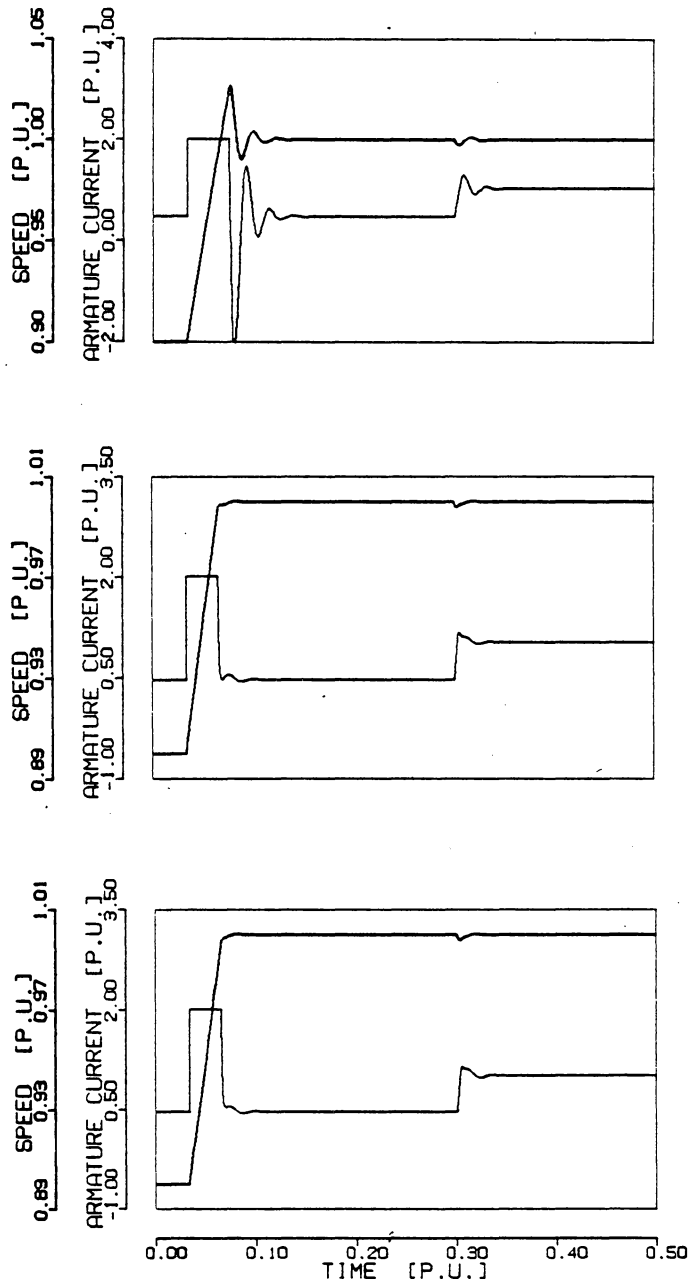

Fig. 6.9: Transient responses of the motor control systems, with the moment of inertia increased 10 times.

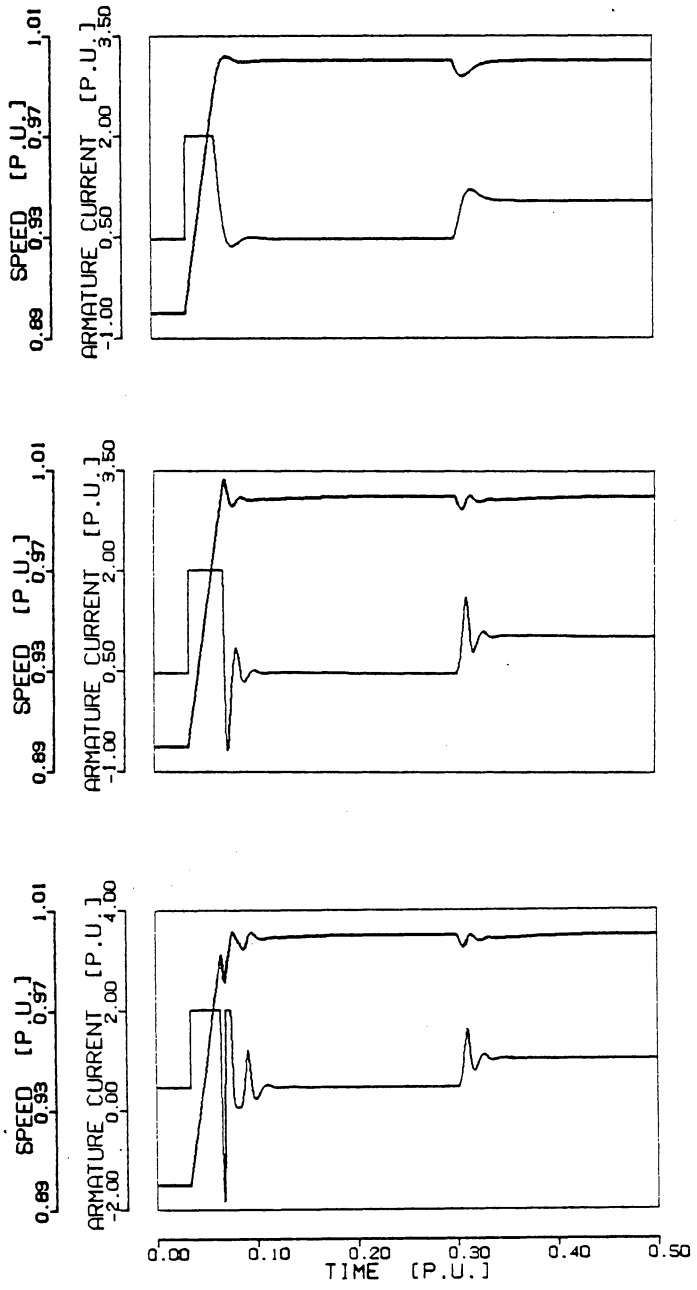

Fig. 6.10: Transient responses of the motor control systems, with the filter time constant T_f increased 2 times.

on the accurate estimation of the speed error and its derivative.

As a conclusion, the simplest of the three algorithms compared, the VLPI control manifested very good robustness to large plant parameter changes. The SVSPI control is the fastest and most robust. It should be used when ultimate performance is required. The SAPI control is inclined to produce larger oscillations, especially when the plant gain is increased and/or the measurement filter bandwidth reduced. These are exactly the same problems that appear in the sliding mode control; however, the proposed SAPI control has the distinct advantage of operating without chattering in steady state.

Chapter 7

ADAPTIVE CONTROL

The central objective of the research presented so far, was investigation of possibilities of using the soft variable structure concepts for handling large parameter variations and nonlinearities of the plant. For that reason, not much attention has been devoted to study of the various, formalized, adaptive control concepts, that are available in the literature [1]. However, any comparison of robust control systems would be incomplete, if at least some possibilities of the adaptive control algorithms are not mentioned. Without any attempt at being exhaustive on this vast subject area, we will just point out the main results and some problems in using adaptive control in electrical drives. Similarities and differences between adaptive algorithms and the algorithms derived in this work will be discussed.

7.1. SURVEY OF PREVIOUS RESULTS

The first example of systematic and formal application of the adaptive control to electrical drives was presented by Courtiol and Landau in 1974 [12]. They used a linear-model-following algorithm, augmented with the model-reference adaptive control. The control was applied to a dc motor driven by line-commutated thyristor converter. The objective was to compensate for the nonlinearities of the converter in the discontinuous conduction mode, as well as for the changes in the mechanical load. The adaptation mechanism was the standard model-reference adaptive algorithm [52].

A similar result was reported most recently by Naitoh [57], with the controller implemented on a microprocessor, in the discrete-time form.

Both examples demonstrated significant improvement of transient response, over PI control, when the moment of inertia, or field current, are changed. In [12] excellent handling of converter nonlinearities is also illustrated, while in [57] very good disturbance rejection is shown.

Characteristically, neither paper discusses the influence of the adaptation gain magnitude on the system performance. (For that matter, even the values of the gains used in the implementations, are not given). This influence is very important because for faster adaptation, larger gains

are needed. However, large gains may cause instability, estimator wind-up, and other phenomena peculiar to the adaptive algorithms [49]. This is especially true when approximate modeling and simplified algorithms are used, as was done in [12,57].

In an earlier paper, Naitoh [56] demonstrated successful correction of the nonlinearities of a line-commutated thyristor converter in the discontinuous conduction mode, using a model-reference adaptive control in the current loop.

Another specific application of adaptive algorithms was reported by Dote et al. [16], who used the fuzzy set theory, to adaptively change the parameters of a digital filter applied to processing signals from a tachometer or torquemeter. Considerable noise reduction was achieved with very small distortion of the signal.

A different approach to the adaptive control is in combining model-reference control and sliding mode control, which was proposed originally by Young [79]. In this algorithm, the error between the reference model output and the plant output is used as the switching function. This generally allows somewhat easier tailoring of the transient response than a simple SLM control, especially in the case of nonlinear and higher order plants. However, in the case of a dc motor, the response is same as with the simple SLM control described in Chapter 3, but the controller structure and design are unjustifiably more intricate. Although Young al-

ready illustrated application of the algorithm to dc drives, Balestrino et al. [3] recently presented a detailed analysis of the application, together with the experimental results. The major quality of the last paper is that it includes a detailed discussion and some solutions to the problem of excessive chattering in practical applications.

An adaptive control strategy, different from the model-reference approach mentioned so far, is the self-tuning control. In that approach, controller parameters are continuously adjusted according to the adaptively estimated plant parameters and disturbances. This type of algorithm was used by Weihrich [75, 76], who implemented an adaptive parameter and torque observer. We will further elaborate on this result in order to demonstrate some of the problems in implementing adaptive control.

7.2. ADAPTIVE CONTROL WITH TORQUE AND PARAMETER ESTIMATION

The differential equation, governing the rotor speed of a dc motor, from (A.27), is given by

$$\dot{\omega} = - \frac{D}{J} \cdot \omega + \frac{k_m}{J} \cdot i_a - \frac{1}{J} \cdot T_\ell \quad . \tag{7.1}$$

Usually, the damping coefficient D, is very small and can be omitted. For the current drive described in Appendix A.3,

the speed measurement y is equal to $c \cdot \omega$, and armature current i_a can be considered equal to the current command i^*. Then from (A.23), the model of the current driven motor can be approximated with

$$\dot{y} = \frac{c \cdot k_m}{J} \cdot u - \frac{c}{J} \cdot T_\ell \triangleq g \cdot u - d \quad , \tag{7.2}$$

where $u = i^*$ when the input is not in the limit, Fig. A.2. From (7.2) it is obvious that estimation of the torque alone, is not possible if the moment of inertia is changing or not exactly known. Therefore, the algorithms which use only torque observers, as in [59], are very sensitive. In order to achieve robustness, Weihrich estimates both g and d, as well as y. The controller that he has presented in [75, 76] has the form

$$u = \frac{1}{\tilde{g}} \cdot [K_p \cdot (r - y) + \tilde{d}] \tag{7.3}$$

By substituting (7.3) into (7.2) one obtains

$$\dot{y} = \frac{g}{\tilde{g}} \cdot K_p \cdot (r - y) + \frac{g}{\tilde{g}} \cdot \tilde{d} - d \quad . \tag{7.4}$$

If $\tilde{g} = g$ and $\tilde{d} = d$, from (7.4)

$$\dot{y} = - K_p \cdot y + K_p \cdot r \quad , \tag{7.5}$$

and the system dynamics is independent of plant parameters g and d, while zero steady state error is also achieved. When there is a change in plant parameters and disturbance, parameters $\tilde{g}$ and $\tilde{d}$ have to be changed adaptively, in order for (7.5) to hold. In [75, 76] a Luders-Narendra adaptive observer [54, 41] is used, which for the plant (7.1), (7.2) has the form

$$\begin{aligned} \dot{\tilde{y}} &= \tilde{g} \cdot i_a - \tilde{d} + K_2 \cdot e \\ \dot{\tilde{g}} &= K_0 \cdot e \cdot i_a \\ \dot{\tilde{d}} &= - K_1 \cdot e \\ e &= y - \tilde{y} \quad , \end{aligned} \tag{7.6}$$

and the control, instead of (7.3) becomes

$$u = \frac{1}{\tilde{g}} \left[K_p \cdot (r - \tilde{y}) + \tilde{d} \right] \quad . \tag{7.7}$$

The equilibrium point of the system (7.1), (7.2), (7.6), and (7.7) is easily obtained as

$$y_e = r \quad , \quad i_{ae} = d/g \quad , \quad \tilde{y}_e = y_e \tag{7.8}$$

$$\frac{\tilde{d}_e}{\tilde{g}_e} = \frac{d}{g} \qquad (7.9)$$

The plant has a unique and desired equilibrium point (7.8), but adaptive gains $\tilde{g}$ and $\tilde{d}$ have a continuum of equilibrium points, belonging to the line (7.9). In order that

$$\tilde{g}_e = g \quad , \quad \tilde{d}_e = d \qquad (7.10)$$

the plant input r must be "sufficiently rich", or, as it is usually called in the estimation theory, "persistently exciting". If this condition is satisfied, in [76, 41] it is proved that the equilibrium point (7.8), (7.10) is globally asymptotically stable.

What is "sufficient", is still a question. Theoretically, the input should contain as many independent time functions as there are adaptive parameters (in our case two, $\tilde{g}$ and $\tilde{d}$). However, if the amplitude of the persistently exciting input is too small, convergence to (7.10) is very slow. Large amplitude will cause larger chattering of the system state variables, which may be unacceptable in many applications (as it was not acceptable with sliding modes). If the input is not sufficiently rich, adaptive gains will tend to drift, especially with the periodic disturbances. This is usually referred to as estimator wind-up [1].

In the case when higher order dynamics of the plant is not modeled (as it is not in (7.1)), a drift of the adaptive gains ($\tilde{g}$, $\tilde{d}$) may be induced by large adaptation gains (K_0, K_1), and/or high frequency components of the input signal ("too rich input"), [49, 62].

The control (7.6), (7.7) was implemented for the current driven dc motor from Appendix A.3. From (A.5) and (A.26), the plant parameters in (7.2) are

$$g \approx 18.2 \quad , \qquad d \approx 15.2 \quad . \tag{7.11}$$

The block diagram of the control system is given in Fig. 7.1. Smoothing filters are added in the paths of $\tilde{y}$, $\tilde{g}$, $\tilde{d}$ and i_a. These filters are not necessary in simulations, but in practice they are required in order to eliminate excessive noise, as was done in [76]. Additional input v provides for the persistent excitation of the control system, and its waveform is shown in Fig. 7.2. Gain K_p was set so that the effective proportional feedback gain, g_p, was the same as in the previous examples of PI control (Section 2.1):

$$K_p = g_p \cdot g = 32 \cdot 18.2 \approx 582 \quad . \tag{7.12}$$

Filter time constants which were used, are

$$T_f = 0.5 \text{ ms} \quad , \qquad T_{fi} = 0.1 \text{ ms} \quad , \tag{7.13}$$

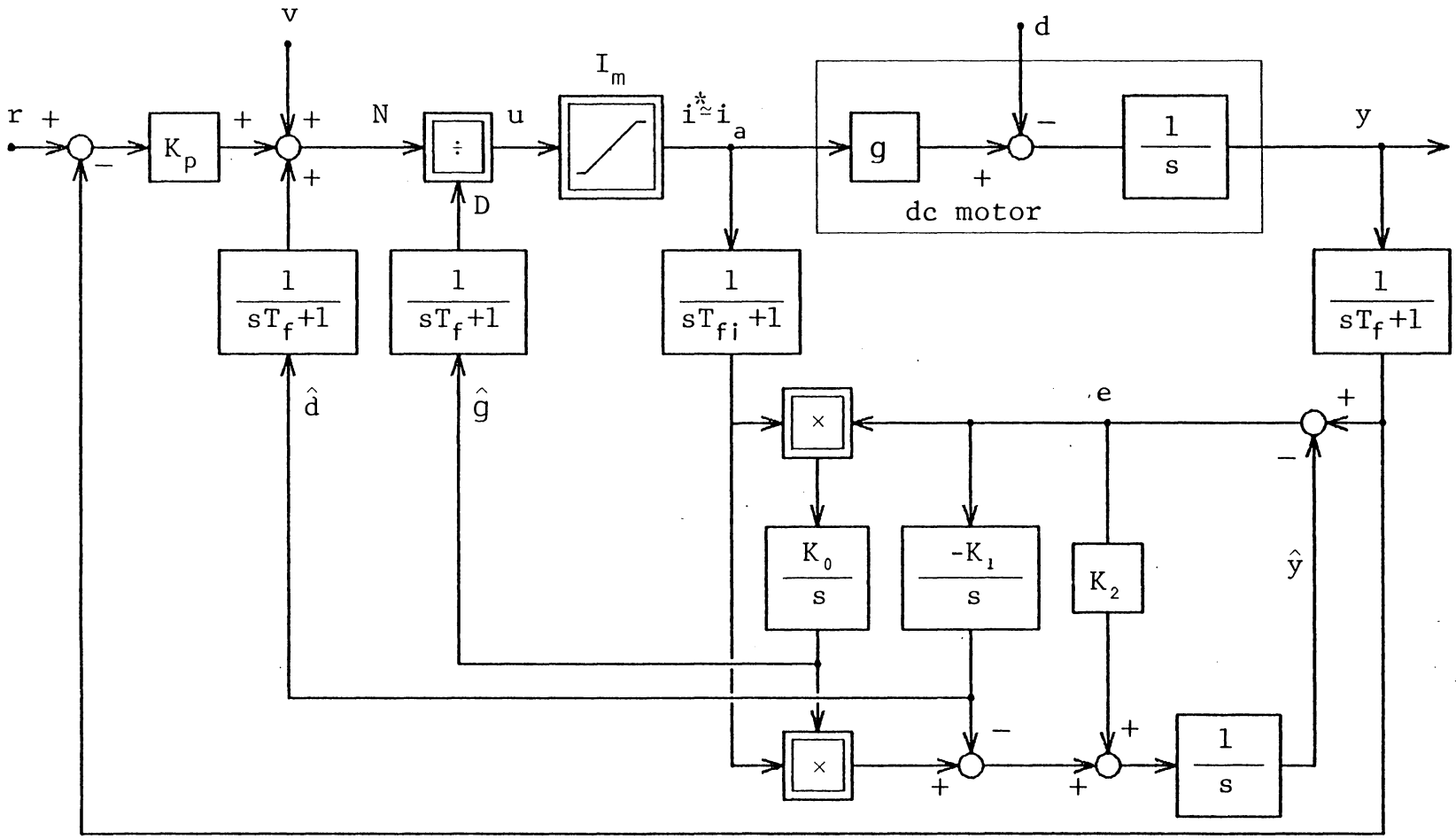

FIG 71

Fig. 7.1: Structure of the self-tuning adaptive control with torque and parameter estimation. (Adapted from [76]].)

so that T_f is same as in the previous examples. The values of the adaptation and observer gains were first chosen as given in [76], and then adjusted by trial-and-error. Finally, the values used are

$$K_0 = 10^5 \ , \quad K_1 = 2\ 10^4 \ , \quad K_2 = 2\ 10^3 \ . \qquad (7.14)$$

When the initial values for the adaptive gains are chosen close to the true parameter values (7.11), as

$$\tilde{g} = 18 \ , \quad \tilde{d} = 15 \ , \qquad (7.15)$$

the simulated waveforms of the motor start-up are shown in Fig. 7.3. Very smooth and fast response without overshoot can be observed. The adaptive gains, after some perturbation, return close to the true values.

In Fig. 7.4 the waveforms of the motor start-up, when the moment of inertia is increased ten times, are shown. The controller is the same, with the same initial settings as in Fig. 7.3. Although the response is still very good, parameter gains settled far from the true values, which now are

$$g \simeq 1.82 \ , \quad d \simeq 1.52 \ . \qquad (7.16)$$

The same kind of behavior was observed by Weihrich [76].

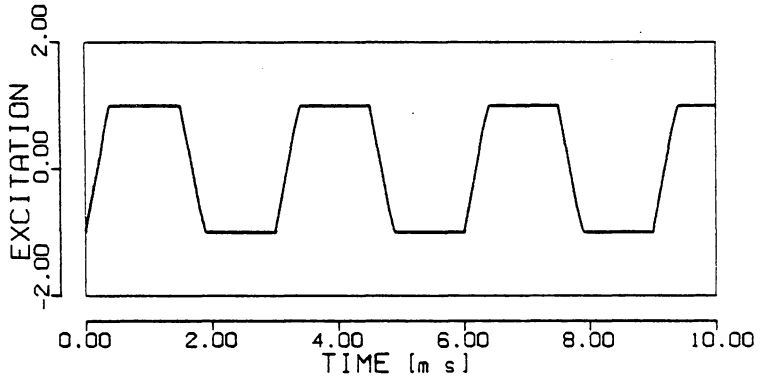

Fig. 7.2: Waveform of the signal v , used for persistent excitation of the adaptive system.

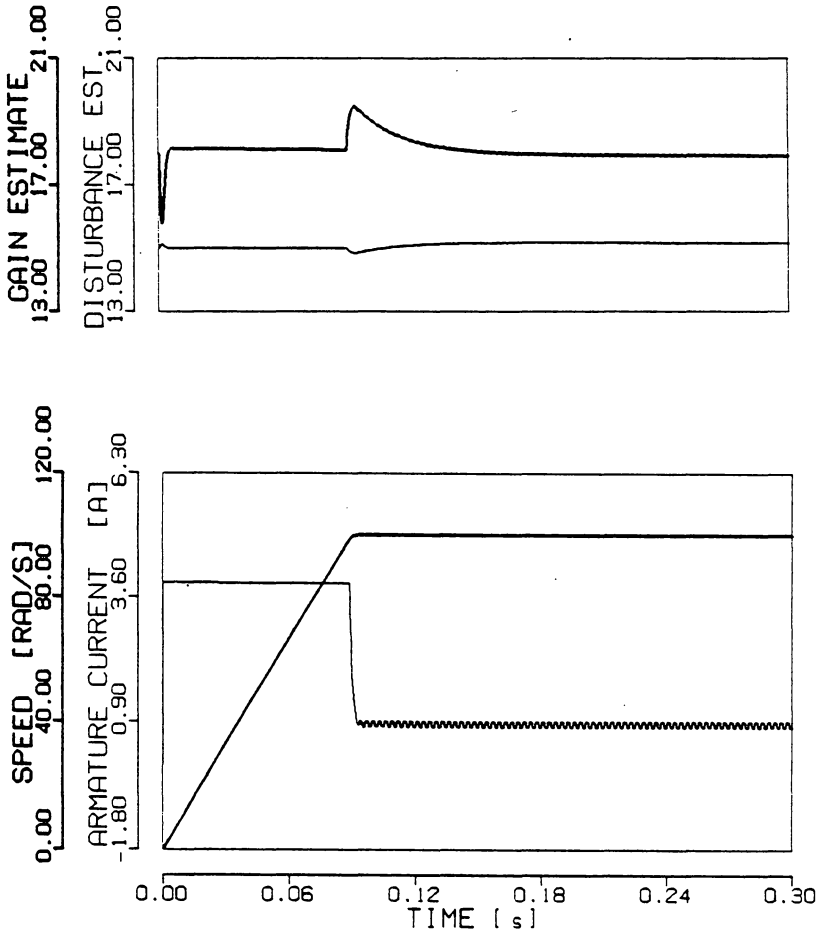

Fig. 7.3: Start-up of the motor with the adaptive controller, and nominal plant parameters.

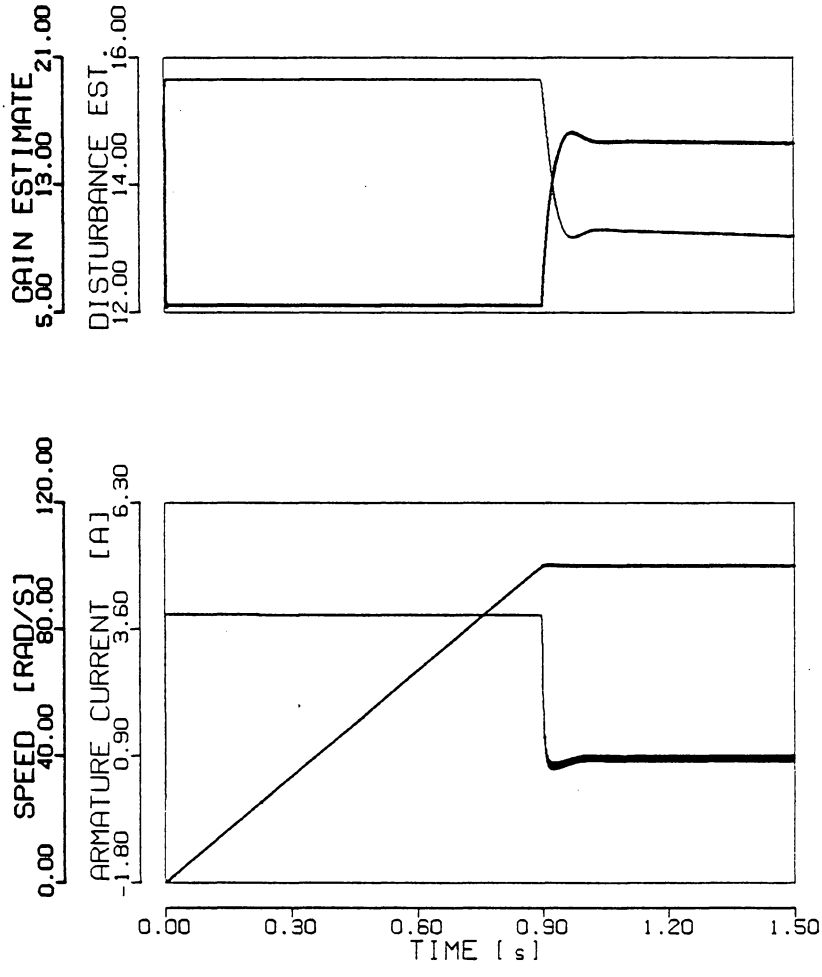

Fig. 7.4: Start-up of the motor with the adaptive controller, and the moment of inertia increased 10 times.

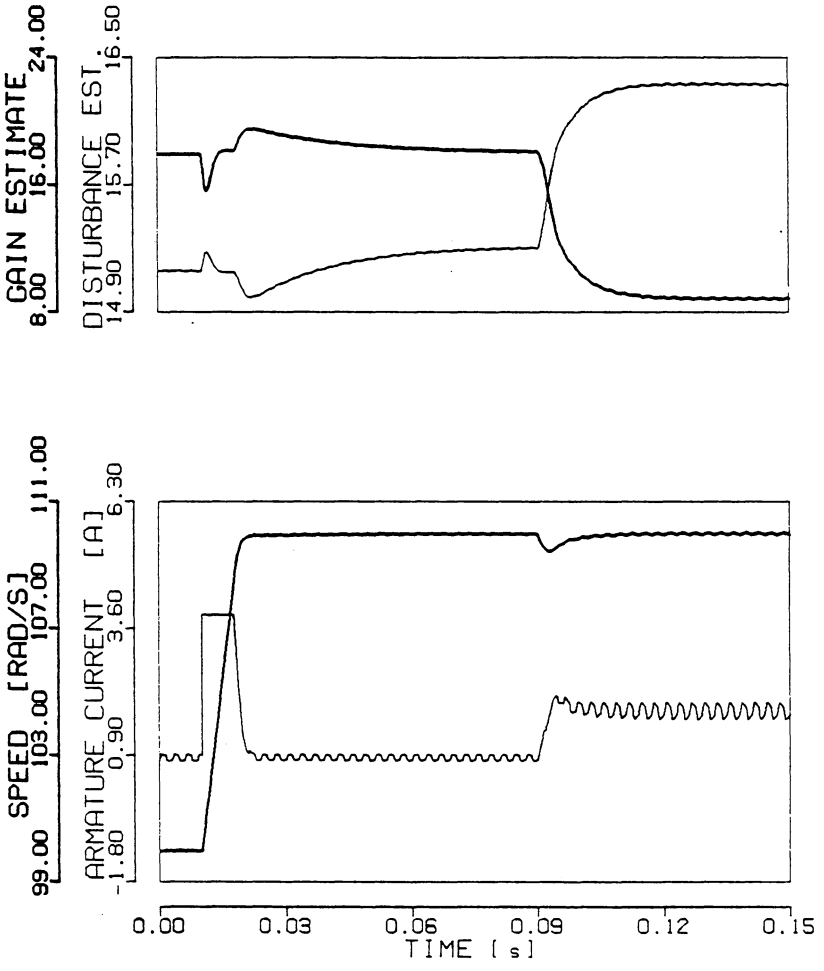

Fig. 7.5: Transient response of the adaptive control system with the nominal plant parameters, for inputs from Figures 2.3b and 2.3c.

When the small input-step from Fig. 2.3b, and the torque change from Fig. 2.3c are applied, the waveforms for the motor with nominal parameters are shown in Fig. 7.5. Excellent behavior is again exemplified in the speed and current waveforms. However, adaptive gains showed a peculiar change after the load torque was applied. The change in disturbance should have caused only the change in $\tilde{d}$, because the plant gain g remained constant. But adaptive gain $\tilde{g}$ decreased considerably, which also caused increased current chattering, because the excitation input v, is now divided by a smaller number.

When the series of torque pulses between $T_\ell = 0$ and $T_\ell = 0.02$ N m is applied to the motor, the resulting waveforms are shown in Fig. 7.6. Drift in the adaptive gains is obvious. If this condition would persist, gain $\tilde{g}$ will decrease so much that the current chattering will become unacceptable, and unstable operation may occur.

In [75, 76] Weihrich proposed a modified algorithm which ensures convergence of the adaptive gains to their true values. However, the rate of convergence is extremely slow, so that the drift conditions of Fig. 7.6 are still present and may lead to instability.

The problems that were illustrated, appeared in the particular example. But, according to the literature cited earlier, they are common for all adaptive control algorithms. Although the resulting dynamic behavior and robustness of

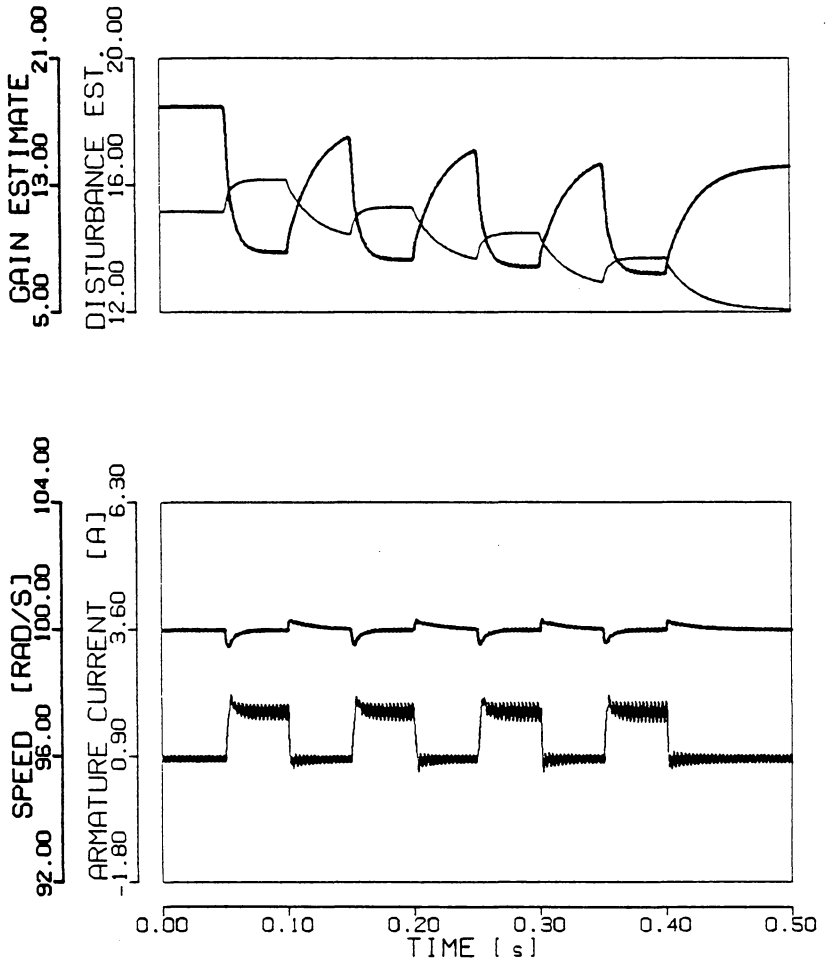

Fig. 7.6: Transient response of the adaptive control system, to the series of load torque pulses between d = 15.3 and d = 33.3 .

adaptive algorithms are very good, these problems still prevent their widespread application.

7.3. SVS CONTROL AND ADAPTIVE CONTROL

All adaptive control systems can be represented by the general block diagram in Fig. 7.7, [38]. Structures of the "feedback control law" may be very diverse, but action of each adjustable coefficient, c_i, may be represented as in Fig. 7.8, by the equation

$$w_i = c_i(\eta,z,t)\ z_i \quad . \tag{7.17}$$

The vector z is a linear function of the output vector y, and the control vector u_c is a linear function of the vector w. Variable η is the "generalized error", representing in some sense, deviation of the actual controlled process from the assumed or desired process behavior. Functions $c_i(\eta,z,t)$ represent the tuning or adaptation algorithm. If the Liapunov direct method is used for the derivation of this algorithm, almost invariably the resulting function has the form

$$\dot{c}_i = K\ \eta\ z_i \quad . \tag{7.18}$$

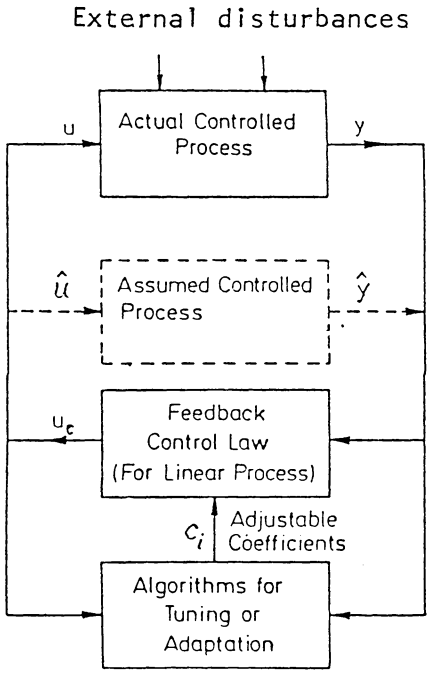

Fig. 7.7: General block diagram of an adaptive control system. (Adapted from [38].)

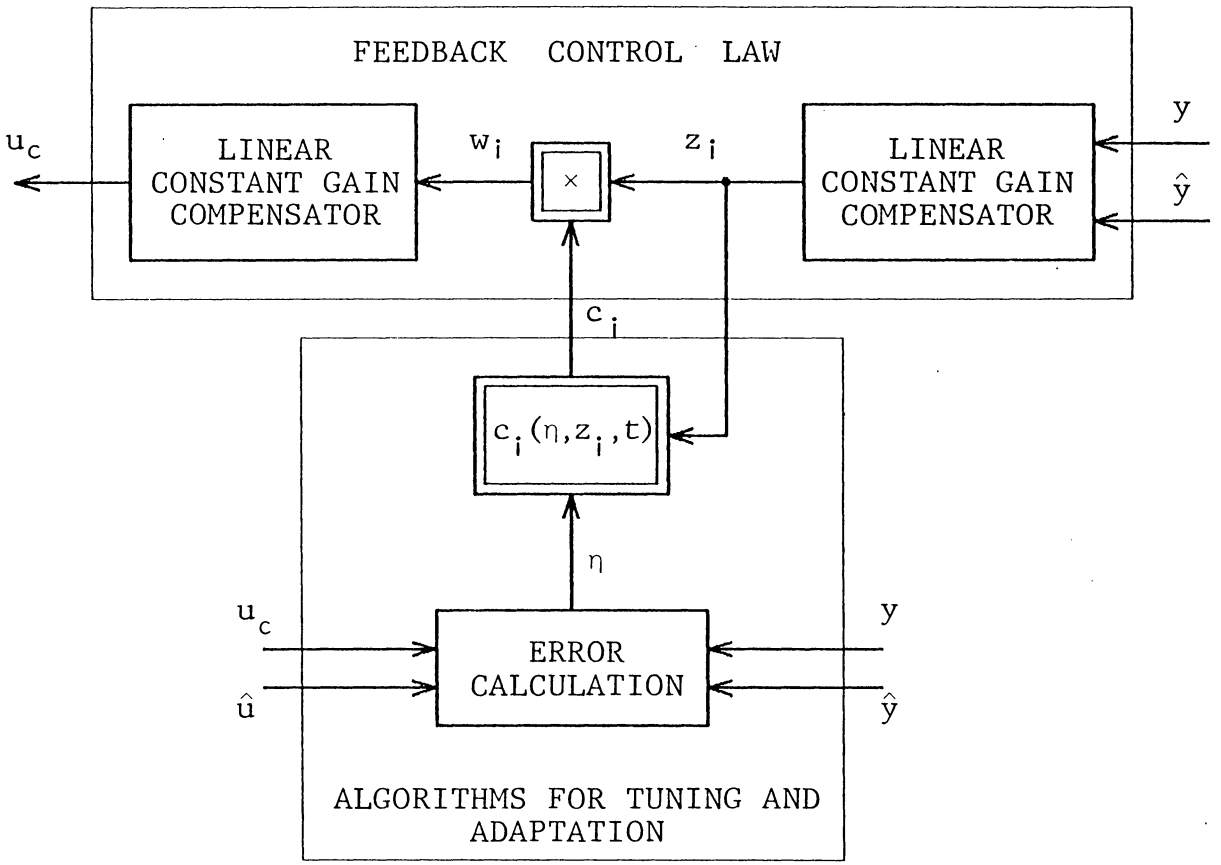

Fig. 7.8: General structure of an adaptive controller.

where K is adaptation gain. It is relatively simple to show that the SVS control of Chapter 4, and two versions of the API control of Chapter 5, have the general form of Fig. 7.7 and equation (7.18).

- SVS control:

  - The actual controlled process is the plant itself, together with offsetting, in Fig. 4.1.
  - Feedback control law is the output feedback $p \cdot y$ in (4.23), with p being the adjustable coefficient.
  - Since $p\ y = u - r$, (4.23) can be rewritten as

$$\dot{p} = - q \cdot [k_1 \cdot (y - r) + k_2 \cdot (u - r)] \cdot y - q \cdot \mu_3 \ . \quad (7.19)$$

    By comparing with (7.18) it follows that the generalized error η is the linear combination of the output and input errors.

- SVSPI control:

  - Actual controlled process in Fig. 5.2, is the VLPI control subsystem.
  - Feedback control law is the proportional feedback $p_2 \cdot e_1$ in (5.24), with p_2 being the adjustable coefficient.

- Since $p_2 \cdot e_1 = u - u_i$, (5.25) can be rewritten as

$$\dot{p}_2 = [e_1 - k(u - u_i)] \cdot e_1 - \mu_5 - \varepsilon(p_2 - g_p') \quad . \quad (7.20)$$

The generalized error is now a linear combination of the output error and the "error" of the controller integral part.

- SAPI control:

- Actual controlled process and the feedback control law are the same as in the SVSPI control.
- Equation (5.38) is

$$\dot{p}_2 = q_2 \, (e_1 + T_c \, e_2) \, e_1 - \mu_5 - \varepsilon \, (p_2 - g_p') \quad , \quad (7.21)$$

and because $e_2 \simeq \dot{e}_1$ the generalized error is a linear combination of the output error and its derivative.

From equations (7.19)-(7.21), the difference between the standard adaptive control and the control algorithms proposed in this work is apparent:

i) Our controllers explicitly include nonlinear limiting function μ. This allows employment of large

adaptation gain q without the possibility of the adjustable coefficient growing out-of-bounds, and causing instability.

ii) In modified SVS control, offsetting of the output y assured that y in (7.19) never becomes zero within the domain of operation. In this way, the equilibrium of the adjustable gain p is unique, so that drifting of p is impossible. In the API algorithms there is the resetting component $\varepsilon(p_2 - g_p')$ which prevents drifting.

In this way, the major problems present in the adaptive control are avoided. The proofs in Appendixes C and D are at least to some extent, general, so that the results presented are not restricted to the speed control of dc drives. They can be used in solving the problems of adaptive control for a wider class of SISO systems.

Chapter 8

POSITION CONTROL

In the control systems of high performance electrical drives, the speed control loop is almost always operating within an outer control loop. Therefore, the performance quality of any speed control algorithm cannot be fully assessed, if its operation is not examined within such a system. The variable which is controlled by this outer loop, in many cases is directly proportional to the position of the motor shaft, i.e., to the integral of the motor speed. Position control systems are very often referred to as servo systems.

This chapter presents a short discussion of design requirements for the position loop, and gives an example of the SVSPI speed control operating within the loop. A possibility of improving the performance of the position control, by applying the SAPI concept in the position loop itself, is demonstrated.

8.1. POSITION CONTROL WITH SVSPI SPEED CONTROL

The block diagram of a position control system for the current controlled dc motor is shown in Fig. 8.1, with the new symbols having the following meaning.

θ - rotor position: $\dot{\theta} \triangleq \omega$,

r_θ - position command,

y_θ - position measurement,

c_θ - position measurement gain,

e_θ - position error,

G_θ - position controller,

G_ω - speed controller,

Ω - speed limit.

The plant model differs from the model for speed control only in the presence of the output integrator. This makes the plant a Type 1 system, so that the output θ is constant when the error e_θ is equal to zero.

The performance requirements of the position control system are the same as for the speed control: accuracy, fast transient response, and robustness. The major difference is that, due to physical restrictions in most applications, an overshoot in the transient response cannot be tolerated.

In the classical approach, design is usually done in two stages. The speed control loop is designed first to produce

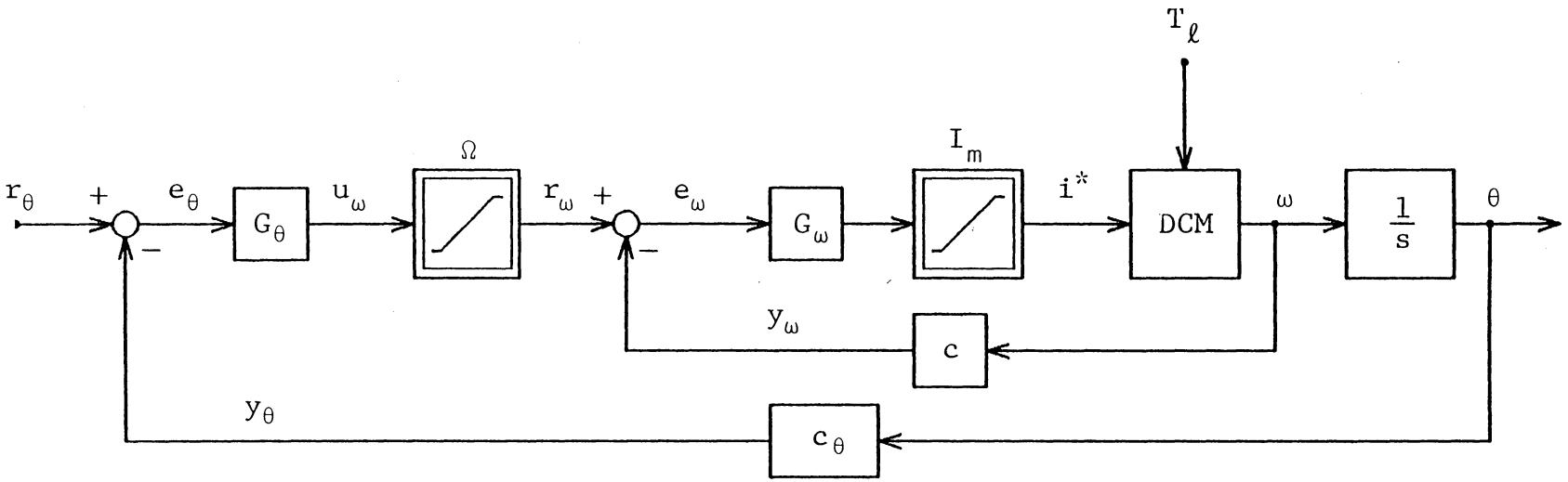

Fig. 8.1: Position control system.

fast and well behaved transient response characterized by a single, or at most double, time constant. It should also compensate for external disturbances and parameter variations.

Once the satisfactory speed control is designed, the position controller should provide desired accuracy and position transient response. Since there is already an integrator at the output of the plant, integral control is not needed for accurate positioning. Namely, in equilibrium $e_\theta = 0$ even if the position controller G_θ is just a constant gain g_θ. On the other hand, if there is an integral component in G_θ, an overshoot is likely happen, either due to the speed limiting, or because the higher order system is more likely to have oscillatory response. Therefore, a simple proportional feedback is almost always used in the position loop.

With the proportional control in the position loop, satisfactory positioning (i.e., response to the step input r_θ) is usually obtained. However, in tracking, both r_θ and θ are changing as a function of time. In that case ω is not zero and therefore e_θ in Fig. 8.1 cannot be zero. This means that $y_\theta(t) \neq r_\theta(t)$. The problem is usually solved, without an additional integrator, by introducing the rate feedforward control. In that case, u_ω in Fig. 8.1 is not any more $u_\omega = G_\theta(r_\theta - y_\theta)$, but is given by

$$u_\omega = G_\theta(r_\theta - y_\theta) + \dot{r}_\theta \quad . \tag{8.1}$$

In this way, provided that the speed loop has zero steady state error, after the initial transient, we have $y_\theta(t) = r_\theta(t)$ and $y_\omega(t) = \dot{r}_\theta(t)$, as required. For positioning $r_\theta(t) = \text{const.}$ so that the same operation is obtained as without the feedforward.

The design considerations mentioned so far are just the fundamental ones. The problems in the position control are much more elaborate, and usually are strongly related to a particular application. However, the subject of this research was speed control, so the detailed treatment of position control will be omitted. Also, although the tracking performance is of the utmost importance in servo systems, only the positioning will be examined here. This will still enable us to observe some phenomena characteristic for position control and suggest a possible solution.

The system in Fig. 8.1 was simulated with the speed controller G_ω implemented as a SVSPI control, described in Section 5.2, and shown in Fig. 5.3. The speed controller parameters are given in (5.29) and the motor parameters in Appendix A.3. The motor speed of $\omega = \pm 100$ rad/s was arbitrarily selected as the maximum allowable speed, so that with the output scaling of $c = 0.05$, the speed limit is

$$\Omega = 5 \quad . \tag{8.2}$$

The position measurement gain was chosen to be the same as the speed measurement gain c, so

$$c_\theta = 0.05 \quad . \tag{8.3}$$

The proportional gain is selected relatively large in order to achieve very fast transient response without overshoot. For our system with nominal parameters, it was

$$G_\theta = g_\theta = 30 \quad . \tag{8.4}$$

The test inputs used are shown in Fig. 8.2. The step in the position command is large enough for the speed limit Ω to be reached. After the transient to the position command is over, a step in the load torque is applied, in order to test the disturbance rejection of the overall system.

Simulation results are shown in Fig. 8.3. Very smooth and very fast transient response can be observed. Due to excellent disturbance rejection by the speed control loop, no influence on the position can be observed after the load torque was applied. Actual maximum deviation of position is less than 0.003 rad.

In Fig. 8.4 the results of simulation of the same control system, but with the moment of inertia increased 10 times, are shown. The disastrous behavior resulted from the

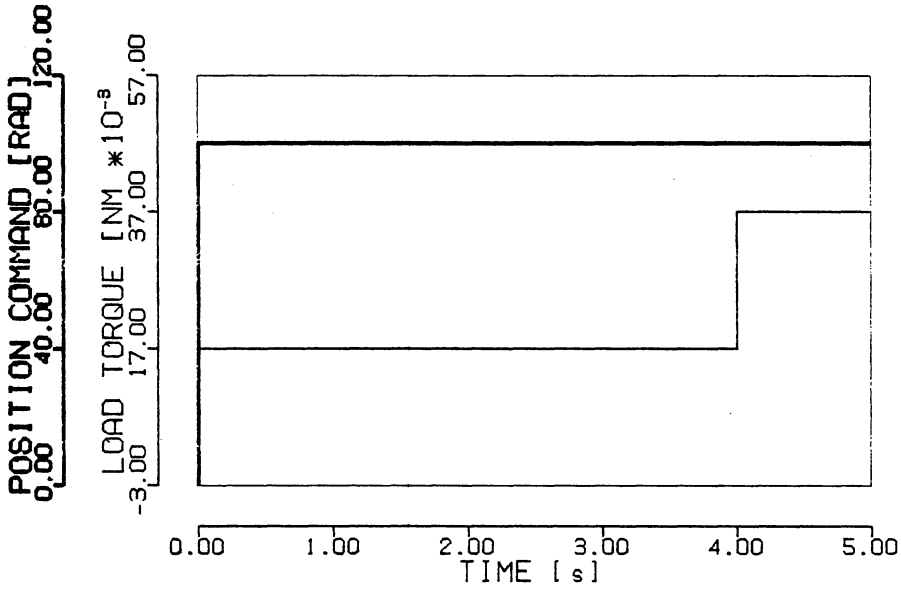

Fig. 8.2: Test inputs.

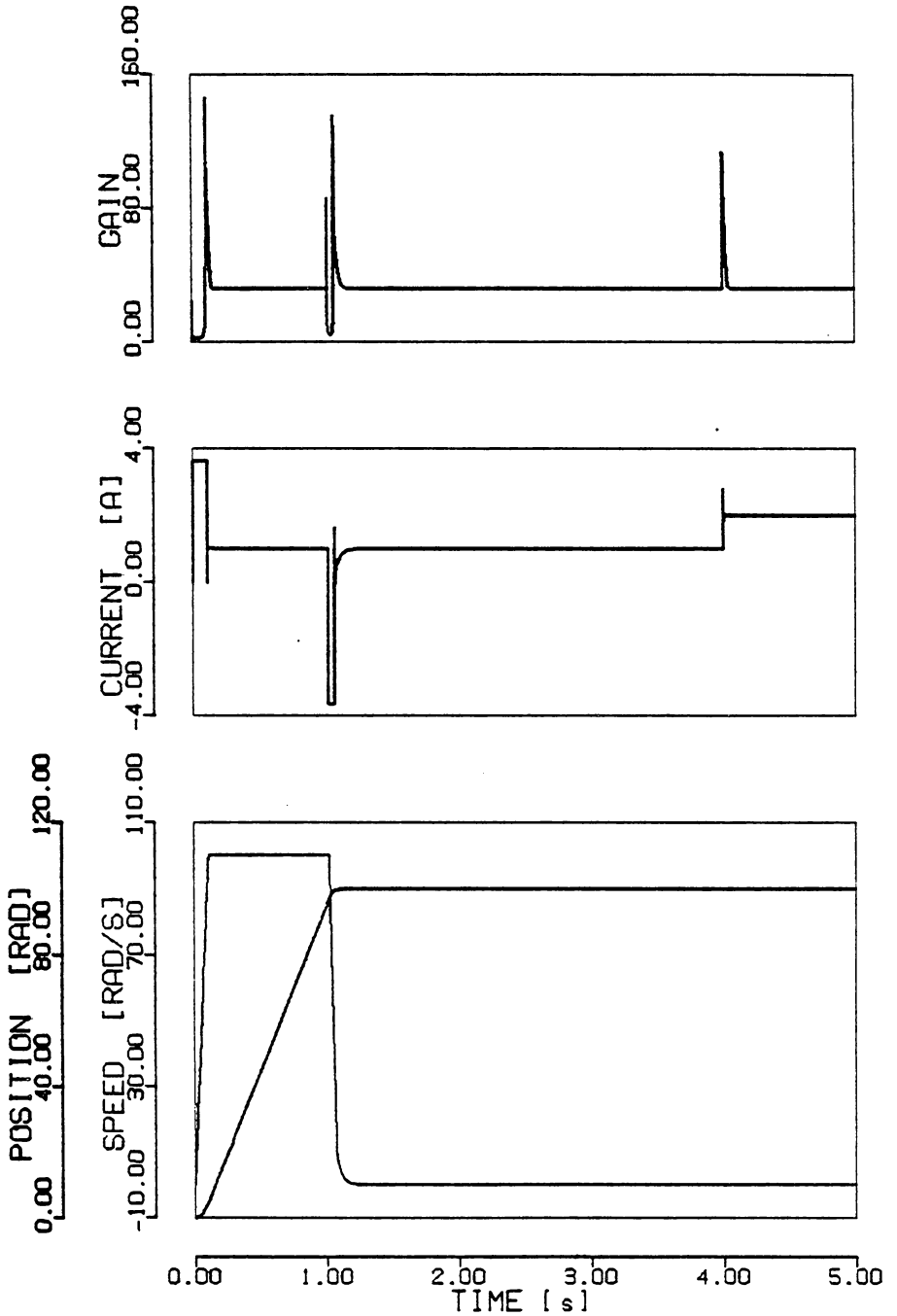

Fig. 8.3: Transient response of the servo system with proportional control, for $g_\theta = 30$.
Nominal plant parameters.

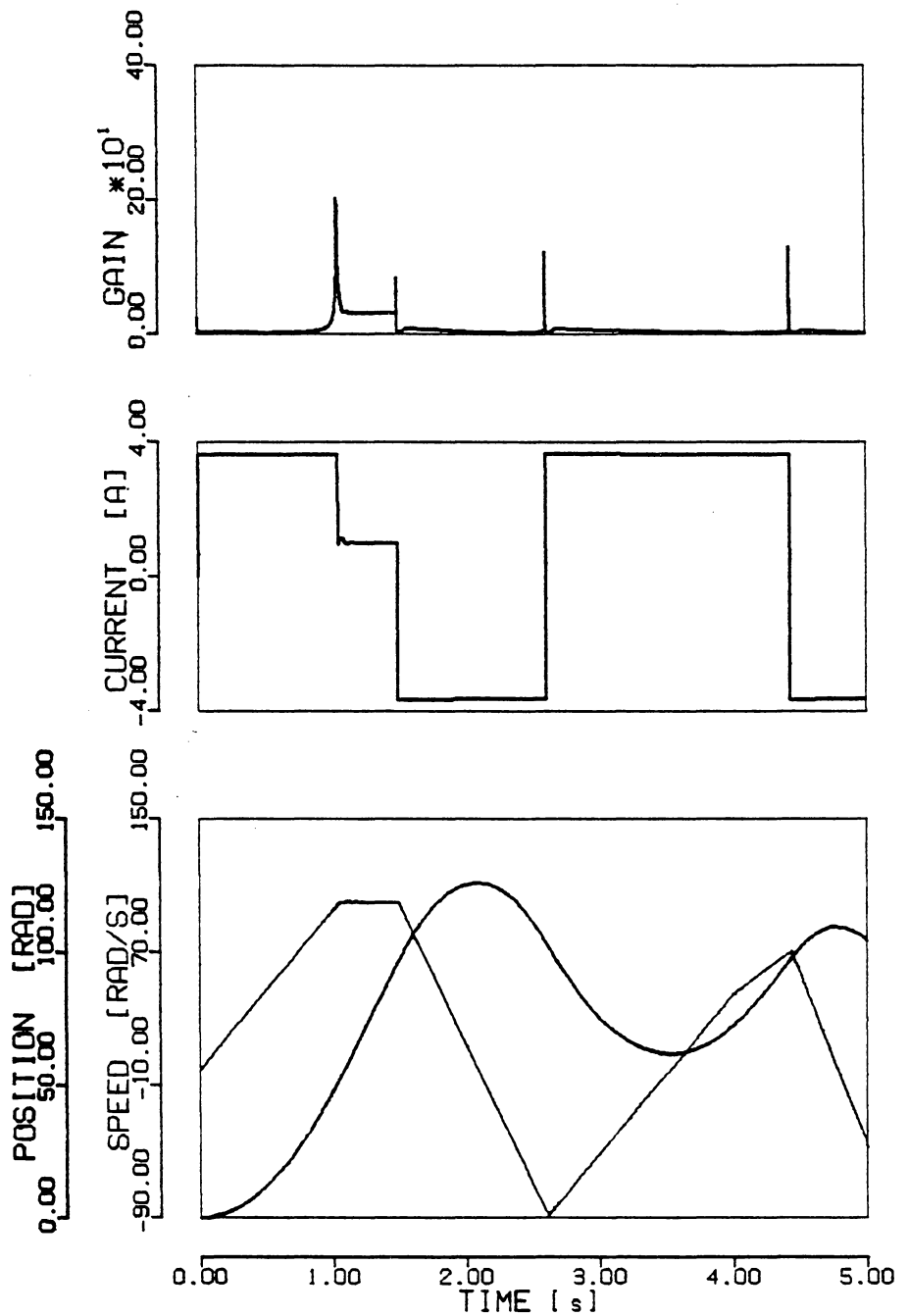

Fig. 8.4: Transient response of the servo system with proportional control, for $g_\theta = 30$.
Moment of inertia increased 10 times.

presence of two nonlinear (saturation) functions in the controller. The current limit restrained the maximum available acceleration in this case, to so small a value, that the speed could not be reduced enough before a large overshoot in position has happened. This then produced decaying but large amplitude oscillations.

The only way of avoiding the above problem is to reduce the proportional gain g_θ . The standard way of designing the position loop is actually to design the system for the largest possible inertia, and then to accept a much slower than optimal response for the low inertias. With the gain of

$$g_\theta = 3 \quad , \tag{8.5}$$

and inertia still ten times larger than nominal the response is shown in Fig. 8.5b. With the nominal inertia, and the same low-gain control, the response is as shown in Fig. 8.5a.

The examples in Fig. 8.5 demonstrated that the speed loop with SVSPI control has almost ideal performance within the position loop. First, the transient response after leaving both saturations (speed and current limits) is governed by the single time constant irrespective of the moment of inertia. The time constant evaluated from the simulations in Fig. 8.5 was the same for both cases and it is

a)

b)

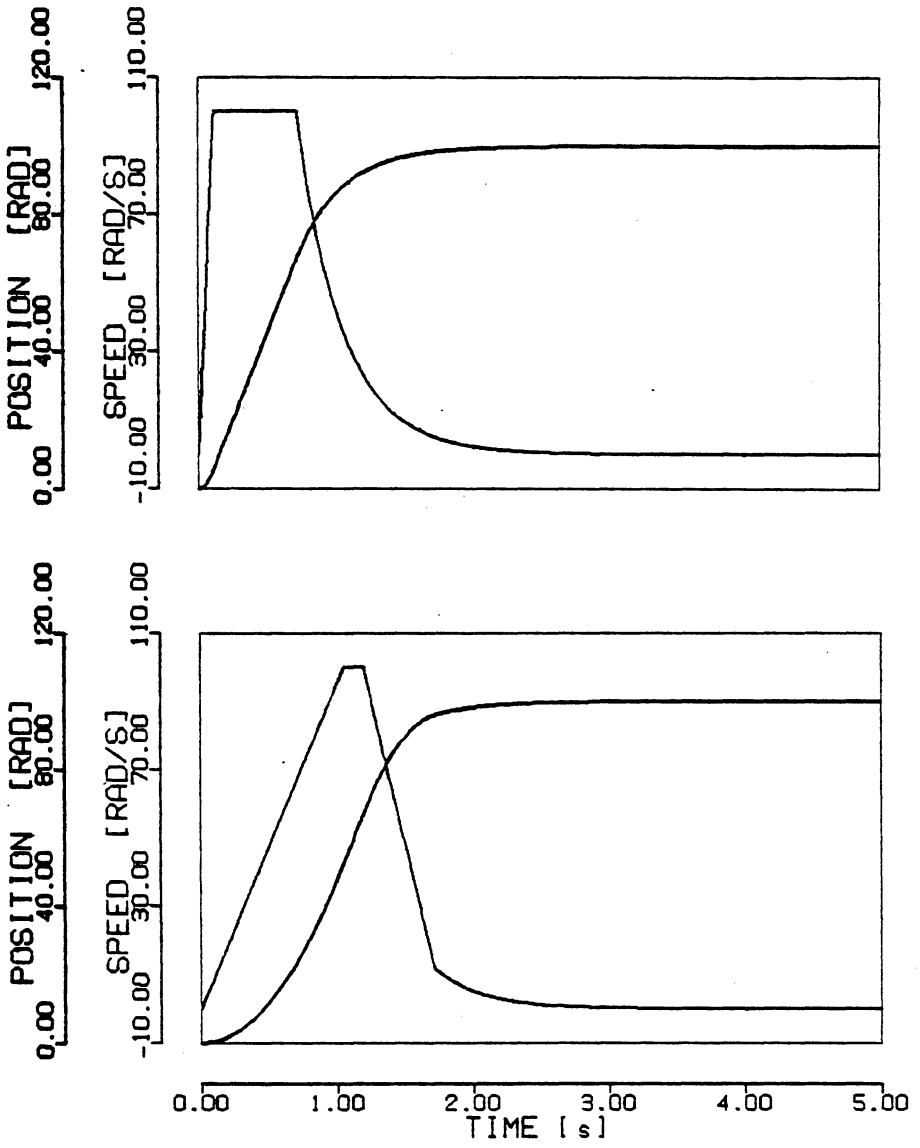

Fig. 8.5: Transient response of the servo system with proportional control, for $g_\theta = 3$.

a) Nominal plant.

b) Moment of inertia increased 10 times.

$$\tau_\theta \approx 0.33 \text{ s} \qquad (8.6)$$

From (8.5) and (8.6) it follows that the speed loop with the SVSPI control, when not in saturation, behaves like a block with constant gain equal to unity. Second, as already mentioned, the disturbance rejection is so good that the load step from about 40% to about 80% of the rated value, caused less than 0.003 radians of deviation in position.

8.2. SLIDING-ADAPTIVE POSITION CONTROL

Excellent performance of the SVSPI speed control, within the standard constant gain position feedback loop, was demonstrated in the previous section. However, one cannot be fully satisfied with the operation of the position controller, because very long settling time has resulted.

The total transient time in Fig. 8.5 can be divided into two parts. During the initial part the system operates with some of its variables in saturation. This means that the response is as fast as possible for the given plant. Proportional gain g_θ has to be chosen such that the system leaves this mode of operation early enough to reach the steady state without overshoot. The resulting small value of g_θ then causes very slow settling in the final part of the transient when the system operates mostly in the linear mode.

Now suppose that a control system is used in the high-performance servo drive with a required accuracy of 0.01%. In that case the appropriate definitions of the transient times are:

t_t - transient time: from the moment when step input is applied until the output is within 99.99% of the steady state value;

t_{is} - initial settling time: from the moment of the step application until the output is 95% of the steady state value;

t_{fs} - final settling time: $t_{fs} = t_t - t_{is}$.

The transient response of the high gain system shown in Fig. 8.3 has the initial settling time $t_{is} \approx 1$ s , and the final settling time $t_{fs} \approx 0.19$ s For the low gain system in Fig. 8.5a we have $t_{is} \approx 1.35$ s and $t_{fs} \approx 2.07$ s. The 35% increase of the initial settling time is necessary in order to achieve proper operation for both low and high inertia, but the tenfold increase in the final settling time is an undesired consequence. Obviously is would be convenient to operate the system with low gain during the initial part and with larger gain during the final part of the transient.

The SAPI control described in Section 5.3 has variable gain which provides for different time constants during transient and steady state. This property makes it suitable

for application in the position loop. Since the integral component of the control is not needed in the position loop, it can be omitted. Then, the sliding-adaptive proportional (SAP) control is obtained. If the resulting controller from (5.38) is applied in the position loop instead of the constant gain G_θ in Fig. 8.1, the following position control algorithm is obtained.

$$u_\omega = p_\theta \cdot e_1 \tag{8.7}$$

$$\dot{p}_\theta = q_2 \cdot (e_1 + T_c \cdot e_2) \cdot e_1 + \varepsilon \cdot (g_\theta - p_\theta) - \mu_6 \tag{8.8}$$

$$e_1 = q_1 \cdot e_\theta = q_1 \cdot (r_\theta - y_\theta) \tag{8.9}$$

$$e_2 = \dot{e}_1 = q_1 \ (\dot{r}_\theta - y_\omega) \tag{8.10}$$

$$\mu_6(p_\theta, e_1, \Omega) = \begin{cases} 0 \ , & -\Omega \le p_\theta \cdot e_1 \le \Omega \\ \mu_0 \cdot \left[p_\theta - \dfrac{\Omega \cdot \mathrm{sign}(p_\theta)}{|e_1|} \right] , & \text{elsewhere.} \end{cases} \tag{8.11}$$

In (8.10), the derivative of the position is calculated directly, instead of using the nonideal differentiator as was done for the speed control. This was done because the speed measurement y_ω is readily obtainable and it is assumed that the derivative of the position command is also available.

Parameter T_c is chosen in such a way that the system enters sliding mode early enough, so that the steady state

is reached without overshoot, in case of the largest expected inertia. From the example in Fig. 8.5b and from (8.6), for our system

$$T_c = 0.33 \text{ s} \quad . \tag{8.12}$$

The gain g_θ is selected to be equal to the largest gain that provides satisfactory response with the smallest inertia. From Fig. 8.3 and from (8.4) we have

$$g_\theta = 30 \quad . \tag{8.13}$$

For the selection of adaptation gains q_1 and q_2, and the resetting gain ε, the appropriately modified Theorem D.1, or the describing function method from Appendix D.2, can be used. However, since the methods are either overly conservative or approximate, the final decision has to be made through simulations. The values we have used are

$$q_1 = 10 \ , \quad q_2 = 30 \ , \quad \varepsilon = 30 \ . \tag{8.14}$$

The limiting gain μ_0 should be as large as possible and we have used $\mu_0 = 10^4$.

The system in Fig. 8.1 with the position controller G_θ implemented by the SAP nonlinear equations (8.7)-(8.11), was simulated. The speed loop remained the same SVSPI con-

a)

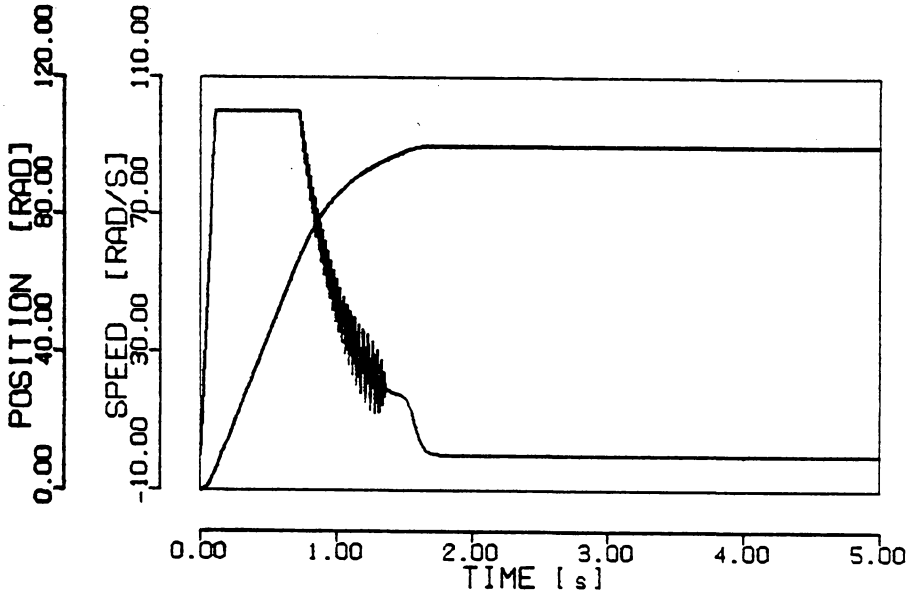

b)

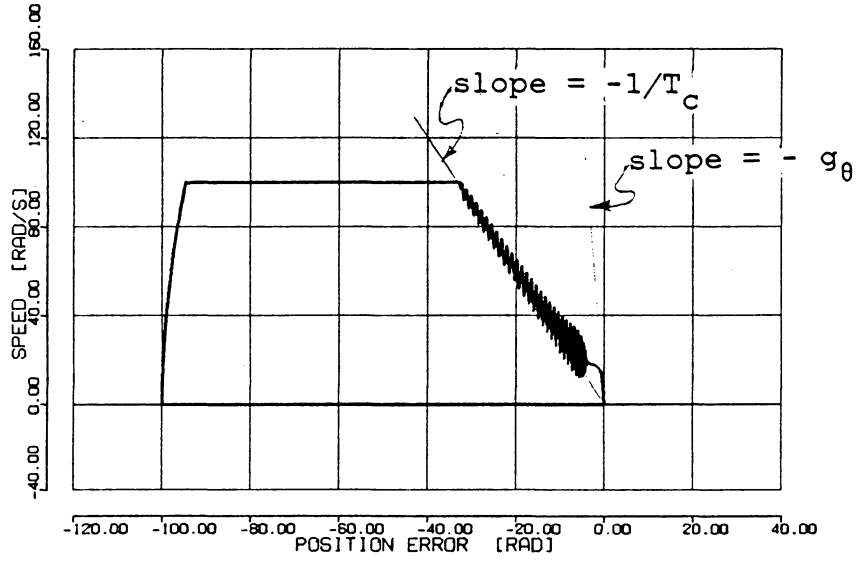

Fig. 8.6: Transient response of the servo system with SAP control, for $q_1 = 10$, $q_2 = \varepsilon = g_\theta = 30$, and nominal plant.

a) Time domain.

b) State plane.

trol that was used for Figures 7.3-7.5. The waveforms that resulted after the test inputs from Fig.8.2 were applied, are shown in Fig. 8.6a. The state plane diagram for the same system, is shown in Fig. 8.6b. During the end of the initial part of the transient the system is in the nonideal sliding mode characterized by the time constant T_c . During the final part of the transient the system leaves the sliding mode and enters the linear mode characterized by the proportional gain $g_\theta = 30$, which corresponds to the time constant $\tau_\theta \approx 1/g_\theta$. The resulting final settling time is $t_{fs} \approx 0.41$ s (a fivefold improvement over the response in Fig. 8.5a), with the initial settling time practically unchanged.

The simulation results of the same control system with the moment of inertia increased ten times are shown in Fig. 8.7. The same decrease in the settling time can be observed again, while no overshoot has appeared.

If the chattering that is present during the sliding mode operation is unacceptably large, it can be reduced by decreasing the gains involved. The simulation results for nominal and a ten times larger moment of inertia with the gains changed to

$$g_\theta = 20 , \quad q_1 = 5 , \quad q_2 = 20 , \quad \varepsilon = 20 , \qquad (8.15)$$

a)

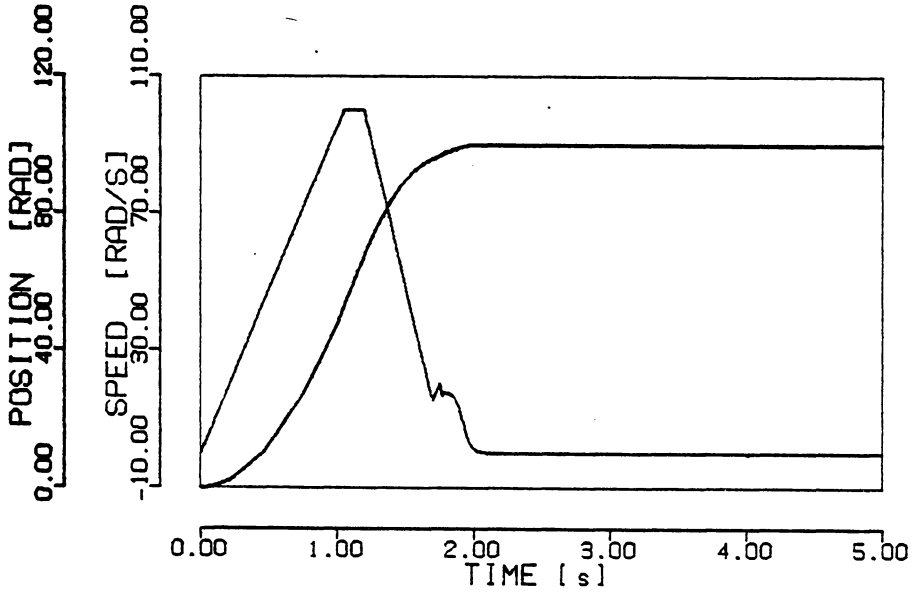

b)

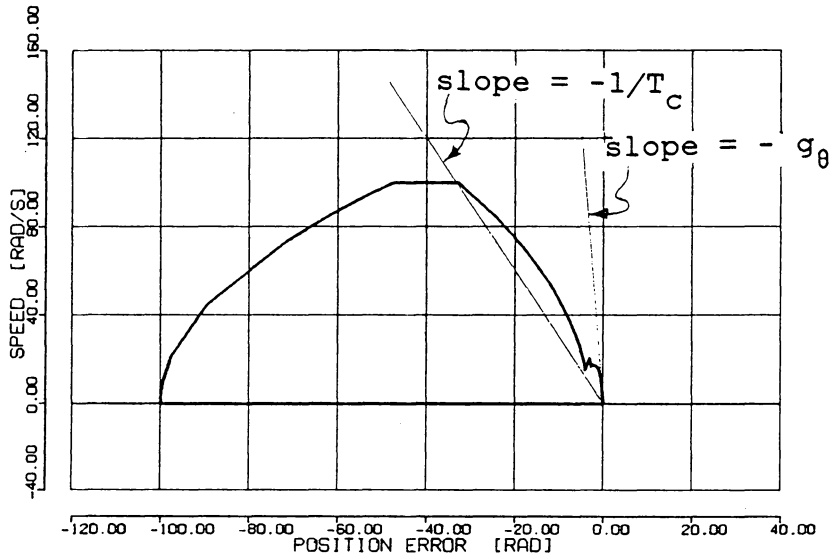

Fig. 8.7: Transient response of the servo system with SAP control, for $q_1 = 10$, $q_2 = \varepsilon = g_\theta = 30$, and moment of inertia increased 10 times.

a) Time domain.

b) State plane.

a)

b)

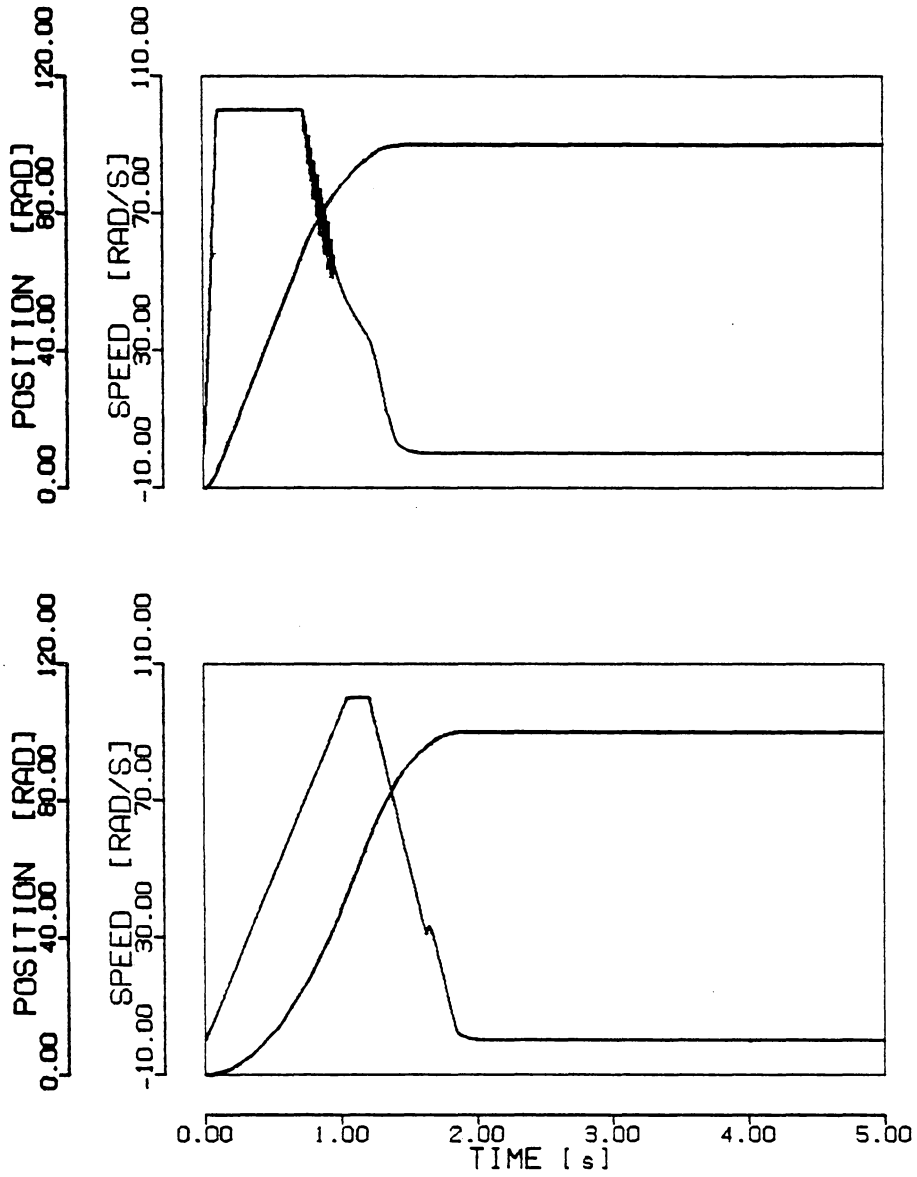

Fig. 8.8: Transient response of the servo system with SAP control, for $q_1 = 5$, $q_2 = \varepsilon = q_\theta = 20$.

a) Nominal plant.

b) Moment of inertia increased 10 times.

are shown in Fig. 8.8. Duration of the period when the system with low inertia is in the sliding mode, is considerably reduced, while the general shape of response remained unchanged. In the case of large inertia the response is changed only slightly.

The sliding mode can be completely eliminated if even lower values of gains are used, as shown in Fig. 8.9, where the gains are

$$g_\theta = 20 \ , \quad q_1 = 5 \ , \quad q_2 = 10 \ , \quad \varepsilon = 10 \ . \qquad (8.16)$$

The price that is paid for the reduction or elimination of sliding mode is in the reduction of steady state gain g_θ. This reduction results in the increase of the equivalent time constant for the small signals.

Improvement achieved by the use of the SAP control in the position loop is not only manifested in the step response. For the very small perturbations around steady state the effective proportional gain is g_θ. It is much larger than the one which would be possible if the constant gain controller is used. This results in the significantly decreased small signal time constant, or equivalently in a significant increase of the small signal bandwidth. Therefore, the small signal properties of the control system are improved, which is very beneficial for tracking and other performance requirements.

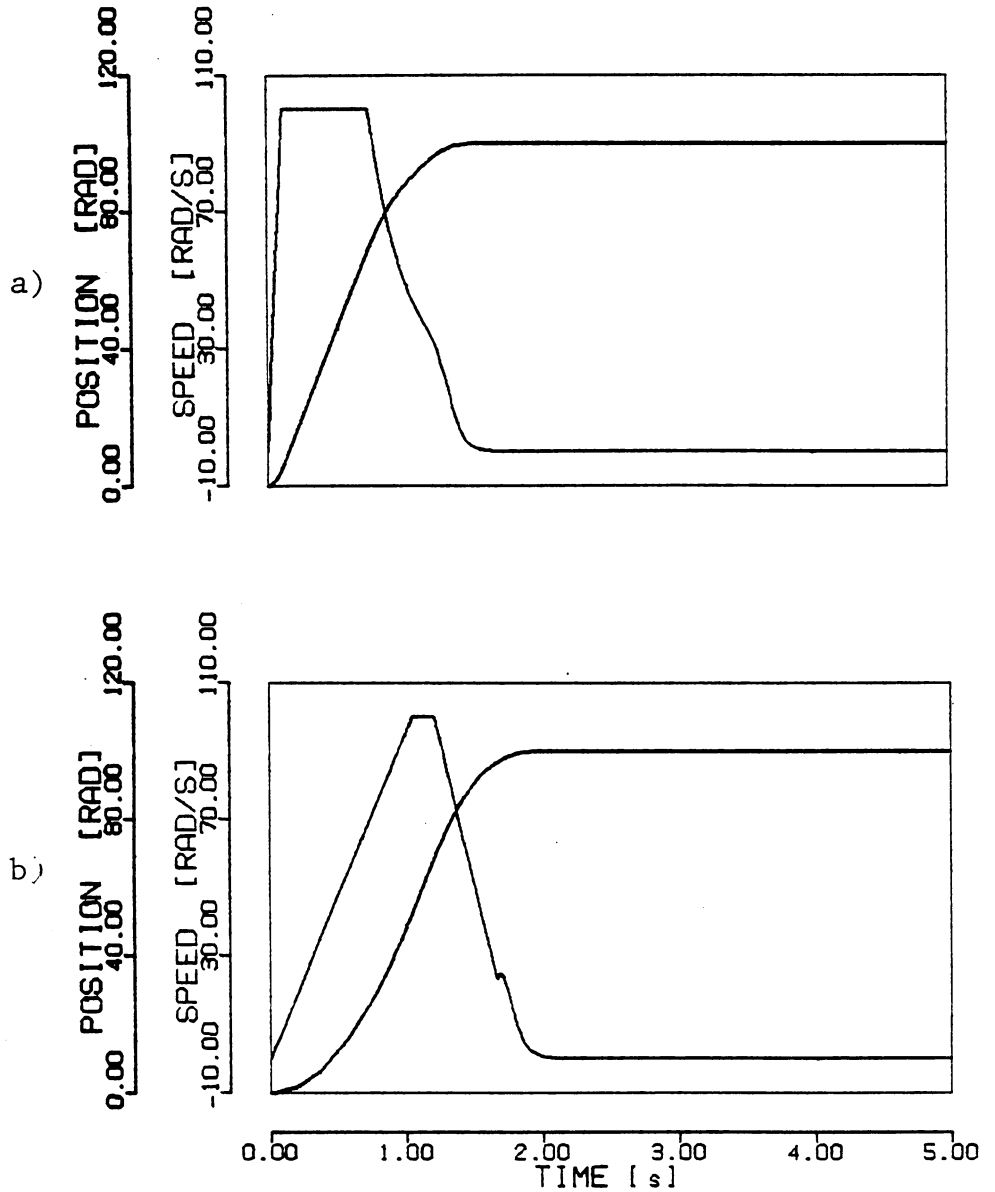

Fig. 8.9: Transient response of the servo system with SAP control, for $q_1 = 5$, $q_2 = \varepsilon = 10$, $q_\theta = 20$.

a) Nominal plant.

b) Moment of inertia increased 10 times.

The systems presented in this chapter were also simulated for the very small step change of the position command. The step amplitude was 1 radian so that the speed limit is not reached. Then the equivalent small signal time constant and bandwidth were evaluated based on the following definitions.

τ_θ - equivalent small signal time constant:

$$\tau_\theta \triangleq \frac{t_t}{\log_2(10^4)}$$

where t_t is the transient time defined before, for the step amplitude of 1 rad.

B_θ - small signal bandwidth:

$$B_\theta \triangleq \frac{1}{2 \cdot \pi \cdot \tau_\theta} \quad .$$

The numerical results for all five cases presented in this chapter are summarized in Table 8.1. Besides the points already discussed, the robustness of the new algorithms is apparent. For the last three cases a tenfold increase in inertia resulted in only 20% increase of the large signal transient time and virtually unchanged small signal bandwidth.

* * *

Table 8.1: Dynamic performance of the position control algorithms, with SVSPI control in speed loop

Case from Fig.	Control G_θ	g_θ	q_1	$q_2 = \varepsilon$	J_n [1]	t_{is} (sec.)	t_{fs} (sec.)	τ_θ (sec)	B_θ (Hz)
7.3	Prop.	30	0	0	1	1.00	0.19	0.033	4.70
7.4					10	oscillating			
7.5a	Prop.	3	0	0	1	1.35	2.07	0.331	0.48
7.5b					10	1.65	2.06	0.330	0.48
7.6	SAP	30	10	30	1	1.31	0.41	0.036	4.39
7.7					10	1.65	0.42	0.039	4.12
7.8a	SAP	20	5	20	1	1.19	0.39	0.052	3.02
7.8b					10	1.61	0.37	0.053	3.00
7.9a	SAP	20	5	10	1	1.19	0.42	0.052	3.00
7.9b					10	1.61	0.44	0.055	2.89

[1] Moment of inertia normalized to the motor moment of inertia from Appendix A, equation (A.2).

The preliminary results presented in this chapter are mostly illustrative in nature. Only one of the proposed speed-control algorithms was tested within a position loop. The SAP control that was proposed for use in the position loop has not been analyzed in any detail, nor were the rules for its design. A consistent comparison with other possible algorithms is also missing. These items need further investigation before the SVS and API control concepts can be applied in practice.

Nonetheless, these preliminary examples have already demonstrated the potential of the API control in achieving fast, well behaved, accurate and robust position control. Specifically, the SAP position control with the SVSPI speed control is faster than the sliding mode position control recently presented by Harashima [37], while the chattering in the steady state is avoided, and the high degree of robustness maintained.

Chapter 9

SUMMARY AND CONCLUSIONS

Eight very diverse algorithms for speed control, and two algorithms for position control of electrical drives, have been presented.

A simple, linear PI algorithm, which was presented in Chapter 2, demonstrated the inability of the linear control to satisfactorily deal with nonlinearities like saturation. The problem of the integrator wind-up was somewhat smaller in the PI control with constant integrator limits. However, this algorithm had a quite unsatisfactory performance in the experiment and can hardly be suggested for future use.

The PI control with variable limits, completely eliminated the problem of integrator wind-up. This enabled the employment of large controller gains for the design of less sensitive and faster control systems. Since the variable limits are relatively simple to implement, this algorithm seems to be the simplest and most straightforward way to improve the performance of speed controllers for electrical drives.

The sliding mode control presented in Chapter 3 is unquestionably the most robust, and also relatively simple. The unavoidable chattering, however, diminishes its usefulness. It is important to note that the increased chattering is not a consequence of the slow power processing devices, but of the inability to estimate the system states accurately and timely. Therefore, the reduction in chattering, without sacrificing the performance, can only be achieved by using higher quality and more expensive transducers and measurement devices.

Recently proposed soft variable structure control, was analyzed in Chapter 4. The analysis resulted in the development of the new, modified SVS control. If used as an output feedback, this algorithm has the disadvantage of having a steady state error, and is not very suitable for microprocessor implementation. Otherwise, as was demonstrated in Chapter 4 and Chapter 6, it has excellent transient response and very good robustness.

Merging of the SLM, PI and SVS concepts resulted in the adaptive PI control, described in Chapter 5. The API control is essentially an adaptive control with a resetting mechanism. The adaptation process takes place during the transient, and the controller resets to the VLPI control during steady state. The SVS version of the API control has performance characteristics similar to the modified SVS control, with the steady state error eliminated. From the simulation

results, it seems to be the best of the presented algorithms for speed control of electrical drives, regarding speed of response, accuracy and robustness.

The sliding API control suffers from the same problems as SLM control when applied for speed control. However, the sliding/adaptive proportional (SAP) control, applied in the position loop in Chapter 8, demonstrated superior performance with respect to the simple proportional control, and the SLM control examples that have been published so far.

When implementing the adaptive control with parameter and torque observer in Chapter 7, the same problems as reported by other authors were encountered. They are the drift of the adaptive gains, and limitations on the maximum value of adaptation gains.

From the analyses of all the algorithms, and especially from the comparison in Chapter 6, the following general conclusions can be made.

- Very fast and nonoscillatory transient response, high accuracy, good disturbance rejection, and robustness to large parameter variations, cannot be obtained with classic linear control.
- It was possible to design all the presented nonlinear control algorithms to approach the above performance requirements very closely.

- All the nonlinear algorithms are quite complex to implement.
- There are no simple and straightforward design rules for the nonlinear algorithms. Most of the theory is still devoted to proving the stability.
- There is a remarkable similarity between the SLM, SVS, API and standard adaptive control algorithms.

Regarding the possible practical applications of the nonlinear control algorithms in the near future, the following remarks seem appropriate.

- Because the performance requirements will keep increasing, there will be more and more attempts to apply nonlinear algorithms for the control of electrical drives.
- These algorithms will not have widespread use, until simple and straightforward design methods are developed.
- At this stage of development, the choice between different nonlinear algorithms will not be based on their relative merits, but on the familiarity of designer, with the particular methodology.

The results presented in this work are not restricted to the control of electrical drives. All the algorithms presented in the dissertation applied are equaly applicable to any stabilizable SISO system.

APPENDIX A

MOTOR MODELS

In this appendix, different motor models used in analyses and simulation, are presented. Parameter values are also given.

A.1. DC MOTOR MODEL

The most common model [25, 33] of a constant field dc motor is shown in Fig. A.1 where the symbols represent

- v_a - armature voltage
- i_a - armature current
- R_a - armature resistance
- L_a - armature inductance
- k_m - electromechanical constant
- D_m - mechanical damping
- J_m - motor moment of inertia
- ω - rotor speed
- T_ℓ - load torque (including constant friction torque).

The parameters k_m, D_m, and the friction part of T_ℓ are usually nonlinear. This was accounted for, to some extent, in simulations (see Appendix E). In theoretical analyses k_m and D_m are assumed constant, and $T_\ell = 0$.

It is customary to include the output impedance of the power amplifier that generates v_a , in the model of the armature circuit with the lumped resistance and inductance of R and L, respectively. Similarly, mechanical load may be combined with the motor model, and in the simplest case, J and D represent total mechanical moment of inertia and damping. Under these conditions the motor speed is given by

$$\underline{\omega} = \frac{k_m}{(s\cdot L + R)\cdot(s\cdot J + D) + k_m^2}\cdot\left(\underline{v}_a - \frac{s\cdot L + R}{k_m}\cdot\underline{T}_\ell\right) \quad . \tag{A.1}$$

From the Appendix F.1, at $\omega = 100$ rad/s, the parameter values are:

$$\begin{aligned} R &= 2.3\ \Omega \quad , & J &= 55\cdot10^{-6}\ \text{kg m}^2 \\ L &= 80\ \mu\text{H} \quad , & D &= 2\cdot10^{-6}\ \text{N}\cdot\text{s/rad} \\ & & k_m &= 0.02\ \text{V}\cdot\text{s/rad} \quad . \end{aligned} \tag{A.2}$$

From equation (A.1), if T_ℓ , the motor transfer function is

$$H_m(s) \triangleq \frac{\underline{\omega}}{\underline{v}_a} = \frac{K_m\cdot s_e\cdot s_m}{(s + s_e)(s + s_m)} \quad , \tag{A.3}$$

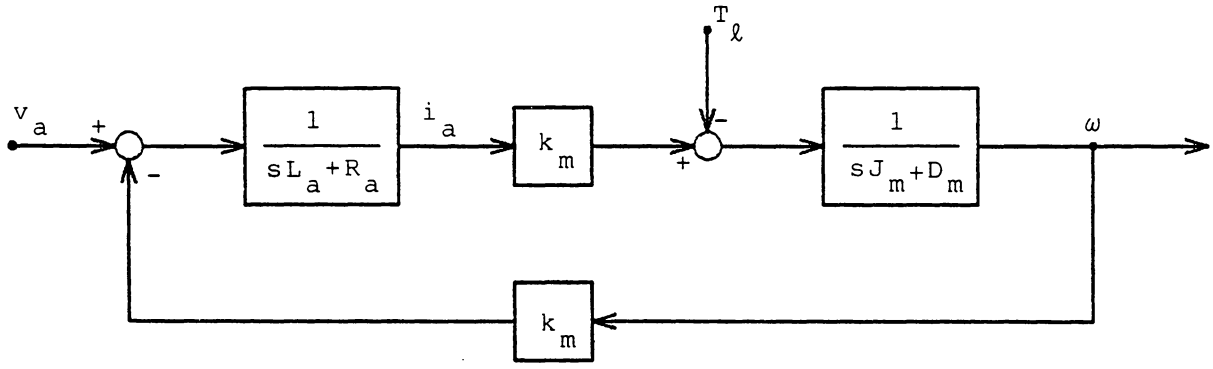

Fig. A.1: Model of a constant field dc motor.

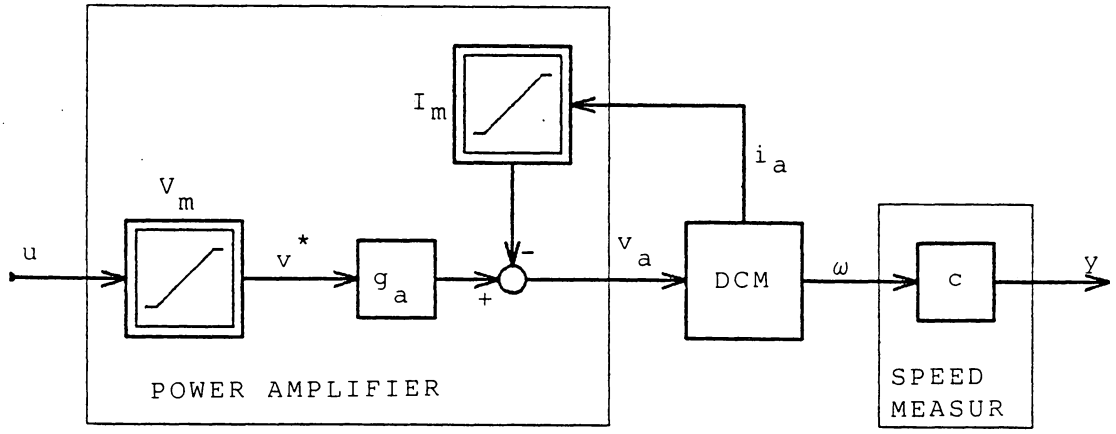

Fig. A.2: Voltage controlled dc drive.

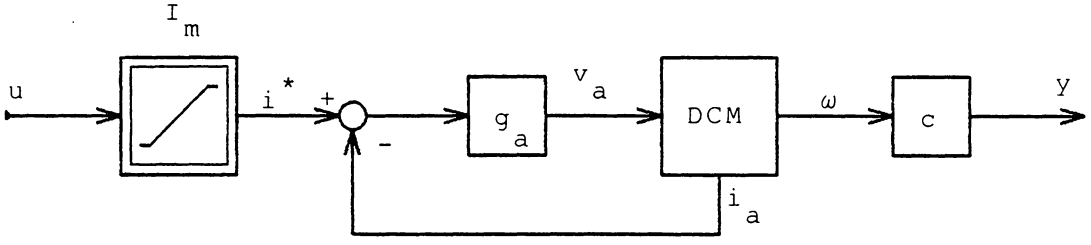

Fig. A.3: Current controlled dc drive.

where numerically

$$K_m \approx 50 \text{ rad/(V s)}$$

$$s_e = \frac{1}{T_e} \approx 3 \cdot 10^4 \text{ rad/s} \qquad \text{(A.4)}$$

$$s_m = \frac{1}{T_m} \approx 3.3 \text{ rad/s} \quad .$$

T_m is mechanical time constant, and T_e is electrical time constant.

From Appendix F.1 it follows that a constant, friction-type torque of

$$T_\ell \approx 0.017 \text{ N} \cdot \text{m} \qquad \text{(A.5)}$$

is present at all times.

A.2. VOLTAGE CONTROLLED DRIVE

To complete a drive, a power amplifier is connected to the armature terminals of a motor, and a speed measurement device is attached to the rotor shaft. In the voltage drive, an auxiliary, current limiting circuit, must be added to the power amplifier, for protection purposes. The block diagram of such system is shown in Fig. A.2, where the symbols represent

u - control input

v^* - reference voltage

V_m - voltage limit

I_m - current limit

g_a - amplifier gain

c - speed measurement gain

y - speed measurement

DCM - dc motor

From Appendix F.2,

$$V_m = 12 \text{ V} \quad , \qquad I_m = 3.6 \text{ A} \quad . \tag{A.6}$$

By using Figures A.1 and A.2, and equation (A.1), the speed measurement y, within the linear region of operation is given by

$$\underline{y} = \frac{c \cdot k_m}{(s \cdot L + R)(s \cdot J + D) + k_m^2} \cdot \left(g_a \cdot \underline{u} - \frac{s \cdot L + R}{k_m} \underline{T}_\ell \right) \quad . \tag{A.7}$$

Gains g_a and c are adjusted so that in steady state

$$u = 5 \text{ V} \quad \Rightarrow \quad \omega = 100 \text{ rad/s} \quad \Rightarrow \quad y = 5 \text{ V} \qquad \text{for } T_\ell = \text{const.} = 0.017 \text{ N} \cdot \text{m} \quad . \tag{A.8}$$

Then

$$g_a \approx 0.8 \quad , \qquad c = 0.05 \text{ V} \cdot \text{s/rad} \quad . \tag{A.9}$$

From (A.7) and (A.3) if $T_\ell = 0$, the transfer function is

$$H_v(s) \triangleq \frac{\underline{y}}{\underline{u}} = \frac{K_v}{(s \cdot T_e + 1) \cdot (s \cdot T_m + 1)} \qquad (A.10)$$

where

$$K_v = g_a \cdot c \cdot K_m \simeq 2 \quad . \qquad (A.11)$$

The constants T_e and T_m are given by (A.4).

If the output filter is used to eliminate the noise from the speed measuring device, the transfer function is

$$H_{vf}(s) = \frac{K_v}{(s \cdot T_e + 1) \cdot (s \cdot T_m + 1) \cdot (s \cdot T_f + 1)} \quad . \qquad (A.12)$$

From Appendix F.3

$$T_f = 0.5 \text{ ms} \quad , \qquad (A.13)$$

and obviously from (A.4), T_e can be neglected. Then

$$H_{vf}(s) \simeq \frac{K_v}{(s \cdot T_m + 1) \cdot (s \cdot T_f + 1)} \quad . \qquad (A.14)$$

A.3. CURRENT CONTROLLED DRIVE

Block diagram of the current controlled drive is shown in Fig. A.3, where i^* is a current reference, and the rest of the symbols are the same as in the previous section. Here,

the current feedback is present at all times. From Figures A.1 and A.3, the speed measurement is given by

$$\underline{y} = \frac{c \cdot k_m \cdot g_a}{(sL + R + g_a)(sJ + D) + k_m^2} \cdot (\underline{i}^* - \frac{sL + R + g_a}{k_m \cdot g_a} \cdot \underline{T}_\ell) \quad . \tag{A.15}$$

If $T_\ell = 0$, the transfer function within the linear region where $i^* = u$, is given by

$$H_i(s) \triangleq \frac{\underline{y}}{\underline{u}} = \frac{c \cdot k_m \cdot g_a}{(s \cdot L + R + g_a)(s \cdot J + D) + k_m^2} \quad , \tag{A.16}$$

or

$$H_i(s) = \frac{K_i \cdot s_1 \cdot s_2}{(s + s_1)(s + s_2)} \quad . \tag{A.17}$$

If the current controller gain is

$$g_a = 100 \quad , \tag{A.18}$$

the parameter values in (A.17) are

$$K_i \approx 170 \ , \quad s_1 \approx 0.11 \text{ rad/s} \ , \quad s_2 \approx 1.3 \cdot 10^6 \text{ rad/s} \ . \tag{A.19}$$

Obviously, $s_1 \approx 0$ and s_2 is undominant so that (A.17) can be approximated with

$$H_i(s) \approx \frac{K_i \cdot s_1}{s} \approx \frac{c \cdot k_m}{s \cdot J} \approx \frac{18}{s} \quad , \tag{A.20}$$

or

$$H_i(s) = \frac{c}{s \cdot \tau_m} \quad , \tag{A.21}$$

where

$$\frac{1}{\tau_m} = \frac{k_m}{J_m} \approx 360 \text{ rad}/(A \cdot s^2) \quad . \tag{A.22}$$

If the load torque is taken in the account, from (A.15) and (A.20), the speed measurement is

$$\underline{y} \approx \frac{c \cdot k_m}{s \cdot J} \cdot \underline{u} - \frac{c}{s \cdot J} \cdot \underline{T}_\ell \quad . \tag{A.23}$$

In the case when output filter is present we have

$$H_{if}(s) = \frac{c}{s \cdot \tau_m \cdot (s \cdot T_f + 1)} \quad , \tag{A.24}$$

or numerically

$$H_{if}(s) = \frac{36 \cdot 10^3}{s \cdot (s + 2 \cdot 10^3)} \quad . \tag{A.25}$$

For $T_\ell \neq 0$, instead of (A.25) we have

$$\underline{y} = \frac{2 \cdot 10^3}{s \cdot (s + 2 \cdot 10^3)} \cdot (18.2 \, \underline{u} - 900 \cdot \underline{T}_\ell) \quad . \tag{A.26}$$

A.4. STATE SPACE MODEL

The motor model in Fig. A.2 can also be represented in the state space form

$$\begin{bmatrix} \dot{\omega} \\ \dot{i}_a \end{bmatrix} = \begin{bmatrix} -\frac{D}{J} & \frac{k_m}{J} \\ -\frac{k_m}{L} & -\frac{R}{L} \end{bmatrix} \cdot \begin{bmatrix} \omega \\ i_a \end{bmatrix} + \begin{bmatrix} 0 \\ \frac{1}{L} \end{bmatrix} \cdot v_a + \begin{bmatrix} -\frac{1}{J} \\ 0 \end{bmatrix} \cdot T_\ell \tag{A.27}$$

For the voltage drive in Fig. A.2, supposing that the current is in the limit only when the voltage is in the limit, we have

$$\begin{bmatrix} \dot{\omega} \\ \dot{i}_a \end{bmatrix} = \begin{bmatrix} -\frac{D}{J} & \frac{k_m}{J} \\ -\frac{k_m}{L} & -\frac{R}{L} \end{bmatrix} \cdot \begin{bmatrix} \omega \\ i_a \end{bmatrix} + \begin{bmatrix} 0 \\ \frac{g_a}{L} \end{bmatrix} \cdot v^* + \begin{bmatrix} -\frac{1}{J} \\ 0 \end{bmatrix} \cdot T_\ell \tag{A.28}$$

$$v^* = \begin{cases} V_m , & u_1 > V_m \\ u_1 , & |u_1| \leq V_m \\ -V_m , & u_1 < V_m , \end{cases}$$

where the symbol u_1 was used instead of u. Now, if the input and load torque consist of the constant values and perturbation,

$$u_1 = r + u$$
$$T_\ell = T_{\ell e} + d \tag{A.29}$$

from (A.28) the equilibrium values of ω_e and i_{ae} can be found. Then by substitutions

$$x_1 = c\cdot(\omega - \omega_e)$$
$$x_2 = \dot{x}_1 = c\cdot\left[-\frac{D}{J}\cdot\left(\frac{x_1}{c} + \omega_e\right) + \frac{k_m}{J}\cdot i_a - \frac{1}{J}\cdot(T_{\ell e} + d)\right] \tag{A.30}$$

$$v^* = r + v$$
$$U_u = V_m - r \tag{A.31}$$
$$U_\ell = -V_m - r$$

the system (A.28) can be transformed into its phase canonical form

$$\begin{bmatrix} \dot{x}_1 \\ \dot{x}_2 \end{bmatrix} = \begin{bmatrix} 0 & 1 \\ -a_1 & -a_2 \end{bmatrix}\cdot\begin{bmatrix} x_1 \\ x_2 \end{bmatrix} + \begin{bmatrix} 0 \\ b \end{bmatrix}\cdot v + \begin{bmatrix} 0 \\ -h \end{bmatrix}\cdot d \tag{A.32}$$

$$v = \begin{cases} U_u\,, & u > U_u \\ u\,, & U_\ell \le u \le U_u \\ U_\ell\,, & u < U_\ell \end{cases} \tag{A.33}$$

where

$$a_1 = \frac{R \cdot D + k_m^2}{J \cdot L}$$

$$a_2 = \frac{R}{L} + \frac{D}{J}$$

$$b = \frac{c \cdot k_m \cdot g_a}{J \cdot L} \quad . \tag{A.34}$$

$$h = \frac{c \cdot R}{J \cdot L}$$

Using (A.2), (A.6) and (A.9), numerically we obtain

$$V_m = 12 \text{ V}$$

$$a_1 \approx 9.2 \cdot 10^4 \quad , \qquad a_2 \approx 2.9 \cdot 10^4 \tag{A.35}$$

$$b \approx 1.8 \cdot 10^5 \quad , \qquad h \approx 2.6 \cdot 10^7 \quad .$$

As mentioned in Appendix A.2, g_a and c in (A.9) are so adjusted that for $T_{\ell e} = 0.017$ N·m , the system has unity steady state gain, i.e., $y_e = c\omega_e = r$. Therefore, in this case

$$x_1 = c \cdot \omega - r$$

$$x_2 = c \cdot \dot{\omega} \quad . \tag{A.36}$$

For the sliding mode control, an external choke was added in order to reduce the armature current oscillations. With

$$L_{ext} = 5 \text{ mH} \quad , \tag{A.37}$$

the total armature inductance becomes $L + L_{ext}$, and the model parameters for (A.30) become

$$\begin{aligned} a_1 &\simeq 1.5 \cdot 10^3 \quad , \qquad a_2 \simeq 460 \\ b &\simeq 2.9 \cdot 10^3 \quad , \qquad h \simeq 4.2 \cdot 10^5 \quad . \end{aligned} \tag{A.38}$$

With $I_m = 3.6$ A a maximum operating torque corresponds to 1.8 A; hence

$$\max|d| \simeq 0.036 \text{ N} \cdot \text{m} \quad . \tag{A.39}$$

APPENDIX B

PROOFS FOR CHAPTER 2

In this appendix a discussion of stability for some cases of the PI control with nonlinear elements, is presented.

B.1. STABILITY OF PI CONTROLLER WITH INPUT SATURATION

For a linear system with a linear compensator, in which plant input has a saturation, the following statement can be proved as a corollary to circle criterion.

LEMMA B: Consider the system on Fig. 2.2. Then if

i) $r(t) = r = \text{const.}$, and an equilibrium point for this r exists;

ii) $G_c(s) \cdot G(s)$ has no poles with positive real part;

iii) $$\text{Re}\,[G_c(j\omega) \cdot G(j\omega)] > -1 \,, \quad \forall\, \omega \in R \,, \tag{B.1}$$

the system is globally asymptotically stable.

PROOF: If the equilibrium point exists, the model of the system in Fig. 2.2 can be transformed into its perturbed form by offsetting the variables e(t), u(t) and y(t), by their respective equilibrium values. The new model obviously, has the origin as its equilibrium point. Its structure is the same as that of the original model, except for the nonlinearity n, which is translated, but still passes through the origin.

After this transformation the assertion comes as a direct consequence of the circle criterion. The special case of that criterion (Vidyasagar, [74, pp. 278-281]), which is applicable to our case, states that the sufficient condition for the absolute stability of a system with nonlinearity $v = n(u)$, which lies between the straight lines $v = 0$ and $v = \beta \cdot u$, is that the linear part of the system has no poles in the open right half plane, and that

$$\inf_{\omega \in R} \{Re[G_c(j\omega) \cdot G(j\omega)]\} + \frac{1}{\beta} > 0$$

In our case $\beta = 1$, and the assertion follows.

□

REMARKS:

1. The condition (i), that the equilibrium point exists, is indispensable for the saturation nonlinearity.

Consider a case when $G_c(0) = \infty$, (as in PI control), and $G(0) = k = \text{const}$. Then for any $r > k \cdot U_m$, an equilibrium point does not exist and the system is unstable. However, in practice, this condition is always implicitly assumed.

2. The conditions of the Lemma are sufficient for the absolute stability, i.e., for any nonlinearity that lies in the sector $[0,\beta]$. The statement also refers to any linear $G(s)$ and $G_c(s)$, not specifically to the PI control. Hence, it may be expected that the condition (B.1) is quite conservative, in our case.
3. Condition (B.1) has a simple graphic interpretation. It requires the Nyquist plot of $G_c(j\omega) \cdot G(j\omega)$ to completely lie to the right of the vertical line passing through the point (-1,0) in the complex plane.

B.2. EXAMPLE

An abstract example of a system which does not satisfy Lemma B, is analyzed using describing functions. Consider a system in Fig. 2.2 with

$$G_c(s) = 6 \cdot \frac{s + 3}{s} \tag{B.2}$$

$$G(s) = \frac{2}{s + 1} \tag{B.3}$$

$$U_m = 1 \quad . \tag{B.4}$$

If there were no nonlinearity, i.e., $v \equiv u$, the closed loop transfer function would be

$$T(s) \triangleq \frac{y}{r} = \frac{12 \cdot (s + 3)}{(s + 9)(s + 4)} \quad . \tag{B.5}$$

In the case when a nonlinearity is present, its effect can be studied with the aid of describing functions. For saturation, the describing function is (Atherton [2, p. 86]),

$$N(a) = m \cdot f_1(\delta/a) \quad , \tag{B.6}$$

where

$$f_1(\rho) = \begin{cases} 1 \\ \frac{2}{\pi} \cdot [\sin^{-1}\rho + \rho \cdot (1 - \rho^2)^{\frac{1}{2}}] \\ -1 \end{cases} \quad . \tag{B.7}$$

Variable a is the amplitude of the first harmonic of an assumed periodic signal at the input of the saturation; m is the slope (gain) of the linear part of the saturation function; and δ is the value of the input at which the saturation is reached. In our case $m = \delta = 1$.

The Nyquist diagram of $G_c(j\omega) \cdot G(j\omega)$ is shown in Fig. B.1 together with the function $-1/N(a)$. It can be observed that the linear part of the system does not satisfy the condition

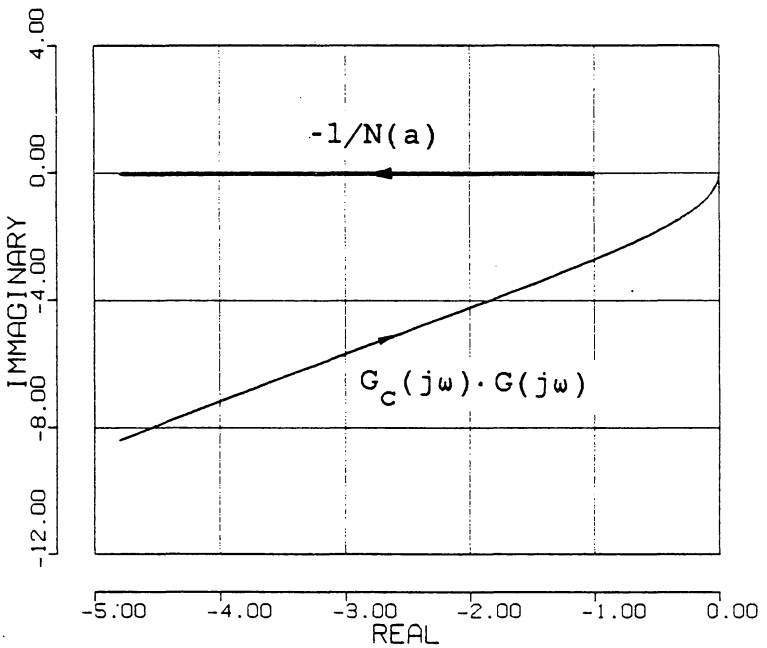

Fig. B.1: Describing function of the saturation nonlinearity, and the Nyquist diagram of the linear part of the system.

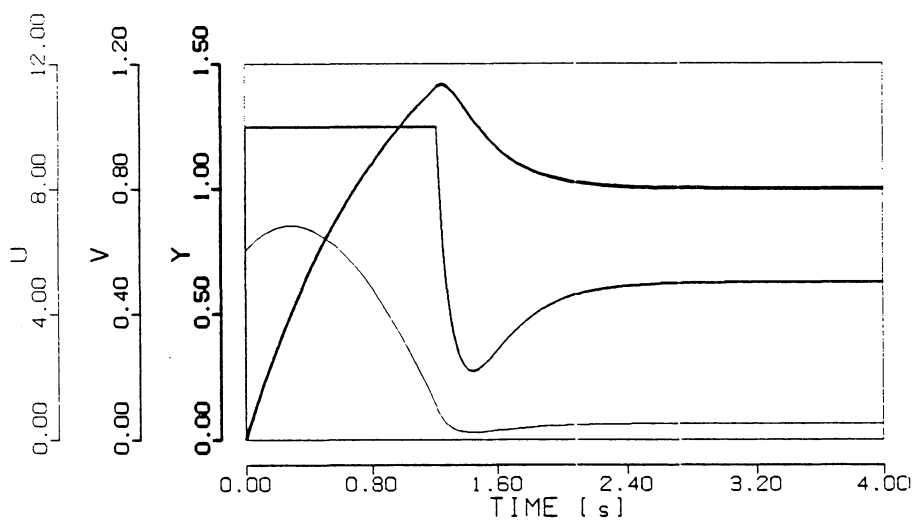

Fig. B.2: Transient response of the system with PI control and input saturation, for the unit step input.

(B.1) of the Lemma B, but also that the Nyquist plot does not intersect with the loci of -1/N(a). Therefore, although the sufficient conditions for stability are not satisfied, neither are the conditions for the existence of limit cycle (Atherton [2, p. 115]).

The time response of the system (B.2)-(B.4), to unit step is shown in Fig. B.2 and stable behavior can be observed.

B.3. STABILITY OF SYSTEMS WITH INTEGRATOR LIMIT

The stability results that are available for handling controller limiting, such as the one shown in Fig. 2.11, are not satisfactory. Both, the absolute stability approach by Jury and Lee [44], Glattfelder and Schaufelberger [32], and the use of Liapunov direct method by Celenteno and Marino [11], have two shortcomings:

i) The nonlinearities are fixed.

ii) The results depend on restraining the nonlinearities to some sector $[\alpha,\beta]$.

In our case, the nonlinearity $\mu_1(u_i,u_p,U_m)$ given by (2.18), with $\mu_0 \to \infty$, belongs to the sector $(0,\infty)$, even with u_p fixed. Therefore, the direct application of the above results is either impossible, or extremely conservative.

The system is singularly perturbed while the limit is exceeded; however it is not, when within the limits. This, formally, results in that the fast subsystem has continuum of equilibrium points, instead of isolated ones. In such a case an existing theory of singular perturbations is not applicable [48].

In spite of these theoretical problems, some conclusions seem to be self-evident. Consider the system in Fig. 2.11 without the nonlinearities in the controller (i.e., $u_p \equiv u_p'$ and $\mu_1 \equiv 0$), but with the input saturation still present. If this system is asymptotically stable it seems plausible to claim that the system will remain asymptotically stable when the controller nonlinearities are included. Indeed, from (2.18)-(2.21), it follows that the controller nonlinearities just ensure that the plant input saturation is never exceeded by the controller output, and otherwise the system is the same. Examples in Fig. 2.12 clarify this statement.

In view of this discussion the following conjecture is proposed.

CONJECTURE:

If the system in fig. 2.11, with the controller nonlinearities removed, is globally asymptotically stable $\forall$ r $\in$ (a,b), then there exists a positive constant μ_0^*, such that the system with the nonlinear-

ities included, and $\mu_1(u_i, u_p, U_m)$ given by (2.18), is globally asymptotically stable $\forall\, r \in (a,b)$ and $\forall\, \mu_0 > \mu_0^*$.

It was not possible to find the proof of the conjecture. However, numerous examples and the reasoning outlined above, led to belief that it is generally true.

In many cases in this work, the proofs of stability rely on the validity of the conjecture. The asymptotic stability is proved for a system without the limiting nonlinearities in the controller, (but with the plant nonlinearities). Then the total system global stability is implied by the virtue of the conjecture. The conclusions are then verified by simulations and experiments.

APPENDIX C

PROOFS FOR CHAPTER 4

In this appendix, the proofs of some stability related statements, given in Chapter 4, are presented.

C.1. COUNTER EXAMPLE TO THE FRANKE'S PROOF

In [28, p. 349] Franke considers the SISO system, which (in his notation) is described by

$$\begin{aligned} \dot{x}(t) &= A\cdot x(t) + b\cdot u(t) \\ \dot{y}(t) &= c'\cdot x(t) \end{aligned} \tag{C.1}$$

with the control

$$u(t) = k_0\cdot w_s + p_1(t)\cdot y(t) \tag{C.2}$$

$$\dot{p}_1(t) = -\frac{1}{q_2}\cdot\{[x(t) - x_s]'\cdot Q_1\cdot b\cdot y(t) + r_2(x,p_1)\cdot p_1(t)\} \tag{C.3}$$

where w_s is a constant reference input, and x_s is equilibrium solution of (C.1) when $u = k_0 w_s$. Further,

$$k_0 = - \frac{1}{c' \cdot A^{-1} \cdot b} \quad , \tag{C.4}$$

$$q_2 > 0 \quad , \tag{C.5}$$

and Q_1 is a solution of

$$A' \cdot Q_1 + Q_1 \cdot A = - R_1 \quad . \tag{C.6}$$

He claims that the system (C.1)-(C.6) is globally asymptotically stable, provided that A is Hurwitz, R_1 is any positive definite matrix, and

$$r_2(x,p_1) \geq 0 \quad . \tag{C.7}$$

It will be shown that the claim fails if $w_s = 0$.

ASSERTION: System (C.1)-(C.6) is not asymptotically stable for $w_s = 0$, if $r_2(0,p_1) = 0$.

PROOF: In equilibrium, if $w_s = 0$, equations (C.1)-(C.3) become

$$\begin{aligned} 0 &= A \cdot x + b \cdot p_1 \cdot c' \cdot x \\ 0 &= x' \cdot Q_1 \cdot b \cdot c' \cdot x + r_2 \cdot p_1 \end{aligned} \tag{C.8}$$

Trivial solution to (C.8) is $x_e = 0$, $p_{1e} = 0$. However, if $r_{2e} = 0$, there is a continuum of equilibrium solutions, described by

$$x_e = 0 \quad , \qquad p_{1e} \in (-\infty, \infty) \quad . \tag{C.9}$$

In that case the system is not asymptotically stable by definition.

□

REMARKS:

1. Franke's proof obviously fails due to (C.7). If that condition is changed to strict relation

$$r_2 > 0 \quad , \tag{C.10}$$

his proof is correct.

2. Since Franke's assertion fails on a particular example which is derived from the general case of multivariable systems in [27], the general case is not true either.
3. In the modified SVS algorithm, described in Section 4.2, condition (C.10) is satisfied by requiring $\varepsilon > 0$, in equation (4.16).

4. Existence of a continuum of equilibrium solutions is standard problem in adaptive control, [1]. There, the adaptive gains usually have an equilibrium solutions on a state space manyfold, not in a single point, [49]. Asymptotic stability is then assured by requiring the inputs to be "persistently exciting", what Franke did not. If the input is persistently exciting, the case $w_s \equiv 0$ is automatically excluded.

C.2. SVS CONTROL AS AN OUTPUT FEEDBACK

LEMMA C: Consider the system (4.1)-(4.9). The necessary condition for

$$(x - x_s)' \cdot Q_1 \cdot b = k \cdot (y - r) \qquad (C.11)$$

to hold, is that

$$c' \cdot b \neq 0 \quad . \qquad (C.12)$$

PROOF: Because $y - r = c' \cdot (x - x_s)$, and (C.11) has to hold for all x, it follows that equality $Q_1 b = k \cdot c$ has to be fulfilled. Then, since Q_1 is positive definite due to (4.9), the following reasoning is true:

$$
\begin{aligned}
& Q_1 \cdot b = k \cdot c \\
\Longleftrightarrow \quad & b = k \cdot Q_1^{-1} \cdot c \\
\Rightarrow \quad & c' \cdot b = k \cdot c' \cdot Q_1^{-1} \cdot c \\
\Rightarrow \quad & c' \cdot b \neq 0 \quad .
\end{aligned}
$$

□

C.3. PROOF OF STABILITY FOR MODIFIED SVS CONTROL

THEOREM C: Consider the system

$$\dot{x} = A \cdot x + b \cdot v \quad , \qquad x \in R^n \tag{C.13}$$

$$\dot{z} = - \lambda \cdot z + \lambda \cdot v \quad , \qquad z, v \in R \tag{C.14}$$

$$y = c'x \quad , \qquad y, u \in R \tag{C.15}$$

$$v = \begin{cases} u & , \quad |u| \leq U_m \\ U_m \cdot \text{sign } u & , \quad |u| > U_m \end{cases} \tag{C.16}$$

$$c' \cdot A^{-1} \cdot b = -1 \quad , \tag{C.17}$$

with the control

$$u = r + p \cdot y \tag{C.18}$$

$$\dot{p} = -q \cdot \{[k_1 \cdot (y - r) + k_3 \cdot p \cdot y + k_4 \cdot (z - r)] \cdot y + \mu_2\} - \varepsilon \cdot p \tag{C.19}$$

where $\mu_2 = \mu_2(p, y, r, U_m)$ is given by (4.7). Then, if the following conditions

i) Matrix A is Hurwitz;

ii) $r = \text{const.} \in (-U_m, U_m)$;

iii) $q > 0$, $\varepsilon > 0$, $k_1 \geq 0$, $k_3 \geq 0$;

are satisfied, there exist some finite $\lambda^* > 0$ and $k_4^* > 0$, such that the system is globally asymptotically stable for all $\lambda > \lambda^*$ and $k_4 > k_4^*$

PROOF: We consider two cases, depending on the value of c'b. If $c'b \neq 0$, the proof is based on the Franke's proof, Lemma C, and Appendix C.1. It is obvious that there exists a Liapunov function for the system (C.13),(C.14) in the form

$$V = [x' \quad z] \cdot Q \cdot \begin{bmatrix} x \\ z \end{bmatrix} \tag{C.20}$$

$$Q = \begin{bmatrix} Q_1 & 0 \\ 0 & k_4 \end{bmatrix} \tag{C.21}$$

where Q_1 satisfies (C.6). Using (C.11) and (C.17), and substituting Q instead of Q_1 in (C.3) we obtain

$$\dot{p}_1 = - \frac{1}{q_2} \cdot [(y - r) \cdot k \cdot y + k_4 \cdot (z - r) \cdot y + r_2 \cdot p_1] \tag{C.22}$$

This equation is same as (C.19) with the following substitutions

$$p = p_1 \quad , \quad q = \frac{1}{q_2} \quad , \quad k_1 = k \quad , \quad k_3 = 0 \tag{C.23}$$

$$r_2 = \frac{\mu_2}{p} + \frac{\varepsilon}{q} \tag{C.24}$$

From the conditions of the theorem, and (4.7), it follows that r_2 in (C.24) is always positive. Then from the Franke's proof [27] with the correction (C.10), the global asymptotic stability follows.

If $c'b = 0$, the system (C.13),(C.14) can be represented, without loss of generality, by

$$\begin{bmatrix} \\ \dot{x} \\ \\ \cdots \\ \dot{z} \end{bmatrix} \triangleq \begin{bmatrix} \dot{y} \\ \\ \dot{x}_r \\ \cdots \\ \dot{z} \end{bmatrix} = \begin{bmatrix} a_y & a'_{yr} & \vdots & 0 \\ & & \vdots & \\ a_{ry} & A_r & \vdots & 0 \\ \cdots & \cdots & \cdots & \cdots \\ 0 & 0 & \vdots & -\lambda \end{bmatrix} \cdot \begin{bmatrix} y \\ \\ x_r \\ \cdots \\ z \end{bmatrix} + \begin{bmatrix} 0 \\ \\ b_r \\ \cdots \\ \lambda \end{bmatrix} v \tag{C.25}$$

$$x_r \in R^{n-1}$$

The equilibrium point of this system, with the control (C.18)-(C.19) is a solution of the following system of non-linear equations.

$$x_e = - A^{-1} \cdot b \cdot (r + p_e \cdot y_e) \tag{C.26}$$

$$y_e = - c' \cdot A^{-1} \cdot b \cdot (r + p_e \cdot y_e) = r + p_e \cdot y_e \tag{C.27}$$

$$z_e = r + p_e \cdot y_e \tag{C.28}$$

$$(k_1 + k_3 + k_4) \cdot p_e \cdot y_e^2 + \mu_2(p_e, y_e, r, U_m) + \frac{\varepsilon}{q} \cdot p_e = 0 \tag{C.29}$$

Equation (C.29) has a trivial solution $p_e = 0$, and that is the only one. Indeed, if $p_e \neq 0$, (C.29) can be multiplied by p_e. Then, due to the assumption (iii) and $k_4 > 0$, the only solution is $p_e = 0$, which is a contradiction. Therefore, the equilibrium point is unique, and is given by

$$x_e = - A^{-1} \, b \, r \quad , \quad z_e = y_e = r \quad , \quad p_e = 0 \; . \tag{C.30}$$

Now define a Liapunov function for the system, as

$$V = w' \cdot Q \cdot w + \frac{1}{q} \cdot p^2 \tag{C.31}$$

where

$$w = \begin{bmatrix} x - x_e \\ \cdots \\ z - z_e \end{bmatrix} = \begin{bmatrix} y - r \\ x_r - x_{re} \\ \cdots \\ z - r \end{bmatrix} \tag{C.32}$$

$$Q = \begin{bmatrix} q_y & q'_{ry} & \vdots & q_{zy} \\ q_{ry} & Q_r & \vdots & q_{rz} \\ \cdots & \cdots & \cdots & \cdots \\ q_{zy} & q'_{rz} & \vdots & q_z \end{bmatrix} = \begin{bmatrix} & & \vdots & q_{zy} \\ & Q_1 & \vdots & \\ & & \vdots & q_{rz} \\ \cdots & \cdots & \cdots & \cdots \\ q_{zy} & q'_{rz} & \vdots & q_z \end{bmatrix} \tag{C.33}$$

and Q_1 is a solution of

$$A' \cdot Q_1 + Q_1 \cdot A = - I \tag{C.34}$$

For V to be a Liapunov function it is necessary that Q is p.d. Matrix Q_1 is positive definite (p.d.), because A is Hurwitz, and then Q is p.d. if $\det(Q) > 0$. Using the expression for the determinant of a partitioned matrix, this is true iff

$$q_z > \begin{bmatrix} q_{zy} & q'_{rz} \end{bmatrix} \cdot Q_1^{-1} \cdot \begin{bmatrix} q_{zy} \\ \\ q_{rz} \end{bmatrix} \tag{C.35}$$

The derivative of V is

$$\dot{V} = \dot{w}' \cdot Q \cdot w + w' \cdot Q \cdot \dot{w} + 2 \cdot \frac{1}{q} \cdot p \cdot \dot{p} \qquad (C.36)$$

Upon substituting (C.13)-(C.19), (C.25), (C.30) and (C.32) into (C.36), and taking (4.7) into account, it follows that

$$\dot{V} = - \Psi_1 - 2 \cdot \Psi_2 - 2 \cdot \Psi_3 \qquad (C.37)$$

$$\Psi_1 = - w' \cdot R \cdot w$$

$$\Psi_2 = \left\{ k_1 \cdot (y - r)' + k_4 \cdot (z - r) - w' \cdot \begin{bmatrix} q'_{ry} \cdot b_r + \lambda \cdot q_{zy} \\ Q_r \cdot b_r + \lambda \cdot q_{rz} \\ q'_{rz} \cdot b_r + \lambda \cdot q_z \end{bmatrix} \right\} \cdot p \cdot y$$

$$\Psi_3 = k_3 \cdot p^2 \cdot y^2 + \mu_2 \cdot p + \frac{\varepsilon}{q} \cdot p^2$$

$$R = \begin{bmatrix} & & \vdots & \\ & I & \vdots & (\lambda I - A) \cdot \begin{bmatrix} q_{zy} \\ q_{rz} \end{bmatrix} \\ & & \vdots & \\ \cdots & \cdots & \cdots & \cdots \\ \begin{bmatrix} q_{zy} & q'_{rz} \end{bmatrix} \cdot (\lambda I - A) & & \vdots & 2 \cdot \lambda \cdot q_z \end{bmatrix}$$

Ψ_3 is p.d. function of p, due to the assumption (iii) and because $\mu_2 \cdot p \geq 0$. Then if Ψ_1 is p.d. and $\Psi_2 \equiv 0$, V will be negative definite. Matrix R (and therefore the function Ψ_1) is p.d. iff

$$2\cdot\lambda\cdot q_z > \begin{bmatrix} q_{zy} & q'_{rz} \end{bmatrix}\cdot(\lambda I - A)^2\cdot\begin{bmatrix} q_{zy} \\ q_{rz} \end{bmatrix} \qquad (C.38)$$

Function Ψ_2 in the expanded form is

$$\Psi_2 = p\cdot y\cdot\{[k_1 - (q'_{ry} + \lambda\cdot q_{zy})]\cdot(y - r) +$$

$$- (x_r - x_{re})'\cdot(Q_r\cdot b_r + \lambda\cdot q_{rz}) +$$

$$+ [k_4 - (q'_{rz}\cdot b_r + \lambda\cdot q_z)]\cdot(z - r)\} \quad .$$

It is identically equal to zero if

$$q_{zy} = \frac{1}{\lambda}\cdot(k_1 - q'_{ry}\cdot b_r) \qquad (C.39)$$

$$q_{rz} = -\frac{1}{\lambda}\cdot Q_r\cdot b_r \qquad (C.40)$$

$$q_z = \frac{1}{\lambda}\cdot(k_4 - q'_{rz}\cdot b_r) = \frac{1}{\lambda}\cdot(k_4 + \frac{1}{\lambda}\cdot b'_r\cdot Q_r\cdot b_r) \qquad (C.41)$$

If the conditions (C.39)-(C.41), (C.35) and (C.38) are satisfied then V and $-\dot{V}$ are p.d. and the assertion of the theorem follows. Now, we will show that there exist positive λ and k_4 such that the above conditions are satisfied.

Because Q_1 is p.d., from Rayleigh's principle [30, p. 142] it follows that there exists a positive scalar $\alpha = \alpha(A)$ such that

$$x' \cdot Q_1^{-1} \cdot x \leq \alpha \cdot x'x \quad , \quad \forall\, x \quad . \tag{C.42}$$

Similarly, because $(\lambda I - A)^2$ is p.d. ($\det(\lambda I - A) = 0$ iff λ is an eigenvalue of A, but $\lambda > 0$ and A is Hurwitz), there exists a scalar $\beta = \beta(A)$ such that

$$x' \cdot (\lambda\, I - A)^2 \cdot x \leq (\lambda + \beta)^2 \cdot x'x \quad , \quad \forall\, x \tag{C.43}$$

By substituting (C.39)-(C.41) into (C.35) and (C.38), and then by applying (C.42) and (C.43), the following two relations are obtained.

$$\lambda \cdot k_4 + b_r' \cdot Q_r \cdot b_r > \alpha \cdot [(k_1 - q_{ry}' \cdot b_r)^2 + b_r' \cdot Q_r^2 \cdot b_r] \tag{C.44}$$

$$2\lambda \cdot (\lambda \cdot k_4 + b_r' \cdot Q_r \cdot b_r) > (\lambda + \beta)^2 \cdot [(k_1 - q_{ry}' \cdot b_r)^2 + b_r' \cdot Q_r^2 \cdot b_r] \tag{C.45}$$

The first one is easily satisfied with large enough λ. However, the second one requires large λ and k_4, to be satisfied. Actually for any $k_4 > k_4^*$, where

$$k_4^* = \frac{1}{2} \cdot [(k_1 - q'_{ry} \cdot b_r)^2 + b'_r \cdot Q_r^2 \cdot b_r] \quad , \qquad (C.46)$$

there exists some λ^* such that for any $\lambda > \lambda^*$ (C.44) and (C.45) hold.

□

APPENDIX D

PROOFS FOR CHAPTER 5

In this appendix, the stability conditions and the describing function, of the sliding-adaptive PI control, are derived.

D.1. PROOF OF STABILITY

First, let us define the nomenclature used in this section.

$|\cdot|$ Euclidean norm of the vector in R^n; absolute value of the complex number.

$\|\cdot\|$ Induced Euclidean norm of the linear operator that maps R^n into R^n.

L_2 Linear space of all measurable vector valued functions, $f(t)$, which satisfy

$$\int_0^\infty |f(t)|^2 \cdot dt < \infty \quad .$$

The space is defined over the field of real numbers. For notational brevity, the dimension of the vector f(t) is not explicitly noted, but it is implicitly understood from the context.

$\|\cdot\|_2$ L_2-norm, i.e., the norm of the functions in L_2 space defined as

$$\|f(t)\|_2 \triangleq \left[\int_0^\infty |f(t)|^2 \cdot dt \right]^{\frac{1}{2}} .$$

We want to prove stability of the control system in Fig. 5.1a with SAPI control from Fig. 5.10. This system can be directly transformed to the system in Fig. D.1, if the substitution

$$p_1 = p_2 - q'_p ,$$

is used. The transfer functions G_f and G_c given in (5.29) and (5.14), satisfy condition (D.3) below. Then the stability follows from the following theorem.

THEOREM D: Consider the system in Fig. D.1 with

$$\varepsilon > 0 , \quad q_1 > 0 , \quad q_2 > 0 , \qquad (D.1)$$

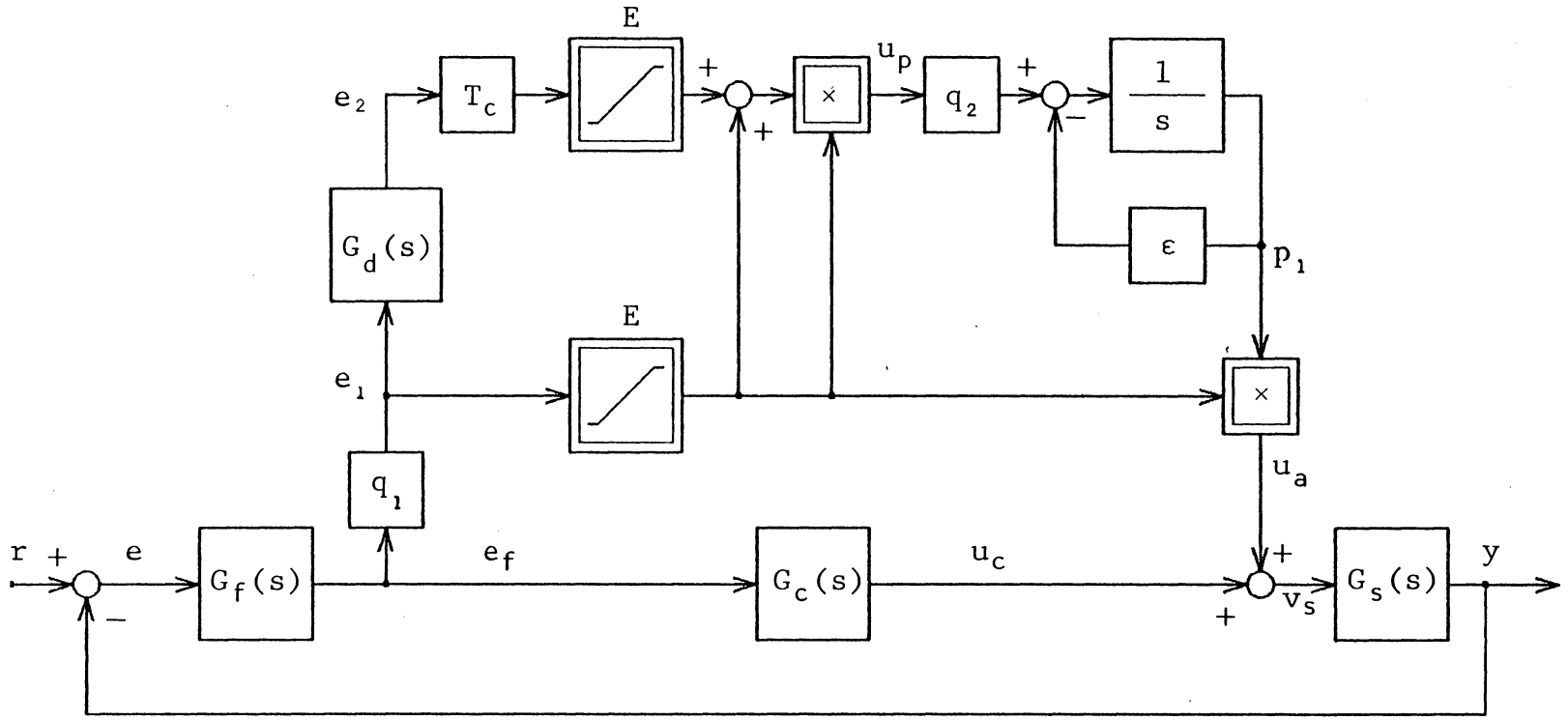

Fig. D.1: SAPI control system, for which the global asymptotic stability is proved.

$$r = \text{const.} \ , \tag{D.2}$$

$$G_f(0) = \text{const.} \ , \quad G_c(0) = \infty \ . \tag{D.3}$$

The sufficient conditions for the equilibrium point $e = 0$, to be globally asymptotically stable, are:

i) The linear subsystem

$$G_1(s) \triangleq \frac{G_s(s)\cdot G_f(s)}{1 + G_s(s)\cdot G_c(s)\cdot G_f(s)} \tag{D.4}$$

is exponentially stable.

ii) The transfer function $G_d(s)$ is exponentially stable.

iii)

$$q_1 < 1/(\sqrt{2}\cdot E\cdot F_m) \tag{D.5}$$

$$q_2 < \varepsilon/(\sqrt{2}\cdot E) \tag{D.6}$$

where

$$F_m = \sup_{\omega\in R} \{|G_1(j\omega)|\cdot[1 + T_c^2\cdot|G_d(j\omega)|^2]^{\frac{1}{2}}\} \ . \tag{D.7}$$

REMARK: Generally, it may not be necessary to require global asymptotic stability. However, if only the I/O stability is

stated, the question of convergence of the adaptive gain p_1 is not answered.

Before proving the theorem we need to transform the system in Fig. D.1, and prove several auxiliary results.

FACT D.1: The stability of the system in Fig. D.1 is equivalent to the stability of the system in Fig. D.2, with $\xi = 0$, and ξ, υ, ϕ, σ given as

$$\xi \triangleq \begin{bmatrix} \xi_1 \\ \xi_2 \\ \xi_3 \end{bmatrix} , \quad \upsilon \triangleq \begin{bmatrix} u_1 \\ u_2 \\ u_3 \end{bmatrix} , \quad \phi \triangleq \begin{bmatrix} f_1 \\ f_2 \\ f_3 \end{bmatrix} , \quad \sigma \triangleq \begin{bmatrix} y_1 \\ y_2 \\ y_3 \end{bmatrix} . \qquad (D.8)$$

PROOF: Because $G_c(0) = \infty$, the input e_f to the block $G_c(s)$ in Fig. D.1, must be equal to zero in equilibrium. Then, from (D.2) and Fig. D.1 it follows that in equilibrium

$$e_e = e_{1e} = e_{fe} = p_1 = 0 \quad . \qquad (D.9)$$

Since this is true for any constant r, and because the nonlinear part of the system depends only on the variable e_1, it is obvious that the stability of the system is uniform in r . Then, it is sufficient to consider only the case $r = 0$.

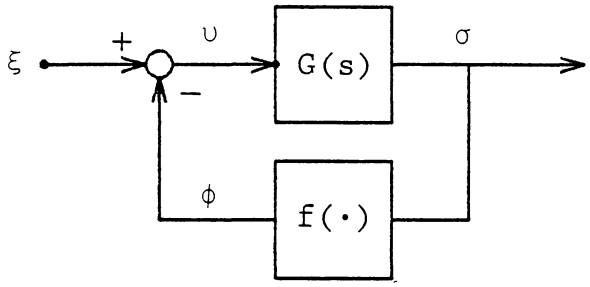

a) Multivariable linear system with memoryless nonlinear feedback.

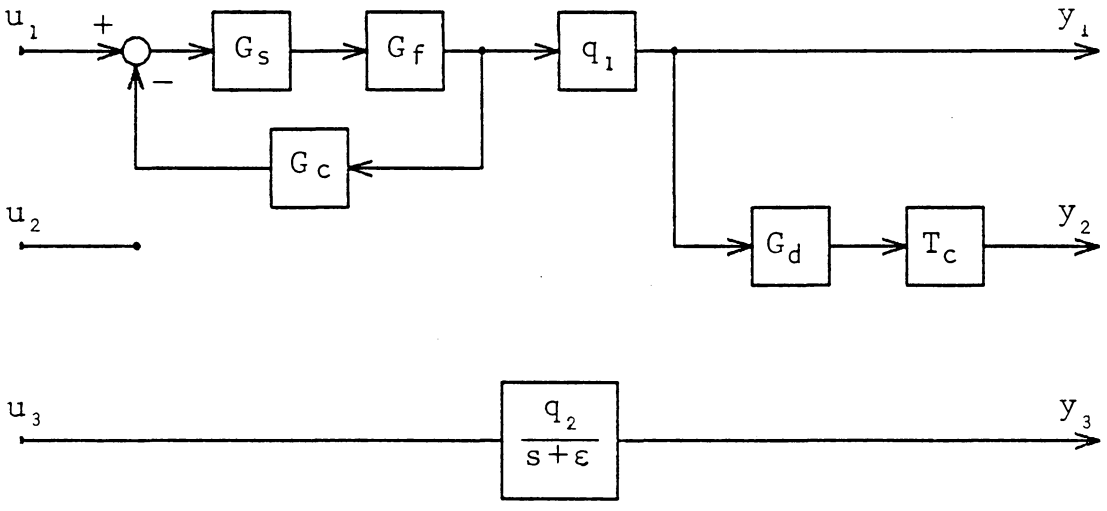

b) Linear part of the system.

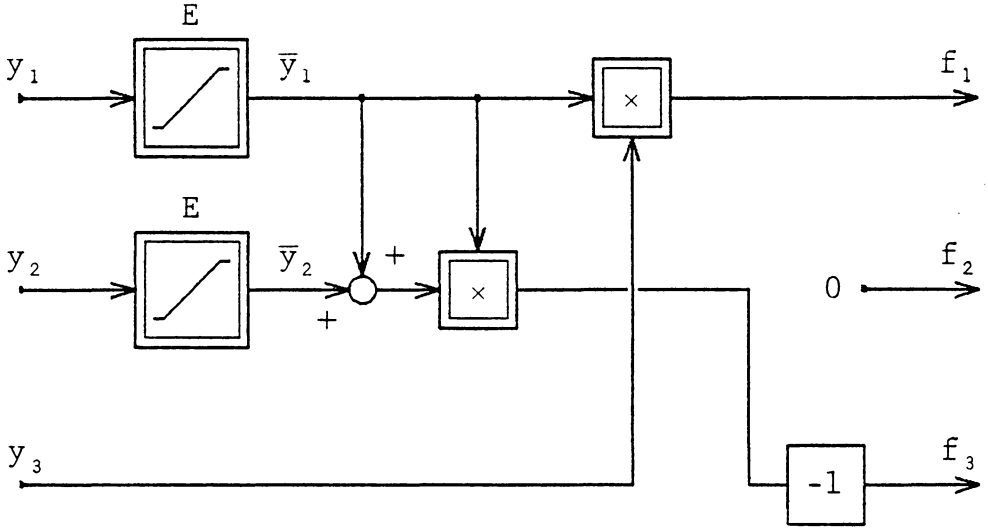

c) Nonlinear part of the system.

Fig. D.2: Multivariable feedback representation of the system from Fig. D.1 with $r = 0$.

The system in Fig. D.1 can be rearranged into the form shown in Fig. D.2a, so that the linear dynamic part is separated from the nonlinear memoryless part of the system. If $r = 0$, and the variables in the new notation are defined as

$$\begin{bmatrix}\xi_1\\ \xi_2\\ \xi_3\end{bmatrix} \triangleq \begin{bmatrix}0\\ 0\\ 0\end{bmatrix}, \qquad \begin{bmatrix}u_1\\ u_2\\ u_3\end{bmatrix} \triangleq \begin{bmatrix}u_a\\ 0\\ u_p\end{bmatrix}, \qquad \begin{bmatrix}y_1\\ y_2\\ y_3\end{bmatrix} \triangleq \begin{bmatrix}-e_1\\ -e_2\\ p_1\end{bmatrix} \tag{D.10}$$

the linear part of the system can be represented as shown in Fig. D.2b, and the nonlinear part as in Fig. D.2c. The resulting system has three outputs and two inputs, but the dummy input $u_2 \equiv 0$ has been added to make the number of inputs and outputs equal. This simplifies notation and does not influence the results in any other way.

The matrix transfer function of the linear part is

$$\sigma = \begin{bmatrix} q_1 \cdot G_1(s) & 0 & 0 \\ q_1 \cdot T_c \cdot G_1(s) \cdot G_d(s) & 0 & 0 \\ 0 & 0 & G_p(s) \end{bmatrix} \upsilon \triangleq G(s) \cdot \upsilon \ , \tag{D.11}$$

where

$$G_p(s) \triangleq \frac{q_2}{s + \varepsilon} \ . \tag{D.12}$$

The nonlinear feedback is described by equations

$$\begin{bmatrix} f_1 \\ f_2 \\ f_3 \end{bmatrix} = \begin{bmatrix} \bar{y}_1 \cdot \bar{y}_3 \\ 0 \\ -(\bar{y}_1 + \bar{y}_2) \cdot \bar{y}_1 \end{bmatrix} \triangleq f(\sigma) \ , \qquad (D.13)$$

where $\bar{y}_1$ and $\bar{y}_2$ represent the limited values of y_1 and y_2, respectively, as in Fig. D.2c.

□

FACT D.2: Consider the system in Fig. D.2a, and let

$$G(s) \triangleq C \cdot (sI - A)^{-1} \cdot B \qquad (D.14)$$

where (A,B,C) is any minimal state space realization of G(s). This system is globally asymptotically stable for $\xi \equiv 0$, if

i) it is L_2-stable for $\xi \in L_2$, and
ii) the linear part (D.14), has all poles with negative real part.

PROOF: The following proof closely parallels the proof of a related theorem by Vidyasagar [74, Theorem 6.4.1, pp. 240-242].

If $\xi \equiv 0$, the system in Fig. D.2a, with (D.14) can be described by

$$x(t) = x(0)\cdot\exp(At) - \int_0^t \exp[A(t - \tau)]\cdot B\cdot u(\tau)\cdot d\tau \qquad (D.15)$$

$$u(t) = \phi(t) \qquad (D.16)$$

$$\sigma(t) = C\cdot x(t) \quad . \qquad (D.17)$$

We need to show that $x(t) \to 0$ as $t \to \infty$, provided that (i) and (ii) are satisfied. Since the state space realization is assumed to be minimal, the pair (A,C) is observable, and therefore

$$\lim_{t\to\infty} C\cdot x(t) = 0 \quad <=> \quad \lim_{t\to\infty} x(t) = 0 \qquad (D.18)$$

Then it is sufficient to show that $\sigma(t) \to 0$ as $t \to \infty$.

From (D.15)-(D.17):

$$\sigma(t) = C\cdot x(0)\cdot\exp(At) - C\cdot\int_0^t \exp[A(t - \tau)]\cdot B\cdot\phi(\tau)\cdot d\tau \quad . \qquad (D.19)$$

From the conditions (i) and (ii):

$$(i) \quad <=> \quad (\xi \in L_2 \quad => \quad u,\sigma,\phi, \in L_2) \qquad (D.20)$$

$$(ii) \quad => \quad \|\exp(At)\| < a\cdot\exp(-\alpha t) , \quad a,\alpha \in R^+ \qquad (D.21)$$

$$=> \quad \|\exp(At)\| \in L_2 \qquad (D.22)$$

$$=> \quad C\cdot x(0)\cdot\exp(At) \in L_2 \qquad (D.23)$$

Therefore if we set

$$\xi(t) = C \cdot x(0) \cdot \exp(At) \quad , \tag{D.24}$$

from (D.23) and (D.20) we have

$$\phi(t) \in L_2 \quad . \tag{D.25}$$

By defining the auxiliary variable z as

$$z(t) \triangleq \int_0^t \exp[A(t - \tau)] \cdot B \cdot \phi(\tau) \cdot d\tau \quad , \tag{D.26}$$

from (D.19) and (D.24) it follows that

$$\sigma(t) = \xi(t) - C \cdot z(t) \quad . \tag{D.27}$$

Vidyasagar [ibid.] has shown that $z(t) \to 0$ as $t \to \infty$, provided that (D.22) and (D.25) hold. Then, from (D.21), (D.23), (D.24) and (D.27) it follows that $\sigma(t) \to 0$ as $t \to \infty$.

□

FACT D.3: Sufficient conditions for the system in Fig. D.2a to be L_2-stable are:

i) Linear part $G(s)$, is proper and has all poles with negative real part.

ii) $\exists \gamma \ , \quad 0 < \gamma < \infty \ : \qquad |f(\sigma)| \leq \gamma \cdot |\sigma| \ , \quad \forall \ \sigma$

iii) $\gamma \cdot \sup_{\omega \in R} \| G(j\omega) \| < 1$

PROOF: This fact is a direct consequence of the small-gain theorem, (Desoer and Vidyasagar [13, pp. 40-43], Harris and Valenca [39, pp. 178-180]). If that theorem is applied to the system in Fig. D.2a, with $G(s)$ being matrix rational transfer function, and $f(\sigma)$ continuous memoryless function, the resulting conditions for L_2-stability are:

a) a solution exists;

b) $\| \int_0^t g(t - \tau) \cdot v(\tau) \cdot d\tau \ \|_2 \leq \gamma_1 \cdot \| v(t) \|_2$

where $g(t)$ is the inverse Laplace transform of $G(s)$;

c) $\| f[\sigma(t)] \|_2 \leq \gamma_2 \cdot \| \sigma(t) \|_2$

d) $\gamma_1 \cdot \gamma_2 < 1$.

The proof is now obvious. The system in Fig. D.2a is continuous, so a solution exists. From (i), G(s) is exponentially stable, and in that case, (b) is satisfied with, [13, p. 139]:

$$\gamma_1 = \sup_{\omega \in R} \|G(j\omega)\| \quad . \tag{D.28}$$

From (ii), (c) is satisfied with $\gamma_2 = \gamma$, and then (d) automatically follows from (iii).

□

FACT D.4: Nonlinear vector function (D.13) from Fig. D.2c satisfies

$$|f(\sigma)| \leq \sqrt{2} \cdot E \cdot |\sigma| \quad . \tag{D.29}$$

PROOF: From Fig. D.2c

$$\overline{y}_1^2 \leq E^2 \quad , \qquad \overline{y}_2^2 \leq E^2 \quad . \tag{D.30}$$

Also, always

$$2 \cdot \overline{y}_1 \cdot \overline{y}_2 \leq \overline{y}_1^2 + \overline{y}_2^2 \quad . \tag{D.31}$$

Then from (D.13)

$$|f(\sigma)|^2 = (\bar{y}_1\ \bar{y}_3)^2 + (\bar{y}_1 + \bar{y}_2)^2\ \bar{y}_1^2$$

$$= \bar{y}_1^2 \cdot \bar{y}_3^2 + (\bar{y}_1^2 + \bar{y}_2^2) \cdot \bar{y}_1^2 + 2 \cdot \bar{y}_1 \cdot \bar{y}_2 \cdot \bar{y}_1^2$$

$$\leq E^2 \cdot \bar{y}_3^2 + 2 \cdot E^2 \cdot (\bar{y}_1^2 + \bar{y}_2^2)$$

$$\leq 2 \cdot E^2 \cdot (y_1^2 + y_2^2 + y_3^2)$$

$$= 2 \cdot E^2 \cdot |\sigma|^2 \quad . \tag{D.32}$$

□

We can now prove Theorem D .

PROOF OF THEOREM D: From Facts D.1 and D.2 it follows that the system in Fig. D.1 is globally asymptotically stable if the system in Fig. D.2, with (D.8) is L_2-stable.

Next, we apply Fact D.3. By using (D.11) and (D.12), the condition (i) of Fact D.3 follows from (D.1) and conditions (i) and (ii) of the theorem. The condition (ii) of Fact D.3 follows from Fact D.4, with

$$\gamma = \sqrt{2} \cdot E \quad . \tag{D.33}$$

By definition

$$\|G(j\omega)\| \triangleq \{\lambda_{max}[G'(-j\omega)\cdot G(j\omega)]\}^{\frac{1}{2}} \quad . \tag{D.34}$$

From (D.11)

$$G'(-j\omega)\cdot G(j\omega) = \begin{bmatrix} q_1^2\cdot|G_1(j\omega)|^2\cdot[1+T_c^2|G_d(j\omega)|^2] & 0 & 0 \\ 0 & 0 & 0 \\ 0 & 0 & |G_p(j\omega)|^2 \end{bmatrix}$$

and the eigenvalues are

$$\lambda_1(\omega) = q_1^2\cdot|G_1(j\omega)|^2\cdot[1 + T_c^2\cdot|G_d(j\omega)|^2] \tag{D.35}$$

$$\lambda_2 = 0$$

$$\lambda_3(\omega) = |G_p(j\omega)|^2 \quad . \tag{D.36}$$

From (D.7) and (D.12)

$$[\sup_{\omega\in R} \lambda_1(\omega)]^{\frac{1}{2}} = q_1\cdot F_m \tag{D.37}$$

$$[\sup_{\omega\in R} \lambda_3(\omega)]^{\frac{1}{2}} = \frac{q_2}{\varepsilon} \quad , \tag{D.38}$$

and therefore from (D.34)

$$\sup_{\omega\in R} \|G(j\omega)\| = \max(\, q_1\cdot F_m \,,\, q_2/\varepsilon \,) \quad . \tag{D.39}$$

Now, by substituting (D.5) and (D.6) from the condition (iii) of the theorem, into (D.39), we obtain

$$\sup_{\omega \in R} \|G(j\omega)\| < \max[\ 1/(\sqrt{2}\cdot E)\ ,\ 1/(\sqrt{2}\cdot E)\ ]\ . \qquad (D.40)$$

Combining (D.33) and (D.40) yields the condition (iii) of Fact D.3 and the assertion of the theorem follows.

□

D.2. DESCRIBING FUNCTION

We propose to derive describing function for the non-linear system in Fig. 5.11, under the assumptions

i) $|\cos \phi_z| > 0.5$

ii) $\omega > 10\cdot\varepsilon$,

where ϕ_z is defined in (D.45) below, and ω is the angular frequency of the first harmonic of e_f.

Suppose that e_f in Fig. 5.11 is the sinusoid

$$e_f = a\cdot\cos(\omega t)\ . \qquad (D.41)$$

If the first harmonic of u_p in Fig. 5.11 is

$$\tilde{u}_p = U_p \cdot \cos(\omega t + \phi_{up}) \quad , \tag{D.42}$$

the describing function $N(a,\omega)$ is defined as

$$N(a,\omega) \triangleq \frac{U_p}{a} \cdot \exp(j\phi_{up}) \tag{D.43}$$

From Fig. 5.11, with e_f given by (D.41), it follows that

$$z_1 = a \cdot g_z \cdot \cos(\omega t + \phi_z) \quad , \tag{D.44}$$

where

$$G_z(j\omega) \triangleq 1 + T_c \cdot G_d(j\omega) \triangleq g_z \cdot \exp(j\phi_z) \quad . \tag{D.45}$$

Then

$$\begin{aligned} z_2 &= z_1 \cdot a \cdot \cos(\omega t) \\ &= \frac{a^2 \cdot g_z}{2} \cdot [\cos(\phi_z) + \cos(2\omega t + \phi_z)] \quad . \end{aligned} \tag{D.46}$$

Variable p in Fig. 5.11 is a linear function of z_2 and g_p, given by

$$\underline{p} = \frac{q}{s + \varepsilon} \cdot \underline{z}_2 + \frac{\varepsilon}{s + \varepsilon} \cdot \underline{g}_p \quad . \tag{D.47}$$

Therefore, by superposition

$$p = g_p + p_0 + a_p \cdot \cos(2\omega t + \phi_p) \quad , \tag{D.48}$$

where

$$p_0 = \frac{q \cdot a^2 \cdot g_z}{2 \cdot \varepsilon} \cdot \cos(\phi_z) \tag{D.49}$$

$$a_p = \frac{q \cdot a^2 \cdot g_z}{2 \cdot (4\omega^2 + \varepsilon^2)^{\frac{1}{2}}} \tag{D.50}$$

$$\phi_p = \phi_z - \tan^{-1}(2\omega/\varepsilon) \quad . \tag{D.51}$$

Then

$$\begin{aligned} z_3 &= p \cdot a \cdot \cos(\omega t) \\ &= (g_p + p_0) \cdot a \cdot \cos(\omega t) + \frac{a_p \cdot a}{2} \cdot \cos(\omega t + \phi_p) + \\ &\quad + \frac{a_p \cdot a}{2} \cdot \cos(3\omega t + \phi_p) \quad . \end{aligned} \tag{D.52}$$

If the conditions (i) and (ii) are satisfied, from (D.49) and (D.50) we have

$$p_0 > 20 \cdot \frac{a_p}{2} \quad , \tag{D.53}$$

so that the third harmonic in (D.52) can be neglected. Then

$$z_3 \simeq a_3 \cdot a \cdot \cos(\omega t + \phi_3) \tag{D.54}$$

where

$$a_3 = [(g_p + p_0)^2 + a_p \cdot (g_p + p_0) \cdot \cos(\phi_p) + (a_p/2)^2]^{\frac{1}{2}} \quad . \quad (D.55)$$

Now, the first harmonic of u_p is

$$\tilde{u}_p = f_1(\rho) \cdot a_3 \cdot a \cdot \cos(\omega t + \phi_3) \quad , \quad (D.56)$$

where $f_1(\rho)$ is the describing function of the unit saturation function given by (B.7), and

$$\rho \triangleq \frac{U_m}{a \cdot a_3} \quad (D.57)$$

From (D.43), (D.52), (D.54), and (D.56) it finally follows

$$N(a,\omega) = f_1(\rho) \cdot [g_p + p_0 + \frac{a_p}{2} \cdot \exp(j\phi_p)] \quad . \quad (D.58)$$

If we set

$$N(a,\omega) = g_p + P(a,\omega) \quad (D.59)$$

then

$$P(a,\omega) = f_1(\rho) \cdot (g_p + p_0) - g_p + f_1(\rho) \cdot \frac{a_p}{2} \cdot \exp(j\phi_p) \quad . \quad (D.60)$$

APPENDIX E

SIMULATION PROGRAM

The SUPER*SCEPTRE simulation program was used for simulations. The dc motor from Appendix F.1 is modeled with the equivalent electric circuit. Coulombic friction is modeled by the table function TJMW, and the nonlinear damping by the resistance RMU. Listing of the source program in the SUPER*SCEPTRE code, used in the simulation of the SVSPI algorithm for generating Fig. 5.4, is given on pages 250 and 251.

The FORTRAN function subroutine FM1 emulates the nonlinear function μ_1 given by (2.18), an the subroutine FM5 emulates μ_5 given by (5.27). The function subroutine FPLOT is used for outputting the data for plotting. Source listings of these subroutines are given on page 252.

On pages 253 and 254 is listing of the JCL statements, which were used for running the program on the IBM 3084 processor with OS/VS2 Revision 3.8 operating system.

The source listing of the main simulation program in SUPER*SCEPTRE code is given below.

```
TRANSFER FUNCTION DESCRIPTION
  MODEL FILTER
     K=2E3
     D=-2E3
MODEL DESCRIPTION
  MODEL DCM (A1-A2-M1-M2)
*******      PANCAKE DC MOTOR  (9FBT)  MODEL      *******
    ELEMENTS
     LA,A2-A3=80E-6
     RA,A3-A4=2.3
     EB,A1-A4=X1(PK*VCMW)
     JMU,M1-M2=X2(PK*ILA)
     CMW,M2-M1=55E-6
     RMU,M2-M1=X3(1./(2E-10*VCMW*VCMW+1E-30))
     JMW,M2-M1=XX01(.0334*XTABLE(TJMW,VJMW))
    DEFINED PARAMETERS
     PK=.02
     DPOS=X4(VCMW)
     POS=0
    FUNCTIONS
     TJMW=-1.01000E-01,-5.00000E-01,-1.00010E-03,-5.00000E-01,
          -1.00000E-03,-6.00000E-01,0,0,
           1.00000E-03, 6.00000E-01, 1.00010E-03, 5.00000E-01,
           1.01000E-01, 5.00000E-01
  MODEL POWER AMPLIFIER (SATURATION)
     M=100
     Y=25
  MODEL CURRENT LIMITER (SATURATION)
     M=1
     Y=3.72
CIRCUIT DESCRIPTION
****   SVS ADAPTIVE PI   *** CURRENT DRIVE; GI=5E3,  GP=32,  SF=2E3 ***
****  PANCAKE  DC MOTOR  ***   Q1=500,  EPS=200,  K=0.1,  M0=1.E7   ***
**** JM=1., GA=1., TF=1. ***        SMALL INPUT STEP & TORQUE       ***
    ELEMENTS
     DM,A1-A2-M1-M2 = MODEL DCM
     PA, 1- 2-A2-A1 = MODEL POWER AMPLIFIER
     CL, 3- 2- 4- 2 = MODEL CURRENT LIMITER
     OF, 5- 2- 6- 2 = MODEL FILTER
     EV, 2- 1 = PVA
     EC, 2- 3 = PU
     EF, 2- 5 = PE
     JTL,M2-M1= TL
    DEFINED PARAMETERS
     PC  = .05
     PGI = 5E3
     PGP = 32
     PQ1 = 500
     PES = 200
     PK  = .1
     PM0 = 1E7
     PVA = X1P(EOCL-ILADM)
     PU  = X2P(PUP+PUI)
     PE  = X3P(PC*(PWR-VCMWDM))
     PE1 = X4P(PQ1*EOOF)
     PUP = X5P(P2*PE1)
     PM5 = FM5(P2,PE1,3.72,PM0)
     PM1 = FM1(PUI,PUP,3.72,PM0)
     PS  = X6P(1-PK*P2)
     DP2 = X7P(PS*PE1*PE1-PES*(P2-(PGP/PQ1))-PM5)
     DPUI= X8P(PGI*EOOF-PM1)
     PP  = X9P(PQ1*P2)
```

```
      PWR = T1
      P2  = .064
      PUI = .884435
      PPLOT=FPLOT(TIME,VCMWDM,ILADM,PP,PUI,PS)
     FUNCTIONS
      T1=0,100,  .01,100,  .01,110,  .15,110
      TL=0,0,  .09,0,  .09,.02,  .15,.02
     INITIAL CONDITIONS
      VCMWDM = 100
      ILADM  = .845
     OUTPUTS
      VCMWDM(SPEED),ILADM(I.ARM),PP,PUI,PS
      PPLOT
     RUN CONTROLS
      COMPUTER TIME LIMIT = 2
      INTEGRATION ROUTINE = IMPLICIT
      STARTING STEP SIZE = 1.E-5
      STOP IF (XSTPNO.GT.10000)
      STOP TIME = .15
END
```

The source listings of the FORTRAN function subroutines used in simulation are given below.

```
C ***********************************************************************
      DOUBLE PRECISION FUNCTION FM1(UI,UP,UM,M0)
C ***********************************************************************
      DOUBLE PRECISION UI,UP,UM,M0,UIMIN,UIMAX
      UIMIN=-UM-UP
      UIMAX=UM-UP
      IF (UIMAX.LT.0.0) UIMAX=0
      IF (UIMAX.GT.12.) UIMAX=12.
      IF (UIMIN.GT.0.0) UIMIN=0
      IF (UIMIN.LT.-12.) UIMIN=-12.
      IF (UI.LT.UIMIN) GO TO 10
      IF (UI.GT.UIMAX) GO TO 20
      FM1=0.
      RETURN
   10 FM1=M0*(UI-UIMIN)
      RETURN
   20 FM1=M0*(UI-UIMAX)
      RETURN
      END
C
C ***********************************************************************
      DOUBLE PRECISION FUNCTION FM5(P,E,UM,M0)
C ***********************************************************************
      DOUBLE PRECISION P,E,UM,M0,PM
      E=DABS(E)
      IF (E.LT.0.01) GO TO 10
      PM=UM/E
      GO TO 20
   10 PM=12.
   20 IF (P.LT.-PM) GO TO 30
      IF (P.GT.PM) GO TO 40
      FM5=0.
      RETURN
   30 FM5=M0*(P+PM)
      RETURN
   40 FM5=M0*(P-PM)
      RETURN
      END
C
C ***********************************************************************
      DOUBLE PRECISION FUNCTION FPLOT(T,A,B,C,D,E)
C ***********************************************************************
      DOUBLE PRECISION T,A,B,C,D,E
      WRITE (7,100) T,A,B,C,D,E
  100 FORMAT (1P6D12.5)
      FPLOT=1.
      RETURN
      END
```

The JCL statements used for running the simulation program are given below.

```
//A000XXXX JOB 99999,SVSPI,TIME=1,MSGLEVEL=(0,0),PRTY=IDLE
/*JOBPARM      LINES=3,CARDS=30000
//SUPERSEP PROC LKLIB='A529D8.SUPER.SCEPTRE.LINKLIB',
//          OVLIB='A529D8.SCEPTRE2.OVERLAY',
//          LKDPARM=,MAXERR=1
//SUPER     EXEC PGM=SUPER
//STEPLIB   DD DSN=&LKLIB,DISP=SHR
//FT01F001 DD UNIT=SYSDA,SPACE=(CYL,(2,1)),DSN=&&SCR1,
//             DCB=(RECFM=FB,LRECL=80,BLKSIZE=800),DISP=(,PASS)
//FT02F001 DD UNIT=SYSDA,SPACE=(CYL,(2,1)),DCB=*.FT01F001,
//          DSN=&&SCR2,DISP=(,PASS)
//FT05F001 DD DDNAME=INPUT
//FT06F001 DD SYSOUT=T
//FT15F001 DD DSN=&&SOURCE,UNIT=SYSDA,SPACE=(CYL,(2,1)),
//             DCB=*.FT01F001,DISP=(,PASS)
//FT16F001 DD DSN=&&LOGIC,UNIT=SYSDA,SPACE=(CYL,(2,1)),
//             DCB=*.FT01F001,DISP=(,PASS)
//SCEPT1    EXEC PGM=SCEPTRE1,COND=(&MAXERR,LT)
//STEPLIB   DD DSN=&LKLIB,DISP=SHR
//FT01F001 DD DSN=&&SCR1,DISP=(OLD,PASS)
//FT03F001 DD DSN=&&SCR2,DISP=(OLD,DELETE)
//FT04F001 DD UNIT=SYSDA,SPACE=(CYL,(2,1)),
//             DCB=(RECFM=FB,LRECL=80,BLKSIZE=800)
//FT05F001 DD DSN=&&SOURCE,DISP=(OLD,DELETE)
//FT06F001 DD SYSOUT=A
//FT08F001 DD DSN=&&PGMSAV,UNIT=SYSDA,SPACE=(CYL,(2,1)),
//             DCB=(RECFM=FB,LRECL=80,BLKSIZE=3200),DISP=(,PASS)
//FT08F002 DD DSN=&&DTASAV,UNIT=SYSDA,SPACE=(CYL,(2,1)),
//             DCB=(RECFM=FB,LRECL=80,BLKSIZE=1680),DISP=(,PASS)
//FT09F001 DD UNIT=SYSDA,SPACE=(CYL,(2,1)),DCB=*.FT04F001
//FORT      EXEC PGM=IGIFORT,COND=(&MAXERR,LT)
//SYSIN     DD DSN=&&PGMSAV,DISP=(OLD,DELETE,DELETE)
//          DD DSN=&&LOGIC,DISP=(OLD,DELETE)
//          DD DDNAME=FORTSRC
//SYSLIN    DD DSN=&&LOADSET,DISP=(,PASS),UNIT=SYSDA,SPACE=(CYL,(2,1)),
//             DCB=(RECFM=FB,LRECL=80,BLKSIZE=3200)
//SYSPRINT  DD SYSOUT=A
//SYSPUNCH  DD SYSOUT=B
//LKED      EXEC PGM=IEWL,PARM='OVLY,SIZE=(180K,50K),&LKDPARM',
//          COND=(&MAXERR,LT)
//SCEPTSIM  DD DSN=&LKLIB,DISP=SHR
//SYSLIN    DD DSN=&&LOADSET,DISP=(OLD,DELETE,DELETE)
//          DD DSN=&OVLIB,DISP=SHR
//          DD DDNAME=FORTOBJ
//SYSLMOD   DD DSN=&&GOSET(MAIN),DISP=(,PASS),UNIT=SYSSQ,
//             SPACE=(CYL,(2,1,1))
//SYSPRINT  DD SYSOUT=A
//SYSLIB    DD DSN=VSP.FRTHXLIB,DISP=SHR
//SYSUT1    DD UNIT=SYSDA,SPACE=(CYL,(1,1))
//GO        EXEC PGM=*.LKED.SYSLMOD,COND=(&MAXERR,LT)
//FT02F001 DD UNIT=SYSDA,SPACE=(CYL,(3,3)),
//             DCB=(RECFM=VBS,BLKSIZE=1028,LRECL=1024)
//FT03F001 DD DSN=&&SCR1,DISP=(OLD,DELETE)
//FT04F001 DD UNIT=SYSDA,SPACE=(CYL,(2,1))
//FT06F001 DD SYSOUT=T
//FT07F001 DD SYSOUT=B
//FT08F001 DD DSN=&&DTASAV,DISP=(OLD,DELETE)
//FT10F001 DD DSN=&&TEMP,UNIT=SYSDA,DISP=(NEW,PASS),
//             DCB=(RECFM=FB,LRECL=80,BLKSIZE=1600),SPACE=(CYL,(2,1))
//END   PEND
```

```
//STEP2   EXEC SUPERSEP,MAXERR=5
//SUPER.INPUT DD *
              .
              .
       Source code of the main simulation program
              .
              .
/*
//FORT.FORTSRC DD *
              .
              .
       Source code of the FORTRAN subroutines
              .
              .
/*
//
```

APPENDIX F

EXPERIMENTAL CIRCUITS

Specifications, circuit diagrams, and photographs of the hardware used in experiments, are shown in this appendix. All designs are functional, although they have not been optimized in any way. Operational amplifiers operate with the ±15 V supply.

F.1. DC MOTOR

Manufacturers specifications of the 9FBT, printed-circuit-rotor, homopolar, permanent magnet, dc motor-tachometer, are given in Table F.1. The parameter values that have been measured, directly or indirectly, are:

Total armature circuit resistance	2.3 Ω
Armature circuit inductance	80 μH
Stiction	0.02 N m
Friction	0.017 N m
Damping	$2\ 10^{-10}\ \omega^2$ N s/rad
Rotor inertia	$55\ 10^{-6}$ kg m^2

A photograph of the motor is shown in Fig. F.1.

Table F.1: Specifications for the dc motor type 9FBT

Parameter	Nominal value in	
	Customary units	SI units
Power	1/40 HP	18 W
Torque	9.0 oz-in	0.063 N m
Speed	2600 rpm	272 rad/s
Voltage	12.0 V	
Current	5.40 A	
Terminal Resistance	0.85 Ω	
Max. Continuous Stall Current	6.40 A	
Pulse Torque	101 oz-in	0.713 N m
Torque Constant	2.80 oz-in/A	0.0198 V s/rad
EMF Constant	2.07 V/krpm	0.0198 V s/rad
Rotor Inertia	0.007 oz-in-s^2	50 10^{-6} kg m^2
Friction	3.0 oz-in	0.021 N m
Mech. Time Constant	0.154 s	
Armature Inductance	100 μH	
Tach. Output Gradient	1.03 V/krpm	0.0098 V s/rad
Tach. Output Ripple	5.0 % p-p	
Tach. Output Impedance	1.0 Ω	

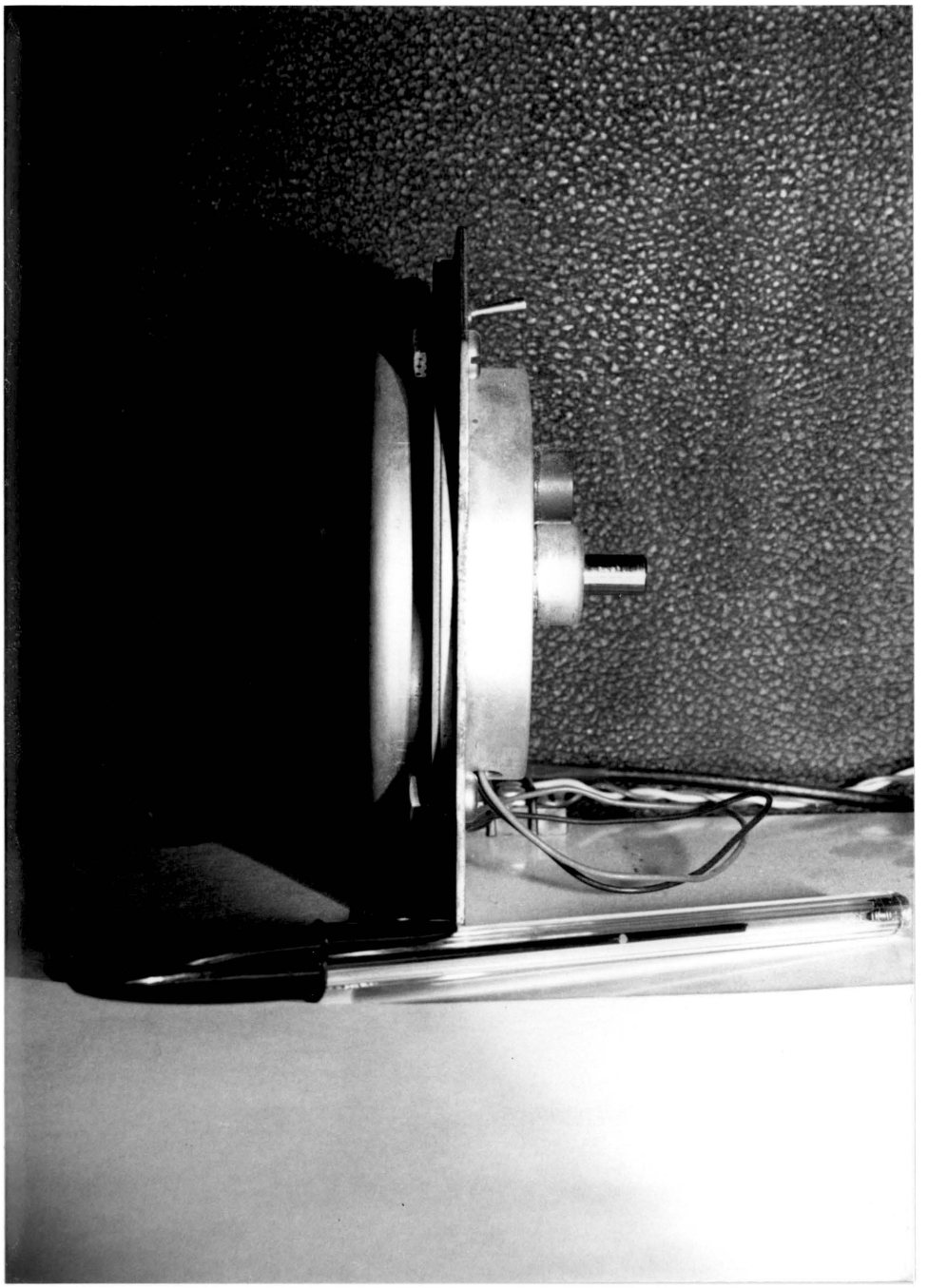

Fig. F.1

F.2. POWER AMPLIFIER

The circuit diagram of the power amplifier is shown in Fig. F.2. The components are:

OA1 - 1/4 of TL074 ;

PA - Apex μtech PA12A ;

RL - 0.24 Ω , 1% , 6 W ;

RC - 1 Ω , 0.1% , 32 W ;

R1 - 13 kΩ , 5% , 1 W ;

R2 - 16 kΩ , 5% , 1 W ;

All other resistors are 1% , 1/4 W .

The current limiting resistors, RL, set the current limit to approximately ±3.6 A.

The voltage limit of the input variable U is approximately ±12 V due to the ±15 V supply for the operational amplifiers.

The resistor RC is used for the current sensing.

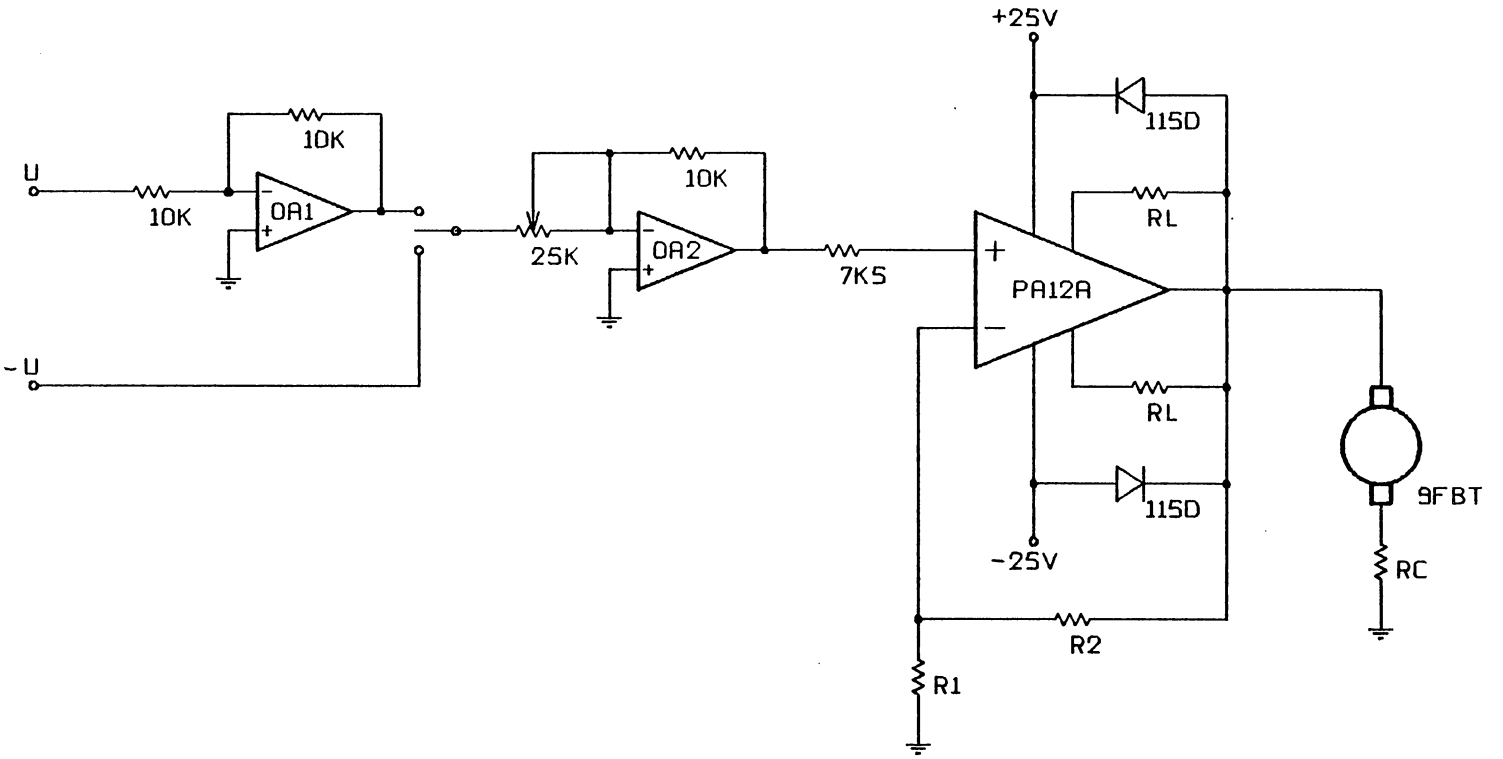
+25V
115D
10K
U
10K
OA1
10K
RL
25K
OA2
7K5
PA12A
-U
RL
115D
9FBT
-25V
RC
R2
R1

FIG. F.2

F.3. INTERFACE CIRCUIT

The interface circuit contains the circuitry for generating the reference signal R , and for processing the tachometer output. Its diagram is shown in Fig. F.3a. The components are:

OA1 - 1/4 of TL074 ;

OA2 - μA741 with input offset voltage null circuit;

All resistors are 1% , 1/4 W ;

All potentiometers are 15-turn , 3/4 W.

A photograph of the interface circuit and the power amplifier is shown in Fig. 3b. The board on the right hand side, also contains additional circuitry, which was not used in the experiments.

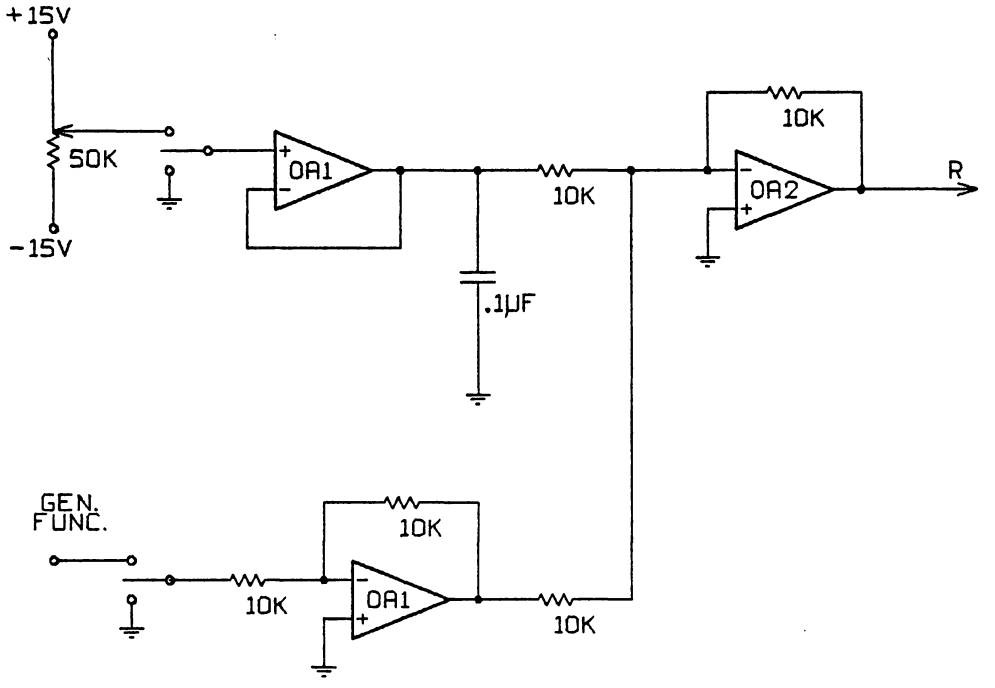

GENERATION OF REFERENCE

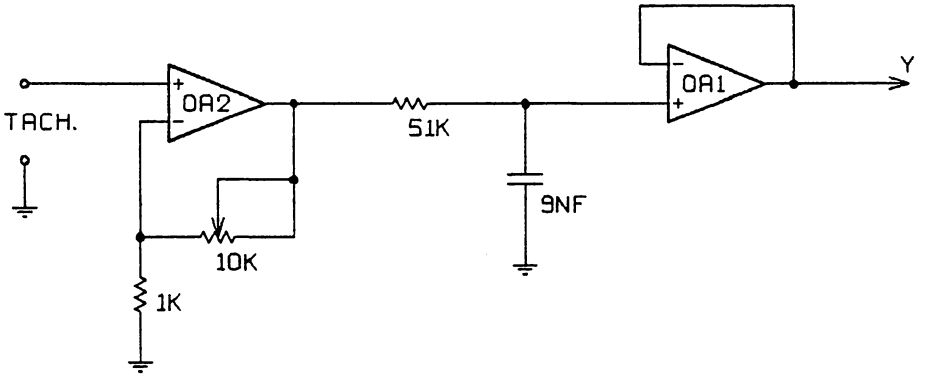

OUTPUT SCALING AND FILTER

FIG. F.3A

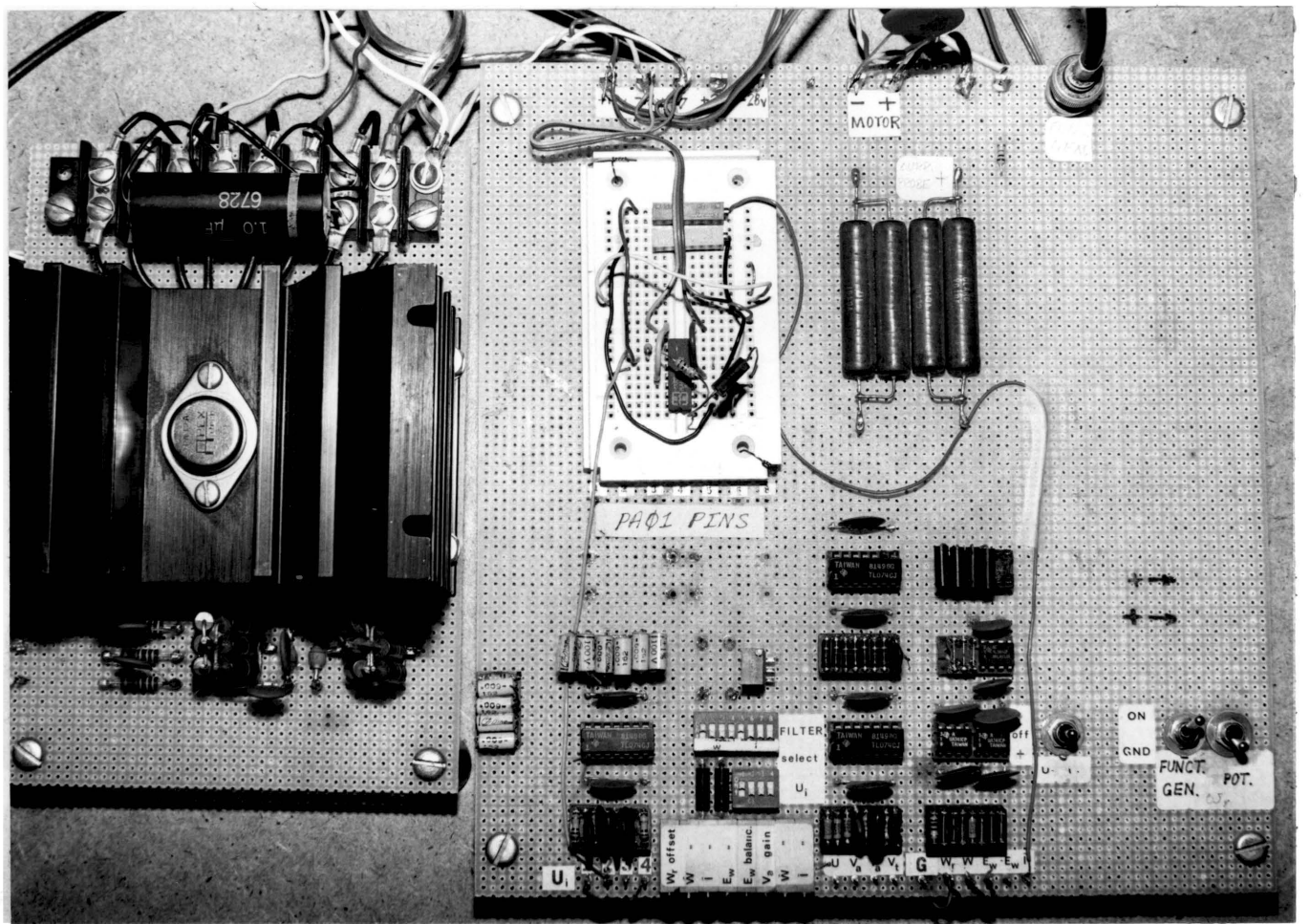

Fig. F.3b

F.4. I-P CONTROL

The circuit diagram of the I-P controller with fixed integrator limits from Fig. 2.7, is shown in Figures F.4a and F.4b. The components are:

OA1 - 1/4 of TL084 ;

OA2 - 1/2 of TL083 with input offset voltage null circuit;

D - 1N4148 ;

R1 - 5 kΩ , 0.1% , 1/2 W ;

All other resistors are 1% , 1/4 W ;

All potentiometers are 15-turn , 3/4 W.

The circuit was built on a protoboard.

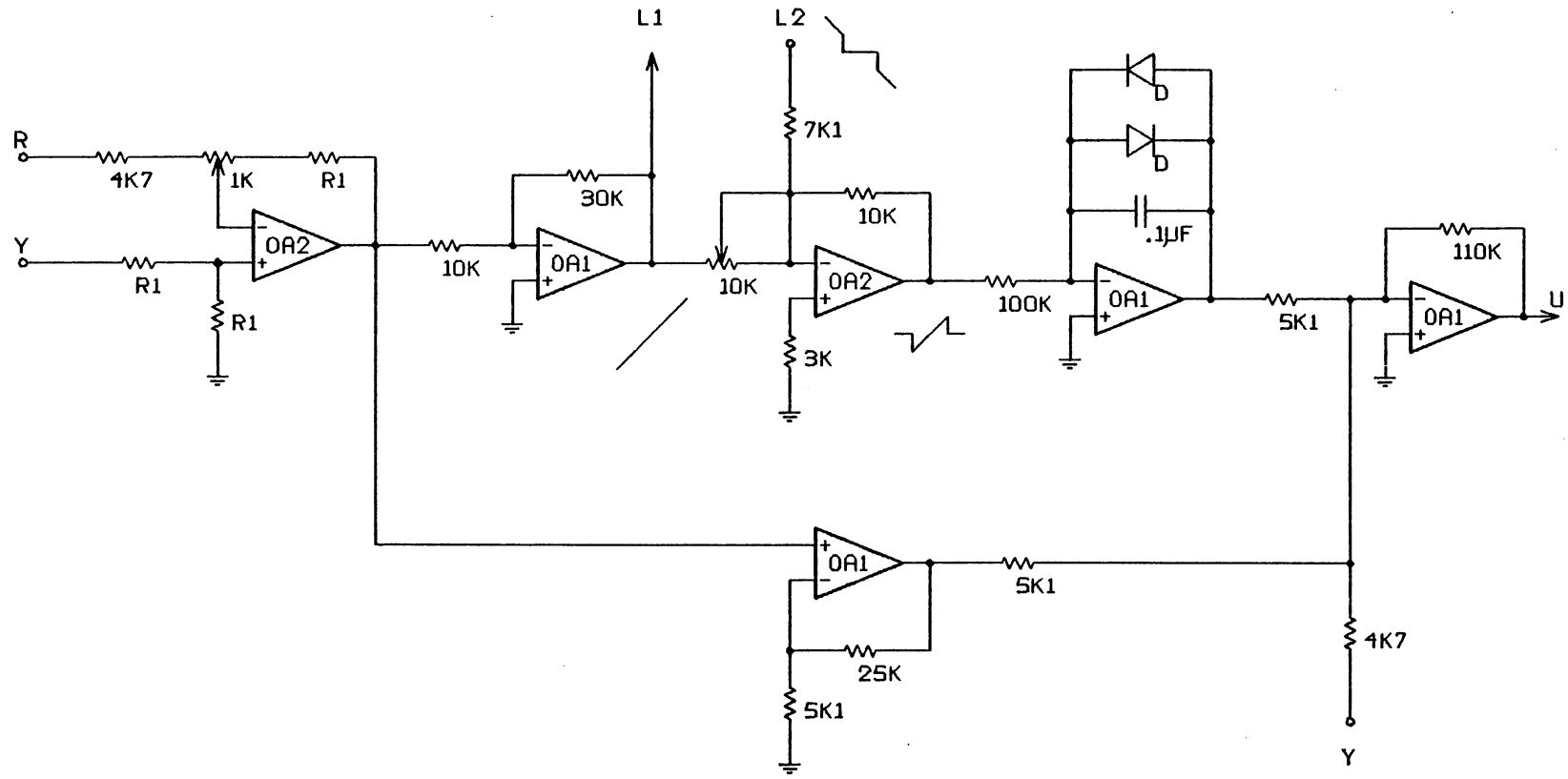
L1
L2
R
4K7
1K
R1
Y
R1
R1
OA2
10K
OA1
30K
10K
7K1
10K
OA2
3K
D
D
.1µF
100K
OA1
5K1
110K
OA1
U
OA1
5K1
25K
5K1
4K7
Y

FIG. F.4A

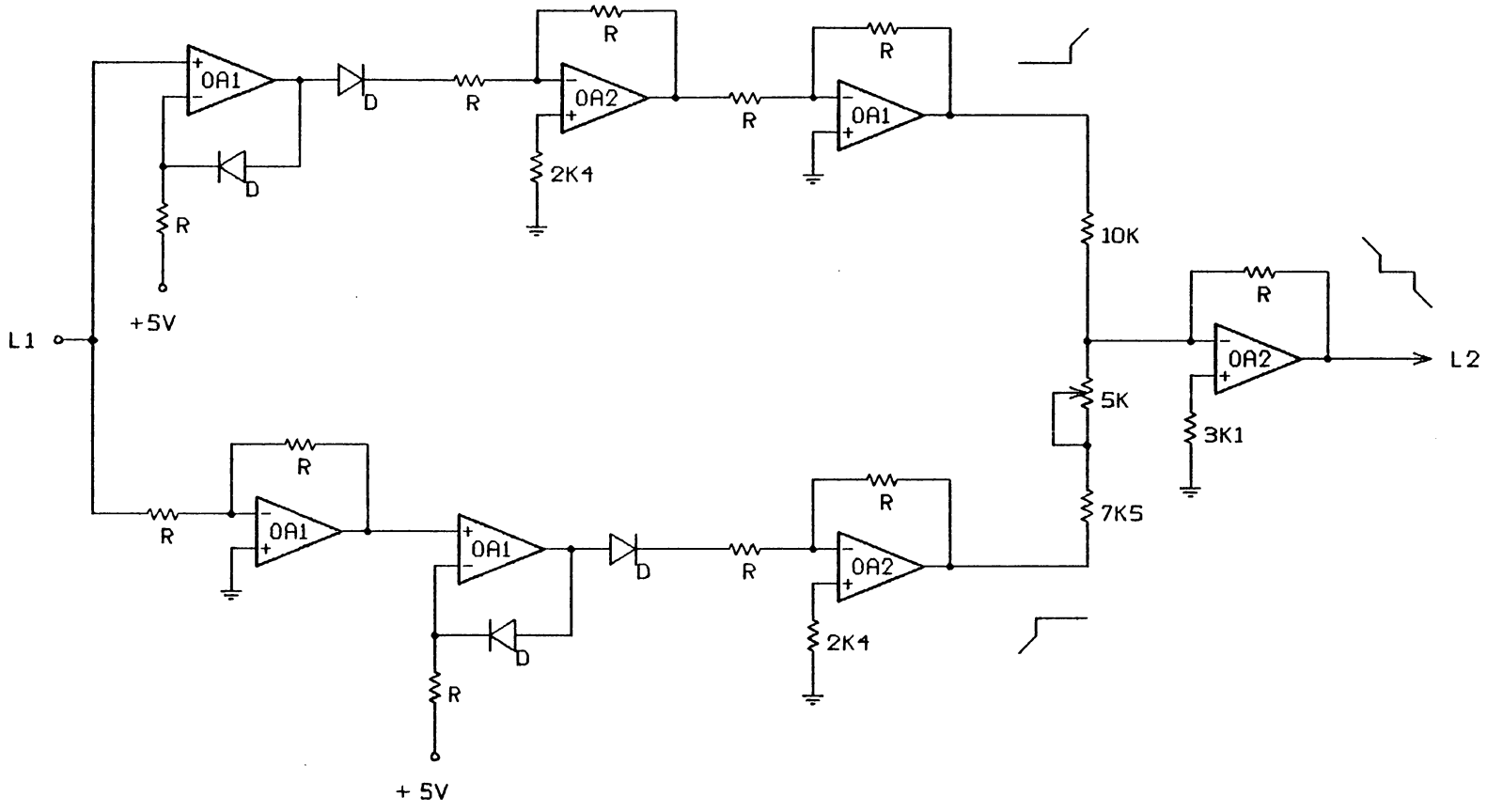
L1
+5V
R
OA1
D
R
OA2
2K4
R
OA1
10K
R
OA2
L2
5K
3K1
7K5
R
OA1
R
OA1
D
R
OA2
2K4
R
+ 5V

FIG. F.4B

F.5. SLM CONTROL

The circuit diagram of the SLM controller from Fig. 3.2, is shown in Figures F.5a and F.5b. The components are:

OA1 - 1/4 of TL084 ;

OA2 - TL081 with input offset voltage null circuit;

ASW - AD7512DIKN ;

XOR - 1/4 of SN74LS86 ;

All resistors are 1% , 1/4 W ;

All potentiometers are 15-turn , 3/4 W.

The circuit was built on a protoboard.

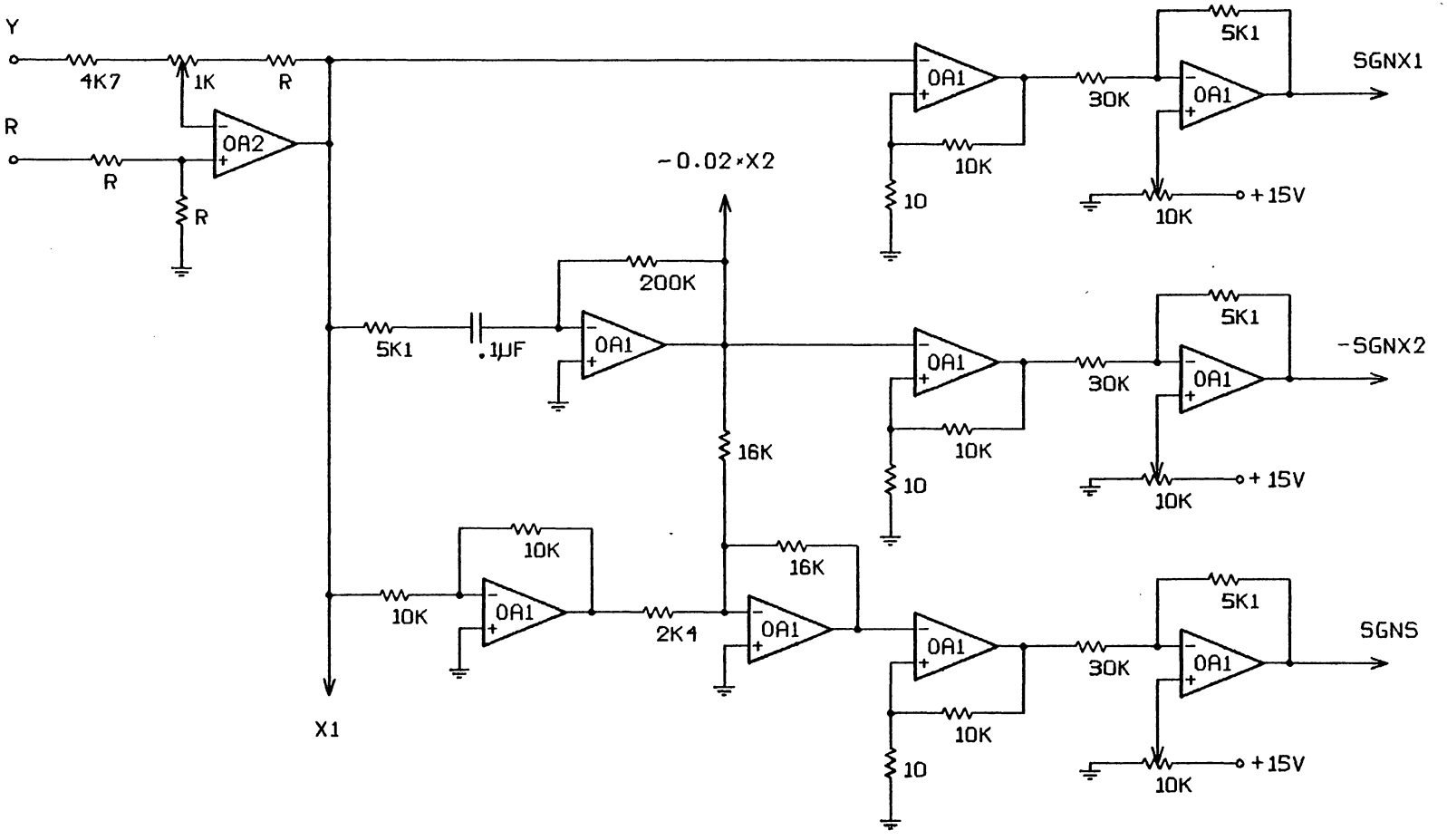
Y
4K7
1K
R
R
R
R
OA2
X1
-0.02*X2
200K
5K1
.1µF
OA1
16K
10K
10K
2K4
16K
10K
10
OA1
30K
5K1
OA1
10K
+15V
SGNX1
10
OA1
30K
5K1
OA1
10K
+15V
-SGNX2
10
OA1
30K
5K1
OA1
10K
+15V
SGNS

FIG. F.5A

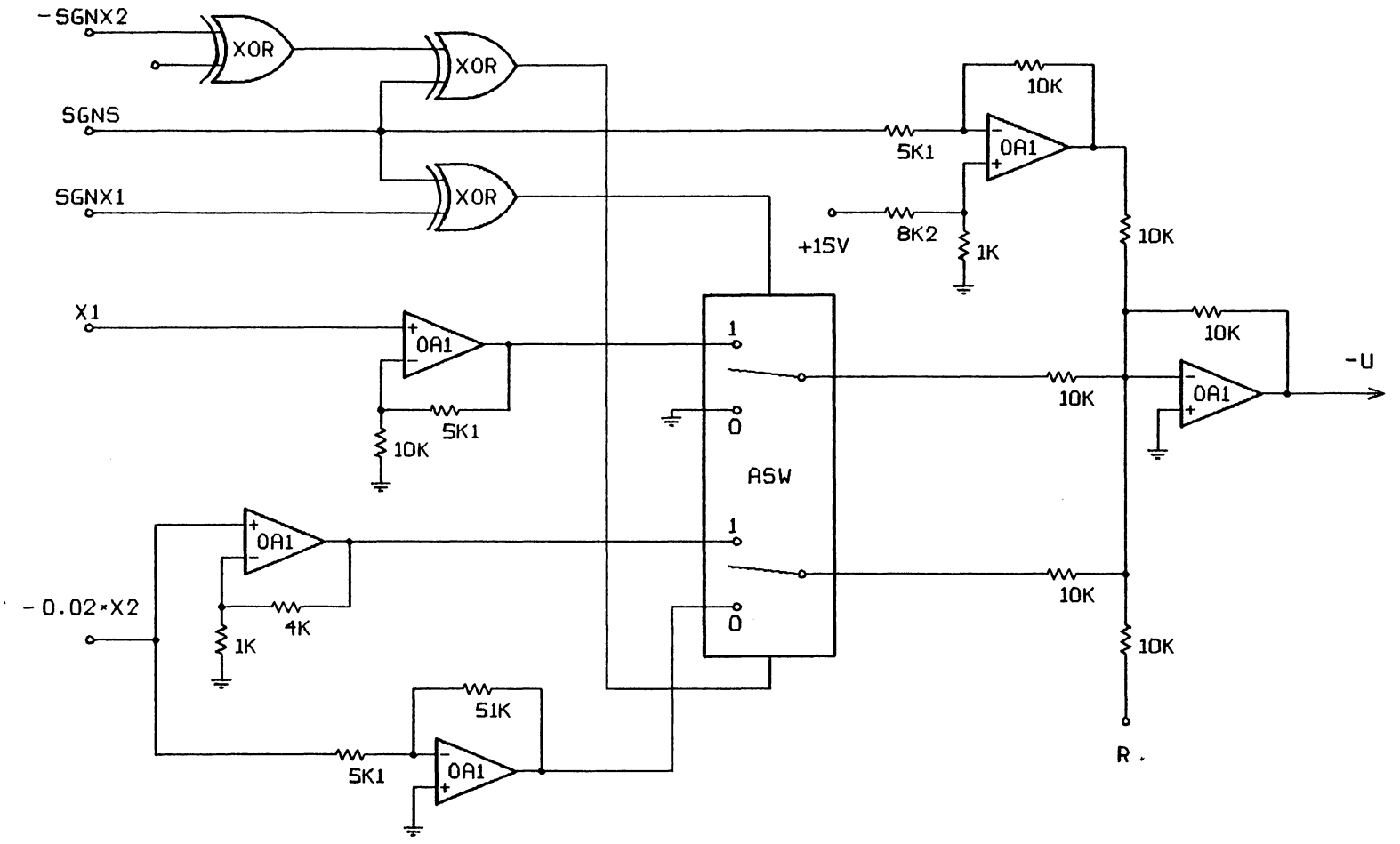
-SGNX2
XOR
XOR
SGNS
SGNX1
XOR
10K
5K1
OA1
+15V
8K2
1K
10K
X1
OA1
1
10K
5K1
10K
10K
OA1
-U
0
ASW
1
-0.02*X2
OA1
4K
1K
0
10K
10K
51K
5K1
OA1
R

FIG. F.5B

F.6. SVS CONTROL

The circuit diagram of the modified SVS controller from Fig. 4.1, is shown in Figures F.6a and F.6b. The components are:

OA1 - 1/4 of TL074 ;

IC1 - AD534KD in the multiplier configuration;

IC2 - AD534KD in the divider configuration;

D - 1N4148 ;

R1 - 10 kΩ , 0.1% , 1/2 W ;

R2 - 20 kΩ , 0.1% , 1/2 W ;

R3 - 1 kΩ , 0.1% , 1/2 W ;

All other resistors are 1% , 1/4 W .

All potentiometers are 15-turn , 3/4 W.

Because the positive voltage range is the same as U_m = 12 V , the signals at the inputs of the controller are divided by 2 and offset by 6 V, and the signal at the output of the controller is multiplied by 2 and offset by -6 V.

A photograph of the circuit is shown in Fig. 6c.

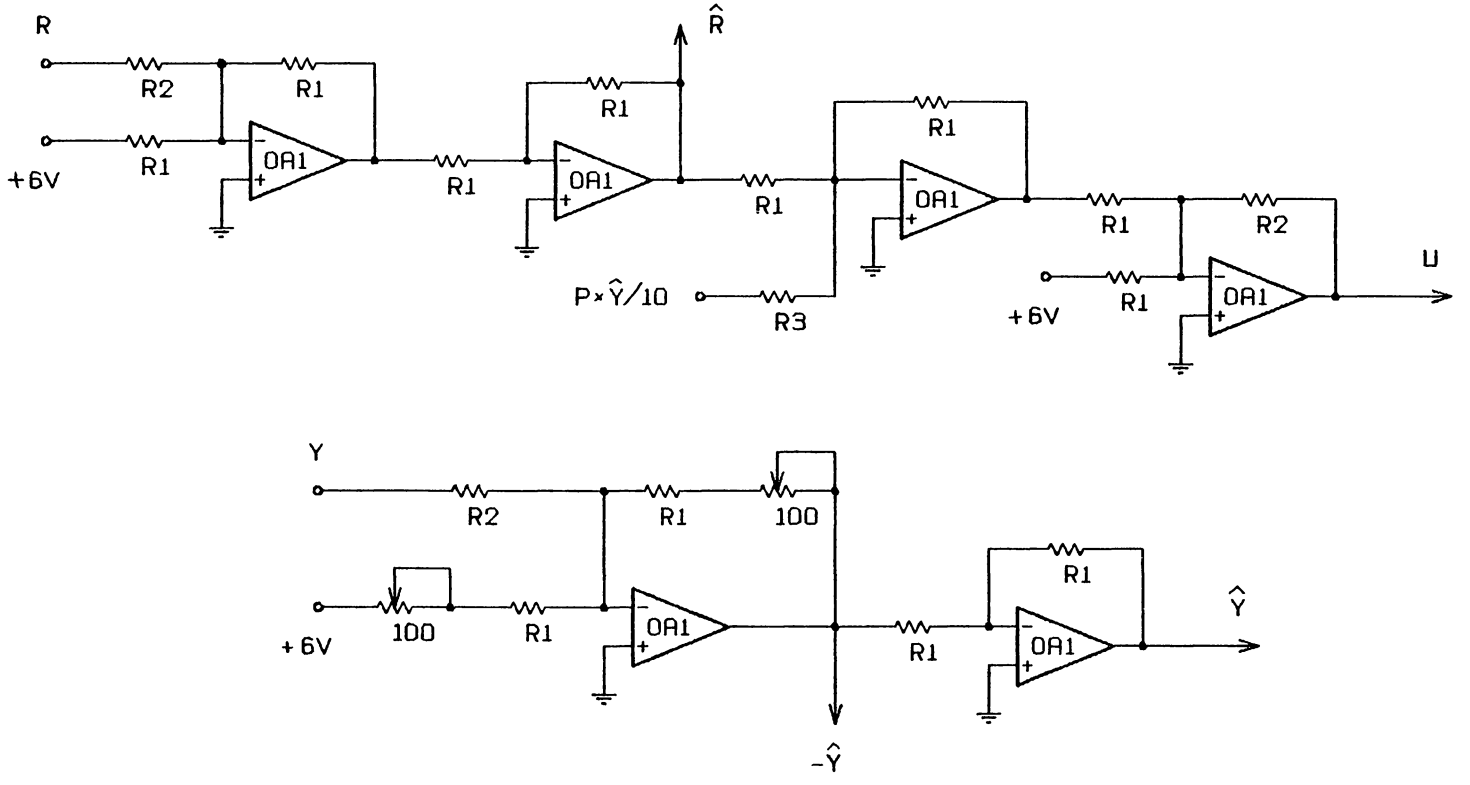
R
R2
R1
+6V
R1
OA1
R1
R1
OA1
$\hat{R}$
R1
OA1
R1
P×Ŷ/10
R3
R1
R2
OA1
U
+6V
R1
Y
R2
R1
100
+6V
100
R1
OA1
R1
R1
OA1
Ŷ
-Ŷ

FIG. F.6A

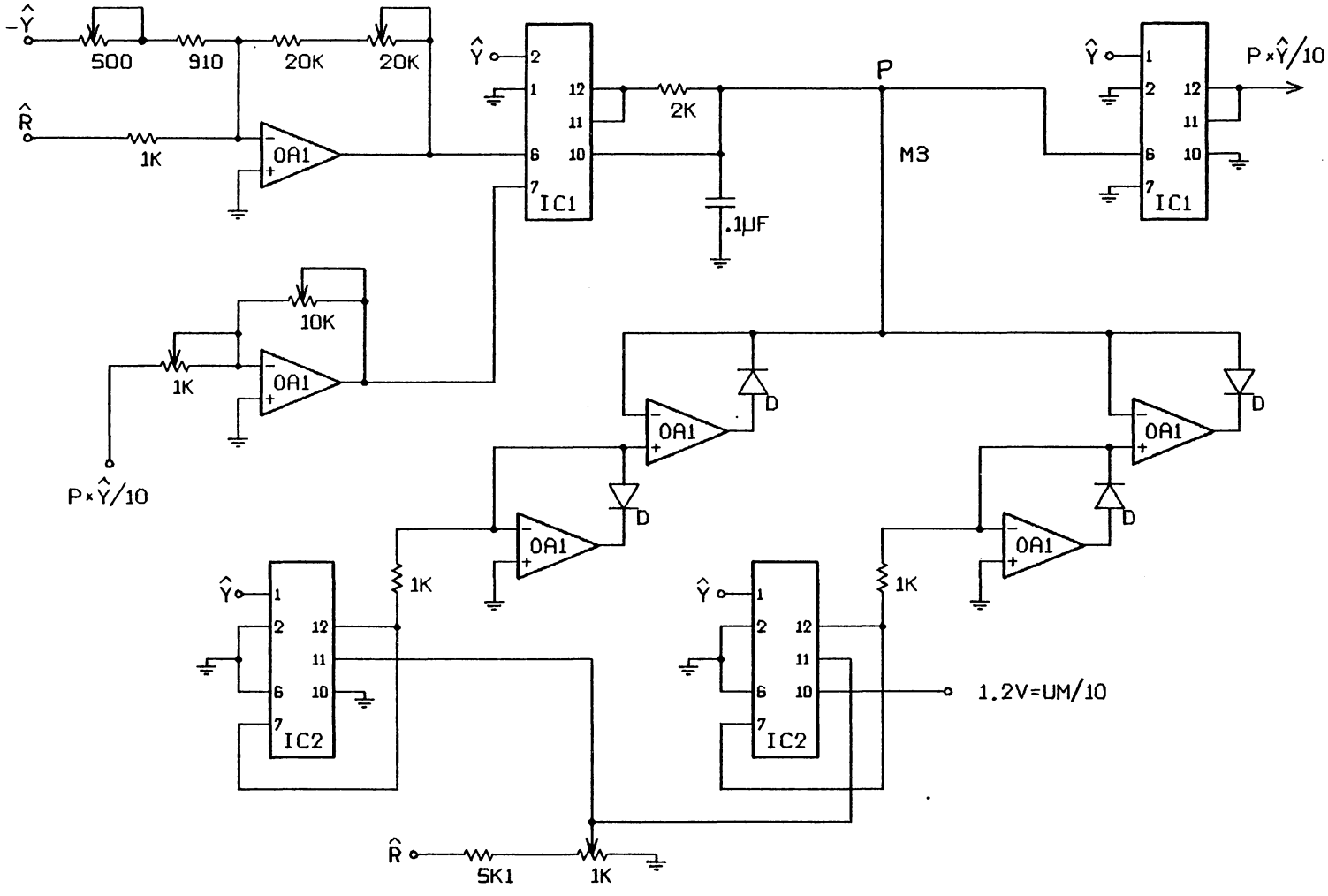
-Ŷ
500
910
20K
20K
R̂
1K
0A1
Ŷ
2
1
12
11
6
10
7
IC1
2K
.1μF
P
M3
Ŷ
1
2
12
11
6
10
7
IC1
P×Ŷ/10
10K
1K
0A1
P×Ŷ/10
D
0A1
D
0A1
D
0A1
D
Ŷ
1
2
12
11
6
10
7
IC2
1K
Ŷ
1
2
12
11
6
10
7
IC2
1K
1.2V=UM/10
R̂
5K1
1K

FIG. F.6B

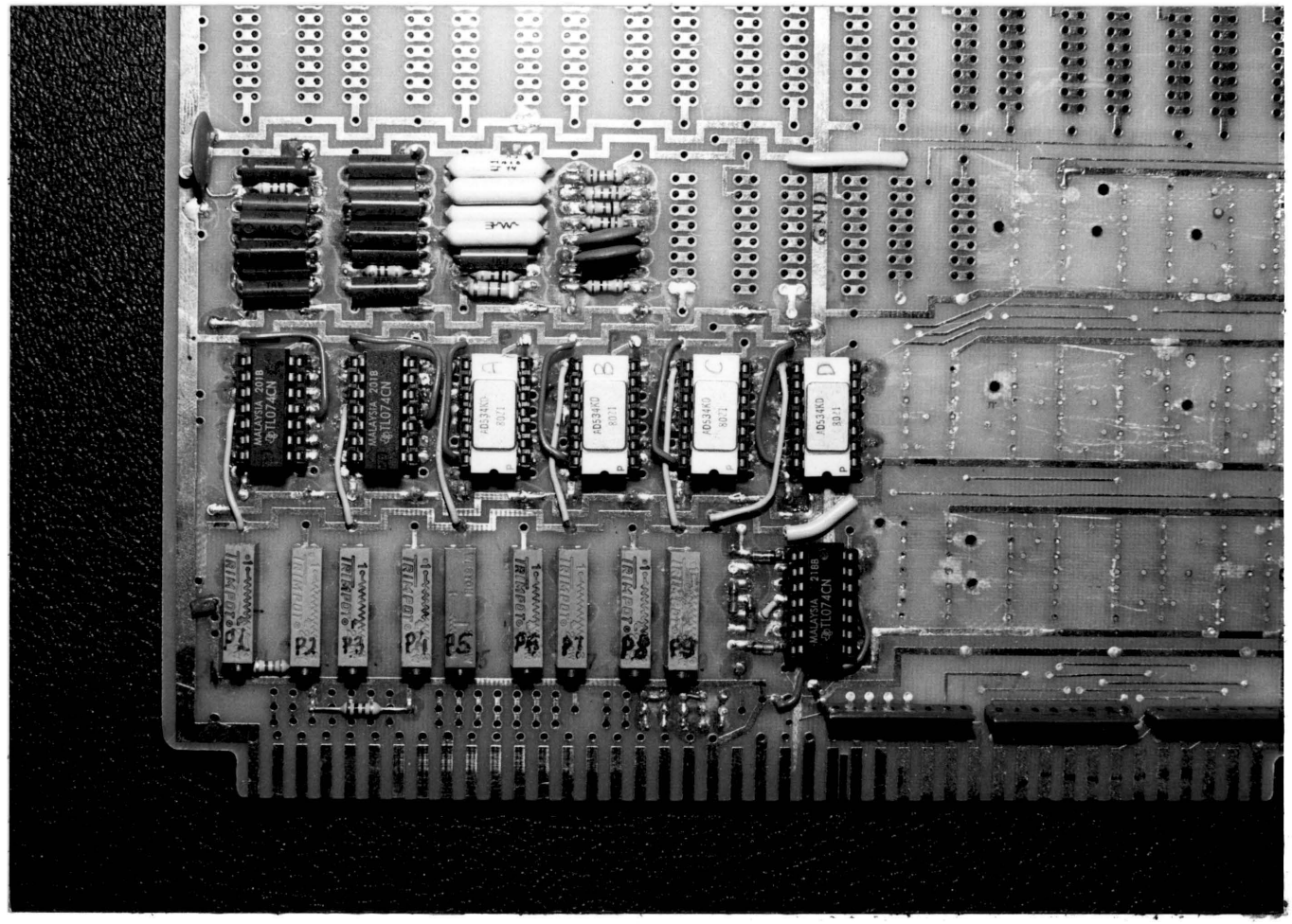
MALAYSIA 7018
TL074CN
MALAYSIA 7018
TL074CN
MALAYSIA 2188
TL074CN
A
B
C
D
P1
P2
P3
P4
P5
P6
P7
P8
P9

Fig. F.6c

REFERENCES

1. Astrom, K. J., "Theory and Application of Adaptive Control - A Survey", Automatica, vol. 19, no. 52, pp. 471-486, 1983.

2. Atherton, D. P., "Nonlinear Control Engineering", New York: Van Nostrand, 1982.

3. Balestrino, A. et al., "Adaptive Control Design in Servosystems", Third IFAC Symp. on Contr. in Power Electron. and Elect. Driv., pp. 125-131, 1983.

4. Bilalovic, F. et al., "A Variable Structure System for Squirrel Cage Induction Motor Control", Proc. of Motorcon, pp. 200-212, Mar 1982.

5. Borojevic, D. et al., "Soft Variable Structure Control for D.C. Motor Speed Regulation", IEEE-IAS 1984 Ann. Meet., pp. 404-410, 1984.

6. Borojevic, D. et al., "Performance Comparison of Variable Structure Controls with PI Control for D.C. Motor Speed Regulation", IEEE-IAS 1984 Ann. Meet., pp. 395-403, 1984.

7. Borojevic, D. et al., "Soft Variable Structure Control for D.C. Motor Control", Presented at the "Conference on Applied Motion Control", University of Minnessota, Minneapolis, June 11-13, 1985.

8. Bose, B. K. (editor), "Adjustable Speed AC Drive Systems", New York: IEEE PRESS, 1981.

9. Bose, B. K., "Sliding Mode Control of Induction Motor", IEEE-IAS 1985 Ann. Meet., pp. 503-509, 1985.

10. Bose, B. K., "Motion Control Technology - Present and Future", IEEE Trans. Ind. Appl., vol. IA-21, no. 6, pp. 1337-1342, Nov/Dec 1985.

11. Celentano, G. and Marino, P., "Nonlinear Controller Allowing for an Upper Bound on the System Internal Variables", IFAC Symp. on Contr. in Power Electron. and Elect. Driv., pp. 77-86, 1983.

12. Courtiol, B. and Landau, I. D., "High Speed Adaptive System for Controlled Electrical Drives", Automatica, vol. 11, pp. 119-127, 1974.

13. Desoer, C. A. and Vidyasagar, M., "Feedback Systems: Input-Output Properties", New York: Academic Press, 1975.

14. Dote, Y. and Hoft, R. G., "Microprocessor Based Sliding Mode Controller for DC Motor Drives", IEEE-IAS 1980 Ann. Meet., pp. 641-645, 1980.

15. Dote, Y. et al., "Variable Structure Control with Sliding Mode for DC Drive Speed Regulation", PESC '82 Record, pp. 123-127, 1982.

16. Dote, Y. et al., "Adaptive Digital Filter with Variable Structure Applied to Processing Signals from Tachometer and Torque Meter", IPEC-Tokyo '83, pp. 1698-1704, 1983.

17. Drazenovic, B., "The Invariance Conditions in Variable Structure Systems", Automatica, vol. 5, pp. 287-295, 1969.

18. El-Ghezawi, O. M. E. et al., "Analysis and Design of Variable Structure Systems Using a Geometric Approach", Int. J. Control, vol. 38, no. 3, pp. 657-671, 1983.

19. Emelyanov, S. V. et al., "Principles of Construction of Control Systems with Integral Coordinate-Parametric Feedback and Their Properties", Tekh. Kibern., no. 5, pp. 140-152, 1981.

20. Emelyanov, S. V. and Korovin, S. K., "An Extension of the Set of Types of Feedbacks and Their Application in Construction of Closed Dynamical Systems", Tekh. Kibern., no. 6, pp. 173-183, 1981.

21. Emelyanov, S. V. and Lozgachev, G. I., "Synthesis of a System with Variable Structure in the Output Variables", Dokl. Akad. Nauk SSSR, vol. 258, pp. 565-566, Jun 1981.

22. Emelyanov, S. V. et al., "Synthesis of Control Systems Using Coordinate-Parametric and Parametric Feedbacks", Dokl. Akad. Nauk SSSR, vol. 266, pp. 792-794, Oct 1983.

23. Emelyanov, S. V. et al., "Synthesis of Systems with Quasicontinuous Generation of Controls", Dokl. Akad. Nauk SSSR, vol. 268, pp. 103-105, Feb 1983.

24. Espana, M. D. et al., "Variable Structure System with Chattering Reduction: A Microprocessor Based Design", Automatica, vol. 20, no. 1, pp. 133-134, 1984.

25. Fitzgerald, A. E. et al., "Electric Machinery", New York: McGraw-Hill, 1983.

26. Franke, D., "Control of Distributed Parameter Systems with Independent Linear and Bilinear Modes", Third IMA-Conference on Control Theory, University Sheffield/England, pp. 827-841, 1980.

27. Franke, D., "Struktur variable Regelung ohne Gleitzustande" (Variable structure control without sliding modes) Regelungstechnik, vol. 30, no. 8, pp. 271-276, 1982.

28. Franke, D., "Ausschopfen von Stellgrossenbeschrankungen mittels weicher strukturvariabler Regelung" (Exhausting bounds on control by means of soft variable structure control), Regelungstechnik, vol. 30, no. 10, pp. 348-355, 1982.

29. Franke, D., "Ein nichtlinearer Dynamischer Regler mit adaptiven Eigenschaften" (A nonlinear dynamical controller with adaptive properties), Regelungstechnik, vol. 31, no. 11, pp. 369-374, 1983.

30. Franklin, J. N., "Matrix Theory", Englewood Cliffs: Prentice-Hall, 1968.

31. Garces, L. J., "Parameter Adaptation for the Speed Controlled Static AC Drive with Squirrel Cage Induction Motor", IEEE-IAS 1979 Ann. Meet., pp. 943-850, 1983.

32. Glattfelder, A. H. and Schaufelberger W., "Stability Analysis of Single Loop Control Systems with Saturation and Antireset-Windup Circuits", IEEE Trans. Automat. Contr., vol. AC-28, no. 12, pp. 1074-1081, Dec 1983.

33. Gupta, D. P. and Lynn, J. W., "Electrical Machine Dynamics", London: Macmillan Press, 1980.

34. Harashima, F. and Kondo, S., "A Design Method for Digital Speed Control System of Motor Drives", PESC '82 Record, pp. 1-9, 1982.

35. Harashima, F. et al., "Mosfet Converter-fed Position Servo System with Sliding Mode Control", PESC '83 Record, pp. 73-79, 1983.

36. Harashima, F. et al., "Arbitrary Trajectory Tracking Characteristics of Sliding Mode Controlled Servo System", PESC '84 Record, pp. 181-189, 1984.

37. Harashima, F. et al., "MOSFET Converter-Fed Position Servo System with Sliding Mode Control", IEEE Trans. Ind. Electron. vol. IE-32, no. 3, pp. 238-245, Aug 1985.

38. Harris, C. J. and Billings, S. A., "Self-Tuning and Adaptive Control: Theory and Applications", New York: Peiter Peregrinus 1981.

39. Harris, C. J. and Valenca, J. M., "The Stability of Input-Output Dynamical Systems", London: Academic Press, 1983.

40. Horowitz, I. M., "Synthesis of Feedback Systems", New York: Academic Press, 1963.

41. Ishikawa, K., "Principles of Luders-Narendra's Adaptive Observer", Int. J. Control, vol. 31, no. 2, pp. 351-365, 1980.

42. Itkis, U., "Control Systems of Variable Structure", New York: John Wiley, 1976.

43. Joos, G. and Barton T. H., "Four-Quadrant DC Variable-Speed Drives - Design Considerations", Proc. IEEE, vol. 63, no. 12, pp. 1660-1668, Dec 1975.

44. Jury, E. I. and Lee, B. W., "The Absolute Stability of System with Many Nonlinearities", Avtomatika i Telemekhanika, vol. 26. pp. 945-965, 1965.

45. Kalman, R. E. and Bertram, J. E., "Control System Analysis and Design Via the 'Second Method' of Liapunov", Journal of Basic Engeneering, pp. 371-393, Jun 1960.

46. Kaynak, M. O. et al., "Microprocessor Controlled Position Servo System With a Sliding Mode", PESC '82 Record, pp. 273-279, 1982.

47. Kaynak, O. et al., "A Variable Structure System with an Invariant Trajectory", IPEC-Tokyo '83, pp. 1688-1697, 1983.

48. Kokotovic, P. V. et al., "Singular Perturbations and Order Reduction in Control Theory - An Overview", Automatica, vol. 12, pp. 123-132, 1976.

49. Kokotovic, P. V., "Recent Trends in Feedback Design: An Overview", Automatica, vol. 21, no. 3, pp. 225-236, 1985.

50. Krikelis, N. J., "State Feedback Integral Control with 'Inteligent' Integrators", Int. J. Control, vol. 32, no. 3, pp. 465-473, 1980.

51. Kuo, B. C., "Digital Control Systems", New York: Holt, Rinehart and Winston, 1980.

52. Landau, Y. D., "Adaptive Control", New York: Marcel Dekker, 1979.

53. Lee, J. R., "Microprocessor-Based Soft Variable Structure Control for D.C. Motor Speed Regulation (Masters Thesis)", Blacksburg: VPI & SU, May 1985.

54. Luders, G. and Narendra, K. S., "A New Canonical Form for an Adaptive Observer", IEEE Trans. Automat. Contr., vol. AC-19, no. 2, pp. 117-119, Apr 1974.

55. Luenberger, D. G., "An Introduction to Observers", IEEE Trans. Automat. Contr., vol. AC-16, no. 6, pp. 596-602, Dec 1971.

56. Naitoh, H., "Model Reference Adaptive Control for Adjustable Speed Motor Drives", IPEC-Tokyo '83, pp. 1705-1716, 1983.

57. Naitoh, H., "Microprocessor-Based Adjustable Speed D.C. Motor Drives Using Model Reference Adaptive Control", IEEE-IAS 1985 Ann. Meet., pp. 524-528, 1985.

58. Namuduri, C. and Sen, P. C., "Variable Structure Control of a Self-controlled Synchronous Motor (SCSM) Drive", IEEE-IAS 1985 Ann. Meet, pp. 479-486, 1985.

59. Ohishi, K. et al., "Torque Speed Regulation of D.C. Motor Based on Load Torque Estimation Method", IPEC-Tokyo '83, pp. 1209-1218 1983.

60. Perkins, W. R. and Cruz, J. B. Jr., "The Parameter Variation Problem in State Feedback Control Systems", Trans. ASME, vol. 87, pp. 120-124, Mar 1965.

61. Phelan, R. M., "Automatic Control Systems", Ithaca: Cornell University Press, 1977.

62. Riedle, B. D. and Kokotovic, P. V., "Stability Analysis of an Adaptive System with Unmodelled Dynamics", Int. J. Control, vol. 41, no. 2, pp. 389-402, 1985.

63. Sabanovic, A. and Izosimov, D. B., "Application of Sliding Modes to Induction Motor Control", IEEE Trans. Ind. Appl., vol. IA-17, no. 1, pp. 41-49, Jan/Feb 1981.

64. Sabanovic, A. et al., "Control of Angular Position, Speed, Acceleration and Shaft Torque of Induction Motor", Proc. of Motorcon, pp. 1-9, Mar 1982.

65. Slotine, J. J. and Sastry, F. F., "Tracking Control of Non-linear Systems Using Sliding Surfaces, with Application to Robot Manipulators", Int. J. Control, vol. 38, no. 2, pp. 465-492, 1983.

66. Stefanovic, V. R., "Present Trends in Variable Speed AC Drives", IPEC-Tokyo '83, pp. 438-448, 1983.

67. Suh, I. H. et al., "A Design and Experiment of Speed Controler with PI-Plus Bang-Bang Action for a DC Servomotor with Transistorized PWM Drives", IEEE Trans. Ind. Electron. vol. IE-31, no. 4, pp. 338-345, Nov 1984.

68. Utkin, V. A. and Utkin, V. I., "Design of Invariant Systems by the Method of Separation of Motions", Avtomatika i Telemekhanika, no. 12, pp. 39-48, Dec 1983.

69. Utkin, V. I., "Variable Structure Systems with Sliding Modes", IEEE Trans. Automat. Contr., vol. AC-22, no. 2, pp. 212-222, Apr 1977.

70 Utkin, V. I. and Yang, K. D., "Methods for Constructing Discontinuity Planes in Multidimensional Variable Structure Systems", Avtomatika i Telemekhanika, no. 10, pp. 72-77, Oct 1978.

71. Utkin, V. I., "Sliding Modes and their Application in Variable Structure Systems", Moscow: Mir Publishers, 1978.

72. Utkin, V. I., "Variable Structure Systems: Present and Future", Avtomatika i Telemekhanika, no. 9, pp. 5-25, Sep 1983.

73. Venkataramanan, R. et al., "Sliding Mode Approach for Speed Control and Speed Estimation in D.C. Motors", Proc. of Motorcon, 1985.

74. Vidyasagar, M., "Nonlinear Systems Analysis", Englewood Cliffs: Prentice-Hall, 1978.

75. Weihrich, G., "Drehzahlregelung von Gleichstromantrieben unter Verwendung eines Zustands- und Storgrossen-

Beobachters" (Speed Control of Direct-Current Drives - Using a State and Disturbance Observer), Regelungstechnik, vol. 26, no. 11, pp. 349-380, 1978.

76. Weihrich, G. and Wohld, D., "Speed Control of D.C. Drives Using Adaptive Observer", Siemens Forsch-u. Entwickl.-Ber., vol. 9, no. 5, pp. 283-287, 1980.

77. West, J. C., and Somerville, M. J., "Integral Control with Torque Limitation", Proc. IEE, vol. 103, p. 407, 1956.

78. Young, K. D. et al., "A Singular Perturbation Analysis of High-Gain Feedback Systems", IEEE Trans. Automat. Contr., vol. AC-22, no. 6, pp. 931-938, 1977.

79. Young, K. D., "Design of Variable Structure Model-Following Control Sustem", IEEE Trans. Automat. Contr., vol. AC-23, no. 6, pp. 1079-1085, 1978.

80. Zames, G., "Feedback and Optimal Sensitivity: Model Reference Transformations, Multiplicative Seminorms, and Approximate Inverses", IEEE Trans. Automat. Contr., vol. AC-26, no. 2, pp. 301-320, Apr 1981.

The vita has been removed from the scanned document